Department of Chemistry

Co-precipitation of Ferrihydrite and Silica from Acidic Hydrometallurgical Solutions and its Impact on the Paragoethite Process

Laurence G Dyer

This thesis is presented for the Degree of
Doctor of Philosophy (Chemistry)
of
Curtin University of Technology

August 2010

To the best of my knowledge and belief this thesis contains no material previously published by any other person except where due acknowledgment has been made. This thesis contains no material which has been accepted for the award of any other degree or diploma in any university.

Signature: _____ Date: 11/2/11

Acknowledgements

The Australian Government, Nyrstar Metals are thanked for the provision of the core research funding via the Australian Research Council, Australian Postgraduate Award (Industry) program. The AJ Parker Collaborative Research Centre for Integrated Hydrometallurgy Solutions and CSIRO Process Science and Engineering are also thanked for additional funding and support. The Nanotechnology Research Institute and its members are thanked for providing much valuable advice and materials for this project, as is Centre for Microscopy, Characterisation and Analysis at the University of Western Australia for the use of instruments and very patient assistance.

My most sincere gratitude to my supervisory panel: Dr. Bill Richmond, Dr. Phillip Fawell, Dr. Mike Newman and David Palmer; for providing such an amazing opportunity and fantastic support, and guidance. Thank you for allowing me to flourish while giving me the occasional shove back on track when I needed it. It was obviously not an easy task as it drove Mike to retirement and Bill away from academia. Also thanks to Dr. Mark Ogden, Dr. Franca Jones, Dr. Kate Wright, Peter Chapman and Dave Walton for discussions, advice and technical aid.

I would also like to thank Fiona Benn, Andrew Owen and Alton Grabsch from the Alumina group for their assistance with instruments, equipment and generally making me feel welcome at CSIRO. Also thanks to Ian Davies, Milan Chovancek, Rick Hughes, Sophia Morrell, Nancy Hanna and all other members of the analytical and PAS teams. Thanks to Dr. Martin Saunders for many hours spent helping with my TEM work and providing new ideas and access to novel techniques, also Steve Parry and Peter Duncan for their technical assistance.

Special thanks to Dr. Geoff Carter, William Rickard and Ross Williams for both technical but more often moral support.

To Jean-Pierre Veder, Michael Rutledge and Graeme Clarke for their tireless efforts in providing respite from my research, and dragging me from my work when I really needed it. The deep philosophical discussions we often found ourselves immersed in will be sorely missed.

My greatest thanks go to my family, specifically my parents Helen and Trevor, for without them I would not be the man I am today and without their continual love and support completing this thesis would not have been something I would have been able to accomplish.

Finally, to Ivana, your constant motivation allowed me to finish my work, you gave me the courage to pursue what I really want and I believe I owe you my sanity. Hopefully now your patience will be duly rewarded, thank you my love.

Abstract

Ferrihydrite is a common iron oxyhydroxide, produced both naturally and industrially. It is often found in association with silica; an example of this is its occurrence in the Paragoethite process applied in zinc hydrometallurgy for the removal of iron from acidic sulphate solutions. In this process, ferrihydrite is the primary constituent of the precipitation residue, but silica also features heavily and is believed to influence both dewatering and the adsorption of ions from solution.

While some information is known regarding the physical interaction of ferrihydrite and silica when they are present as distinct phases, the process by which they simultaneously precipitate remains poorly understood. This thesis details investigations leading to a clearer understanding of this process and provides valuable insights into the factors influencing precipitate behaviour.

Ferrihydrite precipitates containing varying proportions of silica were prepared *via* continuous crystallisation, with the aim of achieving a simplified laboratory-based simulation of the reactions that occur within plant liquors during the Paragoethite process. Multiple anionic environments including sulphate (predominant anion in the Paragoethite process), nitrate (common in natural systems) and chloride were used to monitor the influence of anions on the co-precipitation reaction. Accurate control of the slurry pH and temperature were critical to this simulation, as was maintaining steady-state solution concentrations for iron and silicate. The latter was achieved by continuous addition of iron and silicate, with the corresponding continuous removal of reaction product slurry. Analysis focused on the removed slurry using advanced structural and morphological characterisation of the solid phases formed and quantification of solution species depletion. Reaction conditions were selected to favour the formation of ferrihydrite ensuring it was the dominant phase produced.

It was found that the presence of ferrihydrite increased both the rate and extent of silica removed by precipitation from solution. This phenomenon is based on surface adsorption and is hindered by the presence of ions that bind strongly with ferrihydrite. Ions such as sulphate compete with soluble silicate molecules for binding sites on the surface, whereas more weakly bound ions like nitrate do not

hinder the process. The level of interference was found to be dependent on available surface area, the affinity for the ion's adsorption and the concentration of both silicate and the ion in question.

Oligomeric and colloidal silica were shown to have a significantly different influence on ferrihydrite to that of monosilicic acid. While the crystallinity of ferrihydrite was seen to decrease when precipitated in the presence of monosilicic acid, no similar effect was observed in the presence of silica in a polymeric state. Although a greater proportion of silica was removed from solution when polymerisation had already progressed to a degree, it still imposed less influence on the product crystallinity. This observation underlines the importance of the adsorption-based process that combines the materials during co-precipitation.

X-ray scattering pair distribution function (PDF) analysis of the residue solids was instrumental in displaying correlations between declining ferrihydrite crystallinity and particle size. The data indicated that silicon atoms were not incorporated into the ferrihydrite crystal structure, but by inhibiting the growth of primary particles through surface adsorption, co-precipitated silica produced an apparent decrease in ferrihydrite crystallinity.

The analyses presented in this thesis were combined to derive proposed mechanisms of co-precipitate formation based on both the presence of monomeric silica and colloidal particles. When monomeric silica (silicic acid) is present ferrihydrite particles form initially followed closely by the adsorption of silicic acid monomers which restrict further growth. The adsorbed silicic acid molecules condense across the ferrihydrite surface and polymerise outward. Particles aggregate before much, if any, silica polymerisation has occurred, and the silica continues to polymerise of the surface of the aggregates. Where oligomeric or colloidal silica is present ferrihydrite particles are produced; there is little or no immediate silica adsorption and therefore the particles grow uninhibited. During aggregation the silica particles aggregate with the ferrihydrite, being incorporated both within and on the surface of the clusters. The results of this work provide the most detailed description of the reaction mechanism in ferrihydrite/silica co-precipitation, and the most thorough analysis of the structure of co-precipitates thus far reported.

Table of Contents

List of Figures

List of Tables

1. INTRODUCTION

A range of iron oxides are produced in association with precipitated silica across many natural and industrial systems (Cornell 1996; Jambor 1998). The common occurrence and association of these co-precipitated materials hold great importance in a wide variety of environments. The greatest degree of practical interest is in ferrihydrite, a metastable iron oxy-hydroxide phase, as well as schwertmannite, goethite and hematite, which will be further discussed in section 1.2.

The purpose of this research is to provide information on the pathways through which iron oxide / silica co-precipitates are formed, the properties of these materials and their effect on the system from which they're produced. The crystallisation process of iron oxides is central to this investigation, therefore a summary of crystallisation and precipitation theory is provided in section 1.1. The factors affecting the co-precipitation are of great importance and control of these will heavily govern the chosen experimental methods.

Iron oxides occur as a range of phases, all with differing stabilities, structures (often quite subtle) and properties. The phases formed depend on a variety of conditions as well as the presence of other materials. A great deal is known about many facets of iron oxide formation and the materials produced, which is reviewed in section 1.2. However, limited knowledge exists regarding the manner in which these phases associate with silica during their simultaneous formation. This study aims to elucidate some of the underlying processes that occur and their influence on the behaviour of the materials.

Silica or soluble silicates are present in such a large range of sands, soils and other minerals that there are few natural environments in which silicon in some form is totally absent (Iler 1979). Its consideration is therefore highly important in large number natural systems and the industries that obtain resources from these systems. Silica formation is a unique process in which the inorganic material is produced ***via*** polymerisation and displays many interesting properties (section 1.3). While similar to organic condensation polymerisation, it should not be confused as the same

reaction. Silicon-containing species influence a wide variety of chemical behaviours, some of which is discussed in section 1.3.

While there has been significant research into composites of silica and iron oxide, however co-precipitates have attracted less examination. Co-precipitation (the simultaneous precipitation of multiple species as a composite) is the common formation reaction for associated silica/ferrihydrite materials in both natural and industrial systems. When produced in this manner, the materials display different behaviour and properties to composites which are simply a combination of two or more distinct phases. During co-precipitation the species interact, influencing the formation and properties of each other. Discussion in section 1.4 is devoted to the formation, characterisation and properties of such materials.

The industrial relevance of this examination of iron and silicon co-precipitation is widespread, with particular relevance to hydrometallurgical processing of ores to recover low level valuable elements from gangue mineral phases. The specific impetus for this research has been the need to better understand the Paragoethite process, which is designed to precipitate iron from zinc-rich leach solutions prior to electrowinning to form the metal. Iron is removed ***via*** a precipitation step with a significant proportion of silicate present. Iron is precipitated by increasing the pH with the addition of calcine, which is primarily zinc oxide. The increase in hydroxide concentration creates supersaturation with respect to iron(III) hydroxide, inducing the precipitation of multiple iron oxide/hydroxide/oxyhydroxide phases, the principal phase of which is ferrihydrite. The process and possible implications of the co-precipitation reaction are discussed in section 1.5.

1.1. Crystallisation

Crystallisation is the process of deposition of a solid crystalline phase from liquid or gaseous materials (Mullin 1972). This process is closely related to precipitation and the terms are often used interchangeably, but they are technically distinct from each other. Precipitation does not necessarily form a crystalline product; it describes the formation of any solid from a liquid or another solid ***via*** a chemical reaction (Walton 1967). Therefore many processes fall under both categories. Crystallisation occurs ***via*** a three-step process, which begins with the achievement of supersaturation, followed by nucleation and ends with crystal growth.

1.1.1. Saturation

Saturation with respect to a given material is the state in which a solution of that material and its solid phase are in equilibrium (Mullin 1993). Solutions are said to be supersaturated or undersaturated if they contain more or less solute, respectively, than at the equilibrium point. When a system is in one of these states, saturation is generally reached either by precipitation/crystallisation from a supersaturated solution, or dissolution into an undersaturated solution. Supersaturation is the driving force behind crystallisation. However, supersaturation alone is unable to induce the phenomenon (Miers 1927). Supersaturated solutions can be stable when prepared without contamination in clean containers, in a dust-free environment and without rapid changes in temperature.

A supersaturated state can be achieved by several methods - altering the temperature, evaporation of the solvent or an absence of material that may aid or induce nucleation (dust, seed particles etc.). Supersaturation is commonly expressed by three quantities, namely the concentration driving force (Δc), supersaturation (S), and relative supersaturation ( ) which are defined in Equation 1.1, Equation 1.2 and Equation 1.3, respectively.

Equation 1.1: $$\Delta \boldsymbol{c} = \boldsymbol{c} - \boldsymbol{c}^*$$

Equation 1.2: $$S = \frac{c}{c^*}$$

Equation 1.3: $$= \frac{\Delta c}{c} = S - 1$$

c is the solution concentration and c* is the equilibrium saturation (Mullin 1972).

Determination of saturation is simple in theory, as the concentration of a given material in solution can be measured once equilibrium is reached. However, obtaining a true equilibrium, extracting supernatant samples devoid of fine dispersed particles and correctly identifying the solid phase can all be difficult to achieve in practice. The difficulty in obtaining a true equilibrium and the problems imposed by impure systems are often the cause of disagreement and disparities between solubility measurements. A wide range of techniques for measuring solubility and thereby saturation have been reviewed by Zimmerman (Zimmerman 1952). Problems associated with solubility measurements in respect to silica will be discussed further in section 1.3.2.

Solubilities are complicated by impurities. The greater the level of impurities in the system, the less accurate the equilibrium point will be. This is due to both soluble and insoluble materials having chemical and physical influences on the solubility of the species of focus. Other than having no effect (which while possible, is rare), there are three scenarios that can occur upon the introduction of soluble impurities (Hildebrand 1950; Lewin 1960):

- The impurity and the solute can react, forming a complex or compound affecting the behaviour of the system.
- The impurity causes the solution to be undersaturated, known as “salting out”.
- The impurity causes the solution to be supersaturated, known as “salting in”.

There are several potential causes for these scenarios, such as the common ion effect, and the influence of water impurity on hydrophobic species (Valdeavella 1994;

Rivera-Rubero 2004). They can result from the type or the proportion of the impurity present. The influence of insoluble impurities is often linked with the energy required for nucleation and is discussed in the next section.

1.1.2. Nucleation

Nucleation can occur spontaneously (homogeneous) or be instigated by other factors (heterogeneous) (Mullin 1993). The latter process is known as secondary nucleation, in which particles form due to the presence of pre-existing crystals. As mentioned above, a system will remain supersaturated if the energy barrier to form nuclei can not be overcome. The nucleation process is difficult to analyse and therefore to define. Due to the extremely low probability of several molecules all arriving at the same point and colliding with each other simultaneously, it is far more likely that metastable particles of a few units occur due to free-molecule collisions. If further molecules collide with these oligomers, the particles grow. If a collision does not occur rapidly after formation, the species redissolve into their original forms. This process should eventually yield particles large enough to be considered stable.

The structure of nuclei is also difficult to determine, as problems arise in observing such a small and dynamic event directly. They may contain randomly distributed molecules or be a diminutive version of a complete crystal containing order and local bonding similar to that present in the bulk material. However, the event has been defined as the aggregation of a freely moving group of molecules into a state that restricts movement and is associated with a release of energy (Gibbs 1928; Volmer 1939). The energy related to the formation of a stable nucleus is a combination of the energy released in forming the bulk of the particle and that required to produce the surface. Based on this and the radius of the particle required to be stable, it can be shown that the energy required to form the nucleus tends towards infinity as the concentration tends towards the equilibrium saturation. This means that stable nuclei will not spontaneously form in a saturated solution. Homogeneous nucleation generally requires supersaturation considerably higher than the saturation level (Buckley 1952).

The critical radius for a particle is the point at which it will be stable and is dependent on the associated free energy, somewhat the reverse of the influence of energy involved in its formation. The energy release resulting from the destruction of the surface favours dissolution, while that required to disassemble the bulk particle opposes it. Therefore, a relationship between surface area and volume determines the size requirement for a stable particle.

In many cases, the energy required to form a particle is greater than the average energy of the system, suggesting nucleation will not occur spontaneously. However, the average energy of the system does not necessarily mean that the entire system is at the same energy, just that the average of the distribution of energies throughout the system equates to that value (Mullin 1972). It is common to have localised areas of higher and lower energy, and it is in the areas of highest energy that nucleation is most likely to occur.

Impurities can strongly influence the nucleation rate even at trace levels (Mason 1957). They also do not necessarily have the same impact on all systems; a nucleation inhibitor in one solution may have no effect or actually induce nucleation in another. Purely spontaneous nucleation is rare, as even filtered solutions tend to carry a significant proportion of minuscule solid particles or heteronuclei and larger systems are more susceptible to contamination.

Atmospheric dust is the most common solid impurity. It can even contain particles of the product itself where samples have been handled. Often it is inert particles in the dust that influence the rate. Seeds such as silica and powered glass are intentionally added in many systems to induce nucleation (Mason 1957). Generally, the most effective seed material is the intended product, as no nucleation event is required. However, other materials have been shown to be very effective in inducing nucleation, such as phosphates nucleating arsenates or silver iodide nucleating rain particles (Mullin 1972). It is proposed that foreign materials can have this effect due to surface charge (Edwards 1962), porosity or similar crystal lattices.

The effect of cavities in foreign bodies or the walls of the container has been proposed and investigated as a cause of nucleation (Turnbull 1950). The capture of

an embryo (large molecule or small oligomer) in a cavity provides stability where it would otherwise be unstable in free solution. The embryo grows, filling the cavity which then acts as a nucleus. The dimensions of the cavity are important for the process, and different cavities may suit different systems (Turnbull 1950). An example of this is the silver mirror test in which silver is precipitated (Vogel 1996). If the precipitate is not readily obtained, scratching the inside of the test tube can induce its formation.

Similarity in the crystal lattice is important in the stability of a captured embryo (Turnbull). The structure of the forming nucleus can be strained into a slightly different arrangement to accommodate that of the material. Therefore the degree of mismatch of the two structures will determine the stability of the particle, based on the energy associated with the structural defects formed by lattice rearrangement. Where the particle can undergo enough strain to match the lattice of the material containing the cavity, it is said to be coherent.

1.1.3. Crystal Growth

The nucleation step ends with the formation of a stable nucleus, and at this point crystal growth occurs. The three general theories describing crystal growth focus either on surface energy, the adsorption layer or diffusion (Wells 1946). Surface energy theories involve the shape of the growing crystal being related to the lowest possible surface energy. Therefore a particle growing in a supersaturated medium should display growth of faces that would provide the crystal with the lowest possible energy. While these pose a useful starting block, they do not provide an explanation of supersaturation and solution movement effects on crystal growth.

The adsorption layer theory proposes that crystal growth occurs ***via*** the adsorption of layers of solute molecules on the crystal face. It is suggested that atoms or molecules of the crystallising material form a weakly adsorbed layer that is free to move about the surface of the crystal face, as opposed to being immediately integrated into the crystal (Volmer 1939). This layer is in equilibrium with the bulk solution. The formation of a two dimensional nucleus on the crystal surface is required for each

subsequent layer. Later models describe imperfections in the process, such as multiple layers forming before the previous layer is complete, vacancies appearing within the forming layers and loosely adsorbed single units (Volmer 1939).

Diffusion theory states that crystal growth is the reverse of dissolution and is governed by the difference in concentration at the solid surface and in the bulk solution (Noyes 1897). It is assumed that a stagnant film is present, through which units have to diffuse. However, at high agitation this film would be almost non-existent, increasing the theoretical growth rate to impossible levels. The theory was modified to a two-step process in which molecules are diffused from the bulk of solution to the crystal surface, followed by rearrangement into the crystal lattice (Berthoud 1912).

Ostwald ripening is a very common process in which small particles are redissolved into solution and the redispersed units bind to larger particles. This greatly increases general particle size and is more commonly mentioned in conjunction with precipitation. This process lowers the free energy of the system by lowering the overall surface area. It is driven by the different solubility “pressure” applied to different sized particles (Walton 1967).

Under favourable conditions stable particles undergo an aggregation process, which can occur well after nucleation and particle growth or simultaneously, depending on the kinetics of the system.

1.1.4. Aggregation

1.1.4.1. Particle-Particle Interaction

Aggregation is described as the process by which dispersed particles bind together due to attractive forces to form characteristic structures (Jullien 1987). Colloids are small particles (often in the order of nanometres) suspended in solution. These are generally stable due to their electrostatic surface charge, which overcomes the

attractive Van der Waals forces. It is when the repulsive force due to the surface charge is negated that the particles will aggregate. This often occurs in solutions containing significant concentrations of electrolytes or large neutral molecules, which are attracted to the surfaces of oppositely charged particles. These species shield the electrostatic force.

In the case of complete shielding, there is no significant repulsive force, therefore when the particles diffuse closely enough together they are attracted by Van der Waals forces and bind together (Jullien 1987). Aggregation can take place between multiple single particles, particles and small aggregates or multiple small aggregates. If only partial shielding is achieved, the energy of the particles (velocity provided by thermal or physical agitation) must be great enough to overcome the residual repulsive force. This generally requires more collisions for success, which creates a slower reaction rate than in the case of complete shielding. The aggregates formed at slower rates tend to be more compact, whereas rapidly formed aggregates tend to be more sparsely arranged (Jullien 1987).

Aggregation is a physical process and strongly influences the physical properties of ferrihydrite, for which the primary particles are less than 10 nm in size and form aggregates containing hundreds or even thousands of particles (Cornell 1996).

1.1.4.2. Fractals

Fractal theory has been applied to aggregates, particularly colloidal aggregates, in an attempt to describe and measure their otherwise non-Euclidean nature (Meakin 1988). It is concerned with symmetry through varying length scales, with objects appearing the same (approximately) at different magnifications. The simplest form of a fractal is perfectly self-similar, in that it does not vary under isotropic contraction or expansion. This means that no matter what factor of the length scale is viewed, the object is perfectly similar, as seen in Figure 1.1. The stages through which the fractal is formed involve the addition of multiple units of the previous stage. The initial cross of five particles (fig 1.2a) is added to four other crosses to form a larger cross (fig 1.2b), which is subsequently added to four similar crosses to make one that is

larger still (fig 1.2c). This can be carried through an infinite number of iterations, creating an infinitely large structure, or can be taken at extremely small length scales by replacing each disc with five smaller discs in the cross arrangement (Meakin 1988). Of course, in the case of aggregates one can't simply exchange particles for infinitely smaller but otherwise identical particles.

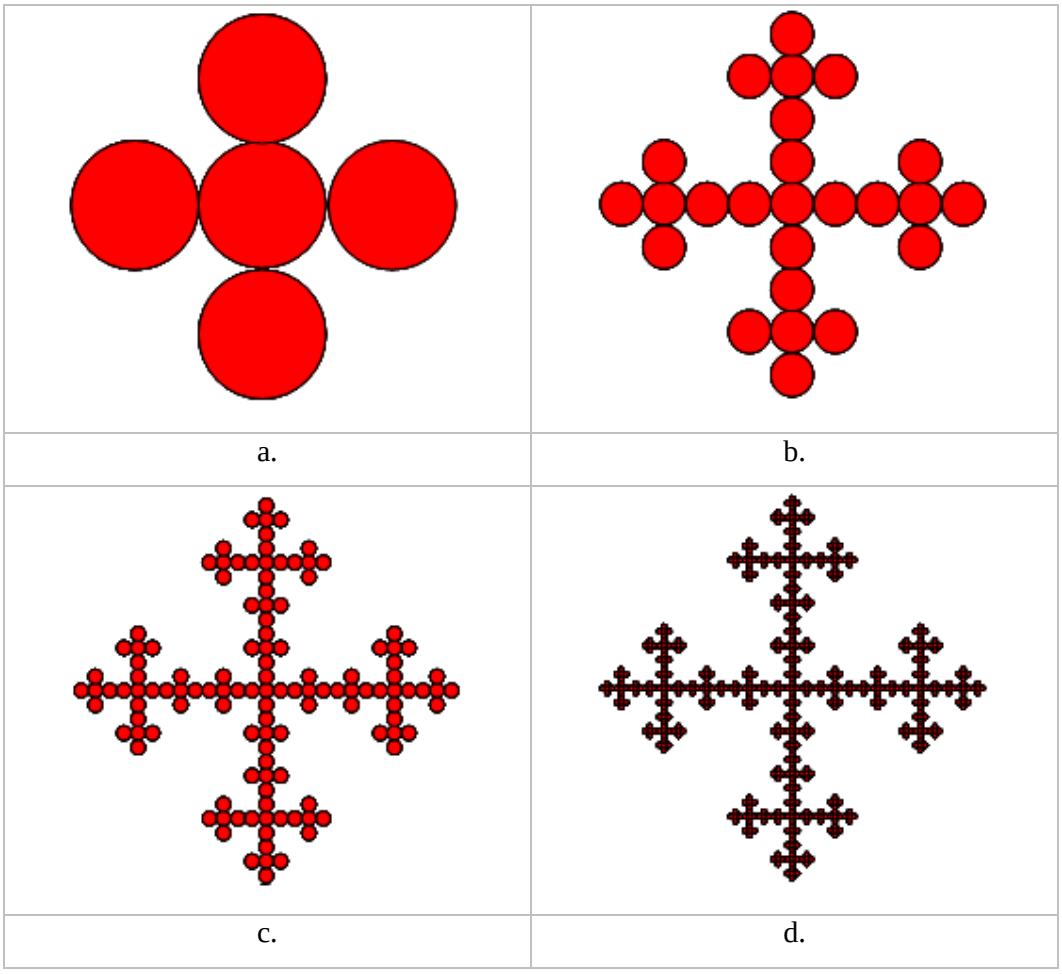

Figure 1.1: The stages of growth of a simple fractal model adapted from (Meakin 1988).

This kind of symmetry is rarely, if ever achieved with aggregates in real systems, but self-similar geometry is still effective in describing their structures. The extent of fractal scaling is limited at the lower end by the particle size and at the upper end by the dimensions of the aggregate, as the tenuous structures are subject to shear and thermal forces which may force them to collapse or break.

For the purposes of this investigation, the fractal dimension refers to the relationship between the mass and volume of the particles. This relationship can be considered as a density in suspension of the aggregates, which is governed by how compactly the particles have bound together. It is indicative of strong binding forces and symmetry within the aggregate, and a high fractal dimension often signifies a more stable aggregate. Equation 1.4 and Equation 1.5 below provide further definition:

Equation 1.4: $$\boldsymbol{M} \propto \boldsymbol{L}^{\boldsymbol{D}}$$

Equation 1.5: $$(\boldsymbol{r}) = \left[\frac{\boldsymbol{MD}}{4\ \boldsymbol{R}^{\boldsymbol{D}}} \right] \boldsymbol{r}^{\boldsymbol{D}-3}$$

Where $\boldsymbol{M}$ is the aggregate mass, $\boldsymbol{L}$ is length, $\boldsymbol{D}$ is the fractal dimension (which must fall in the range $1 \leq \boldsymbol{D} \leq 3$), is the density, $\boldsymbol{r}$ is the sphere radius, and $\boldsymbol{R}$ is a given length with in the aggregate (where $\boldsymbol{R} < \boldsymbol{r}$, $(\boldsymbol{r}) = 0$).

1.1.4.3. Cluster-Cluster Aggregation

There are several models for the aggregation process, based on lattices and particles having random approaches and motion until reaching a nearest neighbour position in the lattice, at which point they are irreversibly connected (Jullien 1987; Meakin 1988). These are based on the premise of a seed particle which is then built upon by a series of particles binding to it and the growing aggregate one by one. This generally renders the initial particle and growing aggregate to be stationary and the free particles to be in motion. However, this produces much higher fractal dimensions (discussed in section 1.1.5) than are typically measured experimentally (Meakin 1988). The overestimation has been overcome with the introduction of cluster-cluster aggregation, in which the aggregates have motion and can interact with other forming aggregates, producing a single, larger cluster (Jullien 1987; Meakin 1988; Adachi 1998).

Cluster-cluster theory assumes a greater level of interpenetration by a single particle into the structure of the cluster than would occur between clusters interacting with

each other, as there would not be interference by the size and shape of the incident particle. As seen in Figure 1.2, the interaction of 2 clusters as opposed to a cluster and single particle creates the more open structure containing far more free space. The fractal dimension obtained from this treatment of the system is very similar to that obtained experimentally, overcoming problem associated with previous models. The integration of cluster-cluster interactions into the models has provided much more accurate descriptions of real aggregates. Computer simulations provide a great deal of information as physical observation is impaired due to the inability to control, and difficulty in monitoring, the chaotic and often extremely rapid process of aggregation.

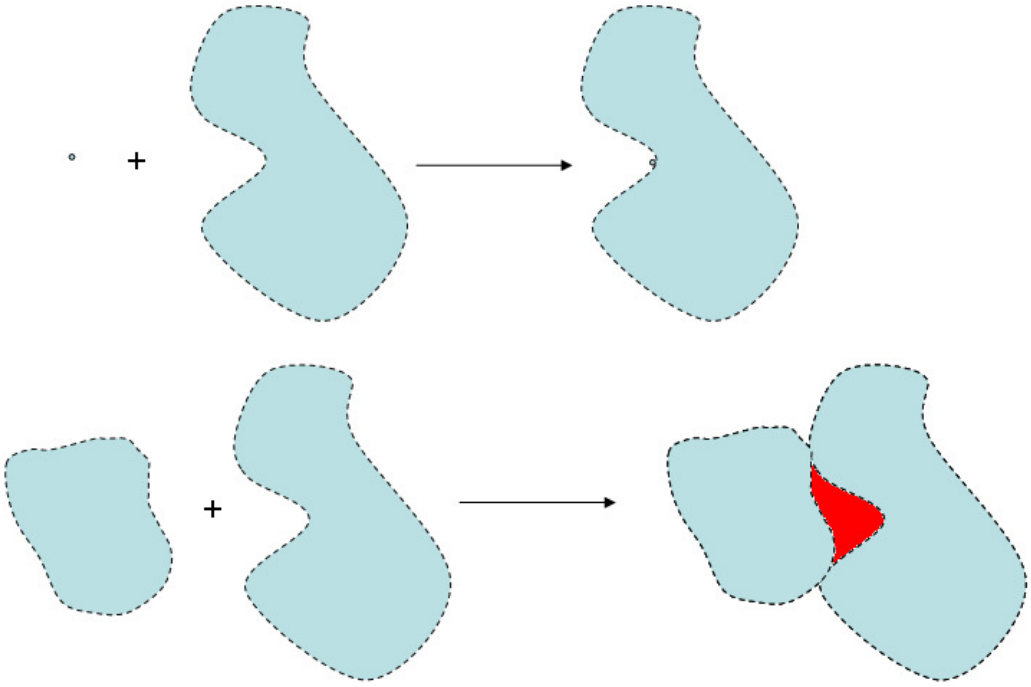

Figure 1.2: Depiction of interactions between a particle and an aggregate (top) and between two aggregates (bottom). The section highlighted in red shows the space created in the interaction between the aggregates that the particle could easily penetrate.

1.2. Iron and Iron Oxides

Iron oxides occur in a wide variety of phases; those that are relevant to this study are listed in table 1.1 along with some related quantities. While ferrihydrite is the principal phase of interest to this research, schwertmannite, goethite and hematite are often produced in conjunction with ferrihydrite. It is therefore necessary to discuss all four materials.

Table 1.1: Structure and properties of the phases relevant to this study.

	Ferrihydrite	Schwertmannite	Goethite	Hematite
Chemical Formula	$5Fe_2O_3.9H_2O$	$Fe_8O_8(OH)_6SO_4$	-FeOOH	$-Fe_2O_3$
Crystal Structure	Hexagonal*	Tetragonal	Orthorhombic	Trigonal
Cell Dimensions (nm)	a = 0.508* b = 0.94*	a = 1.066 b = 0.604	a = 0.4608 b = 0.9956 c = 0.30215	a = 0.50340 b = 1.3752
Principle Morphology	Spheres / hexagonal	Hedgehogs – core, needles	Acicular – needles / laths	Hexagonal prisms, plates
Density (g cm^{-3})	3.96	-	4.26	5.26
Colour	Dark reddish brown	Reddish yellow	Brownish-reddish yellow	Red
Type of Magnetism	Speromagnetic	-	Antiferromagnetic	Antiferromagnetic
Solubility Product (pFe + 3 pOH)	37-39.4	-	43.3-44	42.2-43.3
Surface Area (m^2g^{-1})	100-400	125-320	8-200	2-90
Iso-electric Point (IEP)	7.8, 8.1**	-	7.5-9.38	7.5-9.48

Adapted from Cornell and Schwertmann (Cornell 1996; Schwertmann 2000). * Based on structure proposed by Michel et al. (Michel 2007), ** (Kinniburgh 1975).

1.2.1. Occurrence and Applications

Iron is the third most abundant cationic element in the lithosphere (earth's crust) behind silicon and aluminium (Cornell 1996). As a result of this, it appears in a wide range of natural systems and will be found, at least in trace concentrations, in all rock

systems. Through the erosion of iron-containing rocks into soil or dissolution and precipitation from aqueous bodies, iron is cycled through the environment. It is present in systems such as magmatic and metamorphic rocks, as well as sediments and sedimentary rocks. Metamorphic rocks contain magnetite and ilmenite, whereas the phases of interest here are found in the sedimentary species. This covers older geological environments, such as red beds, ores, ferricretes, and bauxites, as well as more recent formation in systems including terrestrial surfaces, aquatic environments (oceans, lakes, streams, springs, etc.), and the Martian surface (Jambor 1998).

Hematite and goethite are found in deeper deposits and those of greater age due to their relative stability, as meta-stable intermediate phases such as ferrihydrite transform to more stable species over time, when buried or at increased temperature (Blesa 1989; Jambor 1998). Hematite is the most thermodynamically stable phase, whereas goethite is technically meta-stable but is far more stable than ferrihydrite. Goethite does not transform as easily, generally requiring high temperatures to induce the transition. Their formation is also favoured under highly basic or acidic conditions, slow reaction rates and exceedingly high or low temperatures. Other phases such as akaganeite are produced in the presence of certain ions (chloride for akaganeite (Kauffman 1975) and sulphate for schwertmannite (Bigham 1994)). Ferrihydrite and schwertmannite tend to exist in recent environments at the surface and in dynamic systems involving the redistribution of species, such as bodies of water.

Also common is the occurrence of iron products in a plethora of industrial environments, including those resulting from acid mine drainage, water treatment and iron smelting. They are often an unwanted by-product; iron is common in Cu, Ni, Zn, Pb, Al, Mn, and Ti bearing ores and as such must be removed during processing (Dutrizac 1987). Not only is removal an issue but in many cases the iron species detrimentally affect processes such as metal refining, ***via*** contamination of the product, complication of solid-liquid separation or adsorption/substitution of a desired species (Loan 2004; Loan 2006). In water treatment, metal oxides (predominantly ferrihydrite and silica) have hampered operations by clogging pipes and reverse osmosis filters(Sheikholeslami 2002). However, its presence is not totally negative; many iron oxides have very high surface areas and adsorb trace

impurities from solution. An example of this is the propensity of ferrihydrite to adsorb arsenic from solution.

Iron oxides have been used as colourants for millennia for artwork and decoration (Cornell 1996). Primitive man used ochre deposits for drawings and as humans evolved these materials decorated pottery and ceramics and were used in murals. Iron oxides are still used as pigments and in recent times have been the second most prolific pigment in the industry behind TiO_2. Iron oxides are used as precursors to ferrites which are produced for ceramic permanent magnets, anti-forgery devices and "hot sources" for tumour treatment. A range of catalysts can be produced from iron oxides or even the phases themselves, as they have a high surface area. The production of abrasives, sulfate-resistant cement and ferrofluids, along with thermite welding and water treatment are some of the many applications of iron oxides. By far the greatest use of iron oxides is for smelting to create iron or steel.

1.2.2. Formation

The varieties of iron oxides, while diverse, share many similarities. Slight variations in conditions will favour one phase over another, and it is common for multiple phases to be produced in a single system. This can occur through the simultaneous formation of species or ***via*** the transformation of metastable phases to other, more stable minerals. There is interplay between phases and transformations occur under different conditions.

1.2.2.1. Ferrihydrite

The hydrolysis reaction through which many iron oxides are formed is included within this section. This is because ferrihydrite is often the first phase formed, is a precursor to other phases and is the principal material of interest in this study. Fe^{III} oxides are produced during the hydrolysis of Fe(III), or oxidation and subsequent hydrolysis of Fe(II) (Cornell 1996; Schwertmann 2000). The rate of precipitation from divalent iron is dependent on both oxidation and hydrolysis steps. The

oxidation step occurs ***via*** Equation 1.6, the rate of which is dependent on many different quantities.

Equation 1.6: $$2Fe^{2+} + 3H_2O + \frac{1}{2}O_2 \rightarrow 2FeOOH + 4H^+$$

The rate increases a hundredfold with each pH unit, increases tenfold with every 15 °C but decreases with greater ionic strength. It is accelerated in the presence of F^-, $H_2PO_4^-$ and HPO_4^{2-} but retarded by ClO_4^-, NO_3^-, Cl^-, $H_3SiO_4^-$, Br^-, I^-, and SO_4^{2-}. The rate increases with small amounts of some cations but generally decreases in the presence of naturally occurring organic ligands.

This study relates only to trivalent iron hydrolysis, and therefore the divalent iron process will not be considered further. For trivalent iron, hydrolysis leads to the formation of a range of iron oxide/hydroxide species, depending on reaction conditions. It proceeds by deprotonation of the hexa-aquo iron solution species (Equation 1.7) (Cornell 1996).

Equation 1.7: $$\boldsymbol{Fe(H_2O)_6^{3+}} \rightarrow \boldsymbol{FeOOH} + 3\boldsymbol{H^+} + 4\boldsymbol{H_2O}$$

As the protons are removed from the ions, dimers and higher order oligomers are formed ***via*** olation and oxolation (formation of hydroxide and oxygen bridges, respectively). A fully deprotonated ion will form an iron oxide or oxyhydroxide.

The hydrolysis rate is governed predominantly by the pH; the greater the OH/Fe ratio, the faster the reaction. The crystallinity of the ferrihydrite produced is dependent on the hydrolysis rate, forming less crystalline material as the rate is elevated. The differences between the phases, ranging from 6-line (most crystalline) to 2-line (least crystalline) ferrihydrite, are outlined in section 1.2.3.1. At high pH the iron(III)-aquo molecules are deprotonated and polymerise very rapidly in a somewhat chaotic manner. However, at lower pH the polymerisation process occurs more systematically, forming larger growth units between iron in solution and ferrihydrite (Flynn Jr. 1984; Blesa 1989; Combes 1989; Lewis 1989; Rose 1997).

Mulit-unit pre-cursor species appear during the nucleation of iron oxides. Schwertmann et al. observed intermediates in the formation of akaganeite; trimers were identified which combined to form the Cl-templated tunnel structure (Schwertmann 1999). The tunnels consisted of double chains of octahedra surrounding anions. From this, the concept of an intermediate containing 24 iron atoms was formulated. A similar species has been proposed to exist during the slow hydrolysis reaction in the presence of nitrate and sulfate (Schwertmann 1996; Schwertmann 1999). These species have been likened to a defect akaganeite structure, in which the oxyanions template the formations of tunnels. These are known as Fe(III) oxyhydroxy salts and some investigations have been conducted to determine whether the same effect occurs in the presence of other anionic species (Hockridge 2009).

However, no further research has been published containing evidence of intermediate nitrate-templated oligomeric units. Therefore, while it has not been conclusively proven that such intermediates do not occur, there is little supporting evidence, nor is there a suggestion of how these defect akaganeite structures then rearrange to form ferrihydrite. Also, there is evidence that schwertmannite is not a defect akaganeite structure with tunnels surrounding sulfate ions (Hockridge 2009), which therefore questions the formation of the Fe(III) oxyhydroxy sulfate intermediate (the proposed precursor for schwertmannite). The contention regarding the structure of schwertmannite and a related possibility for the oxyhydroxy salts is discussed in section 1.2.2.2.

Oligomeric units (be they small polymers or the aforementioned intermediates) coalesce to form the solid ferrihydrite. At relatively low pH values or under forced hydrolysis, the particle size is larger and 6-line ferrihydrite is the predominant product. Not only is the nucleation and growth of oligomers a rapid reaction step, but aggregation also occurs extremely fast. This gives rise to the large spectrum of aggregate sizes achievable and the randomness of morphology. The phase precipitated has also been shown to be influenced by the presence of soluble silicates. Schwertmann et al. produced a series of ferrihydrites with declining crystallinity by adding progressively more silicate to the reaction of oxidising $FeCl_2$ to the point of producing 2-line ferrihydrite (Schwertmann 2004). A similar effect

has been noted in natural and synthetic samples when precipitated with humic substances (Schwertmann 2005).

1.2.2.2. Schwertmannite

Schwertmannite is similar to ferrihydrite, and they often form in tandem. Claassen (Claassen 2007) has shown that slower hydrolysis rates at low pH and/or supersaturation favour schwertmannite formation over ferrihydrite. This phase is only formed in sulfate-containing media and requires a threshold concentration of the anion to be present. The proposed intermediate for this species is the Fe(III)-oxyhydroxy sulfate, which forms in the distorted akaganeite structure with tunnels templated by sulfate ions (Schwertmann 1999). Schwertmannite resembles ferrihydrite in many of its spectra, with the most notable difference being in terms of aggregate morphology (Loan 2004). Conditions that favour ferrihydrite precipitation will also favour the formation of schwertmannite.

Schwertmannite can be synthesised in other manners that produce a more pure sample (Schwertmann 2000; Loan 2005; Claassen 2007); although a separate ferrihydrite phase may still be present, it will only be as a minor constituent. When an Fe(III) bearing solution that contains a significant amount of sulfate ions is heated for approximately 15 minutes, the product displays the characteristic schwertmannite morphology and diffraction pattern (Loan 2004).

The formation of schwertmannite and even its declaration as a distinct mineral are points of contention. Recent studies have provided evidence that schwertmannite is a combination of ferrihydrite and nanocrystalline goethite (Hockridge 2009). It has been proposed that the formation mechanism involves the generation of ferrihydrite aggregates in the early stages of precipitation. The subsequent formation of the needles that create the characteristic hedgehog morphology is then believed to be the consequence of the aggregation of nanoscale goethite particles. If the reaction continues well beyond the 15 minutes mentioned above, larger goethite particles are produced and goethite peaks begin appearing in the XRD pattern. This will be discussed further in section 1.2.3.2.

1.2.2.3. Goethite and Hematite

Goethite is one of the most stable iron oxyhydroxides. It is formed both ***via*** direct crystallisation and as a result of the transformation of meta-stable intermediate phases, such as ferrihydrite and schwertmannite (Cornell 1996). It is often formed in combination with hematite, but can be generated in a pure form under favourable conditions. Meta-stable phases such as ferrihydrite are kinetically favoured once the pH (or OH/Fe ratio, depending on how it is described) reaches a critical value. At low pH, where full hydrolysis is not achieved, monomeric and perhaps dimeric species exist but do not polymerise further. Where these species are in great enough concentration (supersaturation with respect to FeOOH) they may combine to form microcrystalline phases. This occurs in areas of high iron concentration and low pH.

While there is evidence that hematite can nucleate directly from solution, the vast majority of preparation techniques involve the formation and subsequent transformation of ferrihydrite. It is also often formed through the thermal dehydration of many iron oxyhydroxides.

Once ferrihydrite is formed, it can transform to more crystalline phases over time if not stabilised. This transformation will only occur in solution or at high temperature. Conversion ***via*** solution has been recorded at relatively low temperature (4 °C) but the rate of transformation is bolstered by elevated temperature, as well as suitable pH conditions. Transformation to hematite can occur in the solid state at high temperature or in slurry, facilitated by the structural similarities between the phases. While the end product is always hematite, some literature states that 2-line ferrihydrite goes through a maghemite intermediate, whereas 6-line transforms directly to hematite (Mazzetti 2002). This has been explained by the apparent structural difference between the 2- and 6-line phases, but as will be mentioned in latter sections, this is a point of contention.

EXAFS research by Combes et al. (Combes 1989) showed that face-sharing between octahedra increases during the transformation, which is followed by vacancy

redistribution and dehydration. Hydroxyl groups and protons from other ligands are lost, expelling water, while oxo bridges are formed. The potential charge imbalance is negated by rearrangement of the iron atoms. It has been shown that transformation begins with denser areas forming in the ferrihydrite particles which act as nucleation events for hematite growth, eventually converting the entire particle. Therefore the size of the hematite particle formed is related to the size of the initial ferrihydrite aggregate.

The transformation to goethite only occurs in solution and is a dissolution/re-precipitation process. Unlike hematite, the goethite structure requires greater mobility of elements than is available in the solid state, even at high temperatures (Cornell 1996). Ferrihydrite is dissolved, followed by the nucleation and growth of goethite particles from predominantly monomeric iron hydroxide ions. The rate of transformation increases greatly with pH until the latter reaches ~12, at which point the rate plateaus then decreases above 13. This is due to the saturation of the ferrihydrite surface with OH^- groups, as well as the inhibition of goethite nucleation and growth at extremely high pH.

The amounts of hematite and goethite produced from transformed ferrihydrite depend on conditions and the presence of other species (Cornell 1996). The temperature at which ferrihydrite is precipitated influences the phase it transforms to; a greater precipitation temperature favours hematite as a transformation product. The pH effect is related to dissolution and aggregation of ferrihydrite, with hematite favoured around pH 7 – 8 where solubility is low and aggregation is at its peak, given the proximity to the iso-electric point (pH at which a zero mean zeta potential exists). In contrast, increased solubility and surface charge in the pH regions around 4 and 12 favours the formation of goethite, supplying a large number of growth units. Hematite is again favoured beyond these zones. Increased ionic strength and increased ferrihydrite concentration are also conditions that aid aggregation, which all favour the formation of hematite.

Investigations have also been conducted into the presence of soluble species on the transformation process (Blesa 1989; Loan 2005; Jones 2009). Species investigated include carboxylic and hydrocarboxylic acids, sugars, glycerol, silicate, phosphate,

humic/fulvic acids, reducing organic ligands, Al, Ti, Mn, Cr, V, Ni, Co, Zn and Cu (See table 13.3 in Cornell (Cornell 1996)). Research into the effects of silicate and zinc is the most relevant to this work; the former is discussed in section 1.3. Cations are required to be at much greater levels than ligands before a significant effect is observed, but act over a much wider pH range and can be incorporated into the iron oxide structure.

Aside from manganese and iron, the divalent, first row transition metals also retard ferrihydrite transformation and of these, zinc has the greatest effect. There is no clear trend or explanation to be gained from examination of the magnitude by which each element stabilises ferrihydrite. While there is a possible ordering relationship with covalency, zinc does not fit the sequence (Cornell 1996; Sheikholeslami 2002). The presence of zinc also favours the formation of hematite over goethite in the transformation (Cornell 1996). As the proportion of zinc increases the products change. At Zn / (Fe + Zn) = 0.09, a mixture of goethite and hematite is produced, while at Zn / (Fe + Zn) = 0.18, there is a mixture of hematite and the spinel phase $ZnFe_2O_4$, and finally at 0.33 the spinel phase alone is formed. The spinel phase is believed to nucleate in close proximity to the ferrihydrite surface in adsorbed or adjacent water layers. Like goethite, the transformation continues ***via*** dissolution of the metal incorporated in ferrihydrite and deposition of Zn-Fe-hydroxo complexes.

1.2.3. Structure and Characterisation

Given that many of the iron oxides share similar chemical compositions and iron oxidation states, it comes as no surprise that a large proportion of them exhibit some structural similarities. While many commonalities do exist, they all have discrete structures and for the most part can be distinguished ***via*** techniques such as XRD. Difficulties can arise in systems containing poorly crystalline material and/or complex matrices comprised of numerous phases.

1.2.3.1. Ferrihydrite

Ferrihydrite is a nanocrystalline iron oxy-hydroxide with the generally accepted chemical formula of $5Fe_2O_3.9H_2O$. The nanoscale particles lead to extremely small coherent scattering domains and therefore create a great deal of difficulty in terms of characterising ferrihydrite samples (Jambor 1998). The broadness of the XRD peaks and low number of reflections make structural determination from this method very difficult. Both X-ray and electron diffraction produce the pattern of an amorphous material from which limited information can be extracted. Therefore, until the relatively recent emergence of improved technology, structural investigations of ferrihydrite were limited, and even the most recent data remain open to interpretation. As a consequence of this, no consensus has been reached as to a definitive structure for ferrihydrite.

Early models of the ferrihydrite structure based predominantly on XRD patterns alone gave significantly different results, highlighting the limitations of the data. Jambor and Dutrizac (Jambor 1998) discuss some of the iterations of ferrihydrite models that have been proposed. These include some suggesting a structure similar to hematite (Towe 1967), with others concluding the iron is tetrahedrally coordinated with oxygen and hydroxide atoms, where it is generally accepted to at least predominantly form octahedra (Brady 1968). None of these proposed structures have been widely accepted, displaying the difficulty of identifying the true structure.

While further evidence suggesting a significant proportion of the iron is tetrahedrally coordinated has been published (Eggleton 1988), other groups have discredited such arguments, insisting the conclusion was based on data that did not provide the required resolution, as well as observations which were irrelevant and possibly incorrect (Manceau 1990; Pankhurst 1992). These authors also responded with synchrotron X-ray absorption spectroscopy (XAS) data showing no evidence of iron tetrahedra. Extended X-ray absorption fine structure (EXAFS) data showed a high degree of similarity between ferrihydrite and hematite, suggesting octahedral coordination of iron.

The most widely accepted structural study is that by Drits et al. (Drits 1993), as it is commonly referenced as providing a proposed structure that most closely fits standard data and unlike most, it is yet to be conclusively disproved. This is one of many models proposing that ferrihydrite is composed of multiple structures. It suggests a combination of three structural components - defect-free ferrihydrite, defective ferrihydrite and poorly crystalline hematite. Electron nanodiffraction work by Janney et al. (Janney 2001) supports Drits' defect-free model, indicating it could account for more than 50% of the material. Neutron scattering by Jansen et al. (Jansen 2002) is also in agreement with the model proposed by Drits et al. (Drits 1993).

Michel et al. (Michel 2007) proposed a structure, based on pair distribution function (PDF) modelling of X-ray scattering data, composed of 20% tetrahedrally and 80% octahedrally co-ordinated iron. These are joined by corner and edge shared oxygen atoms. However, a comprehensive rebuttal article has been presented by Manceau (Manceau 2009), citing multiple reasons as to why this structural model is flawed. Manceau's evidence includes the fact that the model proposed by Michel et al. is defect-free, contains tetravalent octahedrons and tetrahedrons and Fe – O distances that violate Pauling's 2nd rule (Pauling 1929). It also doesn't explain data from XRD or EXAFS studies, and is not aligned with X-ray scattering and electron microscopy data (Rancourt 2008; Hiemstra 2009). This rebuttal has also reiterated support for Drits' model, suggesting it remains as the best all-round model for the system based on any data acquired to date.

A point of interest that has been mentioned in the literature, generally in an offhand manner, is the asymmetry of the (110) peak in the diffraction pattern. It was raised in Jambor and Dutrizac's (Jambor 1998) review that there is a shift in this peak's position between 6-line and 2-line patterns. The asymmetry in the 6-line phase was suggested by Eggleton and Fitzpatrick (Eggleton 1988) to be due to the presence of some 2-line ferrihydrite in their 6-line sample. Several authors have noted the asymmetry in passing as a feature but not offered any explanation. Generally, an asymmetric peak is a sign of two adjacent peaks of different broadness overlapping to give the appearance of a single peak with greater incline on one side. However, the

published literature has yet to identify a source that has demonstrated this by separating or defining multiple peaks.

Another point of contention surrounding the structure of ferrihydrite is the difference between the 6–line and 2-line phases (and those that lie between). Some literature states that 2-line has a different structure to 6-line (Drits 1993; Janney 2000; Janney 2000; Janney 2001), while others suggest that the difference in X-ray response is due to the size of the coherent scattering domains (Michel 2007). Commonly known is the fact that a very small particle size has a detrimental effect on the crystallinity of a material (Hlavay 1977). The primary particle size of the most crystalline ferrihydrite phase has been shown to be below 10 nm (generally given as 6 – 8 nm), while 2-line is even smaller (accepted as 2 – 3 nm).

PDF studies by Michel et al. (Michel 2007) (similar to those from which they derived their structural model (Michel 2007)) display similar structures throughout spectra for samples of varying crystallinity. The signals attenuate at different points, governed by their average primary particle size (see section 4.4). The more crystalline material has greater long range order due to the larger primary particles and therefore provides coherent structural information at greater length scales. The exaggerated broadness and limited reflections seen in the 2-line spectrum is a result of the predominantly 2-3 nm particles, which limits any possible structural ordering.

1.2.3.2. Schwertmannite

Schwertmannite has been generally accepted as having a defect akaganeite structure containing tunnels formed by double chains of octahedra surrounding sulfate ions (Bigham 1994; Schwertmann 2000). It has been stated that the reason for the broadness of the schwertmannite XRD peaks and the absence of some peaks expected from akaganeite are due to the sharing of oxygen atoms between iron and sulphur (Cornell 1996). This differs from akaganeite, in which the chloride is said to be the template of the tunnel structure and stabilises it, but is not linked to iron in the structure ***via*** oxo-bridges, as is proposed for schwertmannite.

However, as mentioned in section 1.2.2.2, there is dispute as to whether this defect akaganeite structure exists in schwertmannite at all. Evidence has been presented that schwertmannite whiskers are made up of goethite nanocrystals that grow outward from a core consisting of an aggregate of ferrihydrite (Hockridge 2009).

1.2.4. Properties

Iron oxides form a large variety of particles and aggregates (Cornell 1996). Metastable, nanocrystalline phases such as ferrihydrite and schwertmannite form primary particles of generally less than 20 nm that aggregate very rapidly. Their aggregates are significantly different, in that ferrihydrite aggregates are completely randomly shaped, while schwertmannite aggregates form the characteristic hedge-hog morphology (Loan 2004). More crystalline materials such as goethite and hematite occur in much larger individual crystals, which under certain conditions will remain monodispersed. Goethite can be produced as nanoscale particles. However, these tend to aggregate and are able to combine to form single crystals if left in solution. As expected, the larger particles are generally denser and will settle from suspension faster than aggregates of small particles, due to structurally associated or encapsulated water. Settling and filtration problems are often encountered in suspensions of the mixed phases as the combinations of morphologies and particle sizes rapidly clog filters (Loan 2004).

Ferrihydrite in particular has been used as an adsorbent for both cationic and anionic species in a range of applications from water treatment to industrial purification techniques (Loan 2004; Sperlich 2005; Zeng 2008). It is useful for this purpose because of its very high surface area, quoted as being between 100 and 600 $m^2\ g^{-1}$ but more regularly between 200 and 300 $m^2\ g^{-1}$ (Carlson 1981; Lewis 1989; Schwertmann 2004). This is due to the microporosity formed during the aggregation of the nanoscale primary particles.

It also displays a strong affinity for the adsorption of many species, such as arsenate, sulfate, cadmium and lead (Swedlund 2003; Richmond 2004; Buekers 2008). The adsorption or presence of some species can reduce or improve the affinity for

adsorption of another. Competitive adsorption occurs in significant concentrations of two or more species that readily adsorb on a surface, and has been documented on multiple materials (Janusz 2003; Smith 2005; Luxton 2008). The presence of some ions can improve the adsorption of others ***via*** surface complexation, or surface charge passivation and reversal (Xue 1995; Swedlund 2001; Swedlund 2003).

More stable iron oxide phases such as goethite and hematite generally have smaller surface areas and thus adsorb smaller proportions of ionic constituents (Trivedi 2001; Buekers 2008). The greater capacity for adsorption and the ease of use of ferrihydrite or other "hydrous ferric oxides" make them the obvious selection for applications such as water treatment (Sperlich 2005). However, the affinity for adsorption is often comparable to more stable phases due to the similarity in the structure (depending on phases in question) and surface chemistry (Cornell 1996).

1.2.5. Interaction with Zinc

Ferrihydrite has been shown to adsorb zinc predominantly above pH 4.5 – 5. However, during co-precipitation of ferrihdyrite and zinc some uptake occurs at much lower values (Martin 2005). This is due to the incorporation of some zinc into the ferrihydrite aggregates as they form. The XRD pattern for the co-precipitate does not indicate structural change, as the reflections associated with both pure ferrihydrite and those containing zinc occur at the same angles.

Waychunas et al. (Waychunas 2002) have presented evidence that zinc adsorbed on ferrihydrite forms tetrahedra, but at ratios greater than Zn / (Zn + Fe) = 0.2 octahedral zinc precipitation occurs. This can occur at zinc concentrations below that of the saturation level of zinc hydroxide (Waychunas 2003).

Zinc adsorption onto ferrihydrite has been found to be governed by pH, temperature and sorbate/sorbent ratios (Trivedi 2004). Zinc was observed at lower sorption densities at higher pH levels, and the zinc uptake also greatly decreased (3-4 orders of magnitude) with a decrease in temperature from 25 °C to 4 °C. The adsorption of zinc appears to be significantly different for goethite and ferrihydrite, due to

differences in microporosity (Trivedi 2001). This is related to silica as it can alter the iron oxide phases produced (discussed further in section 1.4). Dyer et al. conducted several tests involving the adsorption of zinc ions on 2-line ferrihydrite under conditions of varying ionic strength and pH (Dyer 2004). Increasing the amount of electrolyte ($NaNO_3$) had very little effect on the adsorption of zinc. This may indicate a very weak association between ferrihydrite and the salt, which is significant to this study as nitrate ions should not influence surface interactions between ferrihydrite and silica.

Multistage adsorption has been shown to be highly effective in reducing zinc concentrations from water samples to very low values (Dyer 2004). The types of ions present also have a significant influence on the adsorption process. The presence of citric acid has been shown to influence the iron oxide surface charge, lowering the iso-electric point and increasing the negative charge (Xue 1995). This increases the amount and rate of both zinc adsorption and desorption from the iron oxide surface.

While ferrihydrite unquestionably binds well with zinc, it has a greater affinity for other species such as cadmium and lead (Martinez 1998). This has positive implications for the Paragoethite process, used for iron removal in zinc hydrometallurgy, as many impurities will be adsorbed before the undesired uptake of zinc from solution.

The effect of the presence of zinc-containing minerals on ferrihydrite has also been investigated. Zinc sulphide has been shown to favour the formation of goethite and hematite over ferrihydrite through surface-mediated reduction of Fe(III) to Fe(II) (Loan 2005). This was further investigated with the finding that natural ZnS promoted hematite and purer, synthetic ZnS promoted goethite (Richmond 2005). The fact that this effect is surface driven is shown by the fact that smaller particles are more effective in driving this phenomenon.

1.3. Silicon and Silica

1.3.1. Occurrence and Applications

Silicon is the single most abundant cationic element in the lithosphere (Cornell 1996). Like iron weathering of rocks to soils, dissolution in aqueous systems and re-deposition cycles silicon throughout the environment. This also means that in any given sample of rock or soil there is likely to be not only some, but rather a significant proportion of silicon. Pure silicon is fairly easily manufactured but rarely occurs naturally, instead tending to form a variety of silicon oxide phases known as silica (primarily SiO_2). Silica occurs in a wide range of structures, ranging from gels and amorphous matter to much more crystalline materials, such as quartz.

Soluble silicates are used in cleaning products such as detergents as well as applications requiring a controlled level of alkalinity. Silicates are a constituent in many adhesives and binders requiring strength or water resistance and appear as precursors in the production of types of silica. Polysilicates are often applied to the field of anti-corrosion coatings where they act as a binder for zinc. Silica gels and powders are used for a wide variety of applications: reinforcing organic solids, reducing adhesion between solid surfaces, increasing adhesive performance, increasing liquid viscosity, creating optical effects, surfactants, hydrophobing effects, adsorbents, catalyst bases, cloud seeding and chromatographic columns. Colloidal silica and silica sols have applications varying from making silica gels and providing an active silica surface to use as a culture medium in biological research; many uses of silica colloids and sols are similar to those of silica gels and powders (Iler 1979).

1.3.2. Formation of Silica

In solution, silicon generally exists as monomeric units of silicic acid in the form of $Si(OH)_4$. The solution is very stable at high pH, which itself increases as silicates dissolve by forming the strongly basic SiO_4^- ions. At low pH, solubility drops

significantly to where it is stable at only a few hundred parts per million or below. Above the saturation point the monomers combine, forming dimers and greater molecular weight species (Schlomach 2004). Polymerisation occurs as a condensation reaction given by Equation 1.8, in which the open-ended dashes refer to further bonding to other oxygen or hydroxide groups.

Equation 1.8: $-SiOH + HOSi- = -Si-O-Si- + H_2O$

The loss of the hydrogen and hydroxide ions from the silanol molecules allow for the formation of the oxo-bridge, creating the siloxane chain (Iler 1979). This is a slow process, especially at low supersaturation; the rate is also governed by ionic strength, temperature and the type of ions present. Aside from the level of supersaturation, polymerisation is driven by ionic concentration - above pH 2 it is governed by $[OH^-]$ and below that level by $[H^+]$.

Formation of oligomers occurs most rapidly at near neutral pH, high silicate concentration and high ionic strength. For low supersaturation levels there is a large induction time (Icopini 2005). Oligomeric units have been found to form a raft of different structures, from simple linear molecules to more complex prisms and multi-cyclics (Sjoberg 1996). The oligomers continue to polymerise, forming particles which then condense internally, removing the majority of the hydrogen and leaving OH^- groups only around the surface. When prepared above 80 °C and pH 7 the silica is approximately anhydrous, thus decreasing the rate of dissolution. Silica polymerisation follows three main steps that are comparable to conventional precipitation. The polymerisation of monomers to form polymers is similar to a nucleation step. The particles grow, and in systems of sufficient concentration, they branch and network through the liquid to form a gel.

Homogeneous polymerisation in silica is a very slow process unless the supersaturation is high, due to either high [Si] in solution, high temperatures, ionic strength and/or high pH. While high temperature and pH decrease the supersaturation with respect to silica, the reaction rates for both precipitation and dissolution increase. It has been found that while high temperatures increase the precipitation rate, the corresponding decrease in supersaturation counteracts the effect (Queneua

1985). There is therefore an optimal temperature in terms of precipitation rate that is around 25 to 50 °C below the saturation temperature (Rimstidt 1980). The increased precipitation rate at high pH is due to the dependence on [OH^-] mentioned above. Increased ionic strength produces a greater proportion of dissociated surface groups which increase the rate of silica dissolution (Vogelsberger 1999), while precipitation occurs more rapidly due to increased supersaturation and surface interactions. Heterogeneous polymerisation occurs much more quickly, on account of the presence of other soluble constituents that induce silica precipitation. Likewise, secondary nucleation is rapid due to an available surface providing binding sites for monosilicic acid. Krauskopf (Krauskopf 1956) has shown that the presence of a pre-formed silica gel increases the rate of silica polymerisation.

By maintaining low supersaturation levels, Chang et al. (Chang 2005) were able to eliminate the nucleation of secondary particles while growing others from seed units. While the growth of existing particles is favoured, the tendency for nucleation increases as supersaturation rises. Matjie and Engelbrecht (Matjie 2007) describe the efficient desilication of gas liquor (ammonia, ammonium carbonate and sulphate containing liquid produced during coal processing) ***via*** the use of seeding particles of alumina, gibbsite and silica with flocculants as adsorptive species. Removal of impurity species from solutions has been carried out by many groups. Sheikholeslami and Bright (Sheikholeslami 2002) show that relatively efficient removal of silicon (starting well below equilibrium solubility) along with cationic elements (Fe, Mn, Mg, Ca, Ni, Co and Ba) is possible by increasing the pH through the addition of basic substances such as NaOH. This would precipitate many of the cations as hydroxide species but should increase the solubility of silicon. The most likely mechanism for this phenomenon is either silica co-precipitation with metal hydroxides or the formation of metal silicates at high pH (>10).

Aggregation and gelation are dependent on the critical coagulation concentration, along with a series of other factors including particle concentration, pH (through surface charge), particle size, surface tension, ionic strength and ionic species present (Allen 1970; Schlomach 2004). At low pH the particles are neutral and thus aggregation occurs extremely rapidly. At silica concentrations above 1 %, aggregation occurs immediately upon the appearance of small particles. At pH 5 – 6

rapid particle formation occurs simultaneously with aggregation. Where the [SiO_2] is greater than 1%, aggregation occurs very quickly between particles and oligomers. Neutral and alkaline sols are strongly negatively charged, which means that aggregation is less favoured and solubility increases.

Aggregate stability decreases with particle size (Schlomach 2004) and the presence of ions such as Al^{3+} and La^{3+}. The concentration of the aggregates increases to the point of gelation. A gel is considered to have formed when 50% or more of the SiO_2 has reached the gel phase. Over time, the solution becomes more viscous and often more opaque, eventually becoming a gel. A depiction of how pH and the presence of ions can alter the aggregation process is given in Figure 1.3.

.

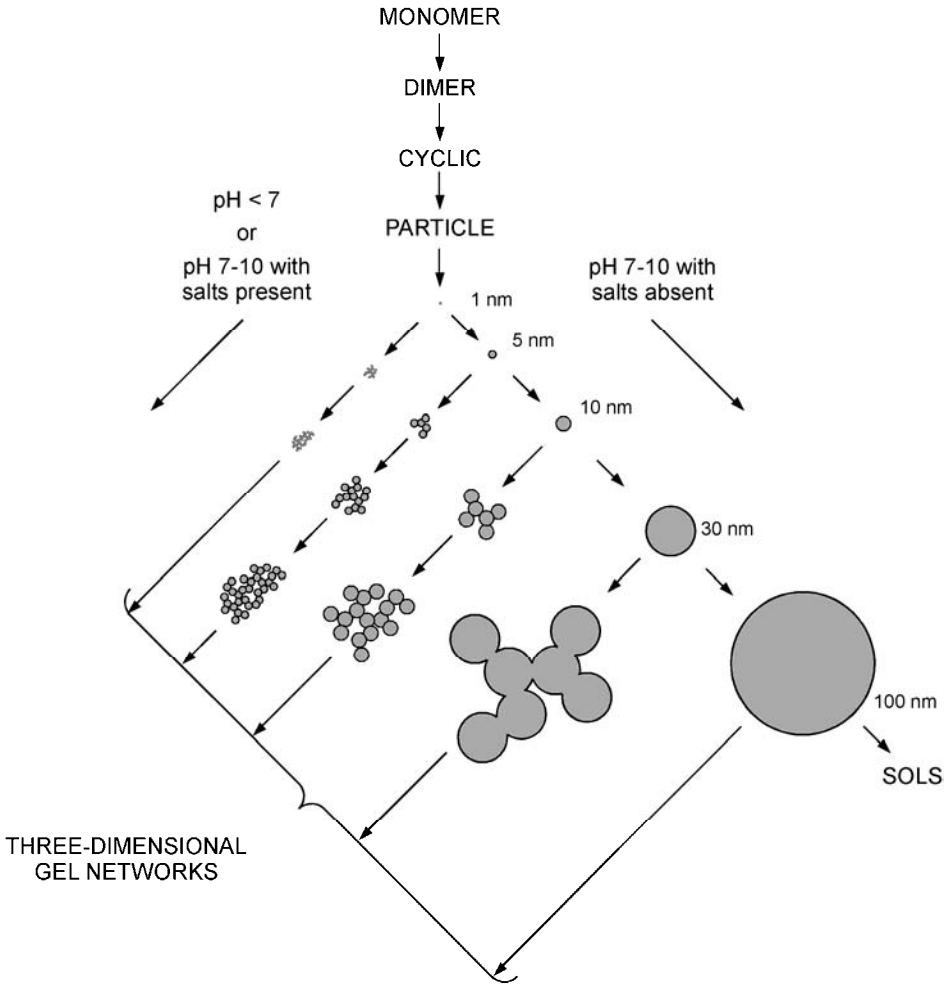

Figure 1.3: Diagram displaying the effect of pH and the presence of ions on the aggregation of silica adapted from Iler (Iler 1979).

The aggregation of sub-micron silica particles is not dependent on agitation; increases in stirring speed have been shown to not increase aggregation in a batch reaction (Schaer 2001). Aggregation has been reported to significantly increase in the presence of ammonia; while charge effects were mentioned, the possible effect of pH (which would increase with ammonia addition) was not discussed (Bagnall 1990). It has been shown that the polymerisation of silica follows an aggregation model more closely than a monomer addition model (Bogush 1991). This allows for meta-stable colloidal particles and deformation in aggregates, introducing some coalescence, which decreases the porosity.

Given the influence that solubility has on the precipitation/polymerisation of amorphous silica, how it changes with pH, temperature and influential ions must be considered. The silicon concentrations within the systems to be studied here will in all cases remain below 2 g L^{-1}, so for the purpose of this investigation the solubility of silica at high pH (>10) can be considered to be infinite. The solubility drops markedly at neutral to low pH to values in the order of a few hundred mg L^{-1}. The exact value of the solubility in this region is dependent on the physical characteristics of the silica and other conditions. When going from solid silica in an under-saturated solution, temperature and particle size alters its solubility and dissolution rate. The generally accepted silica solubility in pure water at 25 °C between pH 2 and 8 is approximately 100 to 150 mg L^{-1} (Iler).

Foloowing a raft of studies that were published with conflicting silica solubility data, Alexander et al. (Alexander 1953) conducted experiments to determine both the solubility with respect to pH and the form the soluble species took. They presented solubilities of between 100 and 140 ppm for pH 2 to 9 and found that it was primarily monosilicic acid was present in solution. Similar studies have come to the same conclusion (Sjoberg 1996). While solubility differs only slightly over the low pH range, it has been found that the rate of dissolution is greatest at the IEP of silica (approximately pH 2) (Vogelsberger 1999). To be certain that equilibrium was obtained, Alexander et al. approached equilibrium from both dissolution of solid

silica and precipitation from supersaturated solution over six months (Alexander 1953). At pH levels above 10.6, not only was the solubility far greater (~ 3600 ppm at 11.4), but also polysilicate ions had formed, as well as monosilicic acid. It has been shown that the adsorption of dimeric silicate ions in alkaline conditions more accurately predicted trends in zeta potential (Davis 2002). This may have been solely due to the pH or also a consequence of the surface onto which it was adsorbing.

Evidence has been presented suggesting that at pH 3 – 4, for both high and low ionic strength solutions, an equilibrium concentration of ~6 mmolal (350 to 400 ppm) of monomeric SiO_2 is reached. At greater pH levels the value drops to the more standard 2 mmolal (100 to 150 ppm) . It is suggested that a metastable equilibrium is established between monomeric silicic acid and nanocolloidal silica particles. It appears that where particle size is limited to such small distributions (given as ~3 nm), the theoretical equilibrium solubility would lie at approximately 6 mmolal, based on the Ostwald – Freundlich equation. However, this would be dependent on the stability of the nanoscale particles, which would also then call into question whether it is a true equilibrium.

The temperature response of silica solubility appears to show a generally linear increase over a range between 100 and 300 °C, but a slower rate of change at temperatures below that, depending on the source of the data (Alexander 1953; Iler 1979; Marshall 1980; Chen 1982). The published results may all have been influenced by the properties of the specific silica sample in each investigation. Chen and Marshall (Chen 1982) have provided molar solubilities which, converted to mass concentrations, give a fairly linear increase from just over 400 ppm at 100 °C to just 1700 ppm at 300 °C. This value tends to plateau around 350 °C, which agrees with the majority of studies that show a decline in solubility upon reaching 400 °C.

Sodium, zinc, nitrate, sulfate and chloride were present in the experimental precipitates formed in this research, therefore their influence on silica polymerisation is of great importance. Marshall and Warakomski (Marshall 1980) conducted a series of studies of amorphous silica solubilities at varying temperatures and in the presence of different electrolytes. Although their values were in the most part

obtained from dissolution of solid silica, as opposed to precipitation from a supersaturated solution, they showed that this only created a shorter required reaction time and the final solubility values were comparable.

The “salting out” effect is a commonly known phenomenon, in which all added salts decrease a species’ solubility. Of all the salts tested at 25 °C, $NaHCO_3$ and Na_2SO_4 showed the least effect on silica solubility (Chen 1982). While in general the increase in salt concentration produces a continued decline in solubility, above 0.2 to 0.25 M there is only a slight effect (Marshall 1980). A solution complex between silicic acid and sulfate has been postulated (Marshall 1982), based on this observed effect and the calculated association constants.

During temperature testing, solubility in Na_2SO_4 solution was contrary to trends in other electrolytes (Marshall 1982). Increasing the concentration of Na_2SO_4 at higher temperatures increased silica solubility, while all other salts tested displayed the opposite trend. $MgSO_4$ was also tested and while the solubility decreased slightly at greater $MgSO_4$ concentrations, it was a minimal effect and negligible compared to those of other materials. $NaNO_3$ decreased the solubility to a much greater extent. These studies quote equilibration times between a few hours and a few days, suggesting that without conditions that catalyse silica dissolution or precipitation, equilibrium will not be reached in a short period of time.

Kinrade and Pole (Kinrade 1992) investigated the effect of alkali-metal cations on silicate solutions, finding three major methods of influence. Lithium increased polymerisation through electrostrictive (structuring induced by applied electric field) water-structuring and the cations form ion pairs with the silicates. The latter decreased the intermolecular repulsive force between silicate molecules. The third effect is that the ion-paired cations stabilised structures by the immobilisation of otherwise flexible formations. The particle size is also dependent on the pH, supersaturation, solvent and the electrolytes present. The aggregate size decreased at greater supersaturation levels and at low levels of electrolytes, the latter due to the increased surface charge (Kim 2004). However, at greater electrolyte concentrations the particle size increased due to surface charge neutralisation. The magnitude of the

effect was related to electronegativity and the effect on zeta potential correlated with that on particle size.

Silica behaviour has been investigated in systems with complex matrices. Thordarson and Tomasson (Thordarson 1989) investigated silica removal from geothermal waste waters in Iceland, showing near neutral pH produced the fastest polymerisation. Aggregation was favoured at higher pH levels, taking days to occur between 7 and 8, but only minutes or hours at greater alkalinity. Overall, a pH of 8 - 8.5 was the most suited for silica removal. The primary conclusion of an investigation by Natesaiyer and Hover (Natesaiyer 1992) was that zinc sulfate retards the dissolution of silica in alkaline media.

Deitzel (Dietzel 2000) showed that polysilicic acids decompose readily in natural waters and the depolymerisation process is inhibited by low temperature, low pH and the presence of heavy metals that complex with the polymers. Silica scale in oil pipes has been reduced using precipitation inhibitors, such as fluoroborates (Gallup 1997).

1.3.3. Structure of Silica

As this thesis deals solely with systems containing amorphous silica, the structure of other phases of silica (such as quartz) will be omitted from the following discussion. In solution, silica takes the form of monosilicic acid at low to moderate pH and forms silicates and polysilicates above pH 10. Amorphous silica is so named for its distinct lack of long range order. Unlike ferrihydrite, primary particles of silica can vary a great deal in size, depending upon the conditions of formation and suspension. While ferrihydrite can appear amorphous due to its nanocrystalline nature, silica is unquestionably an amorphous material. It is composed of silicon atoms tetrahedrally coordinated with oxygen anions, which join and form locally ordered networks, as opposed to a crystalline structure (Balas 2007). The bulk of the particles are anhydrous SiO_2 which result from internal condensation reactions. The surface will not have reacted completely as it is not surrounded by silicon atoms, therefore surface silicon atoms will have silanol groups remaining.

The amorphous silica XRD pattern consists of a single broad peak appearing between 25 and 30 degrees. As a consequence of the general lack of information such patterns provide, silica is more productively characterised using infrared techniques. Pure amorphous silica produces an array of bands between 3400 and 3800 cm^{-1} relating to O – H bonding on surface hydroxyl groups. A large peak is also observed at approximately 1100 cm^{-1} which corresponds to the Si – O – Si bridges within the structure (Hanna 1965; Chukin 1977; Iler 1979; Morioka 1998; Balas 2007; Hong 2007). There is also a smaller peak at ~810 cm^{-1} that is characteristic of silica. The structure of the solid can be altered after formation ***via*** annealing. The elevated temperature produces cristobalite and quartz, which alter the IR spectrum (Morioka 1998).

1.3.4. Properties of Silica

The properties of silica depend on a range of variables during formation. These can affect the phase, particle size, surface chemistry, solubility, aggregate size, fractal dimension and interactions with other species, and these properties often influence each other. The primary particle size will affect the degree of aggregation and the surface area. Small particles introduce a higher degree of porosity during aggregation, which in turn influences other properties.

Values for typical surface areas of silica found throughout the published literature are extremely varied. However, all of these measurements may be valid, such is the variation of the material depending on the conditions under which it is prepared. It has been quoted to be as low as 12.5 $m^2 g^{-1}$ (Balas 2007) for some discrete particles and above 600 $m^2 g^{-1}$ (Iler 1979) for powder produced by vapour condensation. A greater surface area increases the solid's adsorptive capacity and is related to increases in the volume of nanopores and mesopores (Gun'ko 2005). The surface charge density and modulus of the zeta potential have been found to decrease at greater surface areas.

The surface chemistry of silica has been extensively investigated and the literature to 1979 has been reviewed in detail by Iler (Iler 1979). Multiple values for the

isoelectric point of silica have been provided, covering a range from less than pH 2 to pH 4 (Parks 1967; Anderson 1985; Xu 2003). This has been described as being the result of differing crystal structures or the extent of hydration. However, a review of IEPs for a range of materials show that generally structure and hydration degree are not the cause of varying measurements (Kosmulski 2002). Interestingly, the choice of analytical technique, such as electrokinetic vs. electroacoustic, can lead to different results for the same material. The effect of ions present in the suspensions being analysed is also highly influential, as well as the temperature (Tewari 1972). The generally accepted IEP value for amorphous silica in pure solution is approximately pH 2.

The reversal of charge is a phenomenon that has been observed on the silica surface in the presence of some ions (Iler 1979). At high enough concentrations of soluble hydrolysed cations (e.g. Zn^{2+}, Fe^{3+} and Al^{3+}), a coverage of polycations forms on the silica surface. As the proportion of the negatively charged surface covered with positively charged ions increases, the overall effective surface charge increases through neutral to a positive value. It must be noted that this only occurs under specific conditions and does not apply to double layer compression (Iler 1979; Xu 2003). This effect can be opposed by the addition of complexing ligands, such as EDTA.

It has been suggested that silica surface behaviour changes in the presence of cations such as Zn^{2+} (Janusz 2003; Phan 2004), Co, La and Th (James 1972). Initially at low pH, the surface is pure silica, but as the pH rises towards neutral the cations adsorb on the surface and eventually begin to nucleate and form metal hydroxides under near neutral conditions. This alters the surface charge toward positive values, as there is a mixture of positive and negative sites across the surface. Eventually, given a high enough concentration of cations in solution, the surface charge is completely dominated by the hydroxide phase as it envelops the silica particles. Similar effects have been noted with other materials, however this has generally been a consequence of a simple secondary precipitation (Rashchi 1998).

Due to the often large surface area and affinity to adsorb certain species, amorphous silica has been shown to be a very effective sorbent. A method of selective removal

of multiple metals from solution ***via*** adsorption onto an activated silica substrate has been patented (El-Ammouri 1997). The silica surface has been shown to facilitate reactions between strongly bound adsorbed reagents (Davis 1978).

Silicic acid adsorption has been investigated on the surface of aluminium hydroxide, which would likely show similar behaviour to an iron oxy/hydroxide material (Hingston 1967). The initial uptake occurred rapidly and was not affected by temperature or ionic strength. The pH decreased upon the uptake of silicic acid by the surface, as these species replaced the adsorbed sulphuric acid that initially occupied the sites. Subsequent layers formed at reduced rates and had greater activation energies associated with them. This is consistent with the initial layer forming ***via*** adsorption followed by silica polymerisation (similar to particle growth) producing subsequent layers. This would provide a rapidly-formed first layer; the slower forming outer layers would have a lower activation energy than homogeneous silica polymerisation, as no nucleation event is required.

Materials like ferrihydrite and alumina have been shown to be effective agents for removing silica from suspension. Activated alumina can remove up to 90% of the silica from water, a process not significantly influenced by the presence of anions such as sulfate and nitrate (Bouguerra 2007). This is a surface adsorption effect and is increased by greater temperatures and sorbent concentration (to a maximum dosage), and is maximised at approximately pH 8. “Waste” Fe(III)/Cr(III) hydroxides have shown to adsorb 12.25 mg of silica per gram of waste material (Namasivayam 2007). The process was not significantly affected by the initial pH or the presence of molybdate, thiocyanate, chloride, nitrate or sulfate, but vanadate, phosphate and selenite impeded adsorption.

1.3.5. Co-precipitation

Silica co-precipitation with other materials can be affected by the presence of anions. It was found that sulfate influences the structure of aluminosilicates and their surface properties (Miyazake 1999) by slowing the aluminium hydroxide precipitation rate (Okada 1986).

1.3.6. Interactions with Zinc

Silica, in combination with other materials, has been shown to be effective for the removal of zinc and other contaminants from solution (Prado 2005). Zinc can adsorb strongly to the silica surface at a favourable pH, especially in cases of small, freshly precipitated particles (Phan 2004). Silica displays a characteristic adsorption edge of multivalent ions, the position and width of which is dependent on several factors, but predominantly ion concentration (Janusz 2003). The adsorption is far less effective at high temperatures or with a heated silica substrate (Kozawa 1961).

In adsorption testing of zinc on both silicon and silicon oxide, more zinc was found associated with the pure silicon and at greater depths (Ochs 1998). This is due to the formation of an oxide layer during the test into which zinc is incorporated, similar to a co-precipitation process. In natural clays containing zinc, over 80 % of the zinc was associated with phyllosilicates (Manceau 2004), As these soils appear to contain ferrihydrite as well, it shows the importance of silica in zinc-rich environments, such as exist with the Paragoethite process liquors.

At pH 7-9, silica suspensions aggregate in the presence of zinc ions (Mirnezami 2003). This is peculiar, as silica has a highly negative surface charge that opposes aggregation at such high pH values. It is proposed that this is due to the formation of zinc hydroxide on the silica particle surface, which either polymerises or flocculates to join particles together. Roberts et al. (Roberts 2003) also found that a phase resembling zinc hydroxide formed on the silica substrate at pH ~7.5. They also noted that zinc adsorbed strongly at all pH values tested (5.1 – 7.52), was octahedrally coordinated at lower pH values, and formed tetrahedra toward the alkaline end of the range. The presence of silicate ions inhibits the dissolution of zinc in alkaline conditions by adsorption on the material surface (Armstrong 1976). This process may also occur in acid media, with the possibility of subsequent polymerisation on the surface. It is reasonable to hypothesise that this may occur on zinc-laden minerals, inhibiting dissolution, which would complicate the dissolution of ores and concentrates in many industrial processing applications.

1.4. Iron oxide/Silicate Materials and Interactions

1.4.1. Composites: Discrete Phases

Iron oxides precipitated in the presence of pre-existing silica tend to form on the silica substrate. It has been suggested that this is due to the adsorption of aqua-complexed iron on the surface followed by precipitation (Xu 2005). It may also result from providing a nucleation point for precipitation or adsorption of iron oxide particles once they have formed. Hong et al. (Hong 2007) produced particles of hematite and magnetite on silica nanoparticle substrates. They found under their conditions that the feed source was important; ferric nitrate produced magnetite while ferric chloride produced hematite. Infrared spectra of the samples gave bands coinciding with the presence of silica and iron oxide, but there were none corresponding to Fe – O – Si bonds. This may suggest that in this case the particles are only physically adsorbed on the silica surface. Xu and Axe (Xu 2005) have produced similar data, showing the change in the Fe – O and Si – O bonding environment.

A similar result was obtained by Mustafa et al. (Mustafa 2002) when they precipitated iron in a silica suspension. Interestingly, while many other groups have found the IEP of composite materials to be a combination of those known for silica and iron oxide (between 2 and 8), these materials displayed two discrete values, one relating to each phase. This result was considered in this case to be unrelated to composition (Si:Fe ratio). They were therefore believed to exist as two discrete phases, the properties of which were completely independent of each other.

Waste silica is often produced when silica is used to purify samples. Unob et al. coated waste silica with iron oxide to use as a further adsorbent for trace metals, such as lead, copper cadmium and nickel (Unob 2007; Wang 2007). The composites were useful, as dissolution of the iron phase only occurs at pH 3 or lower and the ideal pH

for metal ion removal is 6 – 7. The presence of salts reduced the efficiency of the adsorption of trace metals.

Core-shell particles of iron oxide and silica have been formed on several occasions (Cheng 2006; Ocana 2006; Wang 2007). Coating an iron oxide core with silica has been shown to form Si – O – Fe bonds that closely bind the two phases. A notable effect of the silica was to increase the resistance to oxidation of the material, shown by the lack of peaks in the Differential Temperature Analysis and Thermogravimetry (DTA-TG) data of the sample containing the greatest Si:Fe ratio. Wang et al. noted a similar protection against oxidation after coating hematite with silica. However, there were no peaks in the infra-red spectrum related to Si – O – Fe bonds (Wang 2007). This was similar to the results of Predoi et al., although no theories were provided as to why this bonding environment was absent from these samples (Predoi 2007).

Sedimentary samples have been shown to contain a mixture of phases of iron oxides, silica species and other minerals, such as kaolinite. Schwartz et al. concluded that even though the amorphous iron oxide constitutes a low proportion of the sediment, it aids in binding it together (Schwartz 1997). Also, a silica phase resembling opal was responsible in part for holding clay particles in a “cementitious web”. Similar behaviour could potentially result in improved aggregation within settled solids produced during experiments in this investigation.

1.4.2. Surface / Solution Interactions

Research has been conducted into the adsorption of silica on iron oxides and ***vice versa***. Monosilicic acid adsorbs on the surface of ferrihydrite at relatively low Si:Fe ratios, and when this ratio is increased the monomers polymerise to form Si – O – Si bonds with the adsorbed units (Davis 2002). The point at which polymerisation becomes significant is between Si:Fe ratios of 0.05 and 0.2. Ferrihydrite appears to act as a template for silica polymerisation, inducing it at lower concentrations than would generally be required. Both the rate and extent of adsorption are pH dependent and peak between pH 8 and 10, where silica deprotonation would occur easily and

the solubility of silica remains relatively high. However, polymerisation is higher below pH 6 (Swedlund 1999).

Several researchers have created iron oxide-silica core-shell particles, as silica is easily deposited on the iron oxide surface. One group used hematite particles to template hollow silica spheres. The hematite was first created, then silica deposited on the surface and the hematite redissolved to leave the hollow silica structures (Han 2007). Khare et al. produced iron-coated sands using green rusts (iron(II) hydroxide) and ferrihydrite, investigating the most efficient method to achieve high levels of deposition (Khare 2008). They ultimately chose ferrihydrite precipitation by raising the solution pH in the presence of the sand.

Williams and Kelsall produced atomised iron silicide (Williams 1988), finding the surface was composed of a mixture of Si, Fe(II) and Fe(III) oxides (predominantly silica) which displayed multiple IEPs. At low pH it behaved as a composite of silica and iron hydroxide having an IEP between 4.82 and 5.48. However, there was a turning point just below pH 7 followed by a sharp increase to a positive surface charge within a fraction of a pH unit. At the turning point it was proposed that iron hydroxide is adsorbed on the surface and the particles behave as pure iron hydroxide from then onward. The constant precipitation and dissolution that occurs in the system over time makes reaching equilibrium difficult and the pH dependence would mean the behaviour of the particles was very easily changed by the conditions.

It has been suggested that at low pH and room temperature, iron and silicon may lead to solution complexes of the form $FeH_3SiO_4^{2+}$ (Reardon 1979). This was proposed as a consequence of the increased solubility of silica in ferric solutions.

1.4.3. Co-precipitates

Doelsch et al. have provided Fourier Transform Infra-red (FTIR) data showing that Fe – O – Si bonds are formed during co-precipitation (Doelsch 2001), consistent with the surface adsorption of silicic acid, which has been confirmed by other groups (Carlson 1987; Seehra 2004). A Si:Fe ratio of 1 produced discrete pockets of silica,

demonstrated by Si – O – Si siloxane bonds, once the opportunity for Fe – O – Si has been exhausted. This was similar to the findings of Herbillon and Tran Vinh An, who showed that below a Si:Fe oxide ratio of 0.1, silica is adsorbed on the iron oxide surface, whereas beyond that value silica begins to polymerise (Herbillon 1969). This suggests the oxygen bridges between iron and silicon atoms are kinetically favoured over the polymerisation of pure silica. They also state that the formation of these bonds inhibits the formation of iron oxyhydroxides, meaning that silica retards crystal growth.

The presence of silicate during co-precipitation decreases the formation of double and single corner sharing Fe linkages, with a crossover from three- to two-dimensional growth occurring as the Si:Fe ratio increases beyond 1 (Doelsch 2000). In addition, they have shown that the majority of the Fe is contained in units smaller than 7.5 Å and the precipitates show a high fractal dimension (2 – 2.7), likely to be due to the presence of Si ligands (Masion 2001).

It is well known that the presence of soluble silicates during the precipitation of ferrihydrite restricts the product's crystallinity (Carlson 1981; Anderson 1985; Cornell 1996; Mayer 1996; Schwertmann 2000; Pokrovski 2003); (Chatellier 2004; Seehra 2004; Tongpool 2004). However, an explanation for this is rarely provided. Mayer and Chatellier et al. both showed that the presence of silicate also affects the precipitation from Fe(II). Lepidocrocite (a meta-stable iron oxy-hydroxide with much greater stability and apparent crystallinity than ferrihydrite) was formed in experiments containing no silicate or low Si:Fe ratios (Si:Fe $\leq$ 0.1) (Mayer 1996; Chatellier 2004). At higher levels (Si:Fe $\geq$ 0.36) ferrihydrite was produced, displaying similar results to those of Carlson and Schwertmann (Carlson 1981). Silicate also had an influence on the settling rate, with the silica-containing ferrihydrite settling far slower than lepidocrocite. One co-precipitate was formed with an Si:Fe ratio of 4.5, the settling time of which was several orders of magnitude slower than most others in the absence of electrolyte.

Vempati et al. (Vempati 1990) produced co-precipitates in batches by adding sodium metasilicate and ferric sulfate, then increasing the pH to 8.2 with sodium hydroxide.

At low silicate levels (Si:Fe ratios ≤ 0.05) they reached similar conclusions to other groups, suggesting that silicate monomers adsorb on the ferrihydrite surface. However, at greater ratios (≥ 0.1) the authors proposed, based on electron diffraction, XRD, IR and XPS results, that silicon is incorporated into the ferrihydrite structure. However they did not provide any evidence to directly show this, only stating that multiple bonding environments exist at high Si:Fe ratios, which could be explained by discrete silica phases. Glasauer et al., conducting precipitation of goethite in the presence of silicate, couldn't find evidence of structurally incorporated silicon and concluded the silica fraction not found on the surface was most likely located between crystal domains (Glasauer 1999).

Pokrovski et al. conducted X-ray Adsorption Fine Structure measurements on the precipitates from experiments involving iron(III) and silicate-containing solutions at varying pH (Pokrovski 2003). In the absence of silicon, iron gave the familiar octahedral formation with water and hydroxide ligands at low pH. Increasing the pH induced polymerisation and the formation of oxo and hydroxo bridges connecting octahedra ***via*** edge and corner-sharing. The introduction of silicate to the system decreased corner-sharing in favour of edge-sharing. Silicon tetrahedra linked some iron octahedra ***via*** corner-sharing. At a greater silicate concentration (Si:Fe = 16), some iron was taken up in the silica structure in tetrahedral coordination, while Fe - Fe linkages appear to have vanished. This is evidence as to how silica could influence the primary particle size of ferrihydrite. They also referred to silica binding to iron oxide, suggesting it would decrease the number of active sites on the surface, thus decreasing the uptake of other trace ions.

Schwertmann (Schwertmann 1982) investigated the influence of silicates present during ferrihydrite precipitation on the resultant surface charge. He found that in general, natural iron oxides produced much lower IEP's than pure synthetic materials and that this was, at least in part, due to the association with silicate species. Of the co-precipitates he analysed, a higher proportion of Si in the material correlated to a lower IEP. However, even with equivalent Si:Fe ratios the synthetic materials produced higher IEPs, which has been attributed to the presence of other materials in the natural samples, such as organic matter, that decrease the surface charge.

Co-precipitates were prepared by Zeng (Zeng 2003) in batch experiments from sodium silicate and ferric chloride at pH values between 3 and 12. They then presented evidence displaying that the presence of silica in the precipitates increased the adsorbent strength but decreased the affinity for arsenic adsorption. The formation of Fe – Si complexes was used to explain the increase in adsorbent strength; the decrease in arsenic adsorption was due to the lesser affinity of silica for the species. He claimed that the iron oxide was in an amorphous form, which would suggest it was most likely ferrihydrite. Interestingly, the adsorbent strength increased with greater proportions of silica while the surface area decreased, although only samples at Si:Fe ratios of 0.33 and 1 were measured producing surface areas of 186 and 140 $m^2 g^{-1}$, respectively.

Anderson and Benjamin (Anderson 1985) conducted batch iron oxide precipitation experiments in the presence of a range of silicate concentrations introduced at different times in the process. They demonstrated that at Si:Fe ratios greater than 0.2 not only does silica decrease the crystallinity of the products when added early during precipitation, it also increases the product's stability against transformation. Conversely, if the silicate was added later in the reaction (after 24 hours) hematite formation was favoured. The IEP decreased with the addition of silicate; greater amounts of silicate and greater aging times enhanced this effect. The greatest IEP difference was a drop from pH 8 for pure iron oxide to 4 for the co-precipitate. They also noted that at an alkaline pH the solution was slowly etching the glass beakers, increasing the amount of silicates in solution.

Predoi et al. (Predoi 2007) produced co-precipitates in the form of iron oxide particles dispersed in a silica gel and annealed them at temperatures of 550 and 1000° C. An infrared spectrum was collected on samples before and after heat treatment. No bands in the spectra of the as-prepared or annealed samples were attributed to Fe – O – Si bonding. This was possibly due to the low proportion of iron in the samples (~3%), which may produce such a weak adsorption as to be unnoticeable above the background. Upon heating, hematite particles had formed in the substrate.

Xu et al. (Xu 2004) conducted similar experiments, heating samples of iron oxide enclosed in a silica matrix to between 900 and 1200° C. The samples contained 15% Fe and IR data obtained after sintering showed a weak peak at approximately 950 cm^{-1} attributed to bonding between SiO- and certain cations (Fe^{3+}, Ti^{4+}, Sr^{2+} and Co^{2+}), which may suggest the presence of Fe – O – Si bonds. There was a band present in some of the analyses conducted by Predoi et al. (Predoi 2007) at 940 cm^{-1}, but this was attributed to Si – OH bonding. Heating produced predominantly hematite with some maghemite at 1000° C, above which the amorphous silica was transformed to quartz and cristobalite.

Cannas et al. (Cannas 2004) produced iron oxide particles dispersed in silica gel ***via*** co-precipitation. The reagents were placed together upon dissolution and allowed to precipitate. The silica was in excess and at high enough concentration to gel, producing the desired product. They produced 2-line ferrihydrite that was much more resistant to the effect of temperature - it did not undergo a phase transformation at temperatures significantly greater than those required to transform pure ferrihydrite.

Anderson and Benjamin showed that the presence of silica in the precipitates appears to increase the adsorption of Cd, whereas Cu, Co and Zn were only affected by whether the solid was fresh (<2 h) (Anderson 1985). An increased presence of silicate pushed the point of zero charge (PZC) down, therefore increasing the operating pH with respect to the PZC. This decreased the adsorption of SeO_3 due to the changing characteristics of the surface. These two effects show the different behaviour of the oxyanions and cations; where surface charge is the governing factor for one, it is not for the other.

1.4.3.1. Ferrihydrite Transformation

As discussed in the previous section, silicate has a high affinity for the ferrihydrite surface and a significant effect on transformation. Small amounts of silica in ferrihydrite inhibit the transformation at pH 12 and favour the formation of hematite over goethite (Cornell 1996). Based on the fact that seeding can overcome the effect of very low silicate levels but not of greater proportions, it would appear that silicate

stabilises ferrihydrite from dissolution. Similar effects indicating less crystalline iron oxide phases due to the presence of silica have been displayed in both pure and complex industrial systems (Schwertmann 1999; Claassen 2002). It has also been shown that the effect is greater when the species are co-precipitated, as opposed to the addition of silicate to a ferrihydrite slurry.

Samples of ferrihydrite produced by Glasauer et al. (Glasauer 2000) contained an Si / (Si + Fe) ratio of 0.11 that were stable at 400 °C. The temperature at which transformation to hematite occurred was 850 °C, which is much greater than pure ferrihydrite (300-400 °C). Campbell et al. (Campbell 2002) obtained similar results in producing Si-containing hematite by heating Si-containing ferrihydrite. The temperature required for the transformation increased from 340 °C for a Si-free sample to 740 °C with as Si / (Si + Fe) ratio of 0.27.

Similar results have been noted for other composites, including silica / maghemite powders, for which the temperature of transformation increases by several hundred degrees with the introduction of silica (Sartoratto 2007).

1.5. Paragoethite Process

While the processes within this investigation are of considerable fundamental interest, the motivation for this study has arisen from the need to understand the iron precipitation step from acidic zinc process solution as part of the industrial Paragoethite (PG) process. The process takes its name from the predominantly iron oxy-hydroxide residue formed that was thought to closely resemble goethite (Claassen 2002). The Paragoethite process is designed to precipitate iron from zinc-rich solutions and is primarily focussed on three basic stages: dissolution of ores and calcine (predominantly roasted ZnO) in leaching stages, removal of iron and other impurities ***via*** precipitation, and collection of zinc through electrowinning.

Iron removal involves precipitation from the acidic process liquors by increasing the pH, predominantly forming the meta-stable phases 6-line ferrihydrite and schwertmannite (Loan 2006). This appears in the residue amongst a raft of other phases, including other iron oxides (e.g. goethite, schwertmannite and jarosite) and undissolved calcine particles. Silicon appears in significant proportions that may vary, depending on the site from which the raw materials are obtained. The effect of the increased level of silicate in plant liquors is not known, and this research is aimed at clarifying whether this causes a significant impact on plant operations. Such questions as whether the silicate is effectively removed from process liquors, whether it impacts significantly on the residue and whether it will influence zinc uptake are highly important to plant operations. If the silica is not satisfactorily removed, other measures will have to be implemented to maintain the purity of the final product (Takemori 1993), which would require more time and capital.

The refinery in Hobart, Australia, currently under the ownership of Nyrstar, has been in operation for almost a century. It has always been concerned with zinc recovery, but has not always employed the same process. For some time the plant used the jarosite process which, as the name suggests, produces jarosite as an iron by-product (Arregui 1979; Kershaw 1995). While it provided excellent zinc recovery, this iron oxide phase proved difficult to dispose of. Disposal issues, coupled with environmental legislation, led to the introduction of the Paragoethite process.

Zinc concentrates processed at the Nyrstar Hobart Smelter contain iron-substituted sphalerite (Zn/FeS) and gangue minerals such as pyrite (FeS_2), pyrrhotite ($Fe_{(1-x)}S$), hematite and chalcopyrite ($CuFeS_2$). Iron typically constitutes between 3 and 10 % of the concentrates. Phase transformation occurs under roasting, forming some franklinite ($ZnFe_2O_4$) and hematite. As franklinite is only soluble under extreme pH conditions it can be separated from zincite by neutral leaching. Franklinite and other sparingly soluble minerals are dissolved in hot and strong acid leaching stages (90-95 °C, 70-130 g L^{-1} H_2SO_4). Concentrate may also contain up to 5 % silica.

The ferric liquor (85 °C, 5 – 10 g L^{-1} Fe^{3+}, ~140 g L^{-1} Zn as $ZnSO_4$ and 2 – 4 g L^{-1} SiO_2) is fed continuously into the PG precipitation reactors at a controlled rate designed to promote dilution and calcine slurry is added to achieve the pH_{33} (pH at 33 °C) of 3.5. This value is highly important, as variation outside a small pH range results in poor solid-liquid separation properties. An advantage of the iron oxyhydroxide residue is that it removes Al, SiO_2, As, Sb, Ge, F, Cd and other trace impurities by adsorption. There are both positive and negative aspects to this process: the residue retains relatively low levels of sulfate, the operating costs are low, but the solid-liquid handling is poor and there are greater zinc losses.

The process (summarised in Figure 1.4) involves flow from multiple vessels, including counter-current flows for further processing of some materials, to deal with both solutions and solid material (Loan 2004). A neutral leach (NL) stage separates soluble zinc oxide from insoluble species such as zinc ferrite (franklinite). The solids from NL go to the Preneutralisation (PN) stage, while the liquor goes to Purification. The solids from PN go to the Hot and Strong Acid Leaching (HAL and SAL) stages, where franklinite dissolves. The dissolved iron is then precipitated in the Paragoethite (PG) stage.

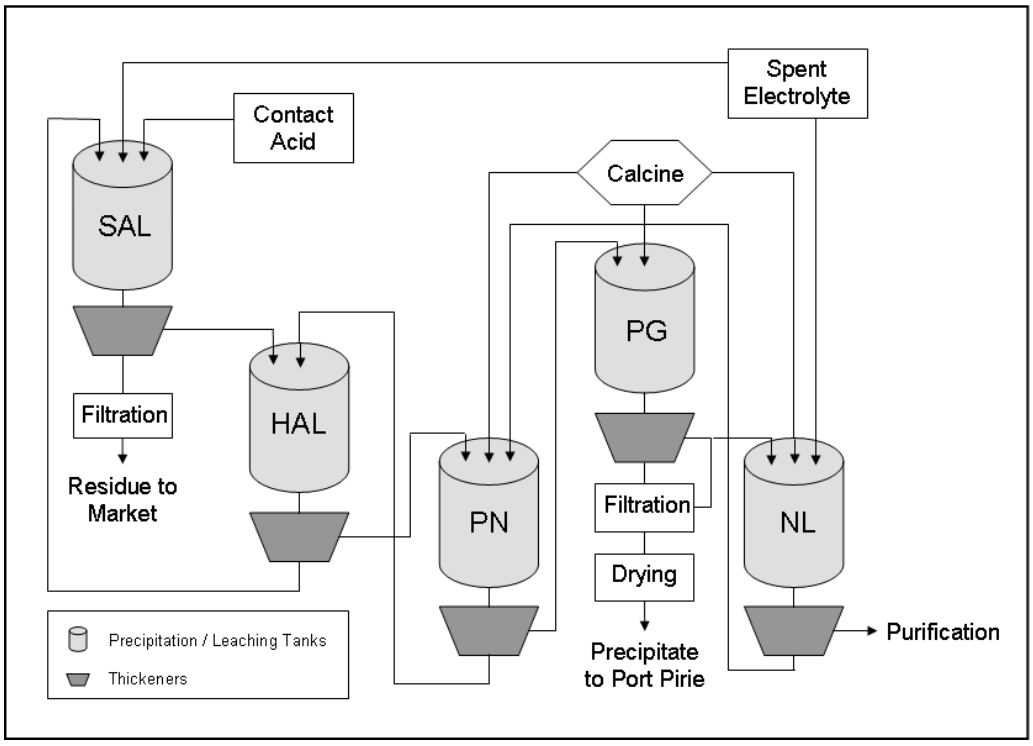

Figure 1.4: Simplified flow sheet describing the process circuit in operation at the Nyrstar Metals Ltd. Hobart Smelter, adapted from Loan 2004 (Loan 2004). Abbreviations as in text.

The Paragoethite precipitation step is carried out in five parallel, 235 m^3 reactors at 85 °C, in which PN overflow is added at a rate of 40 - 50 m^3 h^{-1} per reactor. Calcine is added to maintain the pH_{33} of 3.6 ± 0.1, which requires approximately 1/8 of the PN flow rate. The calcine is added as a slurry at ~500 g L^{-1} solids loading of ≤ 85 m particles in solutions from the NL stage. The pH is measured every 3 minutes through an external cell, by which slurry is automatically sampled from the reactor and cooled to 33 °C for the measurement. The overflow (clarified solution) goes to the NL stage and the underflow (high solids slurry) is delivered to a thickener. The thickening process occurs in an environment where the temperature and pH are not controlled. The temperature decreases as the thickener is not heated and the pH increases to approximately 4. This change in conditions can be the source of undesired reactions, such as greater zinc uptake. The thickener underflow is then filtered and dried to reduce the moisture content from ~38% to ~20%.

The residue generally displays an average particle size of ~20 m but can reach ~100 m (this is an aggregated size, not primary particles). It contains insoluble phases from the calcine including franklinite, anglesite, sphalerite, willemite and quartz, along with the precipitated phases such as ferrihydrite, schwertmannite, goethite, jarosite and amorphous silica. The major components are iron, zinc, lead and sulfate at 34, 14, 2.7 and 12 wt%, respectively. The suggested formula of the bulk of the residue is Fe_2O_3. 0.64 H_2O. 0.2 SO_4 which is consistent with schwertmannite, or ferrihydrite with high levels of adsorbed sulfate.

The zinc level in the residue can be reduced with a higher degree of washing, but this introduces more water to the residue. An increase in the temperature and pH increases the levels of zinc in the residue but decreases the level of sulfate which is consistent with adsorption studies (Loan 2004). Increases in pH may also increase zinc losses due to less dissolution of calcine or precipitation of a zinc phase.

Paragoethite residue is sent to lead smelters for further recovery of associated zinc. Another form of treatment for the Paragoethite waste residue is to combine it with ferric oxides (or steelmaking scraps), silicon (or electronic industry by-products of high enough grade) and aluminium and igniting the mixture to render toxic constituents (As, Pb, Cd) inert to meet environmental standards for disposal (Porcu 2004). However, this can only accommodate up to 30 wt% Paragoethite residue and still leaves a solid waste product.

Work has been conducted on iron precipitate properties resulting from a hydrometallurgical zinc process similar to the PG process. The Zincor process differs in some reaction conditions from the PG process operation in Hobart but primarily produces poorly crystalline iron oxy hydroxides during precipitation (Claassen 2002). Claassen and Sandenbergh have presented the impact of mixing on the iron residue, displaying significant improvements in filterability and decreased zinc uptake under ideal mixing conditions (Claassen 2007). They also found that higher temperatures provide greater dry solids densities and mean particle sizes, but greater zinc uptake (Claassen 2007). Greater reaction pH values also have higher associated D(0.5) (the median aggregate diameter) measurements, but induce a decline in dry solids density and greater zinc adsorption. In relation to silica, Claassen et al.

mention that an absence of more crystalline iron oxide phases is due to the silica associated with the residue.

There are other examples of substantial levels of silicates in processed ores, as zinc silicate is the next richest source of zinc after zinc sulphide deposits (Bodas 1996). The silicates have often proven difficult to dissolve, creating more problems for the plants concerned.

1.6. Thesis Aims and Themes

This thesis is focussed on understanding the processes leading to the formation of ferrihydrite / silica co-precipitates and examining some of the associated properties. Conducting these reactions under a varied range of conditions will provide insight into the reactions occurring and how they are typically influenced. By preparing the composites ***via*** continuous crystallisation, information of greater relevance to both industrial and natural systems can be obtained.

The major themes of the project are the elucidation of the mechanism of co-precipitate formation and how this knowledge can be used to possibly influence the PG process as operated at Nyrstar Hobart, e.g. by identifying options that reduce zinc uptake or improve dewatering. Providing insights into the fundamental processes occurring during co-precipitation alone are very valuable. It will also allow us to determine the driving force behind the behaviour of certain species and allow us to predict how the process may be affected and provide possible solutions to associated problems that may arise.

2. SMALL-SCALE CRYSTALLISATION EXPERIMENTS AND CHARACTERISATION

2.1. Introduction

This chapter discusses the characterisation and analysis of iron oxide/silica samples produced from a continuous crystallisation reaction and the conclusions drawn based on the findings. A significant proportion of iron oxide research has employed non-continuous processes such as batch and sol-gel preparation (Tongpool 2004; Xu 2004; Predoi 2007; Soderberg 2007), continuous crystallisation differs by reaching and maintaining pre-determined reagent concentrations and pH. It better simulates dynamic systems in nature and industry that reach equilibrium and have a virtually infinite source of reagents (Cooper 1998; Loan 2006; Loan 2006).

The experiments described in this chapter are a simplified simulation of the precipitation step in the PG process. The complex matrix of materials in the industrial process makes characterisation of the residue difficult (Loan 2006), as well as clouding the study of some of the fundamental processes. By using pure analytical reagents, as opposed to plant liquors and calcine, it was possible to eliminate the factors of very high zinc concentrations, large amounts of added acid, trace impurities, and undissolved calcine particles. This provided a more practical focus on the behaviour of the iron and silicon species in solution and the phases precipitated.

The co-precipitates were prepared in the presence of three common anions, although the experiments focused predominantly on nitrate and sulfate. The sulfate experiments were of great importance, as there is an abundance of sulfate in zinc process liquors, due to the use of high concentrations of sulphuric acid during leaching. The impact of sulfate on the co-precipitate structure and properties will therefore also influence the effectiveness of impurity removal in the precipitation step. The comparison with nitrate served to show the significance of the anionic environment in which these materials are formed. Both of these anions are commonly associated with environments that produce iron oxide / silica composites

and can at least partially account for differences seen between systems. Experiments were also conducted in chloride media to provide another reference point with which to compare the data.

To obtain sufficient information on the reactions involved and the residues produced, several analytical techniques were required. XRD was highly important in this investigation for several purposes. Distinction between different iron oxide phases has proven to be generally possible from their characteristic diffraction patterns, although low proportion phases and similar amorphous phases can be more difficult to identify (Loan 2002). XRD also provided insight into the type of silica produced, be it amorphous or a more crystalline phase, such as quartz. Furthermore, XRD patterns aided in the determination as to whether the co-precipitates were a combination of pure phases (iron oxide(s) + silica) or were more like a single phase containing a mixture of iron and silicon.

Elemental concentrations obtained ***via*** ICP-MS and ICP-AES provided a measure of how the rate and extent of silica precipitation was governed by the presence of an iron oxide phase and other conditions. Surface charge measurements highlighted the different surface behaviours of some of the precipitates, showing the dependence on silica content and the anionic media in which the residue was formed. While these were the major techniques employed, laser Raman spectroscopy, attenuated total reflectance Fourier transform infra-red spectroscopy (ATR-FTIR), fractal dimension determinations and scanning electron microscopy all provided useful supporting information.

2.2. Experimental

A previous study has found that for the production of 6-line ferrihydrite in a continuous crystallisation system, an iron concentration of 6.3 g L^{-1} (0.113 M) is ideal (Loan 2006). This concentration was therefore used as the baseline for the silicon-free systems. The intention was to maintain constant ionic strength of the solutions across the systems as much as possible, such that when silicon was introduced, the concentration of iron would be reduced by the same amount as that of the silicon being introduced. For example, in the N-5-1 experiment the solution contained 0.0056 moles of silicon (5 % of 0.113) and 0.107 moles of iron (95 % of 0.113) per litre. However, due to the acid required to lower the pH of the dissolved silicate solution, and the differing proportion of caustic required for pH control, the ionic strength was impossible to completely control to a constant level. It may have varied by up to 5 %over the duration of a precipitation experiment.

The iron/silicon feed solutions were prepared immediately prior to the commencement of the experiments to minimise aging as a source of uncertainty. The sources of iron were ferric nitrate ($Fe(NO_3)_3.9H_2O$), sulfate ($Fe_2(SO_4)_3.7H_2O$) and chloride ($FeCl_3.xH_2O$). The silicon-free feed solutions were prepared by simply dissolving the iron source material in deionised water. Where silicon was required, sodium metasilicate ($Na_2SiO_3.5H_2O$) was dissolved and the pH was lowered to between 1 and 1.5 using the acid (Analytical Reagent Grade) corresponding to the iron source (for a ferric sulfate system, sulphuric acid was used). The sodium hydroxide solution was made using NaOH pellets dissolved to 8 M (320 g L^{-1}); small-scale solutions were produced in volumes of 1 L at a time.

The small-scale crystallisation apparatus (Figure 2.1) comprised of a reactor, three Gilson Minipuls 3 pumps, an impeller, a water bath and a pH/temperature probe with Walker meter. The pumps were used to provide continuous streams of reagent addition and corresponding removal of the reaction products, Masterflex norprene tubing was used in the pumps. One pump injected the iron/silicon feed solution, another provided a constant flow of sodium hydroxide solution to maintain the pH, while the final pump removed slurry at a constant rate.

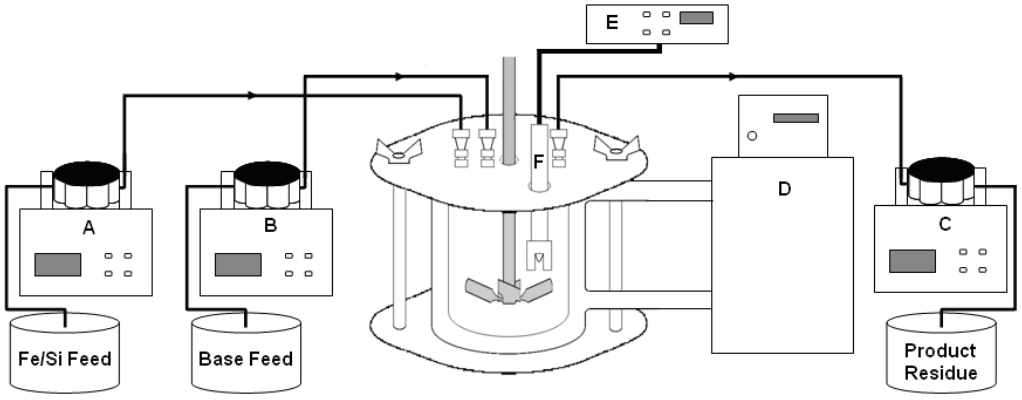

(a)

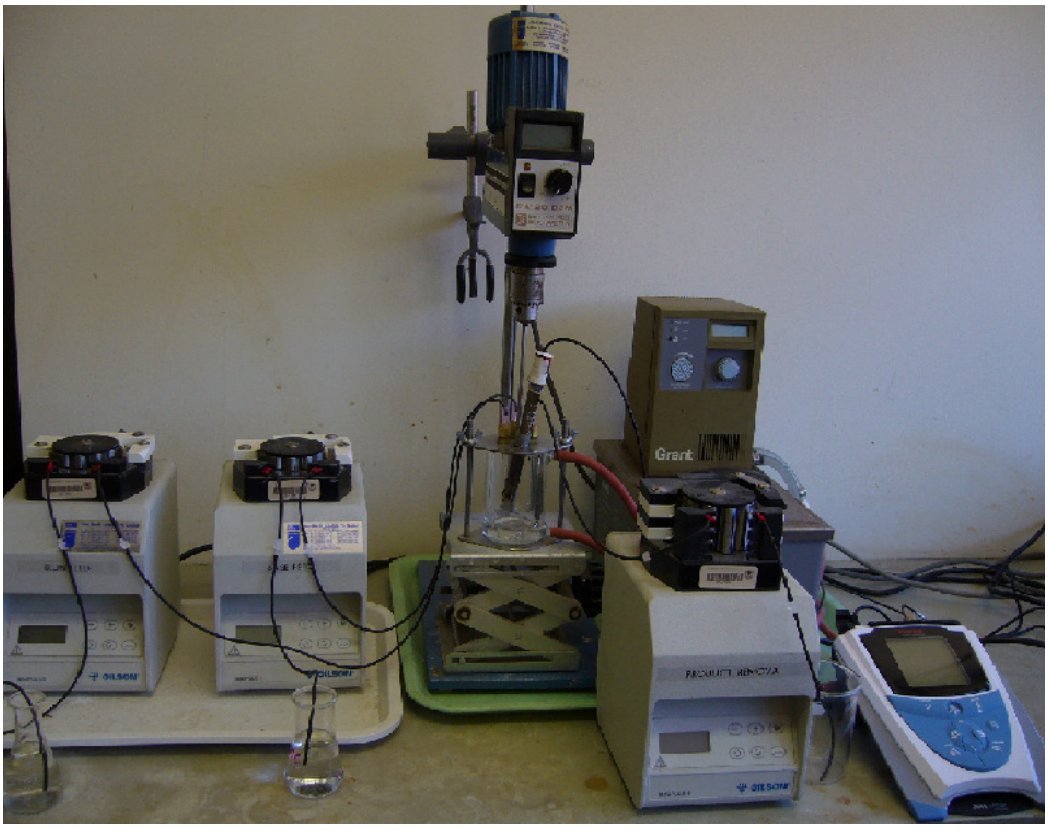

(b)

Figure 2.1: (a) Diagram of the precipitation setup. A, B and C are medical dosage pumps, D is a water bath feeding the reactor jacket, E is a pH meter and F is a pH probe and (b) photograph of actual apparatus in the laboratory.

The product removal served as both a sampling method and a mechanism for maintaining constant volume in the reactor. For all standard tests, the product removal rate was set to 147 ± 1 mL per hour. The iron/silicon solution feed rate remained approximately constant, while the rate of base addition changed depending on the composition and initial pH of the feed solution.

The reactor was a 110 mL glass container (5 cm internal diameter), which was jacketed and connected to a water bath to ensure a constant reaction temperature. A purpose-built stainless steel base and lid were produced to support and stabilise the reactor. The lid was removable and when attached was held in place with wing-nuts. It was also designed to hold the pH probe, with a 5 mm diameter hole at the centre for the agitator shaft and 3 needle entry points for the feed and product removal lines.

As a first step, some simple flow tests were conducted using water to calibrate the pumps to the correct liquid transfer rates. The flow rates would change depending on the solution viscosity and slurry solids loading in each test, and thus the initial tests only provided a general guide, with finer adjustments made for each system.

“Residence time” in this case refers to the time required for one full volume of the reactor to pass through under continuous operation of the system. At the point at which 110 mL of product has been removed from the reactor (also 110 mL of combined feed and base introduced) a single residence time has been completed. At the start of an experiment, the reactor was initially filled with deionised water, thus the concentrations of the chemicals steadily increased throughout the crystallisation process, reaching a plateau at similar levels to the feed solution. It has previously been shown that in this type of system, approximately six residence times are required to reach a steady-state in the system (Loan 2006), which was verified throughout the experiments described in section 2.4.

Throughout all standard experiments, the reaction temperature, pH and residence times were maintained at 85 °C, 2.65 and 45 minutes, respectively. The correct pH value at 85 °C was obtained based on the ideal pH at 33 °C, which is 3.5. To determine this, the reactor was heated to 33 °C, filled with 0.113 M ferric nitrate

solution and adjusted to pH 3.5. The pH was monitored while the temperature was then elevated to 85 °C, at which point the pH reading from the electrode was 2.65.

Slurry samples, taken from the reactor are identified by their corresponding residence time. For example, the RT 1 (residence time 1) sample corresponds to the slurry removed from the reactor during the first 45 minutes of the experiment thus producing 110 mL of material. The “reactor contents” relates to the remaining slurry left in the reactor upon completion of the experiment, at which point the pumps are switched off. This sample may sit in the heated reactor for some time (up to 30 minutes) before removal and preparation for analysis.

In an attempt to better simulate the industrial process, some crystallisation experiments were conducted with feed solutions containing varying concentrations of zinc. The zinc was introduced to the systems by dissolving zinc sulfate separately from the other constituents. This produced a slightly acidic (~pH 4) solution, in which the pH was adjusted down with sulfuric acid before being added to the iron and silicate feed solution. More detail on the procedure for such experiments is given in section 2.6.

A number of operating variables were considered and examined. The residence time was changed by adjusting the pump rates to decrease or increase the amount of time that slurry remained in the reactor. The concentrations of some constituents were varied either by adding a different amount or by the addition of other species (e.g. to increase sulfate levels, sodium sulfate was introduced).

The slurry was sampled for several different types of analyses; powder samples were used for X-ray Diffraction (XRD) and Laser Raman Spectroscopy, supernatant samples were analysed using Inductively Coupled Plasma – Atomic Emission Spectrometry (ICP-AES), and slurry samples were used for Dynamic Light Scattering (DLS). Solid samples were also taken for Transmission Electron Microscopy (TEM) and Pair Distribution Function (PDF) analysis, which will be discussed in a subsequent chapter.

Hematite standard samples were produced based on the process outlined by Sugimoto et al. (Sugimoto 1993); was selected as it offered monodisperse hematite particles that would be consistent and not complicated by impurities and therefore represent an ideal standard given how well the material has been characterised. Solutions of $FeCl_3.6H_20$ (2 M, 100 mL) were stirred by a mounted agitator, with 5.4 M NaOH (100 mL) added over a period of 5 minutes. The solution was continuously stirred for a further 10 minutes before being placed in an oven at 100° C for a period of 10 days. The brown suspension initially observed is expected to go through phase changes, from a mixture of ferrihydrite and goethite to solely goethite, before finally producing pure hematite ***via*** a series of dissolution and reprecipitation steps. Once removed from the oven and cooled the hematite slurry was used in light scattering experiments as a standard in fractal dimension analysis. SEM was also carried out on hematite samples which had been dried onto SEM stubs and sputtered with gold.

2.2.1. X-ray Diffraction

Samples for XRD were generally derived from the entire slurry volume produced in a particular residence time. They were vacuum filtered using a 47 mm diameter Supor® membrane with a 0.45 m pore size. The filter cake was washed with deionised water and left to dry in an oven at 60 °C for several days. The solid samples were then crushed in a mortar and pestle to form a powder and either packed into flat aluminium XRD sample holders or delivered for analysis.

Curtin University's Siemens D500 powder diffractometer employs a copper source (40 kV, 30 mA) producing Cu K emission. Diffraction patterns from this instrument were taken from 3 to 70 degrees 2 theta with a step size of 0.02 and a step length of 1 second. The Phillips X'Pert powder diffractometer used at CSIRO Process Science and Engineering, Waterford, contains a cobalt long fine focus tube. Measurements were taken between 5 and 90 degrees 2 theta with a step size of 0.02 and a step length of 1 second. The majority of XRD analyses were obtained with the CSIRO instrument, as iron species (especially those containing sulfate) flare under the characteristic radiation frequency from Cu K emission.

2.2.2. Elemental Analysis

ICP-AES was employed to quantify the proportion of each element being precipitated relative to that remaining in solution. To measure this, supernatant samples were taken from the slurries and filtered through two 0.45 m syringe filters to remove all solids. A sample of the feed solution was obtained to compare the initial and final concentrations of elements. Both ICP-AES Vista and 735-ES instruments were utilised for the analysis.

2.2.3. Light Scattering and Dynamic Light Scattering

The zeta potential of various samples was investigated using the Malvern Zetanano DLS analyser using the Phase Analysis Light Scattering (PALS) technology. This analysis required a more rigorous sample preparation than first anticipated. Initially, buffer solutions were prepared at pH 2, 3, 4, and 5, using 100 mM concentrations of the required reagents (see Table 2.1). However, this proved to be an unsuitable procedure, as the buffer species interacted with the precipitate in suspension, adsorbing on the surface and altering the surface charge. As a result, all samples analysed produced much lower than expected IEP values.

Table 2.1: Composition of buffer solutions for DLS.

pH	Reagent 1 / Concentration (mol L^{-1})	Reagent 2 / Concentration (g L^{-1})
2	Phosphoric Acid / 0.0446	Disodium Phosphate / 0.0054
3	Phosphoric Acid / 0.0286	Disodium Phosphate / 0.0214
4	Citric Acid / 0.0325	Trisodium Citrate / 0.0175
5	Citric Acid / 0.0183	Trisodium Citrate / 0.0317

A revised sample preparation protocol was therefore introduced. Slurry samples (50 mL) were dialysed in 2 L volumes of deionised water for 7 days, with the dialysate being changed for fresh water every 24 hours. Subsamples were taken and adjusted to the desired pH using nitric acid and sodium hydroxide, where appropriate. Fresh subsamples were used for each pH value. Approximately 1 mL of each sample was loaded into a specialised u-shaped cell (Figure 2.2) and analysed using a Malvern Zetanano DLS particle sizer.

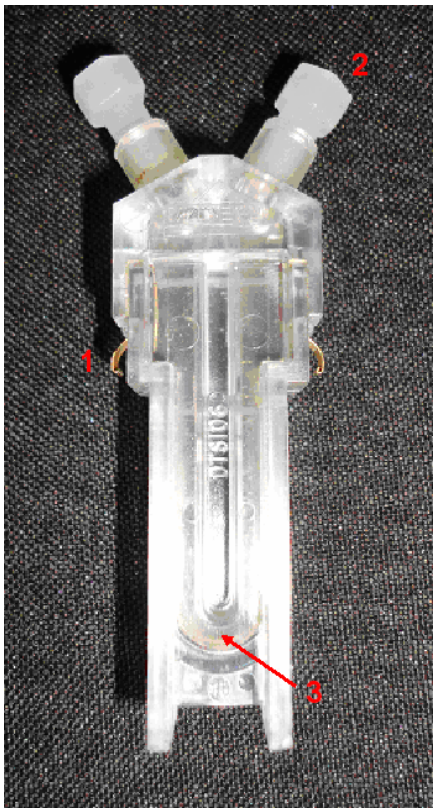

Figure 2.2: The U-shaped cell used in the Zetanano particle sizer to obtain zeta potential measurements. Current is passed through the slurry ***via*** electrodes (1) on either side which induces the electrokinetic movement. The labels (2) and (3) indicate the filling inlets and the point at which the velocities of the particles are measured respectively.

Samples from the chloride series of experiments were also used in an attempt to determine a fractal dimension from light scattering data. Slurry was taken and dialysed in deionised water for 7 days, the water being replaced every 24 hours (as for DLS) to prevent further silica polymerisation. The samples were then analysed using the particle size distribution routine of a Malvern Mastersizer 2000, in which

the slurry is added to MilliQ water under agitation and light scattering is used to measure particle size. A spreadsheet (provided by Malvern Instruments, UK) converts the Malvern scattering data into Microsoft Excel and calculates the log of the angle and intensity values for each detector. Upon plotting this data, the fractal dimension can be obtained from the gradient of the curve taken from the linear region. Similar methods have been used in the study of latex aggregates (Selomulya 2001) and silica particles flocculated by cationic polymers (Zhou 2006), the fractal dimension measurement of aggregated alumina particles has also been correlated with rheological properties (Franks 2004).

2.2.4. Laser Raman Spectroscopy

Laser Raman spectroscopy provided additional characterisation of co-precipitate structure. Grains were simply sub-sampled from the powders created for XRD. A Dilor Labram model 2b dispersive Raman spectrometer was used. Calibration was conducted using a neon lamp, which has a sharp emission spectrum of precise and well known frequency response. The laser is focussed on a single grain of sample and the scattered photons are collected and compiled by the instrument and software. Scans were collected between 100 and 1150 cm^{-1}, for which multiple measurements were made to provide a series of patterns and to detect sample deterioration.

2.2.5. ATR-FTIR

Attenuated Total Reflectance – Fourier Transform Infrared (ATR-FTIR) spectroscopy was used on silicate solutions prepared to the same concentration as some feed solutions for the small-scale reactor experiments. The purpose of this analysis is to determine whether silica polymerisation would occur spontaneously at reaction concentrations, and if so on what time-scale. Solutions of 0.0226 and 0.0564 M sodium metasilicate were prepared, followed by an adjustment of the pH to reaction level (3.5) using hydrochloric acid. Before each measurement, the signal obtained from milliQ water was obtained to be subtracted from that of the samples.

Measurements were taken at 0 hours (minutes after the solutions were prepared), 5 hours, 29 hours, 5 days and 10 days after preparation.

2.3. Silica Solution Stability

2.3.1. Silica Polymerisation in the Feed

Understanding the potential effects of an aged silicate feed solution was also a subject of interest. In early experiments, feed solutions were on occasions prepared days in advance, and for those containing Si species it was necessary to determine whether polymerisation could occur prior to the precipitation reaction. ATR-FTIR (section 2.2.5) was carried out on silicate-loaded solutions to observe the vibrations associated with silica polymerisation (Si – O – Si). The solutions were prepared at two concentrations typical of the co-precipitation experiments, with measurements taken immediately upon preparation and at increasing time intervals.

The characteristic peaks of silica are situated at 810 and 1100 cm^{-1} (section 1.3.3) and there are related hydroxyl groups peaks between 3400 and 3800 cm^{-1}. Increases in absorbance in the silica bands and possible decreases in the bands related to the hydroxyls would be expected as silicic acid monomers condense. The spectra in Figure 2.3 (the 0.0226 M solution) do display a relative increase over time in the 1100 cm^{-1} peak compared to the broad hump centred on ~3400 cm^{-1}. This suggests that there was a significant amount of silica polymerisation and that the proportion of hydroxide groups associated with silicon atoms was diminishing.

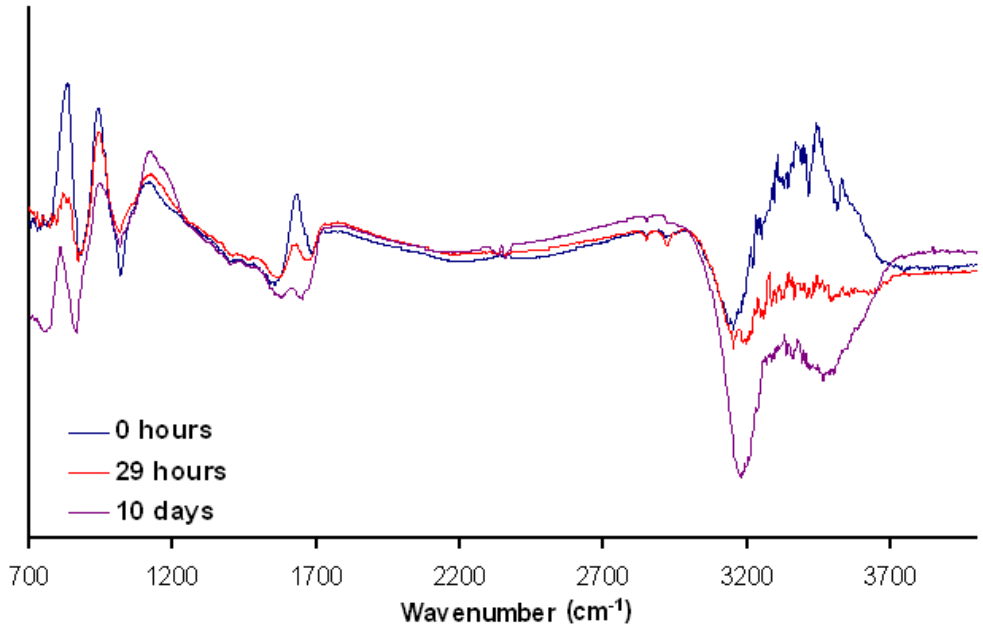

Figure 2.3: Infrared spectra obtained from the 0.0226 M sodium metasilicate solution at pH 3.5 at 0 hours, 29 hours and 10 days.

Figure 2.4 contains similar data for the more concentrated system. It can be seen that the 1100 cm^{-1} peak was greater even at the initial stages than in the 0.0226 M solution. This polymerisation was most likely induced by the addition of acid during the feed preparation; dropping the pH to such a degree decreases the solubility of silica markedly. Polymerisation occurs to a greater degree in this solution as the higher concentration leads to a higher level of supersaturation. As in Figure 2.3, silica polymerisation occurs to a greater extent at each time interval, even out to 10 days, as the kinetics of this reaction are slow. Kinetically fast reactions would have reached equilibrium in a short period, which would thus produce similar patterns between extended time frames.

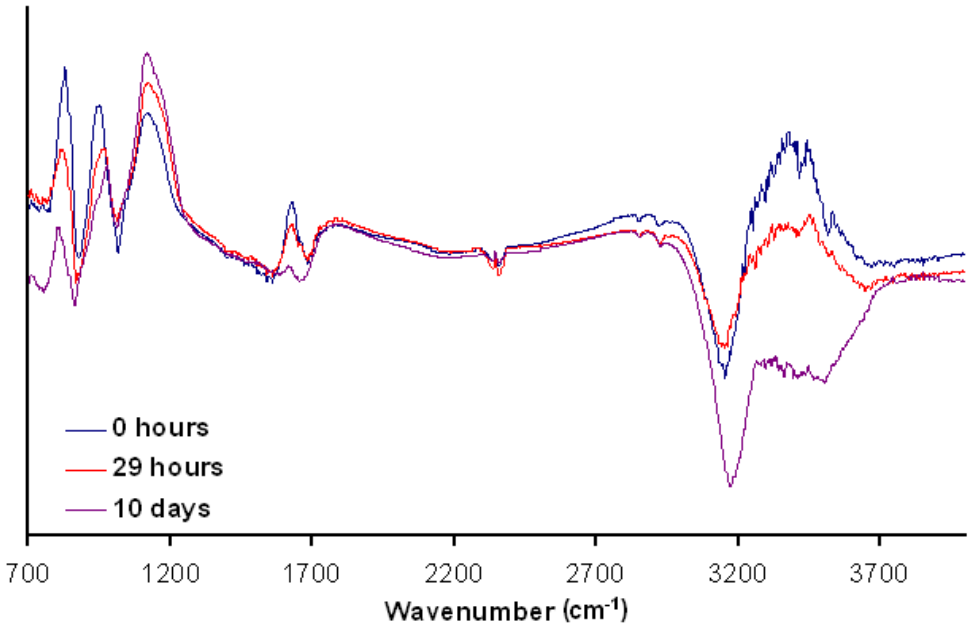

Figure 2.4: Infrared spectra obtained from the 0.0564 M sodium metasilicate solution at pH 3.5 at 0 hours, 29 hours and 10 days.

It should be noted that the correction for the background was fairly poor for the 10 day samples, as there was an apparent negative adsorption (3000 to 3700 cm^{-1}). This was most likely due to the use of pure water as the background solution, whereas an electrolyte solution containing the same concentrations and at the least the same pH of the sample should have been used. The lower pH in the samples is a possible contributor to this effect, as the apparent negative adsorption is in the hydroxyl region. Irrespective of this oversight, the conclusion that silica polymerisation would occur in solution over time is inescapable. Therefore any feed solutions with significant silicate concentrations left to stand for time before use would contain somewhat polymerised species, as opposed to pure monosilicic acid. As a consequence of these findings, the feed solutions were prepared as close to the commencement of experiments as possible.

2.3.2. Silica Polymerisation in the Product Slurry

As stated in section 1.3.2, in solutions of low pH, silica begins to polymerise spontaneously (albeit slowly) at concentrations in the order of a few hundred parts

per million. Given this fact, it was considered a distinct possibility that solution aging could have an impact on the reactions being investigated. The sampling procedure for supernatant elemental analysis was to extract and filter a volume of the slurry immediately after each residence time. Silica polymerisation is a relatively slow process, but a non-trivial amount of silicates remained in solution, and therefore further polymerisation could occur between completion of the precipitation reaction and sampling from the product collection vessel.

As the samples are constantly removed throughout the duration of the experiment, the majority of the slurry spends some time in the collection vessel before filtration. To determine whether this could have a substantial impact one set of experimental conditions (Si:Fe ratio of 0.429, for further detail see Table 2.4, system N-30-1) was repeated using different sampling and preparation methods. The product slurry of one experiment was filtered at the end of each residence time, while the other was continuously fed into a filtration system, thereby being filtered immediately after removal from the reaction vessel. The data presented in Table 2.2 suggests that there was no significant silica precipitation when samples were filtered upon completion of the residence time. In fact there appeared to be a greater residual silicon concentration in the supernatant solution where this method was applied. This was simply normal fluctuation between experiments and perhaps reflected very slight dilution in supernatant collection in the immediately filtered system.

Table 2.2: Elemental concentrations in supernatant solutions taken from steady-state samples of experiments in with different sample handling procedures. In one experiment product slurry was filtered at the end of the residence time (up to 45 minutes after removal from the reactor) and the other filtered immediately upon removal from the reactor.

System	Fe Concentration ($mg\ L^{-1}$)	Si Concentration ($mg\ L^{-1}$)
Filtered at end of residence time	0.69	89.6
Filtered immediately	0.39	75.8

2.4. Initial Scoping Experimental Series

A series of experiments were conducted to provide an initial screening of the behaviour of the iron and silicon containing species under a range of reagent concentrations (Tables 2.3 and 2.4). Knowledge of the solution and residue properties was required to demonstrate the impact that each element / solution species had on the other. The data acquired from these systems also provided the direction for further more detailed investigations.

Table 2.3: Masses of reagents required in each system. The letter in the coding system refers to the primary anion present (N = nitrate, S = sulfate, C = chloride), the first number refers to the Si / (Si + Fe) ratio of the system and the second number refers to the iteration of that experiment (some where repeated) or a particular condition.

System	Mass Ferric Nitrate (g)	Mass Ferric Sulfate (g)	Mass Sodium Metasilicate (g)
N-0-2, S-0-1	45.6	29.7	0
N-5-1, S-5-1	43.3	28.2	1.20
N-10-1, S-10-1	41.0	26.7	2.39
N-20-1, S-20-1	36.5	23.7	4.79
N-30-1, S-30-1	31.9	20.8	7.18

Table 2.4: Experiments producing the samples referred to in this section. Ideal feed concentrations are given; small variations occurred but are insignificant with regard to influencing the reaction.

System	Conditions					
	Feed Concentration		pH_{85}	Residence Time	Temp (°C)	Anion present
	Fe (g L^{-1})	Si (g L^{-1})				
N-0-1	6.3	0	3.00	45 min	85	NO_3^-
N-0-2	6.3	0	2.65	45 min	85	NO_3^-
N-5-1	6.0	0.16	2.65	45 min	85	NO_3^-
N-10-1	5.7	0.32	2.65	45 min	85	NO_3^-
N-20-1	5.0	0.63	2.65	45 min	85	NO_3^-
N-30-1	4.4	0.95	2.65	45 min	85	NO_3^-
S-0-1	6.3	0	2.65	45 min	85	SO_4^{2-}
S-5-1	6.0	0.16	2.65	45 min	85	SO_4^{2-}
S-10-1	5.7	0.32	2.65	45 min	85	SO_4^{2-}
S-20-1	5.0	0.63	2.65	45 min	85	SO_4^{2-}
S-30-1	4.4	0.95	2.65	45 min	85	SO_4^{2-}

2.4.1. Structural Analysis

The first experiment completed was N-0-1, from which samples were collected for XRD analysis. The measured pattern showed predominantly 2-line ferrihydrite (Figure 2.5). This was a clear indication that at least one of the reaction conditions for the experiment favoured the formation of 2-line ferrihydrite over 6-line, i.e. either the temperature was too low, the iron concentration too high or the pH too high (section 1.2.2.1). Given that control of temperature and reagent concentration were known to be sufficient, a test was then conducted to determine the exact pH which would produce the intended product. The reactor was filled with 6.3 g L^{-1} ferric nitrate solution and heated to 33 °C, at which point 8 M NaOH solution was added to

achieve the intended pH of 3.5. Once a steady pH was reached the temperature was raised to 85 °C at which point the pH was measured. This provided the correct pH_{85} of 2.65 required to operate under.

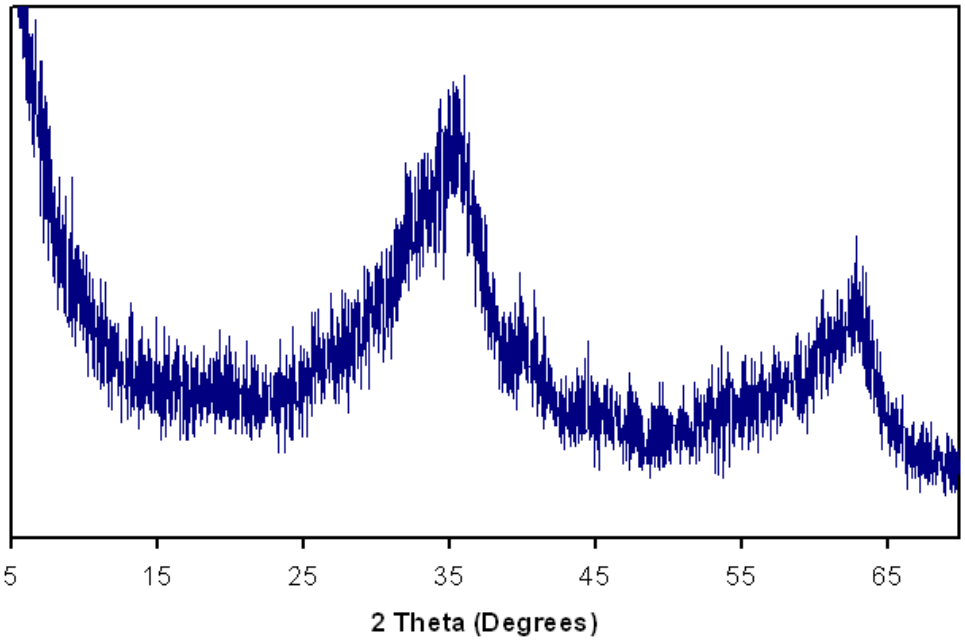

Figure 2.5: XRD pattern of steady state sample from N-0-1.

The products from all residence times for each system in Table 2.4 were analysed to view the progression over time. There was expected to be some formation of more crystalline phases early in the experiment, when the concentrations of species in the reactor were low. However, this was not obvious in most systems, suggesting that this was not a significant effect in a small environment such as this. Figure 2.6 displays the XRD pattern of samples collected from each residence time of S-10-1 as an example, showing that there was little difference in the phases present over the full duration of the experiment.

Given that an industrial system runs at steady-state (unless operations need to be shut down), the most interest is in the properties of samples from the latter residence times. It was also necessary to be certain that steady-state was indeed reached by the sixth residence time, as had been concluded from earlier studies of the Paragoethite system (Loan 2004). To establish this, several systems were run over eight complete

residence times (a total of six hours) to investigate whether any precipitate properties or reaction conditions changed. The XRD results from system S-10-1 shown in Figure 2.6, also includes results from the additional residence times.

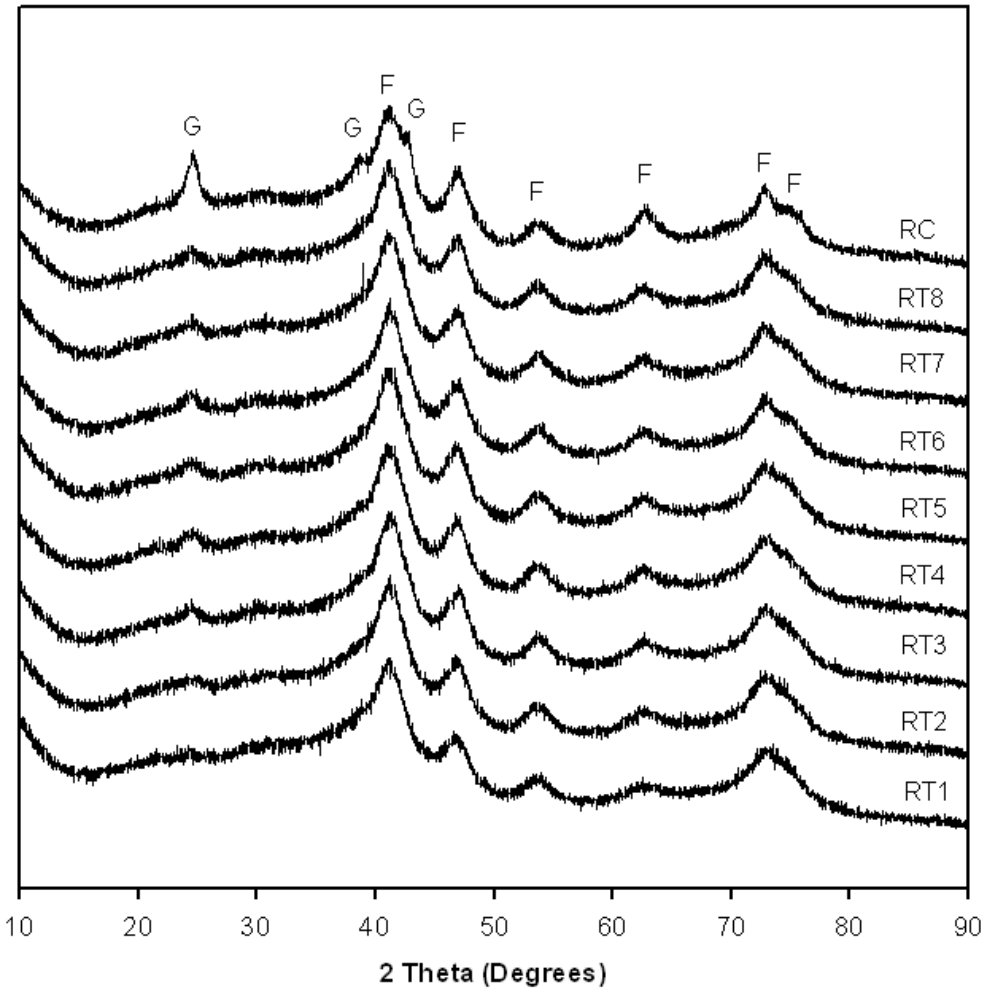

Figure 2.6: XRD Patterns of samples from all eight residence times and the reactor contents (slurry remaining in reactor at the completion of the experiment) from S-10-1. The samples are shown in sequence from the first residence time (bottom) to the eighth residence time (second top) and reactor contents (top) as signified by the labels (RT = residence time, RC = reactor contents). G refers to goethite peaks and F to ferrihydrite.

XRD patterns in Figure 2.6 show slight differences in the first four residence times but do not vary beyond that in the continuous samples. The conclusion was therefore reached that steady-state is reached by the sixth residence time, this was confirmed through elemental analysis (discussed in sections 2.4.3).

The peaks and shoulders observed in the reactor contents sample not attributable to ferrihydrite are associated with poorly crystalline goethite (Cornell 1996) and are observed in the reactor contents of many of the silica-containing systems. This phase is produced from Fe(III) solutions ***via*** transformation of ferrihydrite, which acts as a metastable intermediate.

There are multiple possibilities as to why goethite is found only in the reactor contents. Incomplete mixing could, in principle, affect the system in this way. The reagents are added a few millimetres from the surface of the reaction mixture. The iron and base feeds are laterally 2 cm apart and between 2 and 4 cm from the region from which the product is removed. There may be more than one nucleation zone in the reactor, containing different conditions and therefore hydrolysis rates. The reagents could also be added and subsequently react at the top, being removed from (in effect short-circuiting) the reactor soon after while the rest of the solution contains lower than intended concentrations of iron, silicates and hydroxide. The lower hydrolysis rate would favour the formation of the more crystalline material.

It is possible that the low concentrations of reagents in the liquor during the first residence time leads to the more crystalline phase being formed. Low silicate concentrations may limit polymerisation across the ferrihydrite particle surface, allowing the initially formed particles to transform. However, such products would be expected to be predominantly removed during the first residence time. Goethite particles tend to be larger and more densely aggregated; such material may be preferentially positioned in the lower regions under poor mixing and not well sampled by the shallow needle. Neither possibility seems likely under the agitation conditions applied in these tests. Alternatively, the 18 gauge needles may not adequately collect large aggregates.

The final reactor contents are allowed to stand for a time prior to sampling at 85 °C and with the absence of new feed the reagent concentrations will be reduced. This provides the opportunity for slow hydrolysis reactions that may lead to the formation of small amounts of goethite, and could explain why the material is not found in any of the continuous samples. This is the most likely explanation in the author’s

opinion. These scenarios may all be possible but further investigation is required to determine which, if any, occurs and causes this phenomenon.

2.4.2. Ferrihydrite Crystallinity and Silica

On comparing the XRD patterns of sampled solids from the nitrate systems, the effect of silicon on the precipitate structure becomes apparent. Increasing the silicate concentration in the feed solution led to the apparent crystallinity of the ferrihydrite being decreased (Figure 2.7), inferred from the broadening of the main peaks and the smaller peaks fading into the background signal. This demonstrates not only that the presence of soluble silicates during the precipitation process alters the final product, but the extent of the impact is dependent on the concentration of the silicate in the feed. The other noticeable difference was the broad peak situated around 25 to 30 degrees that appears and increases in intensity with increasing silicate. This peak is attributed to amorphous silica, suggesting that the phase was produced in significant volumes in systems containing greater silicate levels (Hernandez 2007).

The XRD pattern of system N-0-2 (containing no Si in the feed) displays the presence of the more crystalline phases, goethite and hematite, at significant levels. There also appears to be a small amount of hematite in N-5-1 adding to the intensity and sharpness of some peaks. However, beyond this there is no evidence of any phase other than ferrihydrite in any samples from the nitrate system. The iron content in the systems decreased from N-0-2 to N-30-1, which would slow the hydrolysis rate. This in turn should favour the formation of more crystalline phases. Therefore the presence of soluble silicates during precipitation inhibits the formation of these species, an effect noted in other research (Mazzetti 2002).

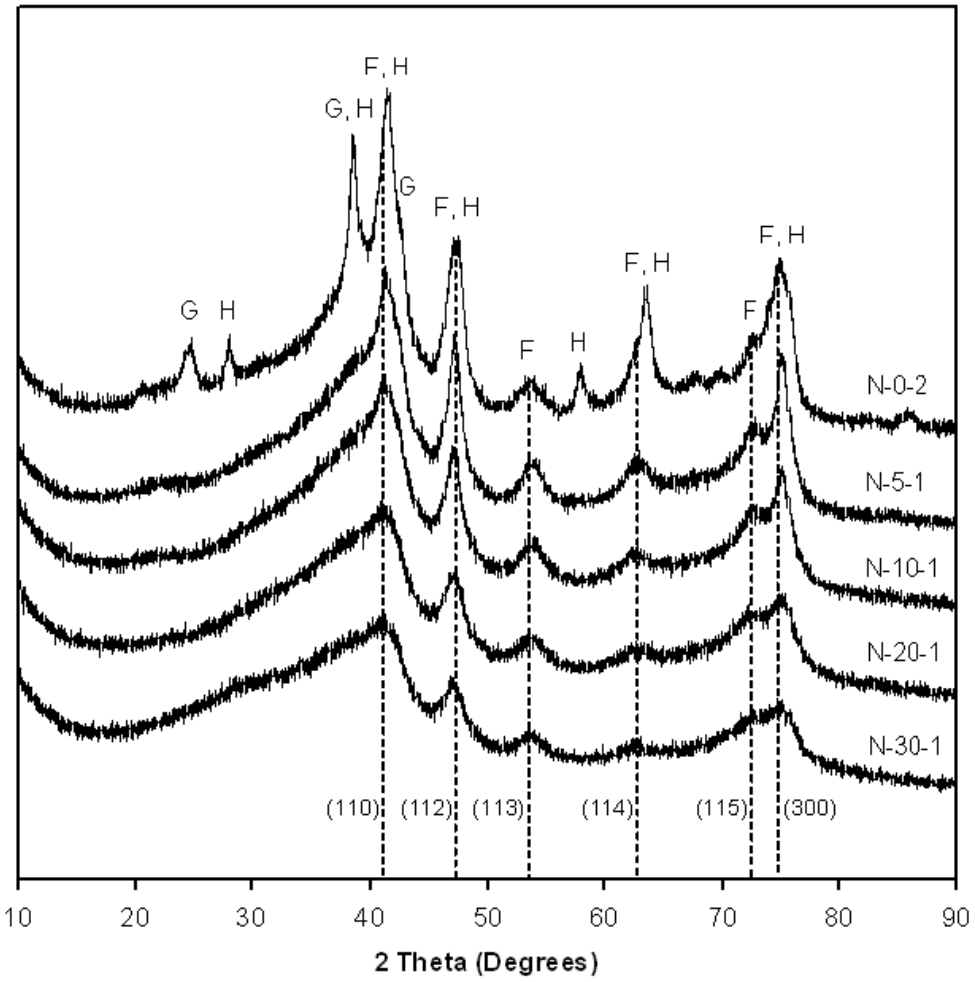

Figure 2.7: XRD patterns from the steady-state samples from each of the five experiments carried out in nitrate media. G refers to goethite peaks, H to hematite and F to ferrihydrite.

Interestingly, the trend of decreasing crystallinity with increasing Si levels is not as apparent in the sulfate systems (Figure 2.8). The peaks show perhaps a small degree of broadening, but no obvious effect is observed. All six characteristic ferrihydrite reflections appear and are distinct even in the system with the greatest presence of silicate. As the concentrations of both iron and silicon and the reaction conditions (temperature, pH etc) are all identical to those in the nitrate systems, the anionic species themselves must be influencing the reactions. Similar to the nitrate systems, goethite is observed in the silica-free precipitate but in none of the others, again providing evidence that there is some effect from the presence of silicates. The

amorphous silica peak at low angle is present, although less obvious than in the nitrate systems.

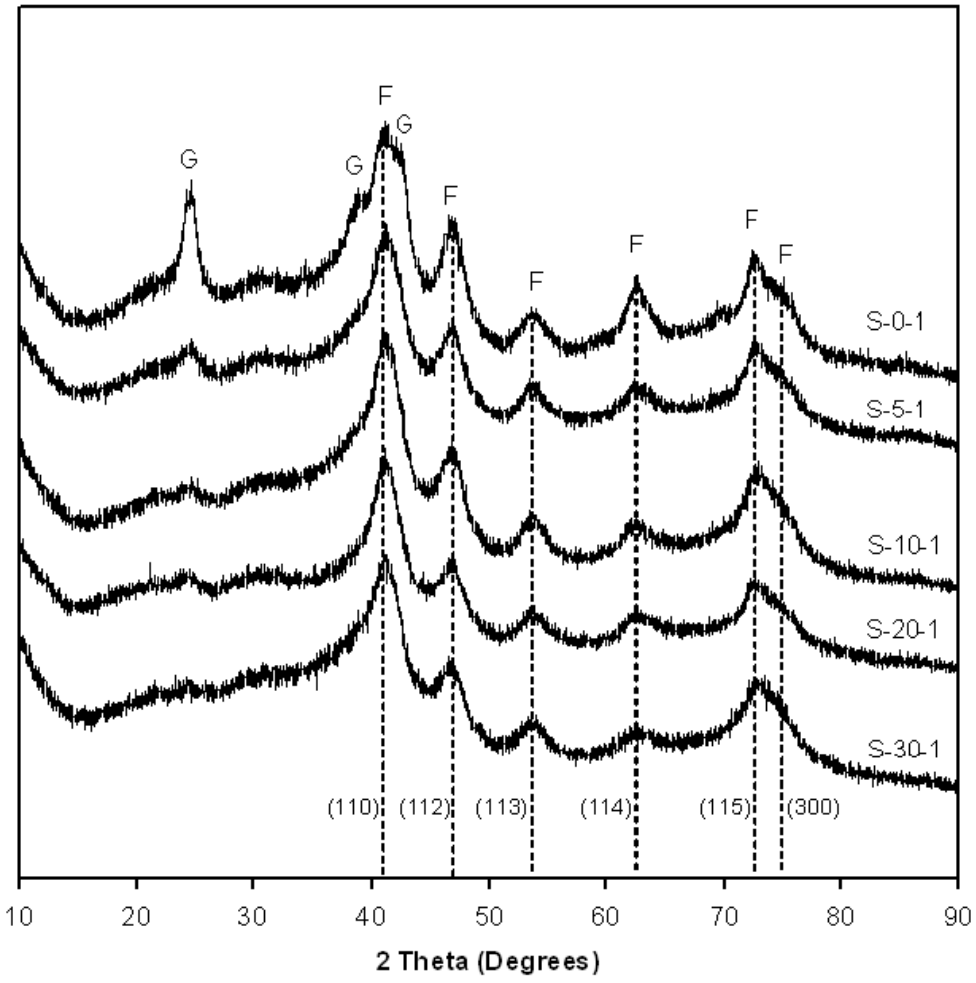

Figure 2.8: XRD patterns from the steady-state samples from each of the five experiments carried out in sulfate media.

As has been the case in many studies involving iron precipitation in sulfate media, schwertmannite also appears to be present. It has a very similar structure and therefore XRD pattern to ferrihydrite, making it difficult to distinguish in mixtures. However, the sharpening of the (110) peak, the decline in the prominence of the (112) reflection and the reversal of the relative intensities of the (115) and (300) peaks all suggest that a significant amount of schwertmannite has been produced along with ferrihydrite. While the goethite in the S-0-1 sample makes it difficult to

judge whether the presence of silicates has an effect on the production of schwertmannite as it convolutes the peaks, there is little difference in the patterns as the silicate concentration increases. The patterns all appear to display a mixture of ferrihydrite and schwertmannite at a similar ratio, suggesting the silicate concentration has little or no impact on the proportions at which the materials are produced. This will also be analysed further with the use of XRD line profile analysis (Table 2.5), Laser Raman spectroscopy (Figure 2.13, Figure 2.14) and PDF analysis (chapter 4).

As mentioned in section 1.2.3.1, it has been proposed that there is no structural difference between 6-line and 2-line ferrihydrite (or any phase that lies between), and the crystallinity is only defined by the size of the coherent scattering domain. Therefore, it would be reasonable to suggest that as silica adsorbs onto the ferrihydrite surface it interrupts further crystal growth, thus decreasing crystallinity by limiting the particle size. However, in many cases where particle crystallinity is affected by the presence of other species, it is due to defects or boundaries formed by the inclusion of that species in the crystal structure. It may then possibly be that the silicon is substituted into the ferrihydrite lattice, altering its structure. It is therefore necessary to determine whether the silicon is incorporated into the structure and alters it, or if it is instead retarding the growth of the ferrihydrite primary particles.

There are multiple mechanisms for the production of goethite and hematite, including the transformation of the metastable ferrihydrite in solution (or at temperature). This transformation is the most likely source of goethite and hematite in the N-0-2 and S-0-1 samples; this may provide an insight into the observed influence of Si. The solution transformation involves dissolution of the meta-stable ferrihydrite and re-precipitation of the more crystalline phase. Silica on the surface of the particles may interrupt this process by stabilising ferrihydrite against dissolution or providing a barrier between the particles and solution.

Peak position in XRD patterns is a simple and reliable method for determining whether or not the structure has been significantly altered. A peak shift should be observable if different elements have been substituted into the crystal structure. Unfortunately, peak shifts can be disguised by overlapping reflections, variations in

instrument parameters and numerous other factors. An internal standard was therefore introduced into the samples to allow accurate quantification of any peak shift associated with the presence of silicon. These standards are materials of high crystallinity and accurately known peak positions, providing sharp, well-defined peaks and in essence calibrating the angular measurements.

Calcium fluoride was selected as the internal standard because many of its peaks do not appear at the same angles as the major ferrihydrite peaks. It was introduced to the sample powders (weighed out to be approximately 5% of the powder mass) prior to micronising, thus ensuring proper dispersion throughout. The patterns that were collected presented sharp, intense peaks associated with CaF_2, from which it was possible to adjust the sample data as required (Figure 2.9). The less intense reflections from the sample and standard tended to interfere somewhat, as they were either at similar angles or directly adjacent. Initially, a simple peak-finding program was used to obtain the peak positions. However, due to the broadness of the peaks, more complex methods were required and line profile analysis was employed.

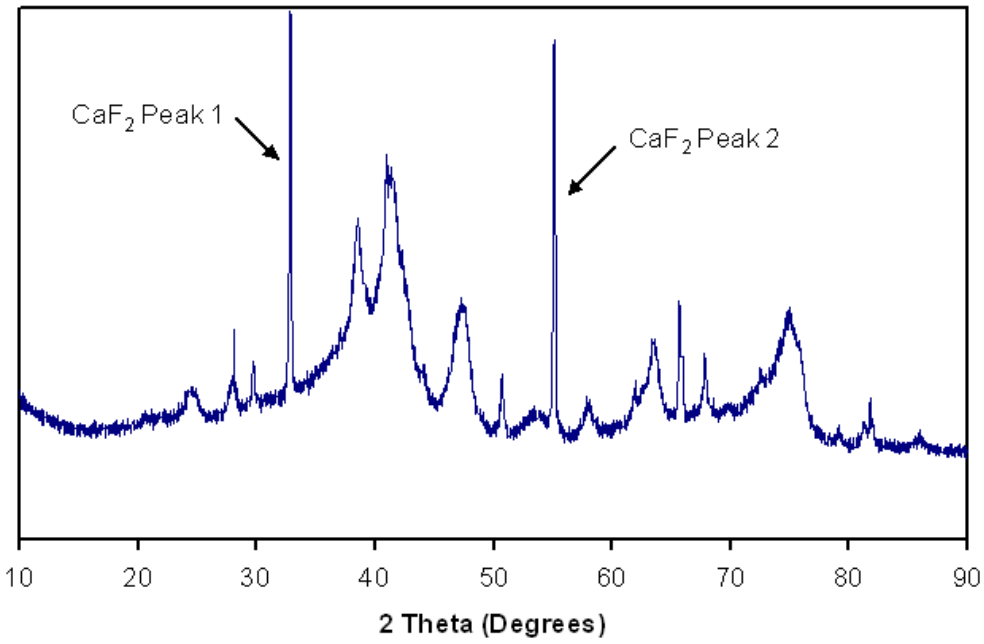

Figure 2.9: XRD pattern obtained from N-0-2 doped with CaF_2 internal standard.

In cases of amorphous samples, getting full width at half maximum (FWHM, a standard measure of peak width) and peak positions is difficult, and therefore pattern fitting is necessary. The program xfit (Cheary 1996) was used to do line profile analysis of the patterns. The Pseudo Voigt function which is an approximate form of the Voigt function, which describes peak broadening and is given in Equation 2.1 (Voight 1912), was applied to fit the data. This fits a series of symmetrical peaks calculated such that their combination with a background function follows the experimental XRD trace. The user selects the number of peaks to be fitted and once a satisfactory fit has been achieved, values for the peak position, FWHM, the shape and area of each peak, along with error values for each fitted quantity can be extracted.

Equation 2.1: $$\boldsymbol{V}(\boldsymbol{x};\ ,\ ) = \int_{-\infty}^{\infty} \boldsymbol{G}(\boldsymbol{x}';\ )\boldsymbol{L}(\boldsymbol{x}-\boldsymbol{x}';\ )\boldsymbol{dx}'$$

Line profile analysis was conducted in this manner on samples both with and without an internal standard. The patterns for samples containing an internal standard were used to quantify the peak positions with respect to CaF_2. Calculated co-precipitate peak positions were compared against those for the samples with the internal CaF_2 standard to check for consistency. The samples without an internal standard were then used to obtain FWHM values, as the extra peaks from the CaF_2 complicate the patterns, and simplicity is desired for the analysis. The interference between some sample and standard peaks increases the difficulty and uncertainty associated with FWHM calculations.

The expected peaks from each individual phase are deconvoluted as part of the line profile analysis process. The peaks in the majority of the samples overlap. In cases where there are many peaks, such as that shown in Figure 2.10 for the N-0-2 sample, the combined peaks become broad and complex, the errors associated with deconvolution then increase and the fit becomes more prone to influence from the user. In addition, the presence of goethite, hematite and schwertmannite influences the broadness of ferrihydrite peaks, as they often appear at adjacent or identical angles. For this reason, the silica-free samples may not offer useful FWHM data for comparison to the other systems.

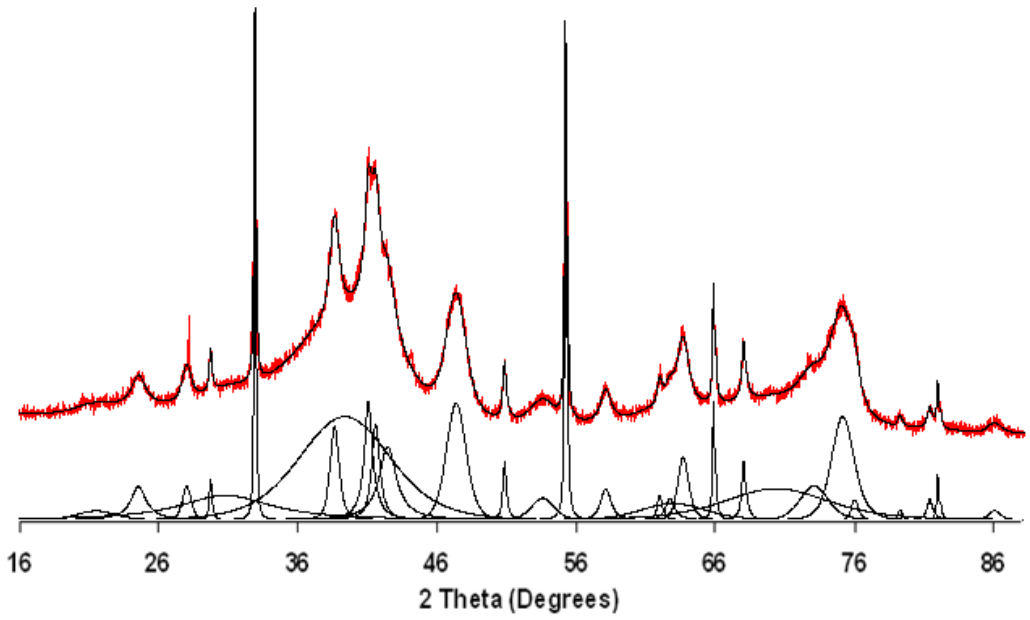

Figure 2.10: XRD peak fit from xfit analysis on the N-0-2 doped with CaF_2.

Figure 2.11 contains the calculated peaks for pure N-0-2 and displays the overlap of reflections from the mixture of phases. In some cases, a single calculated peak contains the reflections of more than one phase, which has little impact on the peak position but can greatly warp the FWHM calculated. Calculated values for all samples are provided in Table 2.5.

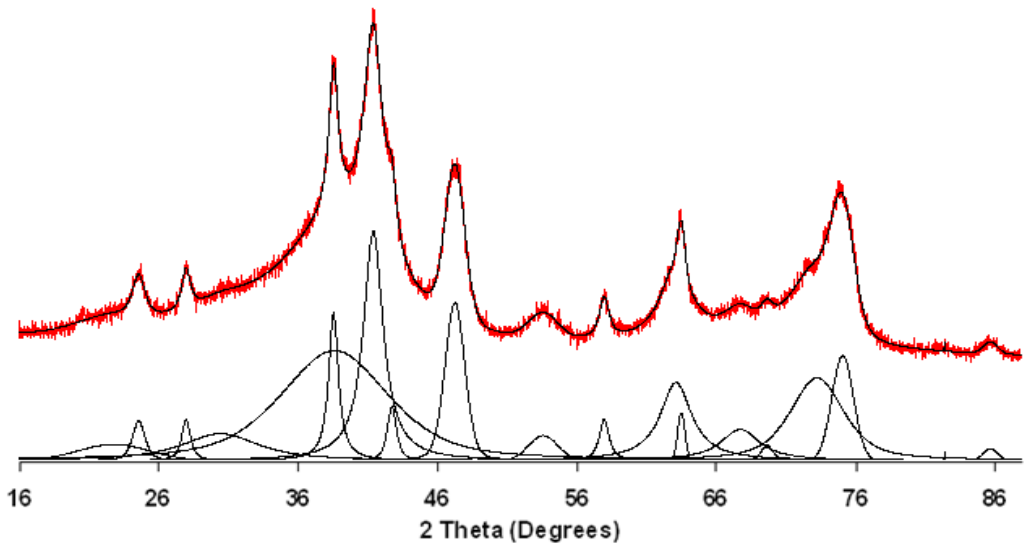

Figure 2.11: XRD peak fit from xfit analysis on the pure N-0-2 pattern.

Table 2.5: Data calculated from peaks fit to XRD patterns using xfit.

	Calculated peak positions from samples doped with CaF_2 (° 2)								FWHM from pure samples (° 2)		
System	CaF_2 Peak 1	CaF_2 Peak 2	(110)	(112)	(113)	(114)	(115)	(300)	(112)	(115)	(300)
N-0-2	32.8	55.1	41.5	47.3	53.4	63.5	72.9	74.9	1.69	4.55	1.81
N-5-1	33.0	55.2	41.9	47.2	53.9	62.6	72.7	75.2	1.35	3.73	1.32
N-10-1	32.9	55.2	41.7	47.2	53.9	63.0	72.8	75.3	1.52	4.06	1.52
N-20-1	33.0	55.2	41.9	47.3	53.8	63.1	72.9	75.4	1.88	5.41	1.97
N-30-1	33.0	55.2	41.8	47.3	53.9	62.9	72.8	75.4	2.01	6.47	2.08
S-0-1	32.8	55.0	41.7	46.6	53.6	62.7	72.5	75.2	2.10	1.89	2.83
S-5-1	32.9	55.2	41.4	47.0	53.8	62.7	73.0	75.3	2.20	2.57	2.89
S-10-1	32.8	55.0	41.4	46.9	53.7	62.5	72.8	75.1	2.14	3.20	2.69
S-20-1	32.9	55.1	41.2	47.0	53.9	64.2	72.7	75.4	2.15	2.85	3.27
S-30-1	32.9	55.1	41.5	46.9	53.7	62.8	72.9	75.2	2.14	2.72	2.49

The calculated peaks from the diffraction pattern of N-30-1 shown in Figure 2.12 indicate the absence of more crystalline phases from the residue. The pattern contains only characteristic peaks of ferrihydrite and the low angle broad reflection of amorphous silica. The analysis of all samples provided an important insight into the (110) ferrihydrite peak. All the systems studied here, as well as equivalent patterns found in literature (Dutrizac 1987; Cornell 1996; Schwertmann 1999; Mazzetti 2002), display a typical asymmetry of the reflection. While this is always labelled as a single peak, the asymmetry actually suggests a combination of two or more peaks. The modelling conducted here shows that assuming two peaks contribute to the (110) peak provides an excellent fit for the measured data. Calculated diffraction patterns based on structural models of ferrihydrite often show two peaks appearing where experimentally only the (110) peak is observed (Jambor 1998), which suggests that two reflections may occur here and would be observed if sharp peaks were able to be practically measured.

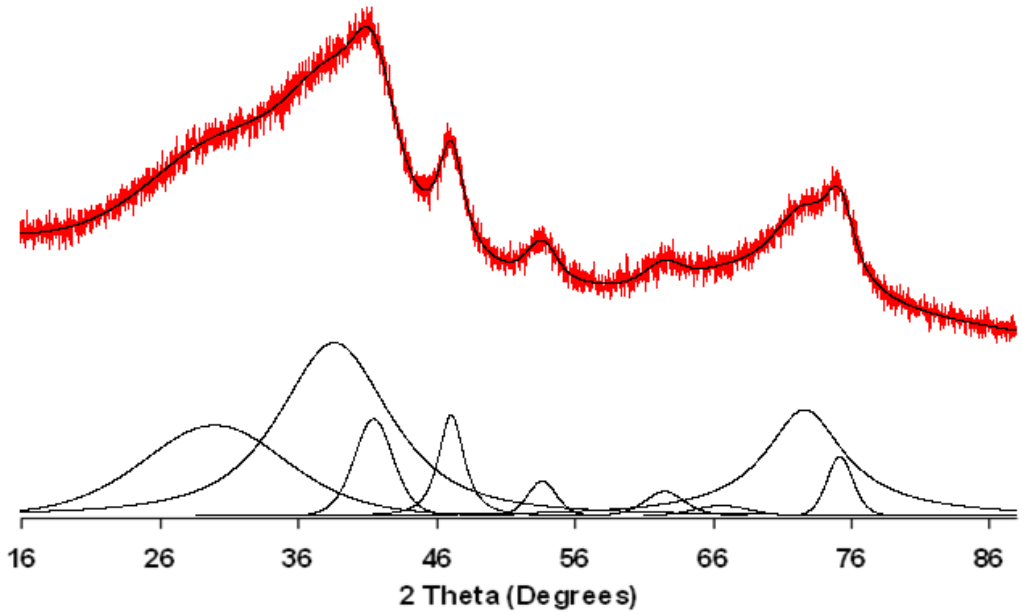

Figure 2.12: Peak fit from xfit analysis on the pure N-30-1 pattern.

The relative position of the characteristic CaF_2 peaks to each other was constant to within 0.06 degrees in the nitrate patterns and 0.01 in the sulfate patterns. Such differences result from normal experimental uncertainty. This correlation suggests that sample reflections have little if any influence on the positions of internal

standard peaks. The absolute positions of the main CaF_2 peaks in the patterns fluctuated slightly but were constant to within 0.2 degrees in all patterns. The variance was again greater in the nitrate patterns than sulfate, but not to a sufficient extent to suggest any interference from the sample.

There was also some variation in the calculated position of the sample reflections but that would appear to be more of an effect of uncertainty and overlapping than any difference in structure. The largest difference, given in the (114) peak between N-0-2 and N-5-1, is 0.9° 2 (Table 2.5), equating to a d-spacing change of 0.0022 nm, which is not of great enough significance to indicate a structural alteration. The error associated with calculated peak positions was less than 1 %, for full width at half maximum values the error was generally less than 10 %, although for some weak and/or overlapping reflections it was between 10 and 20 %. In addition, if the presence of silicates during precipitation were to change the structure, then it would be expected that the greatest difference should occur in the sample with the highest Si content (N-30-1).

The sample peaks vary more than the internal standard as they are less sharp and of lower intensity. As a consequence, the associated error quoted by the fitting program is greater, indicating the slightly reduced accuracy to which it can calculate the peak position. Although no evidence of structural inclusion of silicon was found from this analysis, TEM and PDF analyses were conducted for further, more detailed investigation and are discussed in chapter 4.

The observed peak broadening in the nitrate samples as the presence of soluble silicates in the feed was increased proved quantifiable (Table 2.5). The FWHM measurements show that peaks became broader with the further addition of silicates during precipitation. While theoretically, samples free of silica should be the most crystalline, the FWHM values obtained were greater from N-10-1 and N-5-1 than N-0-2. However, this is a misleading result, as it is influenced by several other factors. As mentioned earlier, the presence of other phases interferes with the calculation of the FWHM values, and N-0-2 has multiple phases. The presence of the more crystalline phases also means that a proportion of the ferrihydrite has been transformed. If there is a slight variation in the crystallite size and the smaller or

larger crystalline proportion was preferentially transformed over the other, then the overall crystallinity would be altered. Due to these factors, the silica-free samples produced in both nitrate and sulfate media can be omitted from comparison in good faith.

The calculated peaks in the sulfate patterns did not show the same trend for the FWHM values, which either remained approximately constant or varied arbitrarily as silicate levels increase (Table 2.5). The observation from patterns in Figure 2.7 and Figure 2.8 that the series does not follow the same declining crystallinity as displayed by the nitrate data is thus confirmed by the analysis. The basis for this discrepancy is discussed in section 2.4.3.

Laser Raman spectroscopy was employed to further analyse the structure of the precipitates. While some flaring occurred in initial measurements, it was overcome with little difficulty by using an appropriate filter to decrease the beam intensity. The nitrate systems produced spectra with peaks at angles corresponding to ferrihydrite (Mazzetti 2002) (~370, ~510 and ~710 cm^{-1}). Precipitates formed in sulfate produced similar major peaks, but with shoulders at (~300 and ~410 cm^{-1}) similar to those expected from the presence of schwertmannite (Figure 2.13).

From the data obtained through the use of this technique, evidence was obtained supporting the conclusions based on the XRD data in terms of the phases present in the co-precipitates (Figure 2.13). While laser Raman spectroscopy did not generate any new information in this regard, it did display an interesting property of the materials. As noted in multiple sources, the presence of silicate during ferrihydrite precipitation stabilises it against transformation, both as dry solid at temperature and in contact with solution (Mazzetti 2002; Jones 2009). The energy from the laser beam was able to transform the samples, which was another reason that the beam filters were required. It was observed that using the same filter, the silica-free sample transformed to hematite, while many of the silica-containing systems remained unchanged (Figure 2.14). This is further proof of the influence of co-precipitated silica in stabilising the ferrihydrite structure.

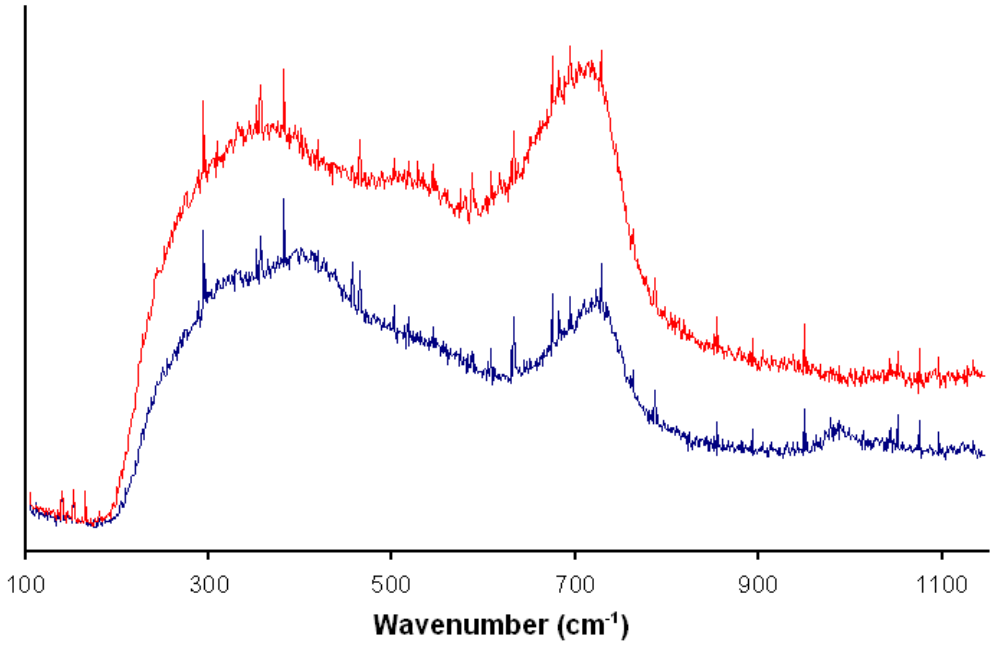

Figure 2.13: Laser Raman spectra obtained from reactor contents samples from the N-5-1 (red) and S-5-1 (blue) experiments displaying the slight differences due to the presence of schwertmannite in the S-5-1 sample.

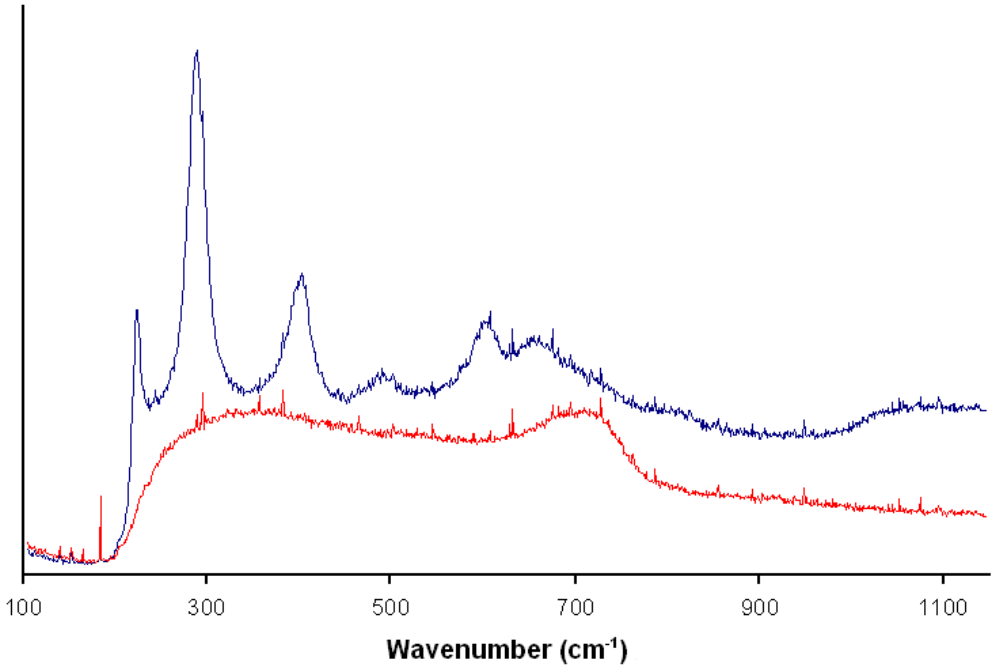

Figure 2.14: Laser Raman spectra obtained from reactor contents samples from the N-0-2 (blue) and N-20-1 (red) experiments. It can be seen that the N-20-1 spectrum appears as ferrihydrite, while the N-0-2 sample contains the sharp peaks at ~222, ~287 and ~399 cm^{-1} indicative of hematite.

2.4.3. Elemental Composition

Elemental solution concentrations were used to gauge the consistency of the reaction at a point defined as steady-state, as well as to investigate the proportions of constituents being precipitated. The concentration of elements from samples of each residence time were determined and compared. For a true steady-state, the values should plateau to a relatively constant value.

Figure 2.15 shows that the concentration of silicon increased over time, reaching a plateau with little variation beyond the third residence time. The iron concentrations tended to fluctuate more as a percentage of the measured concentration, but the magnitude of variations between residence times were not significantly greater than for silicon. Figure 2.15 is representative of the general behaviour of iron and silicon in all experiments.

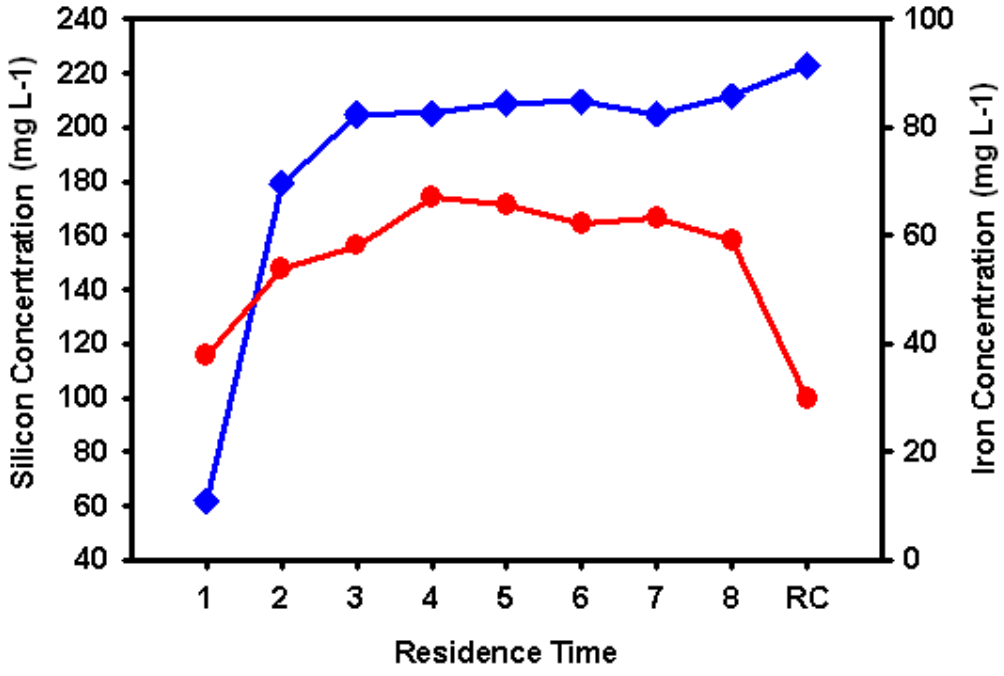

Figure 2.15: S-10-1 as an example of iron (red) and silicon (blue) concentrations measured on samples from each residence time.

The concentrations of iron, silicon and sulphur (where appropriate) were measured in the feed solution and the supernatant solutions taken from product slurries. By comparing these, the proportion of the constituent being reacted and appearing in the precipitate can be calculated. Table 2.6 contains the elemental concentrations in the supernatant solutions and percentages of the elements in the feed that were removed from solution during the reaction.

Table 2.6: Elemental concentrations obtained from supernatant solutions of the sixth residence time samples of each experiment and their associated precipitation percentage. The percentage given is the proportion of the original amount of each element removed from solution ***via*** the co-precipitation reaction.

Sample	Fe in liquor (ppm)	% Fe Precipitated	Si in liquor (ppm)	% Si Precipitated
S-0-1	179	97.2	-	-
S-5-1	61.5	99.0	119	25.00
S-10-1	59.1	99.0	212	33.3
S-20-1	88.6	98.2	433	31.7
S-30-1	99.7	97.7	696	26.9
N-0-2	0.38	>99.9	-	-
N-5-1	8.14	99.9	71.7	54.8
N-10-1	<0.2	100	19.3	93.9
N-20-1	0.81	>99.9	87.2	86.3
N-30-1	0.69	>99.9	89.6	90.6

Sulphur concentrations were also tested, but initial results were unreliable and latter results showed no obvious trend between sulfate adsorption and the concentration of silicate present. This may be due to the higher uncertainty based, on large concentrations of sulphur in the solutions. It may also indicate the absence of an effect of silicate on sulfate ion behaviour in the scope of these experiments.

Although less than 3% of the initial iron remained in solution in all cases, there was still a significant difference between the nitrate and sulfate systems. In all but one of the nitrate experiments, the residual iron concentration dropped below 1 ppm, whereas no sulfate solution measured below 50 ppm. Although this effect may be considered negligible in high concentration environments, it becomes highly significant where there are low initial iron concentrations or purity is required in the final solution.

In all cases there was a greater concentration of silicon remaining in solution than iron. Given that the initial concentrations of iron were well in excess of those for silicon, a much greater proportion of the initial silicon remained in solution. This reflects the higher solubility of the silicates under these conditions. However, this is not simply a case in which silica precipitates to the point at which the silicates in solution are below the level of saturation.

Based on the findings of Marshall (Marshall 1980) for nitrate solutions at 85 °C, the residual silicon concentrations in the nitrate systems are well below the equilibrium solubility. Interpolating their results to 85 °C, the level of silicon in solution at equilibrium is expected to be approximately 195 ppm. It appears the ferrihydrite surface, which presents binding sites for silicic acid monomers, promotes silica precipitation beyond normal levels governed by solubility alone. The equilibration times involved in silica solubility testing are generally at least several hours. The 45 minute residence time in the current study should not provide the opportunity to reach the equilibrium solubility, showing the catalytic effect of the ferrihydrite surface. This type of effect is observed in many systems (Alexander 1953; Marshall 1980; Chen 1982) in which a surface providing adsorption or nucleation sites for particle formation, growth or polymerisation increased the precipitation rate and proportion of the species removed from solution.

A much greater proportion of the silicates remain in solution where sulfate was present as opposed to than nitrate. The silicon concentration remained well above the theoretical equilibrium saturation (approximately 190 ppm (Chen 1982)) in S-10-1, S-20-1 and S-30-1. This displays the influence of sulfate on the co-precipitation process as silica solubility in nitrate and sulfate media only differ by ~5 ppm. The

percentage of Si precipitated remained relatively constant across the series of increasing Si:Fe ratios. It was also at a much greater percentage than for the nitrate systems, suggesting that there was some disruption to the co-precipitation reaction. Given the evidence that silicate species adsorb on precipitated ferrihydrite particles and subsequently polymerise, the presence of sulfate appears to interfere with one or both of these processes.

All the steady-state solutions from sulfate systems carried a Si concentration greater than the expected equilibrium solubility. This further demonstrates the retarding influence of sulfate on the templating effect of the ferrihydrite surface. The 45 minute residence time did not allow the systems to reach equilibrium, in terms of solubility, in the reactor before removal and sampling without the iron oxide particles inducing faster precipitation. In Chen and Marshall's (Chen 1982) experiments, the solutions stood for more than ten hours to equilibrate.

Sulfate ions are known to associate strongly with iron in solution and adsorb to iron oxide particles such as ferrihydrite; in contrast, nitrate ions bind weakly. The sulfate ions would therefore be more likely to compete with silicates for binding sites on the ferrihydrite surface. With less opportunity for adsorption of monomeric silicic acid, silica precipitation would be left to occur spontaneously in solution, which is much less likely.

The data suggests that the adsorption on the ferrihydrite surface provides a template and polymerisation occurs more easily across the surface as no nucleation event is required. There have been other reported circumstances of sulfate impeding the formation of silicon containing species. During hydrothermal treatment of zinc oxide and silica in acid, willemite (Zn_2SiO_4) was formed in the presence of hydrochloric acid, however, sulphuric acid converted all of the zinc oxide into zinc sulfate (Kodaira 1975).

2.4.4. Surface Behaviour

Dynamic light scattering ***via*** the Malvern Zetanano particle sizer proved ineffective for measuring particle size on the samples studied here. As mentioned in Section 2..2.3, the instrument uses scattered light to measure particle velocity due to Brownian motion. Hence there is an upper limit to the particle size that can be measured, as larger particles behave differently and can influence the motion of smaller particles. The upper limit quoted for the instrument is 6 m. Using a Malvern Mastersizer on other samples, it has been found that the PSD range fro the samples produced extends from the hundreds of nanometres to well in to the tens of microns. In the majority of the samples, more than 50% of the particles were greater than the 6 m upper limit that can be reached using the Zetanano, and therefore the Malvern Mastersizer instrument was preferred for sizing purposes.

However, the Zetanano instrument was still able to provide zeta potential measurements on the samples. Given the driving force of the particle motion in this case is the applied current, larger particles are less of a negative influence on the process. As mentioned in section 2.2.3, buffers were initially used for pH control. However, when similar results (IEP below pH 6) were obtained from N-0-2 (a system containing no silica) it highlighted the problems with the measurement procedure, as the IEP values of iron oxides are expected to range from 7 to 10 (Cornell 1996). It became apparent that the buffer species were adsorbing onto the precipitate surfaces, influencing the results. Plant precipitate slurries obtained from the Hobart refinery were also tested in this sequence of measurements. The precipitates appeared to behave as though they had significant proportions of silica on the surface as the IEP for each system was below 6 (Figure 2.16). This was initially considered astounding, given the relatively low silica content of some samples and complexity of the plant materials.

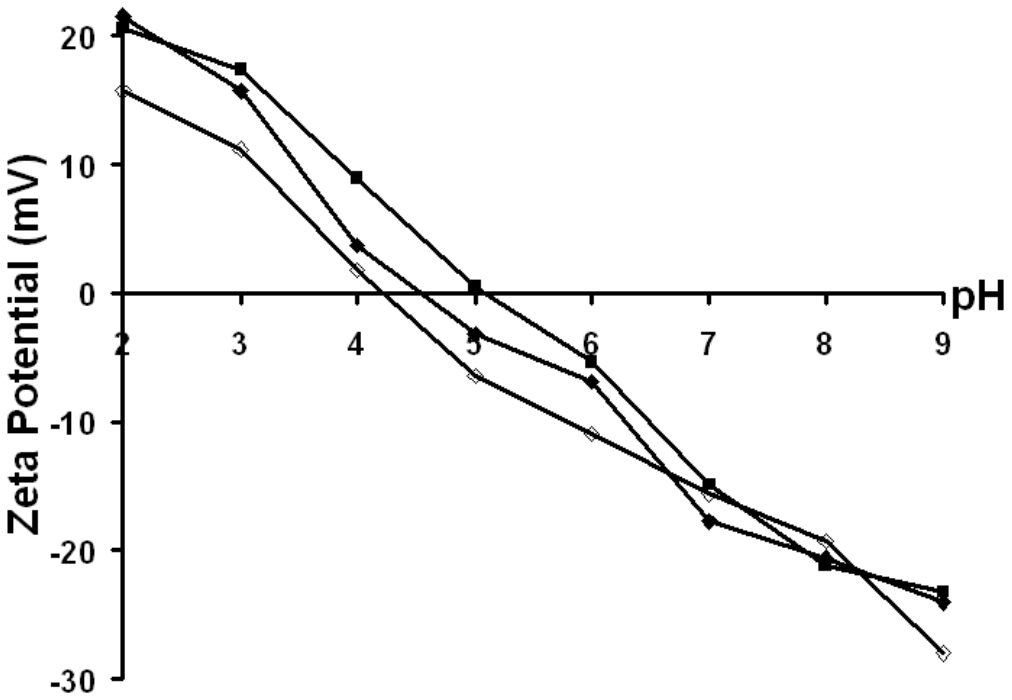

Figure 2.16: Zeta potential measurements from a series of samples produced in Paragoethite process simulation experiments. The distinction between measurements is not shown as that information is inconsequential.

Several approaches to achieve pH adjustment without interference were examined. Samples were dialysed to remove interfering ions while strong acids and bases were trialled as pH modifiers. Nitric acid was preferred, due to its much weaker association with the iron phase, thus limiting adsorption and influence on the results. Dialysis proved necessary and was conducted on all samples obtained for surface charge analysis (section 2.2.3). Zeta potentials were then measured on samples containing no silica and those containing the greatest proportion of silica prepared from both nitrate and sulfate media (Figure 2.17).

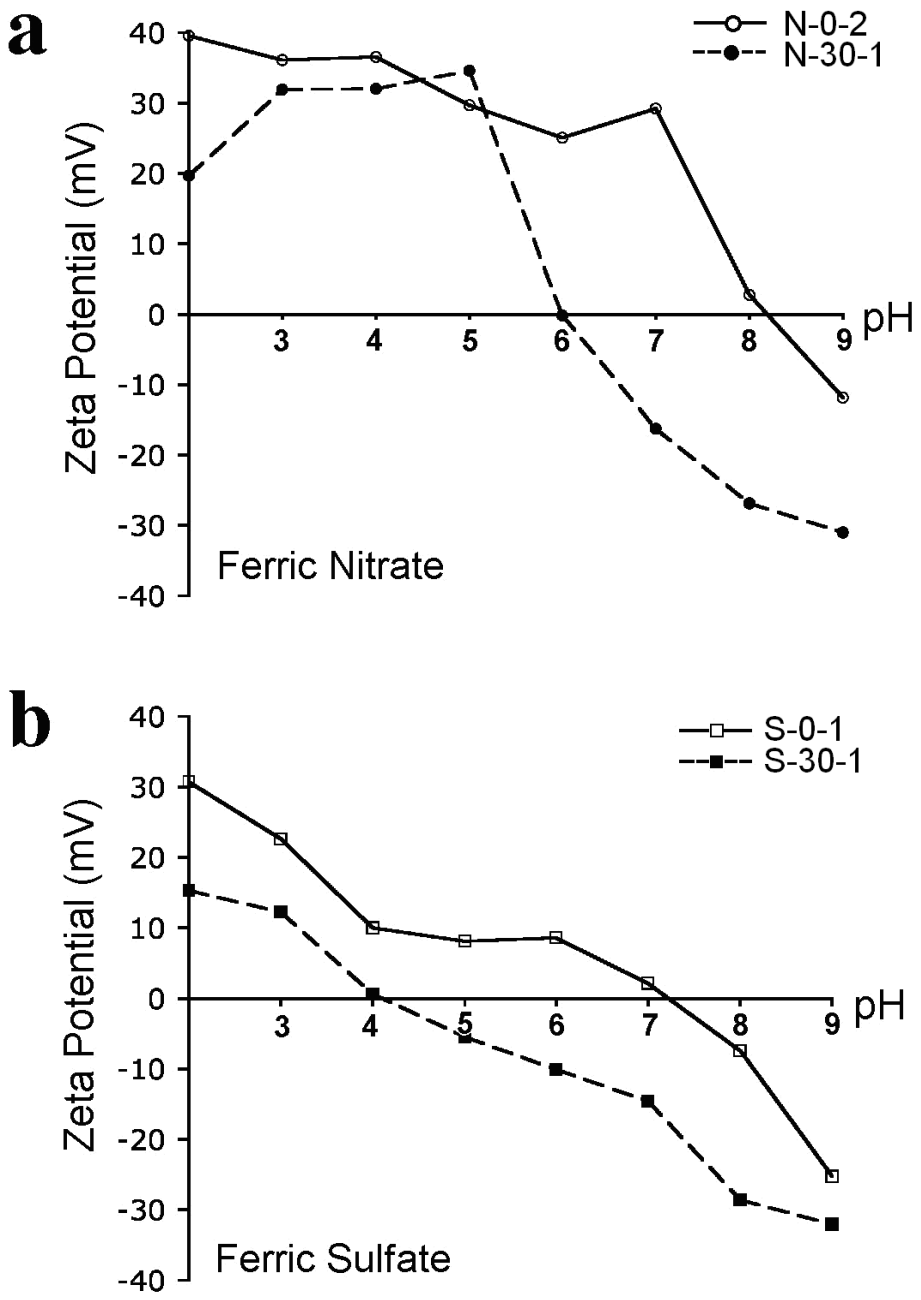

Figure 2.17: Zeta potential measurements conducted on samples from (a) N-0-2 and N-30-1 and (b) S-0-1 and S-30-1. These measurements were obtained following dialysis and strong acid / base pH adjustment, as opposed to buffers.

Over the pH range tested (2-9), all samples passed through an isoelectric point (IEP). Both systems displayed a marked decline in the value of the IEP with the introduction of Si. This was to be expected, as the IEP for ferrihydrite is

approximately 8 while that for silica is stated as being anywhere between 0 and 4, but is generally accepted as about 2 (Kosmulski 2003). As silica occupies some of the co-precipitate surface, the IEP should represent a combination of the two, thereby appearing between 8 and 2.

The products formed in the presence of sulfate had lower IEP's and did not reach the same positive magnitude at low pH. This was due to the adsorption of sulfate on the particle surface. Although the samples were dialysed, it is difficult to remove all adsorbed sulfate without chemical treatment or pH adjustment. Therefore the negative ions adsorbed on the surface, lowering the zeta potential and giving a decrease in the IEP. Interestingly, there was still a significant drop in the IEP between S-0-1 and S-30-1, despite the lower amount of silica in the precipitates from the sulfate system and the relatively low IEP of the Si-free sample. It stands to reason that the majority, if not all, of the silica is therefore located at or near the surface.

N-30-1 would be more representative of the pure co-precipitate surface, due to the lack of influence from adsorbed sulfate ions and a greater Si:Fe ratio in the residue. The observed decline in IEP means that the aggregation and adsorption behaviour of residue will change, based on the pH of the system. The difference would be most marked in a system of neutral pH; and pure ferrihydrite would have a positive surface charge, whereas a co-precipitate similar to N-30-1 would be negatively charged. This would create opposite interactions with charged species, and the co-precipitate would weakly repel negatively charged ions (such as sulfate) that would be attracted to the pure ferrihydrite surface.

Plant liquors have high concentrations of sulfate, and hence the sulfate systems are more representative of plant residues. The lower zeta potential magnitude and IEP observed will decrease the repulsive force between particles, increasing the prospect of aggregation. During the precipitation and thickening portions of the process, the pH may range from 2.5 (pH at 85 °C, pH_{85}) to just above 4. The thickener is not heated and therefore the temperature is lower and slightly variable. The decrease in temperature would lead to a corresponding increase in pH, affecting the surface properties of the slurry.

2.5. Experiments at Greater Silicate Concentrations

Precipitates were prepared from systems containing a greater proportion of Si to determine whether the effects observed in other systems would increase in magnitude. Co-precipitates containing greater Si, which would be expected to have lower crystallinity, would also prove valuable in later analyses, such as PDF and TEM.

Three systems prepared from liquors of different anionic species were examined, each containing Si:Fe ratios of 1. Co-precipitation reactions were conducted in nitrate, sulfate media and a combination of the two (described in Table 2.7). The third system (designated NS) was prepared using ferric nitrate as the iron source but with sulphuric acid used subsequently to adjust the pH of the silicate solution.

Table 2.7: Experiments producing the samples referred to in this section. Ideal feed concentrations are given (variation occurred due to experimental uncertainty).

System	Conditions					
	Feed Concentration		pH	Residence Time	Temp (°C)	Anion present
	Fe ($g\ L^{-1}$)	Si ($g\ L^{-1}$)				
N-50-1	3.2	1.6	2.65	45 min	85	NO_3^-
S-50-1	3.2	1.6	2.65	45 min	85	SO_4^{2-}
NS-50-1	3.2	1.6	2.65	45 min	85	NO_3^- & SO_4^{2-}

2.5.1. Structural Analysis

As can be seen on comparison of the XRD patterns obtained from N-50-1 and those residues containing lower Si:Fe levels (Figure 2.18), the propensity of silicates to decrease the crystallinity of ferrihydrite continues to increase at higher silicate

concentrations. This follows the expected trend and observations of Schwertmann and Cornell (Schwertmann 2000), who describe using the presence of soluble silicate to favour the formation of less crystalline ferrihydrite. Considering a possible mechanism, it is reasonable to assume that with greater silicate concentrations and lower iron levels in the reaction liquor, the collisions between newly formed ferrihydrite particles and silicic acid monomers would be much more frequent, while less frequent between ferrihydrite growth units. The kinetics of the adsorption of silicic acid on the ferrihydrite surface would be greater, thereby increasing the likelihood that particle growth would be inhibited at an earlier stage. This would lead to very small primary particles (such as found in 2-line ferrihydrite) and therefore the marked decrease in crystallinity seen in Figure 2.18.

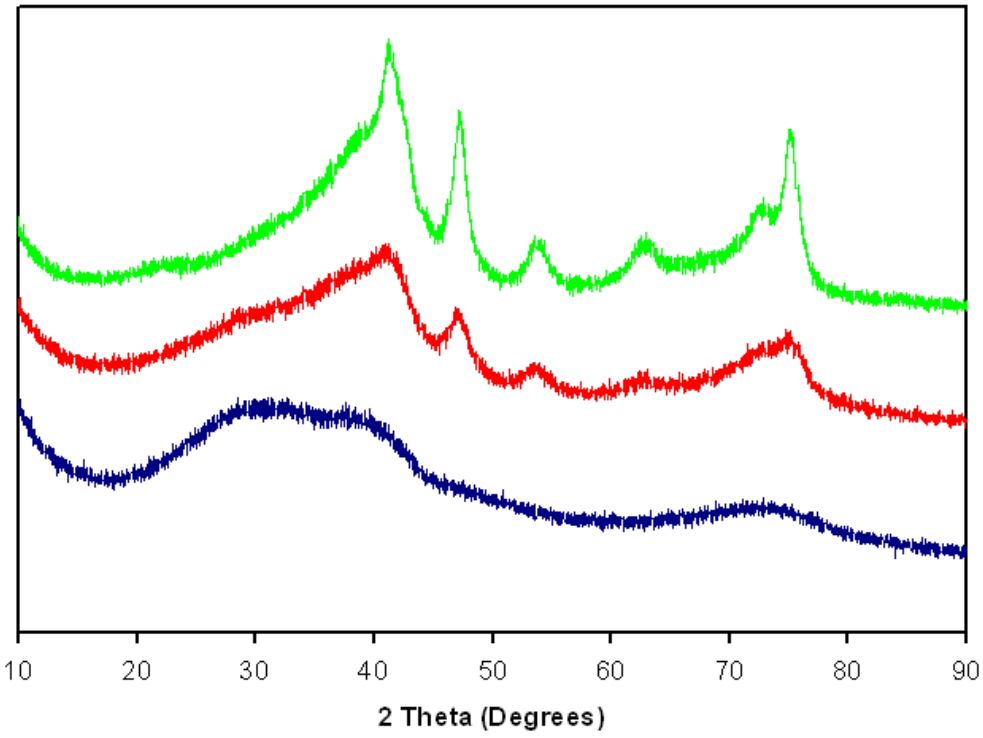

Figure 2.18: XRD patterns of samples N-5-1 (green), N-30-1 (red) and N-50-1 (blue).

As in the initial series of samples produced in sulfate, the pattern from S-50-1 (Figure 2.19) displays some characteristics that would suggest the presence of schwertmannite. The patterns also show that although there is very little difference in the crystallinity between S-5-1 and S-30-1, there was a noticeable broadening of some reflections in S-50-1. FWHM values are provided in Table 2.8. This would

suggest that there is a point at which the precipitated silica affects the crystallinity of ferrihydrite in sulfate media. This point may be simply related to the concentration of silicate in the feed or be based on a ratio of soluble constituents, such as an $Si(OH)_4^-$:SO_4^{2-} relationship. While some broadening occurred, it was far from the magnitude of the effect observed in nitrate media.

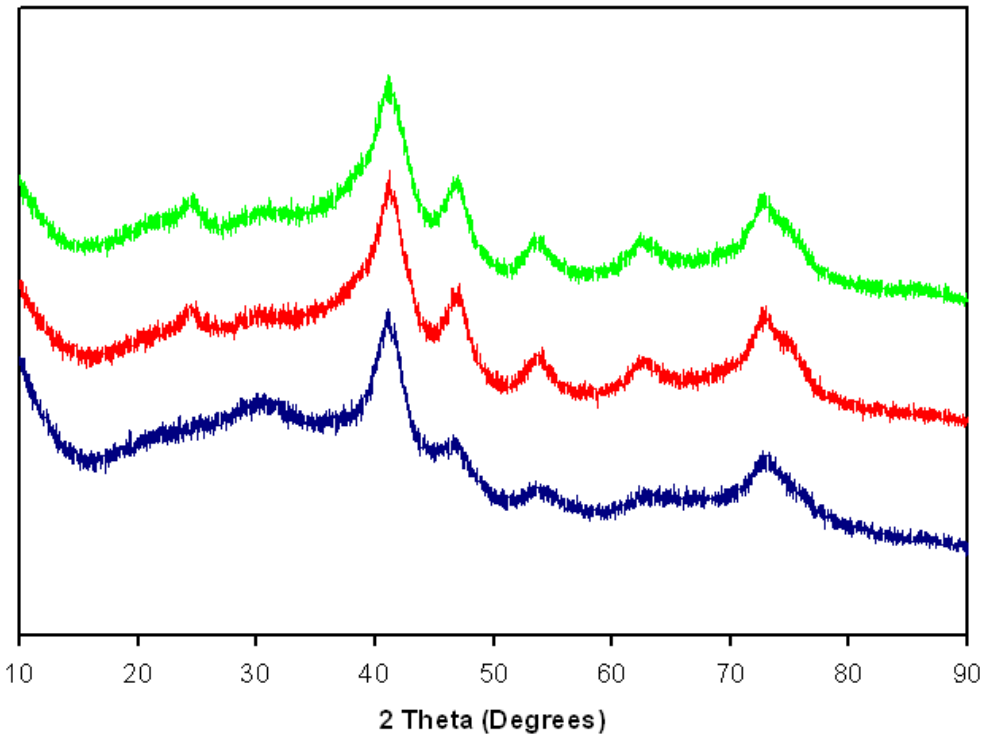

Figure 2.19: X-ray diffraction patterns of samples S-5-1 (green), S-30-1 (red) and S-50-1 (blue).

Structurally, the co-precipitate from the system containing both nitrate and sulfate was similar to that of a system containing only sulfate (Figure 2.20). It can therefore be concluded that it is not the presence of the nitrate ion that increases the effect of precipitated silica on the residue formed, but the presence of sulfate that retards it. The strong binding characteristics of sulfate ions inhibit the adsorption of the silicic acid monomers, allowing the ferrihydrite particles to grow. Interestingly, the similarity of the patterns for the two sulfate-containing systems suggests that even at lower SO_4^{2-} concentrations there is still a comparable effect on the crystallinity of the product. This aspect will be discussed further in Section 2.5.2 with respect to elemental concentrations in both feed and supernatant solutions.

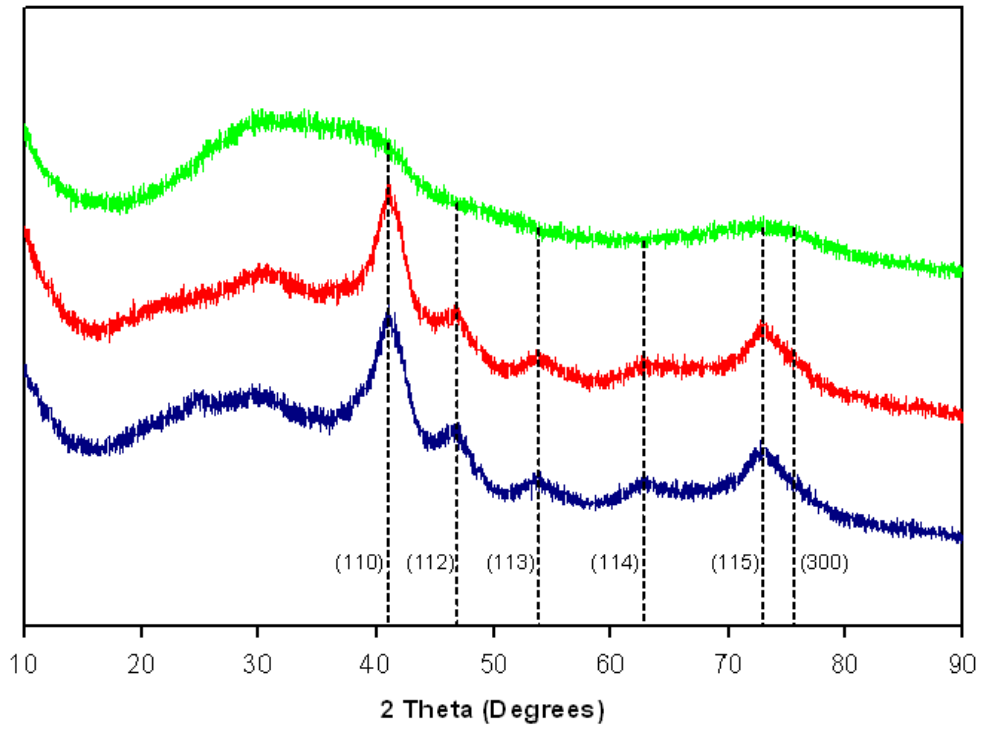

Figure 2.20: X-ray diffraction patterns of samples N-50-1 (green), S-50-1 (red) and NS-50-1 (blue).

Table 2.8: FWHM values from some peaks N-30-1, S-30-1, NS-50-1, S-50-1 and N-50-1, calculated using xfit. Peaks are labelled with the indices associated with characteristic ferrihydrite reflections.

	FWHM Values at Reflection Index:					
Sample	(110)	(112)	(113)	(114)	(115)	(300)
N-30-1	3.09	2.01	2.32	3.28	6.47	2.08
N-50-1	10.5	-	-	-	10.8	-
S-30-1	2.76	2.14	2.21	2.74	2.73	2.49
S-50-1	2.81	2.52	2.63	-	2.36	7.37
NS-50-1	3.62	2.49	2.94	2.54	1.49	6.43

Note that the system containing both nitrate and sulfate has many peaks that are sharper (lower FWHM values) than the respective peaks in the purely sulfate system. For example, the (114) peak, which corresponds to the reflection at approximately 62° 2 , can be seen from Figure 2.20 to be very weak and barely visible for sample

S-50-1. In fact the (114) reflection was not fitted as a discrete peak, but rather as part of a very broad reflection centred on ~ 64° 2 . Statistically there is no discrete peak at 62° 2 and therefore no FWHM value is quoted. The small reflection at ~25° 2 is only apparent in the mixed system and suggests the presence of a small amount of poorly crystalline goethite. From this analysis, it would appear that the mixed system is almost more crystalline than the purely sulfate experiment, which creates greater interest in the results of the elemental analysis.

2.5.2. Elemental Composition

Table 2.9 shows that in the high-silicate system containing virtually no sulphur (perhaps none in the form of sulfate ions), iron was precipitated to the point where the Fe^{3+} ion concentration was below the detection limit of 0.2 ppm and the soluble silicate concentration was below the approximate level of silica solubility. This was consistent with the results of the experiments containing lower Si concentrations. The continued removal of Si down to or below the solubility of silica suggests that there is still sufficient ferrihydrite surface available to template such an extent of polymerisation from the elevated concentration of soluble silicate in the feed. The values obtained from the sulfate samples were also consistent with previous experiments, removing just over 30% of the Si from solution and leaving the silicate level well in excess of the silica solubility (by an order of magnitude). The incomplete removal of the iron was also characteristic of the sulfate systems.

Table 2.9: Elemental concentrations in feed and supernatant solutions of steady-state samples taken from the three high-silicate systems.

System	Fe in liquor (ppm)	%Fe Precipitated	Si in liquor (ppm)	%Si Precipitated
N-50-1	< 0.2	100	140	90.6
S-50-1	87.9	97.3	1151	31.1
NS-50-1	47.7	98.5	675	59.4

Much more iron and silicon remained in solution in the mixed system than the nitrate system, while the concentrations in the purely sulfate system were far greater still. Although the XRD patterns of NS-50-1 and S-50-1 are similar, the elemental concentrations reveal a significant variation. There is a clear trend that the proportion of sulfate present during the precipitation reaction impacts greatly on how efficiently both iron and in particular silicon are removed from the reaction liquor.

As previously indicated, sulfate is believed to competitively adsorb on the ferrihydrite surface, thus decreasing the available binding sites for the silicic acid monomers. Therefore the fact that a decreased amount of sulfate present during the reaction is important allows for several possibilities. Either the sulfate coverage of the ferrihydrite surface is less complete or the diminished sulfate level in solution decreases the rate at which the surface is covered, allowing more adsorption of the silicon species. It is also possible that the observed effect is a combination of both factors. The percentage of both iron and silicon removed from solution is dependent on the sulfate concentration and not necessarily on any ratio of $Si(OH)_4^-$:SO_4^{2-}.

2.6. Chloride Systems

As a consequence of the significant role played by the two different solution anionic species associated with the iron source, a third solution anion was investigated to better understand this effect on the co-precipitation process. Ferric chloride was chosen, as it is readily available and should bind to iron less strongly than sulfate but more so than nitrate (Swedlund 2003). The expectation is that it will display properties that lie between those of the nitrate and sulfate systems. All conditions remained consistent with those in the experiments described in section 2.2 and 2.3, with the chloride experiments detailed in Table 2.10.

Table 2.10: Experiments producing the samples referred to in this section. Ideal feed concentrations are given (variation occurred due to experimental uncertainty).

System	Conditions					
	Feed Concentration		pH	Residence Time	Temp (°C)	Anion present
	Fe (g L^{-1})	Si (g L^{-1})				
C-0-1	6.3	0	2.65	45 min	85	Cl^-
C-5-1	6.0	0.16	2.65	45 min	85	Cl^-
C-10-1	5.7	0.32	2.65	45 min	85	Cl^-
C-20-1	5.0	0.63	2.65	45 min	85	Cl^-
C-30-1	4.4	0.95	2.65	45 min	85	Cl^-

2.6.1. Structural Analysis

There was evidence of more crystalline phases in early residence times in the XRD patterns of residue solids obtained from C-0-1 (Figure 2.21), which was consistent

with corresponding sulfate and nitrate systems. The presence of hematite was displayed by the shoulder at approximately 39° 2 , the extra peak at ~58° 2 , and an increase in the intensity of the (114) ferrihydrite reflection (~63° 2), the latter being difficult to distinguish. Hematite was most prominent in the first three residence times, decreasing in the fourth and fifth and finally not being apparent in the steady-state sample or the reactor contents. It would appear that it was formed in the early stages of crystallisation process while reagents were increasing in concentration and equilibrating, subsequently being removed through the course of the experiment to the point at which none remained.

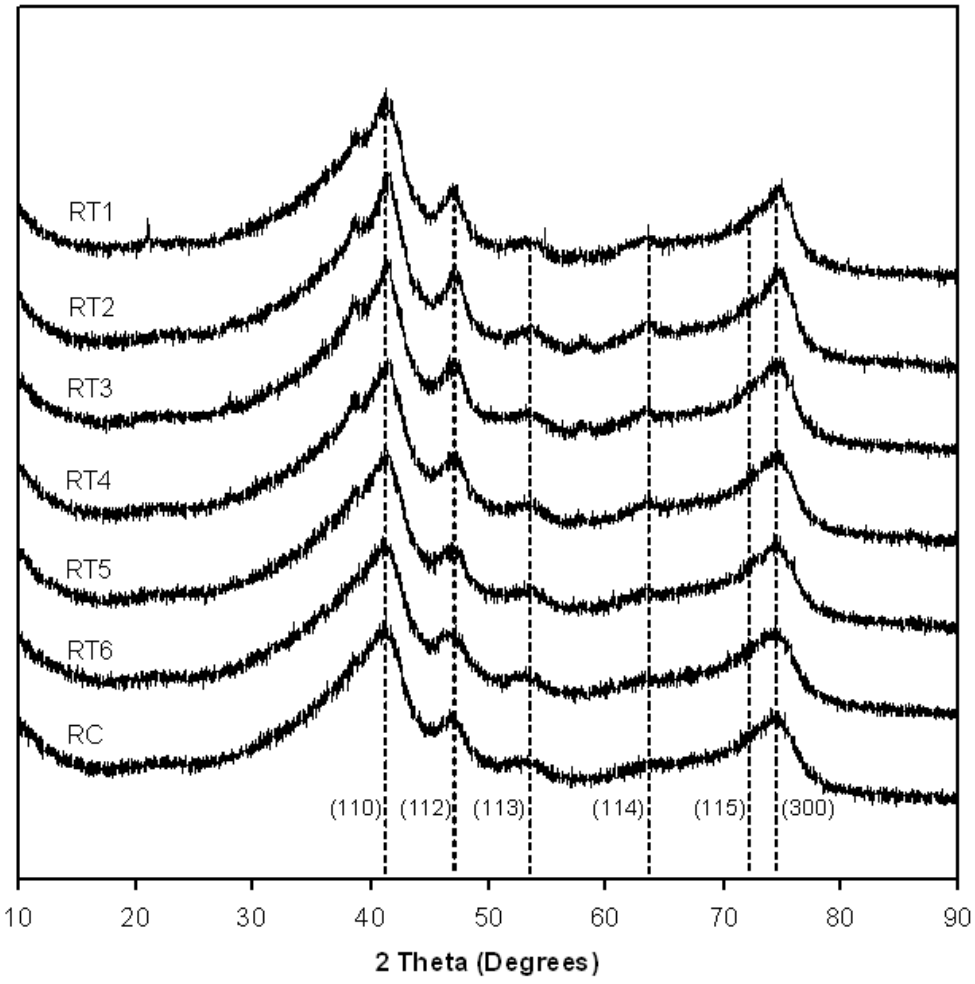

Figure 2.21: XRD patterns obtained from each residence time from C-0-1.

There was not a great deal of difference between the XRD patterns of the steady-state samples from C-0-1, C-5-1 and C-10-1 (Figure 2.22). Interestingly, the silica-free sample appears to be the least crystalline of the three. However, this may be due to a small difference between conditions. This unexpected result was most likely due to the higher iron concentration in C-0-1 increasing the hydrolysis rate.

There was a lack of more crystalline phases in the steady-state sample of C-0-1 and all systems generally display relatively low product crystallinity in comparison to those in nitrate and sulfate media. Given that reaction conditions are identical to those in the nitrate and sulfate experiments, this may suggest that the hydrolysis rate is increased in chloride media.

The effect from the presence of silicate becomes obvious in C-20-1 and C-30-1, for which crystallinity decreased markedly (Figure 2.22). C-30-1 resembled 2-line ferrihydrite, containing very few distinct reflections. Based on the properties of the precipitates in section 2.3, it was likely that the majority of the Si present in the system precipitated in the reaction.

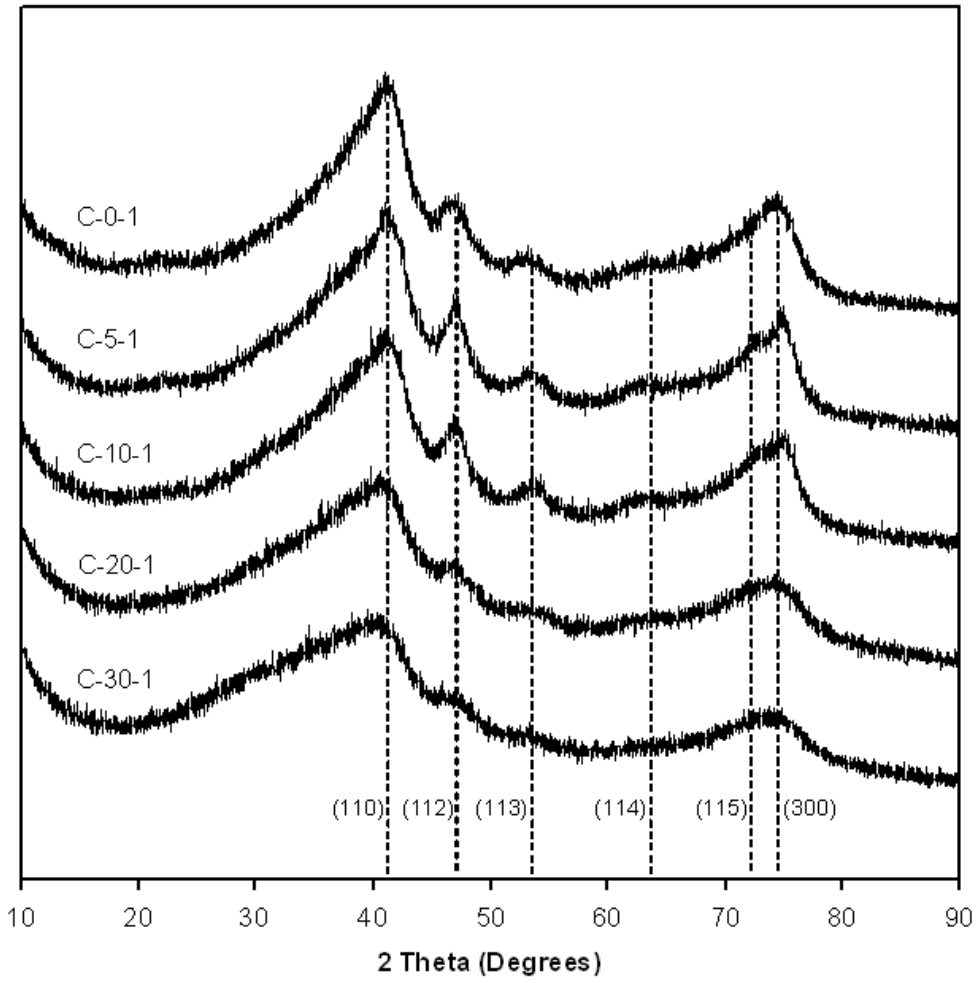

Figure 2.22: XRD patterns from the steady-state samples from the chloride systems.

2.6.2. Elemental Composition

The silicon concentrations presented in Table 2.11 show that chloride as the main anionic species in solution did not inhibit the precipitation of silica. All systems contained a final Si concentration well below the solubility of silica at the experimental concentration of chloride (~140 mg L^{-1}, (Chen 1982)). The amounts of Si removed from each of the C-10-1, C-20-1 and C-30-1 systems were similar to those in nitrate media, suggesting chloride has a similarly weak association with the ferrihydrite surface. The proportion of silicon precipitated in the C-5-1 system was far greater than in any other medium at the same feed concentrations. While N-5-1 left more than 45% of the initial silicate remaining in solution, less than 11%

remained under the same conditions in ferric chloride. This may actually suggest that the chloride is even more effective in Si removal from low concentration solutions than nitrate.

This was an interesting result, as chloride typically complexes iron more strongly in solution and should associate more strongly with the ferrihydrite species, however, no evidence of this was apparent. It would appear that chloride did not significantly compete with silicic acid for surface binding sites, or that any small effect was countered by the decrease in silica solubility (0.0063 mol L^{-1} to 0.0045 mol L^{-1}) due to the presence of chloride ions (Marshall 1980; Chen 1982).

Table 2.11: Elemental concentrations of iron and silicon in the supernatant solutions and percentage removed during the reaction.

System	Fe in liquor (ppm)	% Fe Precipitated	Si in liquor (ppm)	% Si Precipitated
C-0-1	2	>99.9	-	-
C-5-1	12	99.8	18	89.2
C-10-1	9	99.9	38	88.0
C-20-1	1	>99.9	66	89.6
C-30-1	0	100	91	90.7

Again, it would appear from Table 2.11 that the reaction was governed by the rate of silica polymerisation. The major phenomenon governing the rate was most likely the concentration of silicate in the feed solution. More Si (total, not percentage) was removed from solution in systems that contain the greatest initial concentration. This is logical, as the greater concentration would allow for more interactions between silicate species and the ferrihydrite surface. There is a question as to whether the greater level of Si remaining in solution in the higher Si systems was due to a lack of time in the reactor or a decreased number of binding sites on the surface of the precipitated ferrihydrite.

2.6.3. Surface Behaviour

Zeta Potential data was acquired for the steady-state samples of all five systems prepared in chloride media, with Figure 2.23 showing the measured zeta potential as a function of slurry pH. Given the knowledge that co-precipitation with silica decreased the IEP of ferrihydrite significantly (section 2.3.3), there was interest in how the effect varied with Si content. The expected effect would be for the IEP to gradually decrease as the proportion of silica in the residue increased.

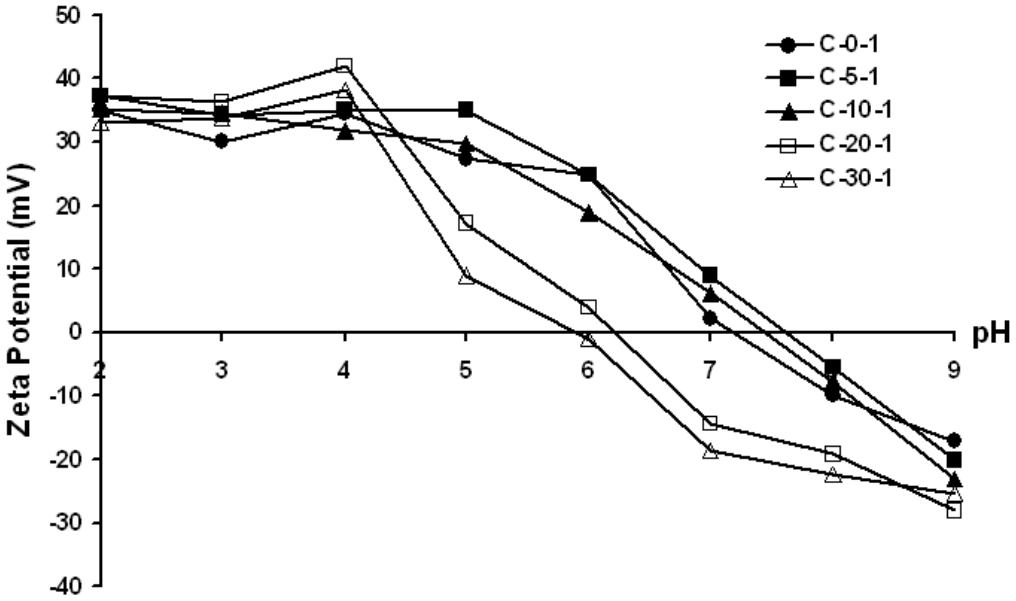

Figure 2.23: Zeta potential measurements of each chloride system taken between pH 2 and 9.

The results were not quite as expected, in that there was little difference between the zeta potential responses for residues from C-0-1, C-5-1 and C-10-1. The silica had no clear effect on surface charge for the lower Si systems, suggesting that ferrihydrite still largely dominated the surface. The slight increase in IEP from C-0-1 to C-5-1 was most likely within experimental uncertainty. The first sign of the influence of silica was for the C-20-1 sample, with a marked decrease in IEP of more than one pH unit. Based on this, the composition at which the surface charge begins to be legitimately altered by the presence of silica was for Si:Fe ratios of between 0.11 and 0.25. Sample C-30-1 displayed the lowest IEP, which was to be expected.

The greatest difference in the Si:Fe ratio between two consecutive systems lies between C-20-1 and C-30-1. It would therefore be expected that the greatest difference in surface charge would be between these two experiments. However, this is not the case as the greatest observed difference is between C-10-1 and C-20-1. The IEPs of C-20-1 and C-30-1 are only separated by 0.3 of a pH unit. It is possible that the increasing silicate concentration at the expense of iron in the feed increases the silica precipitation rate with respect to both the ferrihydrite precipitation and aggregation steps. As a consequence, a greater proportion of the silicic acid adsorption would occur on primary particles and therefore not be on the outer surface of the aggregates being measured. The silica would then be more uniformly distributed throughout the core of the aggregate, rather than being predominantly surface associated.

2.6.4. Aggregate Properties

The method described in section 2.2.3 for the measurement of fractal dimension ***via*** light scattering data from the Malvern Mastersizer has only begun to be employed in about the last decade. Publications employing this technique often focus on narrowly dispersed particles which were more easily analysed, and generally do not provide significant detail of the measurement process (Selomulya 2001; Zhou 2006; Jarvis 2008). The data obtained for both this section and presented later in Tables 3.3, 3.5, 3.7 and 3.11 proved more difficult to analyse with regard to determining the region of the curve to be measured.

The most difficult part of the analysis is determining the angular range over which to measure the gradient. This can be a very subjective process, as the region of the curve to be measured is not always clear therefore it is somewhat subject to the user's judgment. As small variations in fractal dimension are quite significant, a firm convention for the calculation process is required. However, the shape of the curves varies and thus the portion of which the gradient is measured also varies (Figure 2.24). The degree of aggregation has a great bearing on the fractal dimension

measurement. A low degree of aggregation will not provide good fractal dimension data.

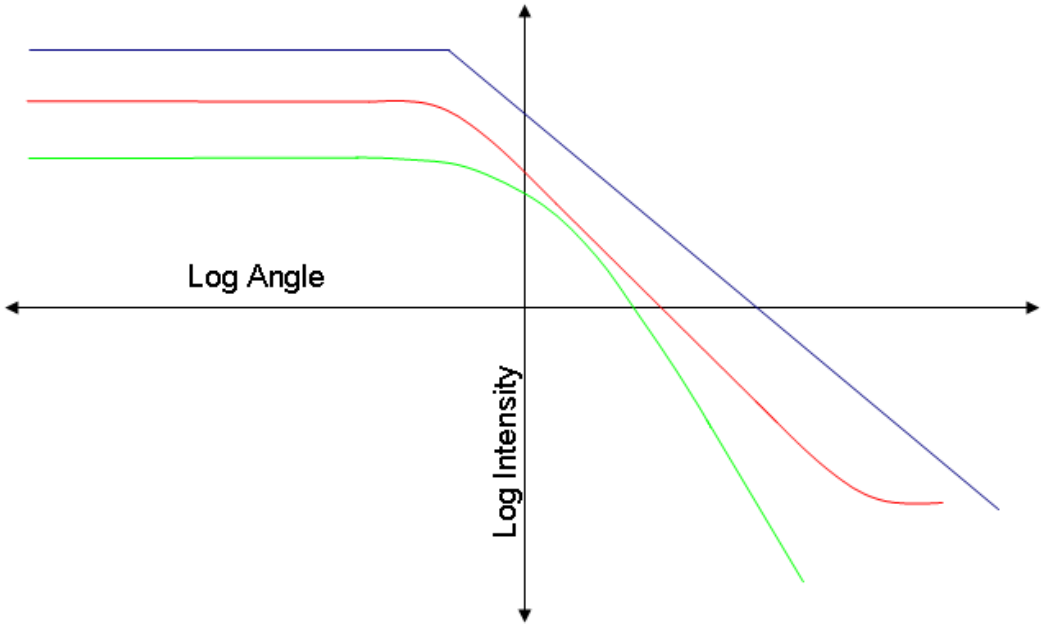

Figure 2.24: Schematic of some types of data sets for the measurement of fractal dimension, the ideal situation is provided in blue, others that would cause some difficulty are presented in red and green. While it is simple to select the linear region from which to measure the slope on the blue curve, the curvature of the green and red lines complicates the analysis.

A fully dispersed standard hematite sample was prepared (section 2.2.1) specifically to test the method, as its fractal dimension has been investigated in this way previously (Zhang 1996). SEM images confirmed that the intended monodisperse particles of a few hundred nanometres in size had been formed (Figure 2.25). Although the images give the impression that some particles had aggregated, much of this was an artefact from the drying process, with very little aggregation observed when suspended in pure water. The scattering data of the pure hematite sample (no additives) was obtained, and upon plotting log(I) vs. log( ) did not contain a section from which the fractal dimension could be obtained (blue curve of Figure 2.26). This however was not necessarily a problem, for if the sample is not well aggregated, a fractal dimension by definition cannot be extracted.

Subsamples of the standard hematite were treated in different ways in order to induce aggregation; 10 g L^{-1} KCl was added to one, and the pH of another was increased to approximately 8, which is near the IEP of hematite. The sample in KCl displayed slight improvement, by way a region of the graph containing a few data points that could be used for the analyses. In contrast, the sample with an elevated pH aggregated well, providing a curve with a relatively distinct turning point and a large data range from which to obtain a gradient. Figure 2.26 shows the difference between the curve shapes obtained under each set of conditions.

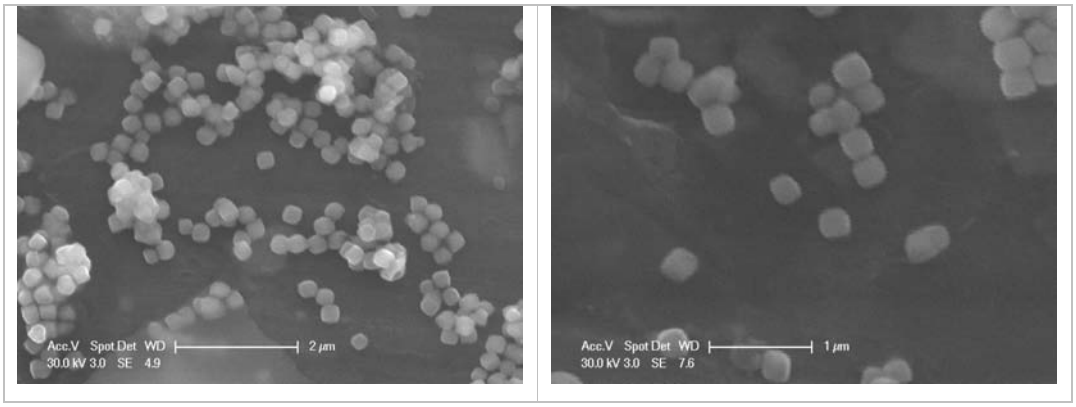

Figure 2.25: SEM images of hematite produced for fractal analysis.

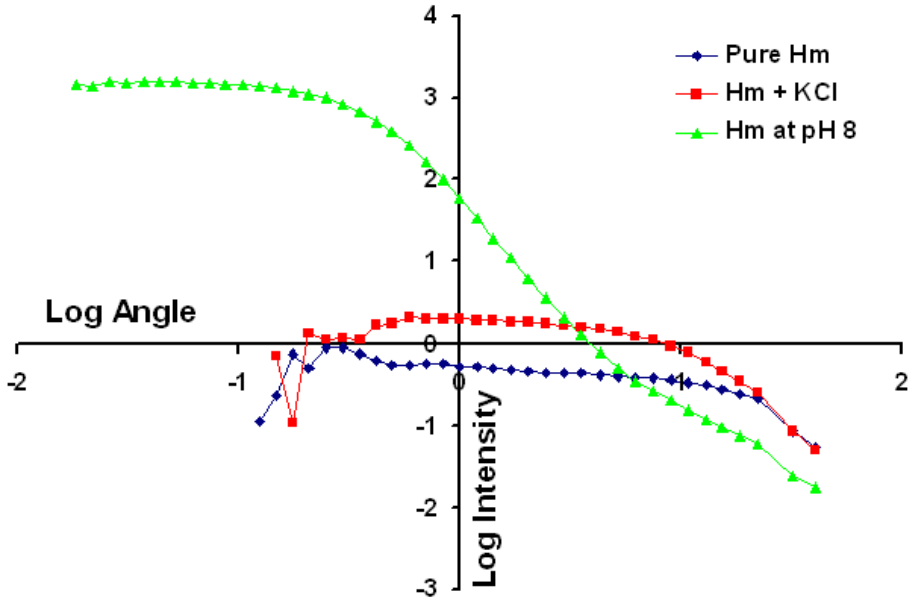

Figure 2.26: Plots of log (I) vs. log ( ) for the hematite suspended in deionised water (blue), KCl solution (red) and deionised water adjusted to pH 8 (green).

The fractal dimension obtained from the sample at pH 8 was then able to be compared with literature values of the fractal dimension of hematite. Amal et al. (Amal 1990) produced multiple values for hematite based on the method of aggregation be it diffusion-limited or reaction-limited. Given aggregation was induced by increasing the pH of a preformed suspension this reaction would be deemed to be a diffusion-limited process. The value obtained of 2.3 (using the region between 0.85 and 22.1°) correlates perfectly with that obtained by Amal et al. (Amal 1990) for their comparable system, which endorses the validity of the technique.

Analysis of the chloride systems served both as a trial for the measurement of fractal dimension and as an investigation of the materials produced. Achieving aggregation was not an issue in this case, as ferrihydrite aggregates both rapidly and extensively, however, it was not known if the nanoscale size of the particles would have any bearing on the measurement.

Figure 2.27 shows that the shape of the curves obtained from the scattering information was not uniform, nor did they show a distinct trend based on the Si/Fe ratios in the feed. The fractal dimension values obtained from the analysis are given in Table 2.12, however, the results are somewhat subjective. The different shapes of the curves makes obtaining reliable estimates of fractal dimensions from the data difficult, as there is a lack of consistency in the regions of linearity. The values obtained from the ferrihydrite samples do not provide the required accuracy to be considered as definitive fractal dimensions. However, trends in the values may prove useful.

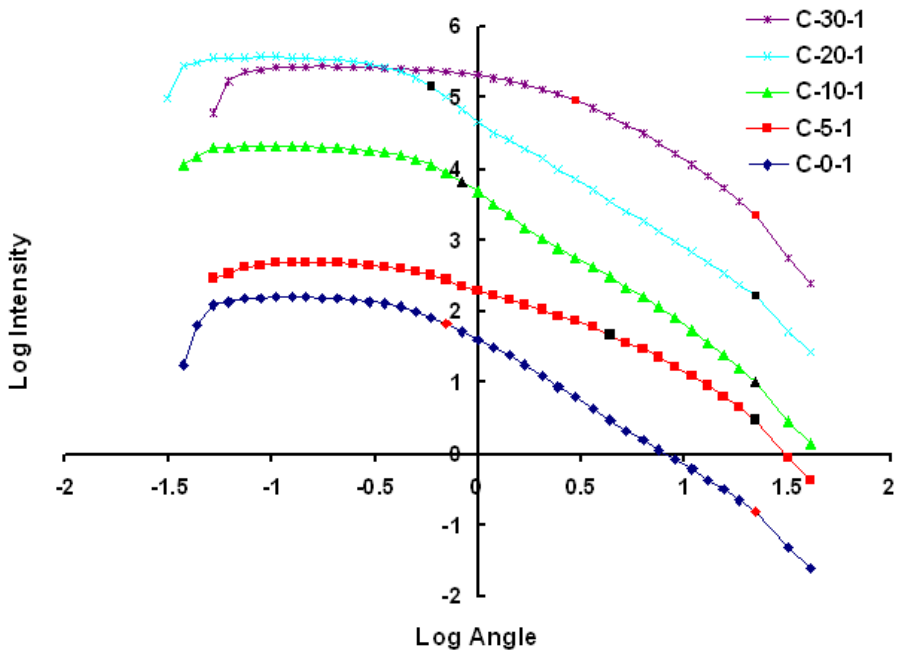

Figure 2.27: Plots of log (I) vs. log ( ) obtained from the five chloride systems. The sections selected to measure the slope lie between the differently coloured markers (i.e. between the two red markers in the data from the C-0-1 sample).

The fractal dimension data (Table 2.12) may suggest that the initial introduction of silica to the precipitate decreases the aggregate's packing, but on increasing silicate concentration in the feed, the particles become more tightly packed. However, the discrepancies may simply be a result of uncertainty. Considering the distribution of silica is primarily surface associated, it would appear that small amounts of silica on the surface interrupt the packing of the aggregates. However, at higher silica levels the particles would have lower surface charge as well as a significant distribution of both positive and negative sites and thus may aggregate more freely.

Table 2.12: Fractal dimension for chloride system samples.

System	C-0-1	C-5-1	C-10-1	C-20-1	C-30-1
Fractal Dimension	1.79	1.68	1.90	1.82	1.84

2.7. Zinc Containing Systems

As zinc is the primary constituent of the liquors within the Paragoethite process, gaining an understanding of how it affects the observed co-precipitation reactions and products is critical. Experiments were carried out on systems with five Si/Fe ratios from 0 to 0.429 (i.e. equivalent to the systems studied in section 2.3), each also doped with varying proportions of zinc. These experiments are detailed in Table 2.13. Three major insights were sought:

- Does zinc affect the structure of the residue?
- Does zinc alter the percentage of silicon precipitated?
- Does the presence of silicon affect the proportion of zinc adsorbed / precipitated?

Table 2.13: Experiments producing the samples referred to in this section. Ideal feed concentrations are given (variation occurred due to experimental uncertainty).

System	Conditions					
	Feed Concentration		pH_{85}	Residence Time	Temp (°C)	Anion present
	Fe ($g\ L^{-1}$)	Si ($g\ L^{-1}$)				
*S-0-80Z	6.3	0	2.65	45 min	85	SO_4^{2-}
S-5-80Z	6.0	0.16	2.65	45 min	85	SO_4^{2-}
S-10-80Z	5.7	0.32	2.65	45 min	85	SO_4^{2-}
S-20-80Z	5.0	0.63	2.65	45 min	85	SO_4^{2-}
S-30-80Z	4.4	0.95	2.65	45 min	85	SO_4^{2-}
**S-0-10Z	6.3	0	2.65	45 min	85	SO_4^{2-}
S-10-10Z	5.7	0.32	2.65	45 min	85	SO_4^{2-}
S-30-10Z	4.4	0.95	2.65	45 min	85	SO_4^{2-}

* S-x-80Z denotes experiments in which feed solution contain ~80 $g\ L^{-1}$ Zn,

** S-x-10Z denotes experiments in which feed solutions contain ~10 $g\ L^{-1}$ Zn.

Attempts were made to match the zinc levels of the process solutions, however, 160 g L^{-1} of zinc is very difficult to achieve under laboratory conditions. Such solutions were also unstable at room temperature. The majority of experiments were conducted at a loading of 80 g L^{-1}; by halving the zinc concentration, problems related to the saturation point at room temperature were avoided.

While these experiments were successful in terms of preparation and stability of the feed solution, zinc containing phases formed a large proportion of the product. The high concentration of zinc also made it difficult to ascertain whether there was any link between silicate concentration and the proportion of zinc removed from solution during the reaction.

Further crystallisation experiments were conducted using feed liquors containing 10 g L^{-1} Zn (S-0-10Z and S-10-10Z in Table 2.13). These samples (also used for synchrotron PDF studies, discussed in Chapter 4) did enable information to be obtained on the interaction between iron, silicon and zinc.

2.7.1. Structural Analysis

Figure 2.28 highlights the difficulty in trying to extract information on ferrihydrite from XRD data obtained from the systems prepared from solutions containing 80 g L^{-1} Zn. Not only did the Zn phases produce peaks of greater intensity, there were multiple phases, and in many cases reflections appeared at angles where ferrihydrite peaks would also be expected. Differential XRD (DXRD) would be required to extract the broad ferrihydrite peaks and thus obtain information about its formation in these systems (Loan 2004). Given that the information DXRD would provide would not show anything substantial than would not be noticed by simple observation, it was not conducted. There was evidence of all six characteristic ferrihydrite peaks, but trying to extract anything meaningful about the sample's crystallinity would be extremely difficult (Figure 2.28).

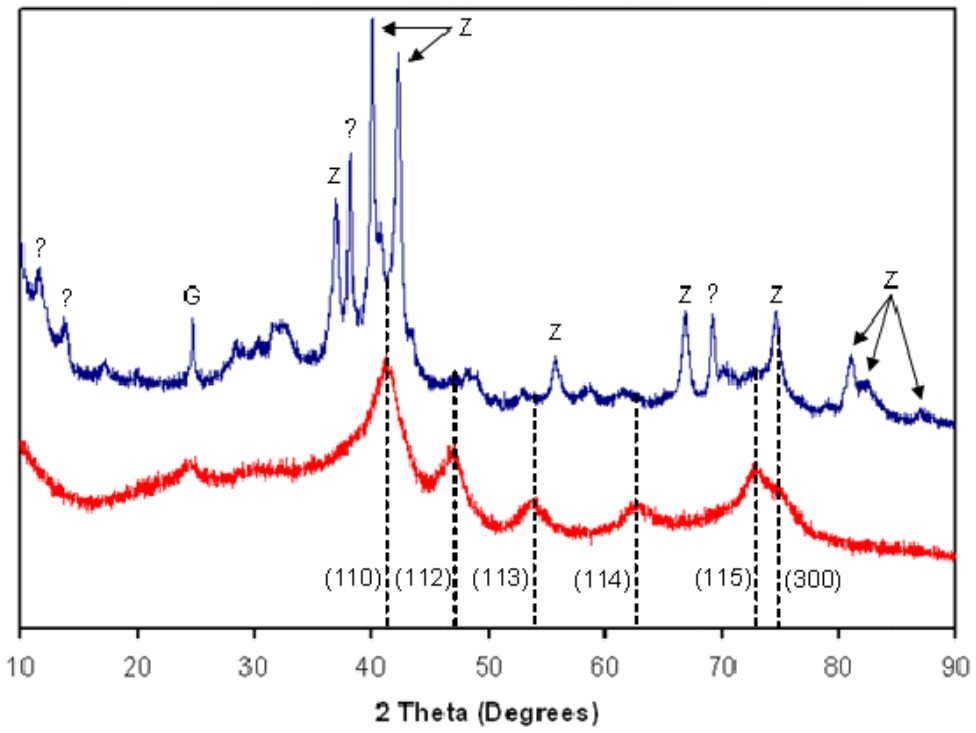

Figure 2.28: XRD pattern of S-30-80Z (blue) and S-30-1 (red). Where reflections related to zincite, goethite and unknown are indicated by Z, G and ?, respectively.

The patterns in Figure 2.28 show the broad reflection centred on ~41° 2 belonging to the ferrihydrite (110) peak, but it is largely obscured by and (could easily be mistaken for) the overlap of the cluster of peaks related to zinc phases in that region. Multiple zinc phases were produced but by far the most prevalent is zincite (ZnO), the peaks of which are marked in Figure 2.28. While zincite is highly soluble in both weak and strong acids, it is less soluble in alkaline conditions and is known to precipitate at approximately neutral pH. The combination of the high concentration and introduction of the sodium hydroxide would likely trigger the precipitation of the material. The other reflections did not match any minerals in the database.

Figure 2.29 displays the XRD patterns from each of the experiments containing 80 g L^{-1} zinc. Trends relating to the proportion of zinc phases observed and the silicate concentration in the feed were generally difficult to ascertain. The zincite peaks are weaker in the S-0-80Z, S-5-80Z and S-30-80Z samples, but more intense in S-10-80Z and S-20-80Z, suggesting no relationship with any silicon species.

One point of note relates to the peak at approximately 12° 2 in Figure 2.29. It appears as a very intense reflection in the pattern from the S-0-80Z sample, but is either greatly diminished or completely absent, replaced by a material (probably a silicon-containing mineral) that has a characteristic reflection appearing at the same angle, in the other four samples. The origin of the peak is difficult to determine as the peaks do not belong to a material in the database and therefore was not identified. Whatever the species may be, the presence of silica severely inhibits the formation of this species. It has been suggested that the reflection may belong to a material known amongst industry as "basic zinc sulfate", which contains a strong reflection between 11 and 12° 2 . However, this zinc sulfate hydroxide hydrate has other characteristic peaks of similar intensity at 21.2 and 31.5° 2 , which do not appear in these diffraction patterns.

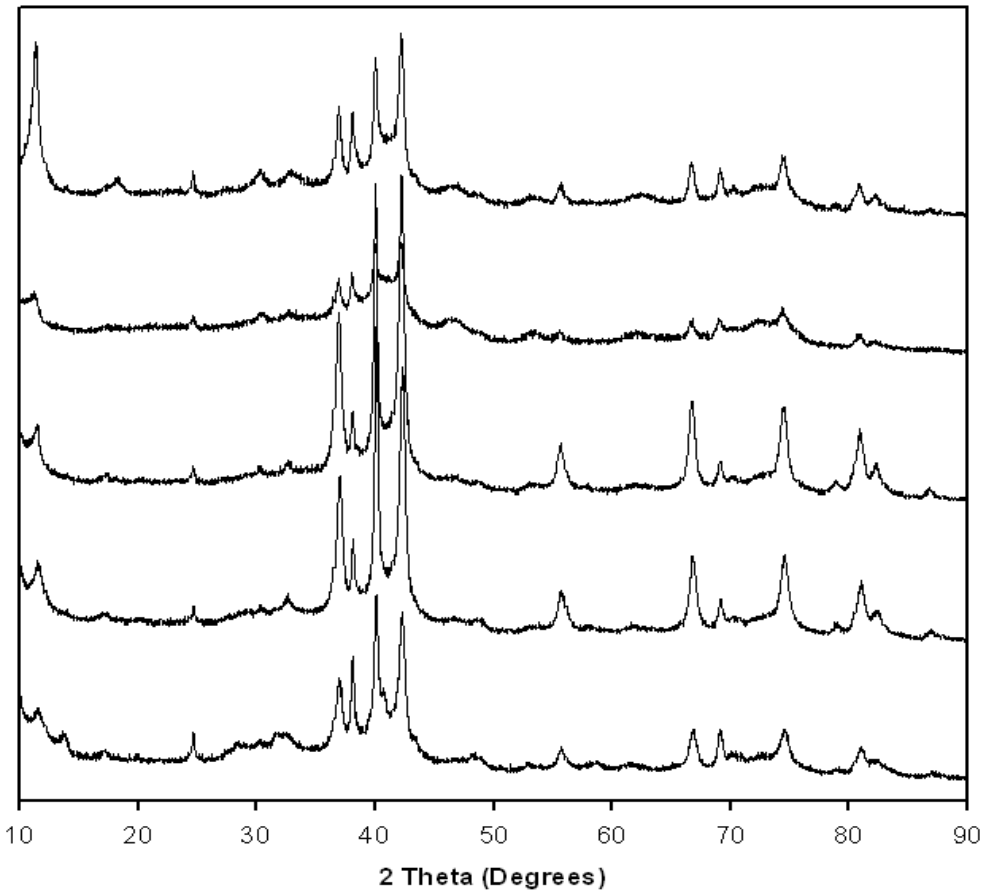

Figure 2.29: XRD patterns of samples from the S-0-80Z – S-30-80Z displayed top to bottom, respectively.

Reducing the zinc concentration in the feed to 10 g L^{-1} produced XRD patterns from the residues that generally resembled data obtained from the standard experiments (Figure 2.30). It appears for the most part that the zinc uptake at these levels was ***via*** adsorption or the formation of zinc phases in low enough proportion to not be visible in an XRD pattern. The only evidence of zinc phases (labelled with * in Figure 2.30) was found in the reactor contents of the S-0-10Z experiment. While there was minimal effect on the crystallinity of the ferrihydrite formed, there was evidence of a smaller proportion of schwertmannite (notable by the broadness of the peak at ~41° 2 , and substantial intensity of the peak at ~47° 2) in all systems other than S-30-10Z RC.

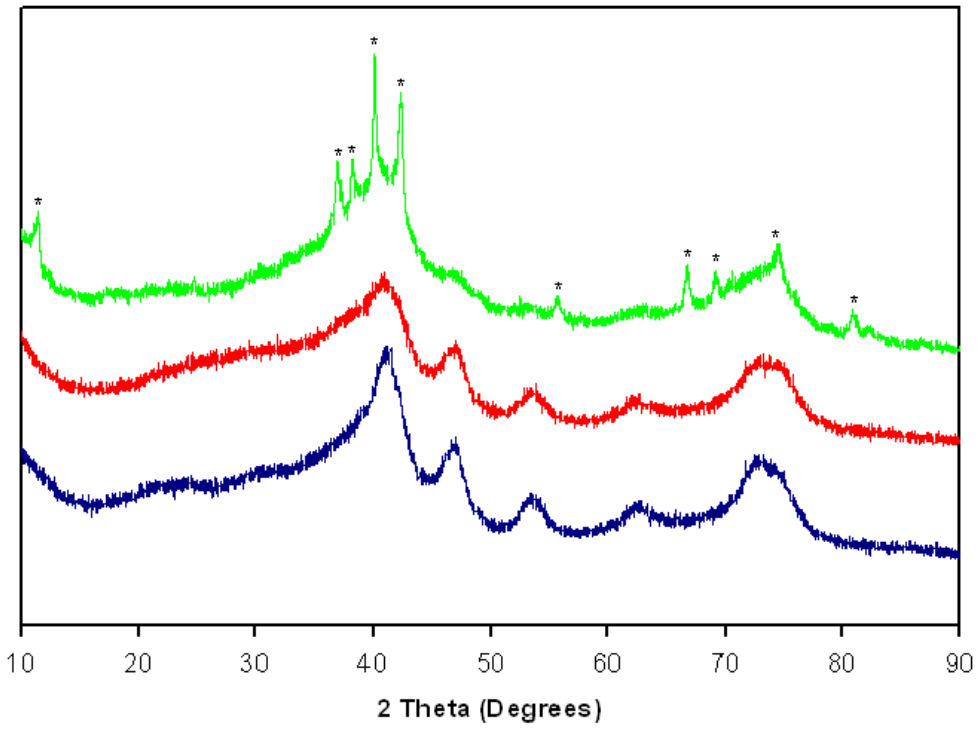

Figure 2.30: XRD patterns of reactor contents samples from S-0-10Z (green), S-10-10Z (red) and S-30-10Z (blue).

2.7.2. Elemental Composition

The measurement of Si and Fe in solution was not impeded by the high concentration of zinc present. This allowed information to be obtained under conditions more like plant liquors without interfering with the analysis of the reaction (Table 2.14). It was difficult to achieve an initial Zn concentration of exactly 80 g L^{-1} due to solubility constraints. At 80 g L^{-1} loading, a zinc sulfate species was also found to precipitate almost immediately where evaporation was allowed to occur. Sulphur concentrations were analysed but were not deemed useful as they showed no trends or bearing on the reaction.

Table 2.14: Elemental concentrations (in ppm) and percentages precipitated during the reactions involving the presence of either 10 or 80 g L^{-1} added zinc.

System	Fe in liquor / % precipitated	Si in liquor / % precipitated	Zn in liquor / % precipitated
S-0-10Z	1 ppm >99.9 %	- / -	8340 ppm 11.3 %
S-10-10Z	25.7 ppm 99.6 %	233 ppm 27.9 %	10200 ppm 0.5 %
S-30-10Z	24.2 ppm 99.5 %	309 ppm 69.1 %	10100 ppm 1.7 %
S-0-80Z	24 ppm 99.6 %	- / -	82300 ppm 1.7 %
S-5-80Z	18 ppm 99.7 %	107 ppm 34.4 %	86000 ppm 0.4 %
S-10-80Z	42 ppm 99.3 %	207 ppm 38.0 %	79000 ppm 7.8 %
S-20-80Z	29 ppm 99.4 %	303 ppm 53.9 %	83800 ppm 4.7 %
S-30-80Z	29 ppm 99.4 %	335 ppm 66.8 %	82000 ppm 3.6 %

The most prominent feature of the data obtained from these experiments is that the addition of a significant amount of zinc sulfate to the system greatly increased the

amount of silica precipitated. The percentages reached in both S-30-80Z and S-30-10Z were approximately twice that of the standard systems.

There are several effects that could have caused this behaviour. By adding the zinc sulfate the ionic strength is increased to more than double of that under standard conditions. High ionic strength increases the rate of silica precipitation and lowers the equilibrium solubility in what is known as the “salting out” effect. However there was a large difference between in the ionic strength of the systems with 10 and 80 g L^{-1} added Zn, but this did not greatly affect the percentages of Si removed from solution.

The precipitation of the zinc species seen in the XRD patterns of the 80 g L^{-1} solutions could also impact the behaviour of Si. Given that we have shown that the presence of the ferrihydrite surface as a template vastly increases the rate of silica precipitation, it is reasonable to assume that some of the zinc phases (ZnO, $ZnSO_4$) may have a similar effect. Even if the effect is many times smaller than that of ferrihydrite, the relatively large amount of the phase produced could induce further precipitation. Similarly if there is zinc co-precipitating with ferrihydrite there may be zinc included in the ferrihydrite structure. Co-precipitation with zinc may increase the amount of ferrihydrite produced (as it will contain the same mass of iron as well as some zinc) thus increasing the available total surface area.

Interestingly, the amounts of zinc removed from solution follow opposite trends between the 10 and 80 g L^{-1} loadings and neither trend is absolute in relation to silica. A large proportion of zinc removed during S-0-10Z (11.3 %), which drops to the lowest value in S-10-10Z and then increases again in S-30-10Z, although still at less than 2 %. Conversely in the 80 g L^{-1} systems there is little zinc removed in S-0-80Z, with the greatest proportion is precipitated from S-20-80Z and decreasing as the initial Si concentration increases from there. This may also be related to the iron, in that at higher silicon concentrations there is a lower the proportion of iron and therefore less zinc would be removed with iron. Based on this data, no conclusions can be reached on how the zinc behaves with respect to the iron and silicon levels in the reaction.

Both the amounts of silica and zinc precipitated in the 80 g L^{-1} systems have a significant bearing on the plant process, given that the reaction is carried out in sulfate media and high zinc loading. Were it not for the presence of the zinc, be it due to ionic strength or surface adsorption, silicon removal from the solution ***via*** ferrihydrite would be much less efficient. Unfortunately, whether or not the soluble silicates or silica presence in the precipitate increase or decrease the proportion of zinc lost to solids is unclear from this study.

2.8. Condition Alterations

A series of experiments were conducted in the sulfate system in which the iron concentration, pH, reactor residence time and hydrodynamics were varied.. Only a single condition was changed per experiment (Table 2.15) to minimise the possibility of confusing the observations.

Table 2.15: Experiments producing the samples referred to in this section. Ideal feed concentrations are given, variation occurred due to experimental uncertainty.

System	Conditions					
	Feed Concentration		pH	Residence Time	Temp (°C)	Anion present
	Fe (g L^{-1})	Si (g L^{-1})				
S-0-1	6.3	0	2.65	45 min	85	SO_4^{2-}
S-30-1	4.4	0.95	2.65	45 min	85	SO_4^{2-}
S-30-3F	8.8	0.95	2.65	45 min	85	SO_4^{2-}
S-30-2F	2.2	0.95	2.65	45 min	85	SO_4^{2-}
S-30-1F	1.1	0.95	2.65	45 min	85	SO_4^{2-}
S-30-2	4.4	0.95	2.65	45 min	85	SO_4^{2-}
*S-0-2	6.3	0	2.65	45 min	85	SO_4^{2-}
*S-30-3	4.4	0.95	2.65	45 min	85	SO_4^{2-}
**S-30-A	4.4	0.95	2.65	45 min	85	SO_4^{2-}
S-30-pH1	4.4	0.95	2.15	45 min	85	SO_4^{2-}
S-30-pH2	4.4	1.90	2.15	45 min	85	SO_4^{2-}
S-30-pH3	4.4	0.95	3.15	45 min	85	SO_4^{2-}
S-0-20m	4.4	0.95	2.65	30 min	85	SO_4^{2-}
S-30-90m	4.4	0.95	2.65	90 min	85	SO_4^{2-}
$^{+}$S-30-2S	4.4	0.95	2.65	45 min	85	SO_4^{2-}

* Experiments were conducted with a different impeller (Figure 2.31).

** Experiment carried out with an aged feed.

$^{+}$ Feed solution contained added Na_2SO_4

S-30-2, was conducted under the same conditions as S-30-1.

2.8.1. Impeller Design

On occasions, experiments conducted under apparently similar conditions behave differently in terms of the proportion of silica precipitated. This section examines whether there was sufficient mixing in the reactor and if hydrodynamic considerations were altering the precipitation process in any way. Experiments for some sulfate containing systems were conducted with agitation using an alternative impeller (Aldrich Z17143-3 stainless steel impeller, shown in Figure 2.31). Poor mixing within a reactor of such low volume was considered unlikely, but required confirmation.

Figure 2.31: The two types of impellers used in these experiments. Standard impeller is at the top, Aldrich Z17143-3 at the bottom.

The XRD data in Figure 2.32 is for samples S-30-1 and S-30-3, in which the only difference is the impeller used. The patterns were close to identical, which suggests little difference in mixing. An unexpected observation is that the patterns obtained from both the silicon-free and silicon containing systems (S-0-2 and S-30-3,

respectively) with the alternative impeller are almost identical. This was interesting, as generally the silicon-free samples produced peaks corresponding to the presence of some more crystalline phases (e.g. S-0-1 Figure 2.10). The pattern obtained from S-0-2 shows predominantly schwertmannite and ferrihydrite, with no indication of goethite. This may be due to the blades mixing through a greater volume of the solution, eliminating some of the possible localised high or low concentration zones.

The absence of goethite in S-0-2 (Figure 2.32) is difficult to reconcile with the XRD and elemental concentrations for the systems with Si. Potentially, there may have also been slight or localised differences in the pH, such as not to favour goethite production at all. Based on the XRD patterns obtained, if there are variations in the hydrodynamic conditions, the impact on the co-precipitation process appears minor or negligible, which was the main concern in this instance.

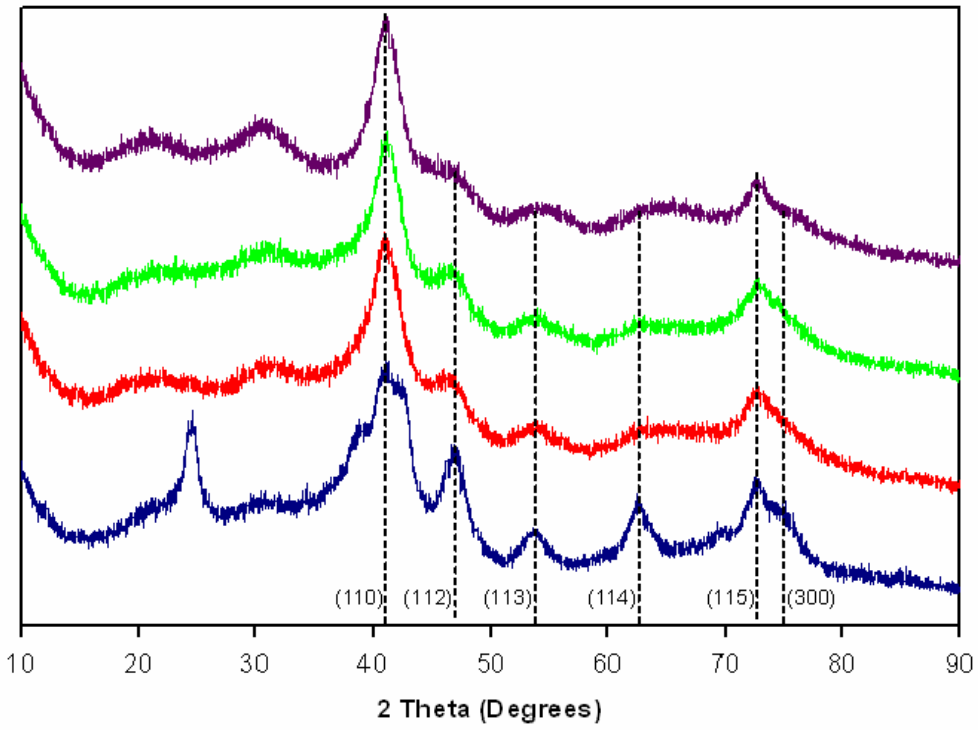

Figure 2.32: XRD traces of samples prepared in reactions employing different impellers. S-0-1 is presented in blue, S-0-2 in red and S-30-3 in green and S-30-2 in purple.

Any significant difference in mixing efficiency should be most evident in the amount of Si removed from the solution, through the provision of more collisions and greater

exposure of silicic acid monomers to particulate surfaces for binding. Through comparison of the elemental concentrations presented in Table 2.16, there was no discernable difference in the behaviour of Si in reactions using either impeller. The proportion of Si remaining in solution was almost identical between S-30-1 and S-30-3, differing by less than 0.5%. An interesting point of note is the difference in the residual iron concentrations between the two silica-free systems. The fact that more than twice the iron remained in solution after the precipitation process using the standard impeller may provide evidence regarding the presence of goethite. The excess iron in solution may be due to less efficient mixing by the standard impeller near the top of the reaction volume where reagents are introduced. The remaining iron in solution at very low concentration would have a much lower associated hydrolysis rate, thus forming more crystalline material.

Table 2.16: Elemental concentrations of iron and silicon in the supernatant solutions from each system and percentage removed during the reactions.

System	Impeller	Fe in liquor (ppm)	% Fe precipitated	Si in liquor (ppm)	% Si precipitated
S-0-1	Standard	179	97.2	-	-
S-0-2	Z17143-3	74.7	98.8	-	-
S-30-2	Standard	84.5	98.2	671	32.1
S-30-3	Z17143-3	65.4	98.6	674	31.8

2.8.2. Iron Concentration

Further evidence was required to support the theory that co-precipitation follows the sequence of iron precipitation → $Si(OH)_4$ adsorption → silica polymerisation processes that has been formulated, based on data from section 2.3. The effect of varying the iron content in the feed was investigated while maintaining a constant silicate concentration. Although this would vary the ionic strength, this was not expected to have a large impact on the reaction. The hypothesis behind these tests was that altered levels of iron would produce different amounts of ferrihydrite. This, in turn, would provide different areas of available surface for adsorption, thus affecting the amount of silicon removed from solution. To test this, variations of the system S-30-1 were made, as this maximised the potential to achieve either increased or decreased Si precipitation (in contrast, the nitrate systems always gave a high percentage of Si precipitation under standard conditions). The matrix of systems used is given in Table 2.17.

Table 2.17: Elemental solution compositions of standard system and systems used for iron content investigations.

System	c(Fe) mol L^{-1}	c(Si) mol L^{-1}	Corresponding % Fe	Corresponding % Si	Si:Fe
S-30-2	0.079	0.034	70.0	30.0	0.43
S-30-3F	0.158	0.034	82.4	17.6	0.21
S-30-2F	0.040	0.034	53.8	46.2	0.86
S-30-1F	0.020	0.034	36.8	63.2	1.72

The XRD patterns in Figure 2.33 show the expected trend, with crystallinity decreasing as the Si:Fe ratio was increased. While this is further evidence that the relative proportion of silicates present has a bearing on the crystallinity of the solid formed, it does not itself provide any new insight. The silica peak at low angle (25 - 30° 2) appears greater in the blue trace, but this is not necessarily an indication of a

greater amount of silica being precipitated, simply a greater silica:ferrihydrite ratio in the residue.

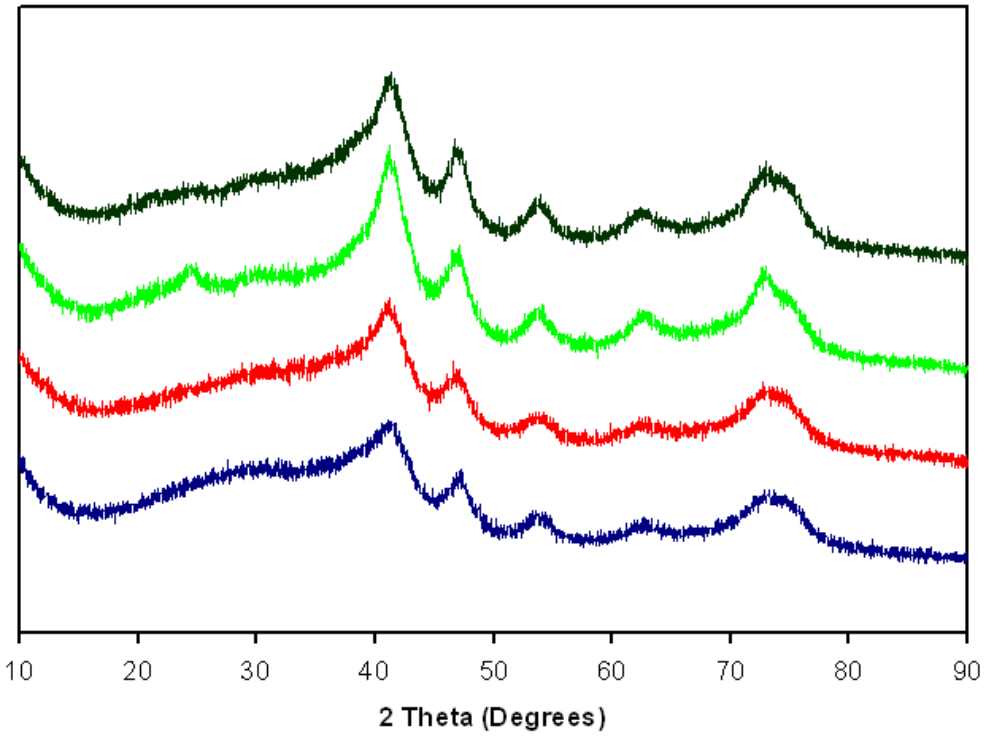

Figure 2.33: XRD patterns of systems containing iron concentrations of 0.020 mol L^{-1} (blue), 0.040 mol L^{-1} (red), 0.079 mol L^{-1} iron (green) and 0.158 mol L^{-1} (black).

The elemental analysis given in Table 2.18 provides the information of greatest interest. The hypothesis was that the amount of Si precipitated from solution would be dependent on the available surface area provided by the formation of the ferrihydrite particles. This trend was observed, especially by the highest iron solution concentration, in which the percentage of Si present in the precipitate was almost doubled compared to S-30-2. The precipitation of Si was correspondingly lower for Fe concentrations lower than in the standard systems, but the sensitivity was much reduced. Obviously a larger difference was expected for the system with double the starting iron concentration, but this does not fully explain why the variation in the other systems is relatively low.

Table 2.18: Percentage of the initial concentration of elements removed as solid during co-precipitation reaction presented in increasing feed iron concentrations.

Sample	Fe in liquor (ppm)	Fe Precipitated (%)	Si in liquor (ppm)	Si Precipitated (%)
S-30-1F	36.4	97.0	722	25.7
S-30-2F	40.0	98.3	640	33.6
S-30-2	131	98.2	671	32.1
S-30-3F	70.0	99.9	425	63.4

Sulfate is thought to play a major part in these reactions, competing with silicate species for adsorption sites on the ferrihydrite surface, and is therefore examined in the next section.

2.8.3. Excess Sulfate Doping

The data already collected from co-precipitates formed in nitrate, sulfate and chloride liquors strongly suggested interference from sulfate on the adsorption and polymerisation of silica in these experiments. Further evidence was required to prove that sulfate inhibited the process, as opposed to the nitrate and chloride, which favoured it. Ferric sulfate feed liquors were doped with additional sulfate (in the form of Na_2SO_4) to observe if the extent of silica precipitation would experience any further decline. The first attempt proved fruitless, as a significant proportion of sodium sulfate itself precipitated during the reaction (XRD pattern given in appendices, Figure 6.1). This both masked the XRD signal of the co-precipitate and provided a greater solid surface area for silicic acid adsorption. The sodium sulfate precipitation was likely due to excessive concentrations as (20 g L^{-1} of Na_2SO_4) was added.

The second experiment, containing only 10 g L^{-1} added sodium sulfate, (S-30-2S) yielded a precipitate did not contain an observable amount of sodium sulfate. The XRD pattern primarily displays the characteristic peaks of schwertmannite as opposed to the mixture of large proportions of ferrihydrite and schwertmannite (Figure 2.34). This is not surprising, as greater sulfate levels would likely favour schwertmannite formation (Bigham 1994).

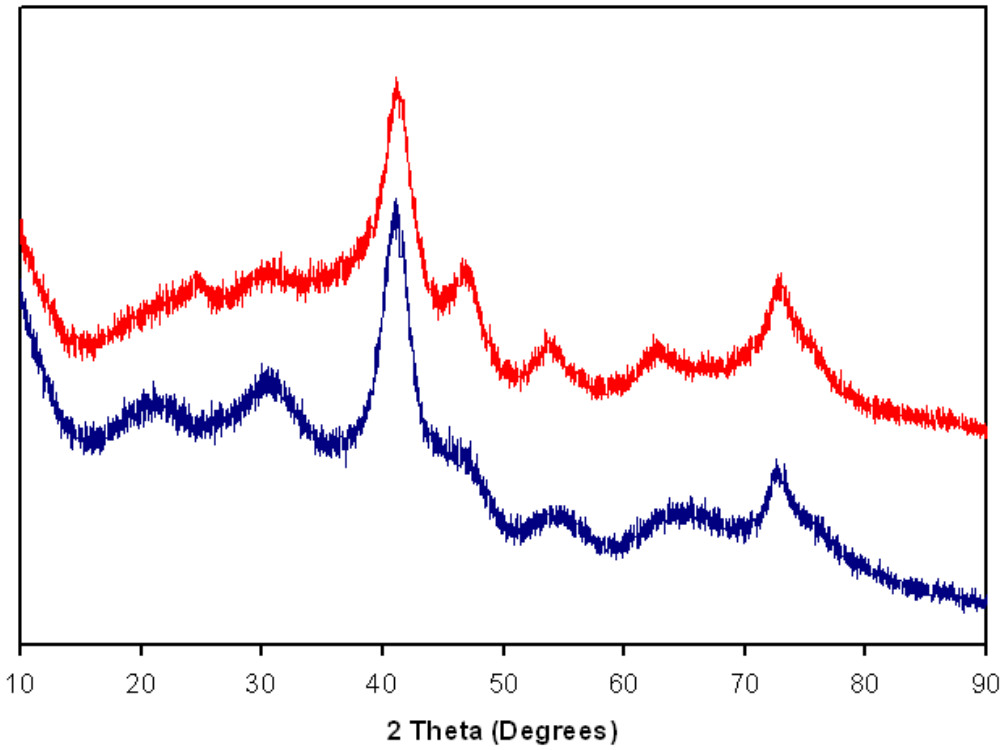

Figure 2.34: XRD patterns of samples S-30-2S (blue) and S-30-2 (red), displaying the difference induced by the additional sulfate in the latter. The peak at ~48° 2 is reduced to a broad shoulder of the previous reflection and those at ~55 and 64° 2 are broader in the S-30-2S pattern. These are indicative of schwertmannite.

The hindering influence of sulfate on the proportion of silica precipitation (seen in Table 2.19) runs counter to the standard "salting out" effect assumed for most precipitation processes, in which greater electrolyte concentrations should in general induce a greater degree of precipitation. However, as mentioned in chapter 1, it has been shown that the presence of some sulfate salts can increase the solubility of silica (Chen 1982), possibly through the formation of a silicon-sulfate solution complex

(Marshall 1982). The predominant effect is the competitive adsorption of sulfate on the ferrihydrite surface, impeding the adsorption of silicic acid and thus the subsequent polymerisation of silica. This is shown by the significant increase in silica precipitation in the presence of ferrihydrite in solutions of anions, such as nitrate, that do not bind to the surface as strongly as sulfate.

Table 2.19: Elemental concentrations in supernatant solutions from experiments S-30-2 and S-30-2S, displaying the impact of elevated sulfate levels (+ 10 g L^{-1} Na_2SO_4) in the latter on the precipitation of silica.

System	Fe in liquor (ppm)	% Fe precipitated	Si in liquor (ppm)	% Si precipitated
S-30-2	84.5	98.2	671	32.1
S-30-2S	131	96.7	705	19.9

The greater presence of schwertmannite within the solids obtained from S-30-2S (indicated by the XRD patterns in Figure 2.34) could also be explained by the proposal from Hockridge et al. (Hockridge 2009) that the phase is composed of a core aggregate of ferrihydrite particles with needles radiating from the surface of the core, formed by direction sensitive aggregation of goethite nanocrystals. The lower degree of silica precipitation in the presence of elevated sulfate levels (S-30-2S) would favour the formation of goethite over time, allowing the nanocrystals to form and aggregate into the characteristic hedge-hog morphology of schwertmannite. However, the greater sulfate concentrations may alone be the cause of the greater schwertmannite levels. Also while there is a correlation between a greater proportion of schwertmannite in the residue and decreasing silica precipitation, it is unlikely that the sulfate-containing phase impacts on the degree of precipitation. It is simply coincidental that the conditions promoting schwertmannite formation inhibit silica precipitation.

The reactor contents (Figure 6.2 in appendix) contained a more intense peak at approximately 25° 2 , suggesting the presence of some goethite. When correlated

with the proportion of silica precipitated in experiment S-30-2S (Table 2.19), it is likely that the decreased amount of silica allows for the formation of a small amount of goethite. This may occur either early in the process or during longer periods (longer than the standard 45 minute residence time) at reaction temperature.

2.8.4. Effect of Residence Time

Since it was apparent that equilibrium with regard to silica solubility was rarely reached in these continuous crystallisation experiments (described in section 2.3.2), the residence time within the reaction vessel will have a strong bearing on the type and proportion of materials that are produced. Variations in the residence time will influence the co-precipitation results by either restricting reactions to shorter times or allowing them to reach a more stable state, both of which may change the concentrations in solutions and proportions of species in the precipitates. With regard to Paragoethite process plant operations, the time in precipitation vessels remains relatively constant, so it is important to maintain the residence time in simulations. This section is devoted to gaining an insight as to how significant the effect of varying the residence would be.

The standard reactor residence time used in all preceding tests was 45 minutes; both the shortening (30 minutes) and lengthening (90 minutes) of this duration was investigated. These times were selected based on the capacity of the pumps used to reach lower or high revolution rates while maintaining stable operation over extended periods. Ferrihydrite precipitation is itself an extremely fast process and therefore was expected to be largely unaffected by such changes. Although there may be a greater proportion of more crystalline material while the concentration is increasing in the early stages of the experiments with longer residence times, the steady-state product will most likely be similar to those conducted under standard conditions. In contrast, Si in solution should not reach equilibrium in the given time, as it precipitates in a slower reaction. Shortening the residence time should further decrease the amount removed from solution, while the opposite applies for a greater time in the reactor.

Although ferrihydrite precipitation is a very fast process, there was in fact a significant difference between the proportions of iron precipitated when the feed rates were varied (Table 2.20). Doubling the residence time decreased the concentration of iron left in solution to 37.4 ppm, from 84.5 ppm in the standard experiment with 45 minute residence times. However, decreasing the time by 15 minutes left 300 ppm more iron in solution than under the standard conditions. It would appear that after the chaotic initial nucleation and short particle growth of the iron phase, it requires a significant amount of time to actually reach equilibrium. To put this into context, even at the shortest residence time, 91% of the solution iron was still precipitated.

Table 2.20: Elemental concentrations of iron and silicon in the steady-state supernatant solutions and percentage removed during reactions employing different residence times.

Residence Time	Fe in Liquor (ppm)	% Fe Precipitated	Si in Liquor (ppm)	% Si Precipitated
30 minutes (S-0-20m)	384	91.0	799	19.3
45 minutes (S-30-2)	84.5	98.1	671	32.1
90 minutes (S-30-90m)	37.4	99.4	511	48.6

The effect on the Si concentrations was, as expected, even greater when viewed in terms of the percentages removed from solution. Primary silica precipitation to reach equilibrium will often take several hours or even days to occur at the temperature and pH of this reaction (Chen 1982). The 15 minute decrease in residence time related to a reduction of more than 12 % in the proportion of silicon removed from solution. Extending the time available to 90 minutes corresponded to the removal of 15% more of the initial silicate level from solution. This proves that equilibrium was not achieved in the reactions under standard conditions and the dissolved silicate concentration was still well above the equilibrium solubility of silica. It also

represents evidence that an effect of the available ferrihydrite surface area is to greatly increase the rate at which silica can be precipitated, and when this templating process is interfered with, such as by the competitive adsorption of sulfate, that precipitation rate is retarded.

2.8.5. Effect of pH

As stated in section 1.2.2.1, the precipitation of iron oxides is highly dependent on the pH. Conversely, silica precipitation in the acidic region is under most circumstances not greatly affected by small variations in pH.

The effect of a pH change (±0.5 of a pH unit) from the standard value (pH_{85} = 2.65) was investigated by again conducting variations on the baseline S-30-1 experiment. The initial pH of the feed solution remained constant throughout the experiments and the reaction pH was adjusted by varying the feed rate of sodium hydroxide solution. The lower pH experiment also served to provide some information as to the extent that associated silica can retard the formation of more crystalline phases. At pH 2.15, goethite formation is more favourable than in the standard reaction; if goethite was absent from the residue formed at low pH, it would show the strength of the inhibition from silica. To further investigate this point, an experiment containing twice as much silicate in the feed was also conducted at the same pH level. Such an experiment would indicate whether the decreased iron hydrolysis rate impacts on the proportion of Si removed during the precipitation process.

Aside from apparent differences in the proportion of schwertmannite in the precipitates, the XRD patterns for samples from S-30-2, S-30-pH1, S-30-pH2 and S-30-pH3 (defined in Table 2.15) displayed little difference (Figure 2.35). There was no evidence of goethite, suggesting that even at lower pH levels, the silicate concentration examined was able to inhibit the formation of more crystalline phases. Interestingly, the sample prepared at pH 2.15 (S-30-pH1) gave the XRD pattern most resembling ferrihydrite, indicating it had the lowest proportion of schwertmannite of the four systems. In addition, there was very little decrease in ferrihydrite crystallinity at the highest pH (S-30-pH3), which was an unexpected outcome. It was

found earlier that an operating pH_{85} of 3 in a silica-free, nitrate experiment produced 2-line ferrihydrite (section 2.3). However, in this case a slightly higher pH (3.15) yielded the 6-line species. Whether it was the presence of silicate or sulfate that caused this effect is unknown, however, it is likely that the interaction between iron and one or both of these species slows the iron hydrolysis rate, thus producing the more crystalline phase.

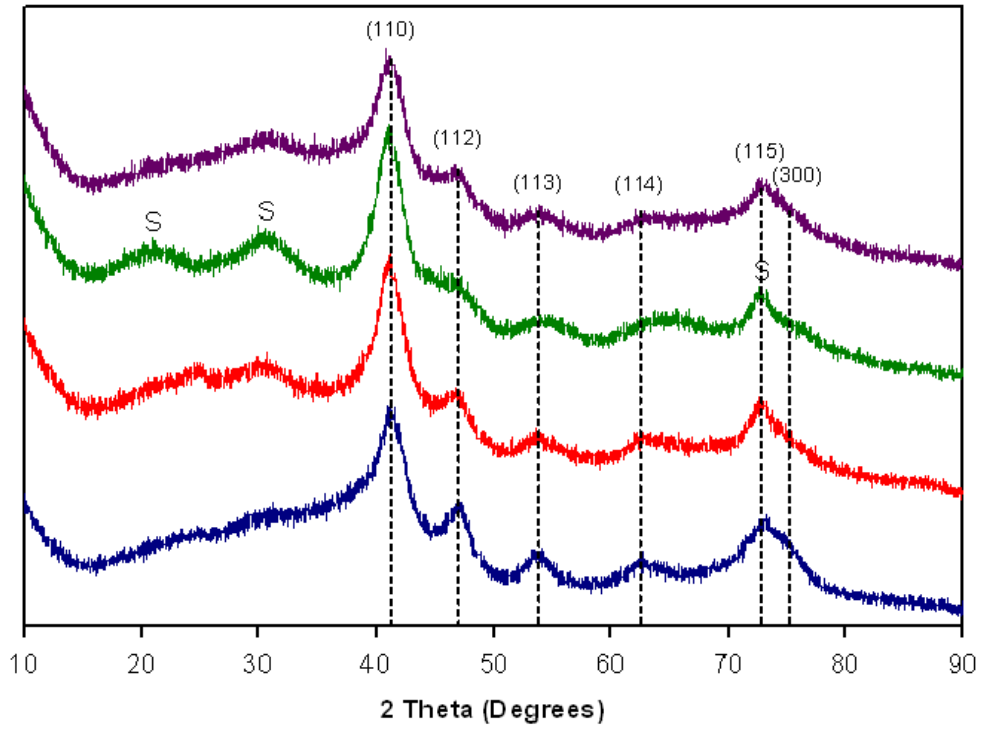

Figure 2.35: XRD pattern of steady-state samples from experiments S-30-pH1 (pH 2.15, blue), S-30-pH2 (pH 2.15, red), S-30-2 (pH 2.65, green), and S-30-pH3 (pH 3.15, purple). Peaks indicating schwertmannite are highlighted by the letter S.

The pH during precipitation had a significant impact on the proportion of silica appearing in the precipitate (Table 2.21). As has previously been shown that silica precipitation is dependent on the amount of iron present (section 2.7.2), it is reasonable to conclude that the difference shown in Table 2.21 was due to the iron hydrolysis rate. The fastest hydrolysis rate would occur at the highest pH, which corresponds to the greatest Si removal from solution. As the hydrolysis rate rises, the primary particle size decreases, particles are produced in greater number and at a

greater rate. This may increase the total available surface area, producing a larger number of binding sites for monosilicic acid adsorption.

Table 2.21: Elemental concentrations in solution and precipitation percentages from these systems.

pH	Fe in liquor (ppm)	% Fe precipitated	Si in liquor (ppm)	% Si precipitated
2.15 (S-30-pH1)	71.9	98.4	580	40.6
2.15 2x Si (S-30-pH2)	246	94.1	1367	34.1
2.65 (S-30-2)	84.5	98.2	671	32.1
3.15 (S-30-pH3)	28.5	99.3	430	51.5

Although there is little difference between the solubility of silica at pH 2.15 and 3.15 (Iler 1979), the rate of polymerisation is dependent on the hydroxide ion concentration. The increase in pH represents an order of magnitude increase to the hydroxide concentration, which would accelerate the silica precipitation rate. This explains why there would be less Si remaining in solution in the pH 3.15 system, but not why there was less observed at pH 2.15 than at 2.65. The surface charge of the ferrihydrite would be greatest at the lowest pH, which would increase the likelihood of silica adsorption. Under these conditions the precipitated silica surface itself would be closest to neutral, increasing the possibility of aggregating with oligomeric units or small particles that have formed elsewhere in the liquor.

2.8.6. Aging Investigation

To investigate the extent to which iron / silicate feed aging might affect the process, a precipitation experiment was conducted with the same feed concentrations as S-30-1 using a feed solution that had been aged for several weeks (S-30-A).

The XRD pattern in Figure 2.36 displays a goethite peak in the precipitate from the S-30-A system (indicated by the G). The system with the fresh feed solution behaved similarly to standard experiments, producing a residue that contained no traces of more crystalline material. It can therefore be concluded that the products of an aged feed are more crystalline, showing far less influence from the presence of Si. This was contrary to what was initially expected, as it was believed that Si would polymerise at least to preliminary oligomers while aging in the feed, which would mean that a greater proportion of the Si content of the solution would reach the solid phase. Based on earlier results (Section 2.4.2), this would in turn have resulted in a reduction in product crystallinity.

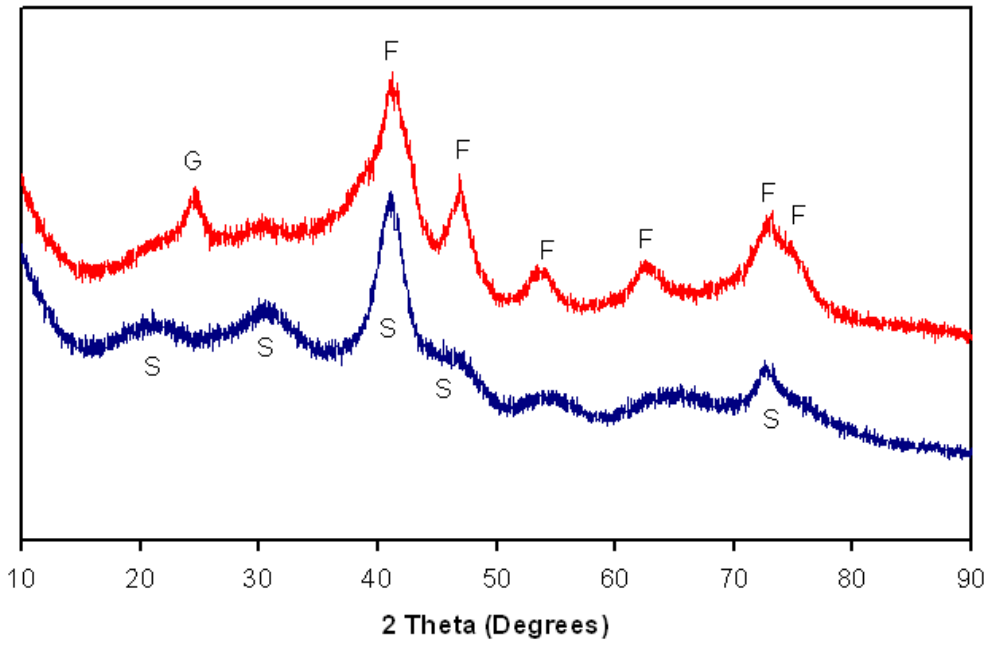

Figure 2.36: XRD patterns of precipitates prepared using S-30-2 (blue) and S-30-A (red) feed solutions.

The product prepared using the aged solution also appeared to be predominantly ferrihydrite, whereas that made from the fresh solution displayed a structure containing a greater proportion of schwertmannite (indications of schwertmannite are highlighted by the S in Figure 2.36). The minor ferrihydrite peaks were much more clearly defined and prominent in the S-30-A sample. The major peak was also broader, an attribute of ferrihydrite. While this was partially the effect of the presence of goethite, the impact on the XRD patterns of the more crystalline phase was small and would not cause such a significant broadening.

There was significantly less silicon in the supernatant solutions from the S-30-A experiment (Table 2.22). As expected, more silica was co-precipitating with the ferrihydrite, no doubt due to polymerisation occurring prior to the reaction. It would appear that polymerisation prior to adsorption on the ferrihydrite particles lessened the impact that precipitated Si has on the crystallinity of the solid. Therefore it was likely that silica particles or at least oligomers were aggregating with precipitated ferrihydrite particles.

Table 2.22: Elemental concentrations in supernatant solutions taken from S-30-2 and S-30-A, displaying the greater proportion of silica precipitated from the experiment using the aged solution.

System	Fe in liquor (ppm)	% Fe precipitated	Si in liquor (ppm)	% Si precipitated
S-30-2	84.5	98.2	671	32.1
S-30-A	53.0	98.8	470	51.8

Due to the greater amount of silica precipitated from the aged solution, it is reasonable to conclude that polymerisation was occurring before the precipitation step, and therefore before adsorption. It was previously shown in section 2.3.2 that the greater the amount of Si in the precipitate, the lower the residue crystallinity. However, the product of the S-30-A experiment behaves differently, being affected less, despite a greater amount of silica. This shows that the reactions differ, and while

it is not possible to completely rule out any polymerisation prior to adsorption in systems with fresh feed solutions, it is reasonable to conclude that the majority of the adsorbed species are in a monomeric state. This stands to reason, as silica polymerisation is slow at room temperature and at relatively low concentrations, whereas once the ferrihydrite particles are formed the adsorption (kinetically fast) would occur immediately.

2.9. Summary

Through the combination of several insights gained into the co-precipitation process in this chapter, it is apparent that ferrihydrite has an influence on the formation of silica and vice versa. Ferrihydrite particle surfaces provide binding sites for the adsorption of silicic acid. As a large number of the sites become occupied, immobilised silica monomers are in close proximity, therefore aiding polymerisation. This process increases the rate and total proportion of silica precipitation. Interference with the adsorption and subsequent polymerisation process can significantly impede silica precipitation. The influence of sulfate in solution has been shown in this chapter; sulfate binds strongly with ferrihydrite surfaces and thus competes with silicic acid for adsorption sites.

The adsorption of silicic acid on the ferrihydrite surface decreases the apparent crystallinity of the iron oxyhydroxide phase, a phenomenon which is further investigated in chapter 4. The ferrihydrite / silica surface association also appears to retard the phase transformation generally observed to occur in the meta-stable ferrihydrite. However, both of these effects are nullified when the feed solution is aged, as silica polymerisation occurs before ferrihydrite is formed, thus decreasing the interaction between ferrihydrite and silicic acid. This suggests that a greater degree of silica polymerisation upon interaction with iron decreases the influence of silica on the structure of the iron oxide/oxyhydroxide formed.

The surface charge of the co-precipitates is dependent on the Si:Fe ratio. At great enough ratios the IEP decreases and continues to do so as the proportion of silica increases. To investigate the physical properties of the co-precipitates, a larger sample volume is required, which is the subject of chapter three.

3. LARGE-SCALE EXPERIMENTS

3.1. Introduction

The experiments described in this chapter were conducted for multiple reasons. The primary purpose was to produce sufficient sample volumes to enable physical property analyses. Preparing a single litre of steady-state sample slurry using the small-scale apparatus would require just over 9 hours; it was therefore not viable to produce sample slurry sizes on a scale of several litres. The experiments also served as an indication of whether the crystallisation process behaved consistently on a larger scale, or if it was strongly influenced by hydrodynamic and other issues associated with the experimental set-up. Experiments at different scales were intended to provide insights when considering the relevance of this study to the full-scale industrial iron removal process.

Knowledge of some physical properties that influence aggregation and adsorption behaviour of the co-precipitates is not only important towards the fundamental understanding of the reactions that produce them, but also to how the findings may be applied in plant operations. The particle surface area will impact on the affinity for the residue to adsorb both impurities (highly desirable) and the product zinc species (clearly undesirable). The majority of the other measured quantities (surface charge, fractal dimension, PSD, density) are related to the solid/liquid separation process and the ease with which it can be achieved, as this step can be a major bottleneck in hydrometallurgical operations. If the particles are aggregated to form larger structures that are permeable and have roughly the same morphology, they will settle rapidly to a high sediment density and filter well. However, structures that retain a high proportion of intra-aggregate liquor can lead to low sediment densities and poor filtration (Farrow 1991). If such a decline in properties is observed, the practical implications for the process could be quite bleak, to the point of requiring condition modification or the introduction of additional treatment steps in the circuit.

A number of experiments were also conducted in which the feed solutions were prepared under conditions that created a temporary high silica supersaturation, with the aim of inducing polymerisation. Process liquors are saturated with respect to silica, as were all silicon-containing feed solutions used in co-precipitation experiments within this study. Homogeneous silica polymerisation requires concentrations well in excess of the equilibrium saturation values. It is also a very slow process, and therefore long reaction times are required for a significant amount of polymerisation to occur, even at the low pH and mild ionic strength of the feed solutions. However, plant conditions involve extremely high ionic strength, as well as some coarse feed material that can aid nucleation of silica particles. This, in combination with long periods of time liquors spend in leaching loops before reaching the precipitation step, makes it likely that polymerisation has occurred to the point where it becomes significant. By inducing silica polymerisation from high supersaturation in the feed, it was hoped to simulate this effect and thereby examine its consequences on the iron removal products.

3.2. Experimental

3.2.1. Scale-Up Details

This set of experiments was designed to be equivalent to those outlined in chapter 2 except on a larger scale. The 110 mL glass jacketed reaction vessel was replaced with a 2.5 L (effectively) stainless steel jacketed container (150 mm internal diameter and 175 mm internal height). The main reaction conditions (concentrations, pH, temperature and residence time) all remained the same. For each experiment, 18 L of the iron/silicon feed solution were prepared. Six residence times within the reaction vessel would consume 15 L; the additional 3 L were in case of problems during the experiment or if more steady-state sample was required to be produced.

Figure 3.1 shows the experimental set-up for the larger scale crystallisation. The feed tank is a 20 L stainless steel vessel; although it is jacketed, the solution was maintained at room temperature.

Much greater flow rates were required for the iron/silicon feed and product removal to maintain the correct residence time, increasing from only 147 mL h^{-1} in the small-scale tests to 3.33 L h^{-1}. The medical dosing pumps used previously were unable to cope with such flow rates and were replaced with Watson Marlow 505J and Masterflex 7518-10 peristaltic pumps with 17 gauge norprene tubing. The original pump remained adequate for the base feed solution, for which the flow rates fluctuated around 100 mL h^{-1}.

Figure 3.1: Photograph of the crystallisation set-up employed in the larger scale experiments.

Flow rate tests, similar to those described in section 2.2, were conducted to calibrate the flow rates of the pumps; unlike the small-scale tests, no alteration of these calibration parameters was required between experiments. As the rates were significantly higher and small differences in viscosity made no observable difference in the large gauge tubing, the pump calibration was maintained without drift over much longer periods of time.

A separate temperature probe was employed in the large-scale experiments to monitor the temperature inside the reactor. There was a larger volume compared to surface area associated with this vessel, due to both its size and the fact that, unlike the small reactor, the jacket does not include the base. As a consequence, the circulated water was required to be 89 °C in order to effectively maintain 85 °C in the reactor. The temperature required was dependent on ambient conditions, as the feed solution temperature and heat loss from tubing varied slightly. However, a difference of less than 5 °C was not sufficient to adversely affect the reaction.

The solutions were made up in a similar way to those required for the small-scale work (section 2.3.1, table 2.4). The solid form of the desired iron species was dissolved in aliquots (the total mass was divided among 2L volumetric flasks to promote dissolution) and added to the feed container using the flasks. Sodium metasilicate was dissolved in deionised water, upon which the pH was dropped to between 1 and 1.5 with the appropriate acid. This solution was then added to the feed container and the total volume was brought to 18 L, if more water was required. The solutions were then agitated for 10 minutes to promote mixing and homogeneity.

As in the small-scale experiments, XRD, ICP and DLS were conducted on selected samples collected at the completion of the relevant residence time. Subsamples of 100 mL were obtained for these analyses, as the majority of the 2.5 L slurry obtained from each residence time was required for other measurements, such as rheology and FDA. Measurements were conducted to obtain particle size distribution (PSD), fractal dimension, settling rate, aggregate density, rheology, surface area and physical density. XRD and ICP were also used to confirm whether the systems were behaving in a similar manner to the previous small-scale experiments.

3.2.2. Preparation for Analysis

Samples taken for XRD were filtered and washed with de-ionised water multiple times. The samples from sulfate media with the highest Si content displayed very poor filtration properties and attempts at vacuum filtration through a 0.45 m membrane proved futile. A pressure filtration vessel was used and was more effective mainly by virtue of greater membrane surface area. It has a diameter of 142 mm as compared to the vacuum system which uses 47 mm diameter membranes, and there was not enough solid to cover and disrupt the entire membrane. The analysis was conducted in an identical manner as the small-scale experiments, using the same equipment (section 2.2).

The procedures and equipment used in obtaining and preparing the ICP (section 2.2.2) and DLS (section 2.2.3) samples were unchanged from those of the small scale

experiments. Particle size and fractal dimension data were obtained in the same fashion as described in the last paragraph of section 2.2.3. Density measurements were conducted using a Quantachrome Multipycnometer MVP-1, slurry samples were filtered through 0.22 m membranes and oven-dried at 100 °C. After similar preparation, samples for surface area analysis were outgassed in a vacuum at 100 °C before being measured using a Micromeritics Tristar 3000. Floc density analysis (FDA) was conducted using slurry samples that were diluted with excess reaction liquor, which was separated from slurries destined for other analyses. The cell through which the samples were viewed was 2 mm deep and 6 mm wide. The cell was flushed with milliQ® water then filled with sample slurry. After isolating the cell, digital video of the settling particles was taken over a total time of approximately 30 minutes per sample, which was refreshed throughout the process to obtain representative data (Fawell 2009).

3.2.3. Settling Rate

Settling rates were measured for each residence time at reaction temperature, both with and without the addition of flocculant. Samples (100 mL) were collected and placed in 250 mL measuring cylinders (38 mm internal diameter) in water baths at 85 °C for at least 10 minutes to equilibrate. Both samples were mixed twice using a plunger (two plunges up and down, 33 mm diameter circular disc plunger), then one sample was dosed with the required volume of flocculant, mixed twice more with the plunger, the plunger removed and the settling rate measured by following the fall of the mudline with time. The settling rate is derived from the initial linear portion of the settling curve, which in this case meant the time taken fall from the 110 to 40 mL marks on the cylinders (73 mm). Given the large percentage of very fine material in the product, many of the non-flocculated samples had poorly defined mudlines and were difficult to measure.

The flocculant used was Magnafloc 800HP (Ciba Specialty Chemicals, now BASF), which is known to be a high molecular weight homopolymer of acrylamide (i.e. nominally 100% nonionic; while some hydrolysis of the amide functionality to acrylamide is possible, this would represent less than 1% of the monomer units

within the polymer). Solutions of such flocculants need to be prepared very carefully to ensure that the “powder” flocculant grains don’t gel or aggregate upon the introduction of water, with the entangled polymer chains leading to the grains swelling substantially. This can occur if water is added directly to the powder without intense mixing (although excess mixing can also lead to degradation), and gels once formed cannot be readily disrupted. A simple and reproducible make-up process involves an initial wetting of the flocculant grains with ethanol (Scott 1996). Approximately 1 g of 800HP is accurately weighed and dispersed in 1 g of ethanol. After 5 minutes, water is added in aliquots of 5 mL with constant shaking. Once approximately 50 mL has been added the remainder of the water can be added at once. The total volume is based on the mass of flocculant to obtain a concentration of 0.5 wt%; if exactly 1 g of flocculant is used, the total solution will be 200 g. The solution is then placed on a shaker table at 200 rpm for 3 hours, then lowered to 120 rpm for a further 20 hours.

3.2.4. Slurry Behaviour Measurements

The solids concentration required for rheological characterisation is many times greater than that produced in the crystallisation process. Slurry obtained upon reaching steady-state conditions was allowed to settle and the supernatant solution was subsequently pumped into another vessel. The remaining concentrated slurry was centrifuged, with any separated liquid removed using a syringe. The supernatant liquor from the settling process was pressure filtered and used for dilution where required. The majority of the rheology measurements were conducted on a Haake Rheometer VT550 using an SV2P cup and rotor sensor. Some further measurements, including tests on diluted residue samples, were conducted using FL-1000 or FL-100 vanes, depending on the amount of slurry produced (some samples would not accommodate the larger vane). The data was compiled with Thermo-Haake Rheowin Pro software.

Once FDA and rheology measurements were completed on a sample, it was then submitted for particle size distribution, surface area and dry particle density measurements. The only drawback with this method is that the PSD will be

potentially distorted due to the process used to concentrate the slurry. By removing the bulk of the liquid by decantation, any particles below a certain size that would not settle naturally or ***via*** centrifugation would be lost and not analysed. However, this would represent a relatively small fraction of the solid and therefore should not interfere greatly with the measurement. PSD measurements were conducted on slurry samples diluted in previously removed supernatant solution, using a Malvern Instruments Mastersizer MS2000.

3.3. Sulfate Systems

3.3.1. Preparation Conditions

In these experiments, the same constituent molar ratios (Si:Fe) in the feed as those described in section 2.3 were used on the larger scale (0, 0.053, 0.111, 0.25, 0.429); condition details are provided in Table 3.1.

Table 3.1: Experiments producing the samples referred to in this section, all were conducted at 85 °C and a pH_{85} of 2.65. Ideal feed concentrations are given, variation occurred due to experimental uncertainty. * LS-x-x denotes the larger scale systems (reactor volume 2.5 L).

System*	Feed Concentrations		Si:Fe Ratio
	Iron (g L^{-1})	Silicon (g L^{-1})	
LS-0-1	6.3	0	0
LS-5-1	6.0	0.16	0.053
LS-10-1	5.7	0.32	0.111
LS-20-1	5.0	0.63	0.25
LS-30-1	4.4	0.95	0.429
LS-20-2 (section 3.3.7.1)	4.0	0.49	0.25
LS-30-2 (section 3.3.7.2)	4.4	0.95	0.429

The conditions were designed to promote silica polymerisation in the liquors before the precipitation reaction takes place are similar to, but an extreme version of, the aging test described in section 2.8.6. To obtain polymerisation in the feed without the need for prolonged aging, the solution was prepared in a way designed to maximise the silicate concentration at the point of pH adjustment. This was achieved by dissolving the total amount of sodium metasilicate required for all 18 L of solution in

only 500 mL of water (this volume was raised to 1 L for the LS-20-1 and LS-30-1 systems, as dissolution of more than 80 g of sodium metasilicate in only 500 mL and adjusting the pH down to below 2 induced rapid gelation). The solutions were left to sit for two hours to provide an opportunity for the silicic acid monomers to polymerise before commencing the precipitation reaction. Although silica polymerisation is slow, it occurs at a greater rate when the concentration is increased. The solubility of silica at low pH and room temperature is between 0.1 to 0.2 g L^{-1}. Experiments in this study containing higher silicon levels had concentrations two orders of magnitude greater than the solubility.

3.3.2. Structural Analysis

XRD measurements were only conducted on samples from the final residence times and the final reactor contents, as the purpose was to determine steady-state behaviour and compare that with precipitate structures from the small-scale crystallisations.

Figure 3.2 shows that the predominant phase in all samples was ferrihydrite, suggesting the reaction was proceeding as intended (ferrihydrite being the desired primary phase). As in the small-scale experiments, the LS-0-1 sample contained detectable amounts of goethite. However, goethite reflections were also observed in the patterns of the large- scale silicate-containing systems, whereas the more crystalline phase was absent from the corresponding small-scale samples. It is possible that insufficient silicon was precipitated during the iron oxide formation to retard the phase transformation from ferrihydrite to goethite. However, it is more likely a similar process is occurring to that in the small-scale aging test, as non-trivial proportions of silica were precipitated in all previous experiments. This is most likely an outcome of the feed preparation method described in section 3.3.1 leading to a substantial degree of silica polymerisation prior to addition. Since the feed solutions were prepared within 3 hours of the experiment commencement, this effect may be due to polymerisation in the feed prior to the reaction, as only a relatively short amount of time would be required for polymerisation at such high concentrations.

Likewise, there is no discernable decline in the crystallinity of the ferrihydrite (no observable peak broadening), which was the observation in the small scale experiments. It seemed that the proportion of amorphous silica in the precipitate was not great enough to provide an observable change. This may again be the case, but if silica polymerisation is occurring prior to the precipitation the crystallinity would again remain unaffected.

Figure 3.2 demonstrates, as expected, that schwertmannite is most likely present in the residue, displayed through the sharpening of the (110) peak and the different relative intensities of the (115) and (300) peaks. Due to the presence of goethite, the sharpening of the (110) peak is difficult to resolve, however, the change in the relative intensities of the two reflections at the greatest angles, and the decreased intensity of the (112) reflection, are both consistent with the sulfate-containing phase. It is also easiest to observe in the LS-20-1 sample where there does not appear to be any goethite present.

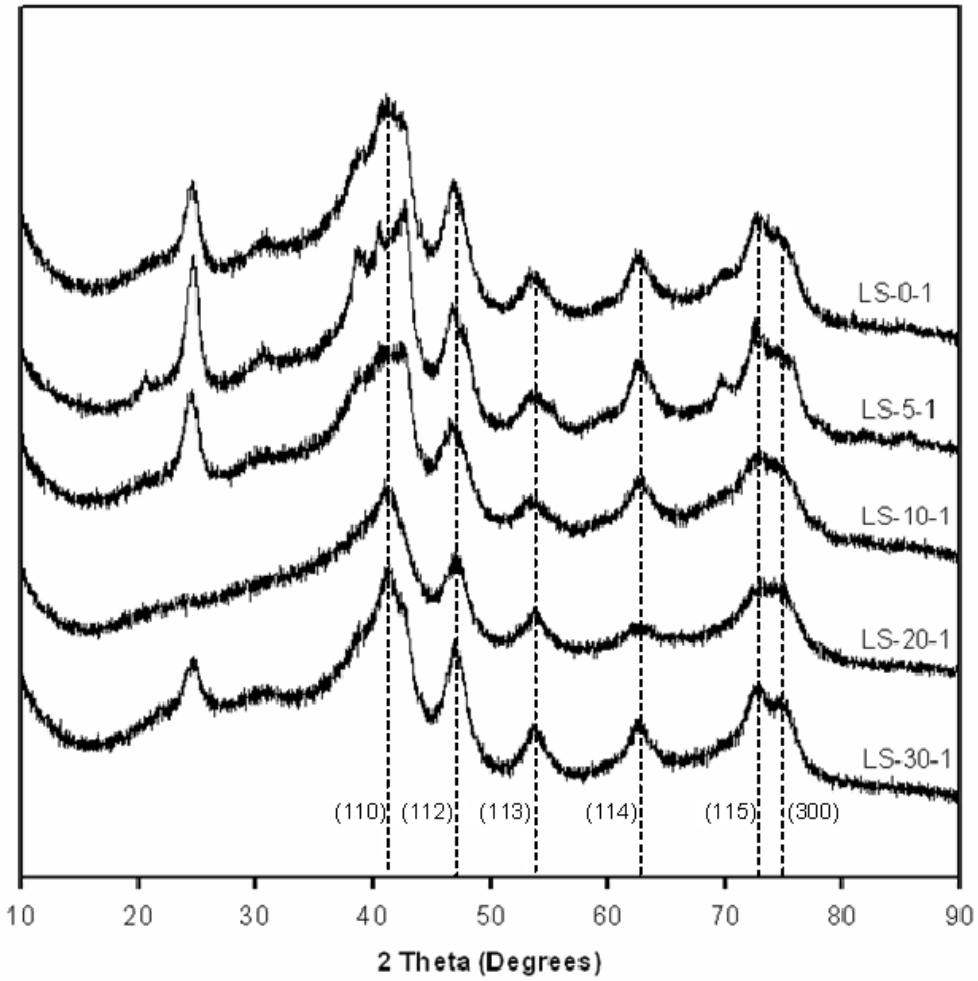

Figure 3.2: XRD patterns obtained from steady state samples of LS-0-1 to LS-30-1.

An interesting point to note is that although prepared in a very similar way, the LS-20-1 sample was the only product from the large-scale tests to not display the presence of goethite. This was most likely because the solution was prepared at a slightly lower concentration thereby not inducing the same degree of polymerisation in the feed prior to the co-precipitation reaction. To determine whether polymerisation had occurred in the feed (and if so then to what degree) required examination of the supernatant solution concentration data.

3.3.3. Elemental Composition

A comparison of elemental concentrations in the liquors before and after precipitation clearly displays the disparity between the small-scale (Table 2.6) and large-scale (Table 3.2) experiments with respect to the proportion of silica precipitated. Between 25 and 35 % silica precipitation was achieved at the small-scale, whereas almost 70 % was observed in the same large-scale systems. Such a high level of precipitated silica excludes the possibility that goethite is present due to a lack of silica in the residue. This would therefore suggest that silica polymerisation was occurring prior to the co-precipitation reactions.

Table 3.2: Elemental concentrations from the steady-state samples of the sulfate systems.

System	Fe in Liquor (ppm)	% Fe Precipitated	Si in Liquor (ppm)	% Si Precipitated
LS-0-1	10.3	99.8	-	-
LS-5-1	2.73	>99.9	92.0	40.1
LS-10-1	2.94	>99.9	108	62.1
LS-20-1	11.9	99.8	261	57.6
LS-30-1	13.7	99.7	263	68.9

The silicon concentration in the large-scale liquors actually dropped below the value reached in the small-scale aging test (S-30-A), suggesting a greater proportion of polymerisation in the large-scale feed solution. The driving factor of an elevated Si concentration has yielded a much faster reaction rate and thus a significant degree of polymerisation has occurred. Note that the concentrations in the liquors from the LS-20-1 and LS-30-1 systems still remained above the solubility of silica (~ 180 ppm at 85 °C (Chen 1982)) and well above the values reached in the nitrate system tests (section 2.4). Therefore it would appear that the significant amount of polymerisation occurring prior to the precipitation reaction still did not allow equilibrium to be reached in these systems. However, in those systems with lower feed concentrations, the Si level decreased to slightly below the equilibrium concentration. This was due

to the low volume at which the silicate solutions were prepared. The sodium metasilicate was dissolved in 500 mL of water (1 L for more concentrated solutions, such as LS-30-1), meaning the concentration was much greater at this point than when it was introduced to the rest of the feed solution. The LS-5-1 system contained approximately 5700 ppm of Si in the 500 mL preparation solution when the pH was adjusted. This would induce a significant amount of polymerisation, as the solubility with respect to silica would be around 60 ppm at room temperature (Marshall 1980). The concentration would be barely above the solubility of silica upon dilution in the total 18 L feed stock. The solubility rises significantly when the solution is heated to 85 °C, and therefore it is unlikely that the solution would be saturated during the reaction.

In terms of the industrial process circuit, this result suggests that a significant degree of polymerisation could occur in the leaching stages, before the liquor reaches a precipitation tank. In some respects this is a positive result, as a much greater proportion of the soluble silicates should be removed during the formation of the residue. However, this may negatively impact upon the physical properties of the product material.

3.3.4. Physical Properties

Measurements were conducted on steady-state samples from each of the reactions; the data obtained is summarised in Table 3.3. The same sampling and measurement processes were conducted for each experiment, with the only difference being in the time between preparation and analysis; this time was subject to the availability of instruments.

Table 3.3: Physical data obtained from LS-0-1, LS-5-1, LS-10-1, LS-20-1 and LS-30-1.

Sample	Fractal Dimension	Surface Area ($m^2 g^{-1}$)	D(0.1) (m)	D(0.5) (m)	Density ($g\ cm^{-3}$)
LS-0-1	2.07	132.0	9.28	16.26	3.56
LS-5-1	1.81	109.1	3.22	17.10	3.62
LS-10-1	1.72	150.2	2.17	15.73	3.39
LS-20-1	1.87	248.8	1.52	8.56	3.42
LS-30-1	1.45	255.3	0.90	6.74	3.05

3.3.4.1. Aggregate Analysis

The particle size distribution statistics and fractal dimension values given in Table 3.3 display decreasing trends with increasing feed silicate concentration. This provides insight into the impact of adsorbed oligomeric silica on the ferrihydrite aggregates. XRD analysis has shown no evidence to suggest that the primary particle size of the ferrihydrite has been affected, meaning these property changes are entirely related to the aggregation process. It would appear that the adsorption of silica oligomers or colloidal particles interrupts the aggregation process by providing physical barriers between ferrihydrite particles and possibly inducing different surface interactions during aggregation (Fe-O-Si as opposed to Fe-O-Fe). This may simply limit the size which aggregates are able to reach, i.e. producing aggregates structures that are easily ruptured by agitation or turbulence.

The LS-20-1 sample produced the only fractal dimension value that did not fit the trend; a possible explanation is provided in the XRD data. The residue produced in that experiment was the only one of the five not to contain goethite. As indicated in section 2.4.1. the formation of goethite (most likely by transformation of ferrihydrite) is inhibited by the presence of silica, however, polymerised silica does not have the same effect, as shown in section 2.8.6. The lack of goethite would suggest that a significant amount of silica was still in a monomeric state or at a low degree of

polymerisation, thereby still having an influence on ferrihydrite transformation. Such an effect would also be seen in the aggregation process, decreasing the detrimental influence of polymerised silica on the aggregates.

The particle size distributions are bimodal, with a small peak related to finer aggregates often centred between 1 – 3 m, and the primary peak relating to more coarse aggregates centred anywhere between 10 and 25 m (Figure 3.3). Interestingly, the percentage of aggregates that appear in the former peak increases as the proportion of silica in the residue increases. In most cases, this constitutes a small fraction of the clusters, often containing less than 10% of the total sample volume. However, in the case of the LS-30-1 sample, these smaller particles constitute a much greater proportion of the total number of aggregates. The percentages of the aggregates falling below 3 m were 4.2, 8.6, 11.4, 13 and 26.8 % for LS-0-1, LS-5-1, LS-10-1, LS-20-1 and LS-30-1 respectively. Such a trend may suggest that a greater number of aggregates are prone to significant breakage from shear forces in the vessel when larger proportions of associated silica oligomers or colloids are present. This correlates well with the low fractal dimension observed for such samples.

The fractal dimension is indicative of the structures formed by the aggregation process and potentially the relative strength of those aggregates (Jullien 1987). Such values refer to how well packed the aggregates are; a decreased fractal dimension suggests that the aggregates are no longer packing tightly, with more space between the individual particle branches (section 1.1.5). A low fractal dimension can also represent weak aggregates, particularly as the size increases (Mullin 1993). This is a far more significant trend than that observed in the fractal dimension measurements of the small-scale chloride systems (section 2.6.4).

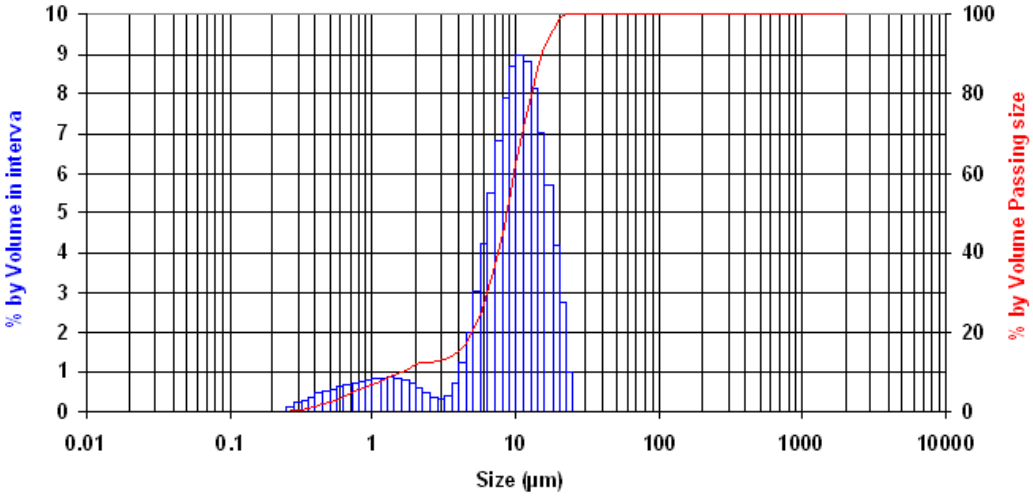

(a)

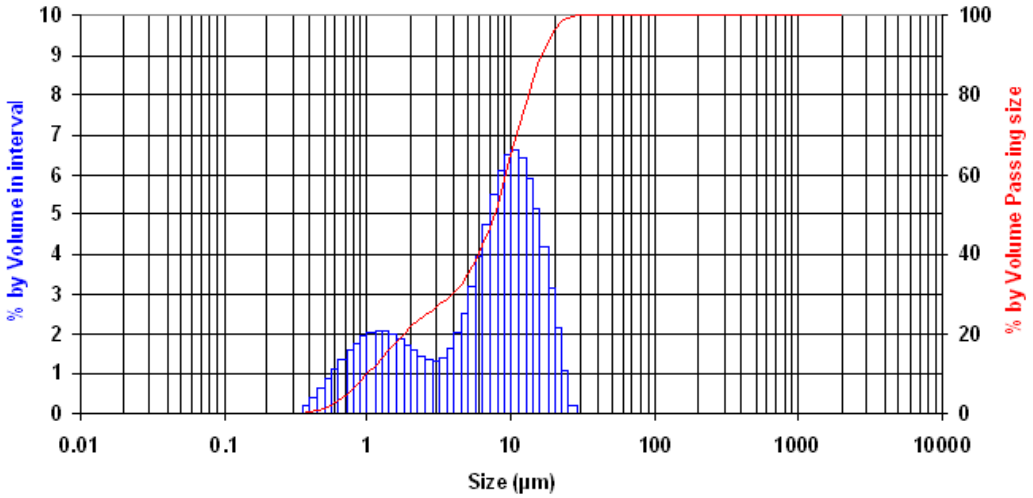

(b)

Figure 3.3: Particle size distribution measurements made on samples from (a) LS-20-1 and (b) LS-30-1 illustrating the bimodal distribution and the increase in the proportion of finer particles (below 3 m) with greater Si:Fe ratios in the residue. PSD data for all large-scale sulfate systems are provided in the appendix in Figure 6.3 and Figure 6.4.

With regard to the plant situation, greater space in aggregates in suspension means more entrained or intra-aggregate liquor. The trend observed suggests the silica will detrimentally affect the process, as displacing liquor from within the aggregates becomes more difficult. At the low solids concentration involved in these lab simulation experiments, variations in the particle size do not significantly affect the efficiency of flocculation and the settling process. However, at the higher solids

levels dealt with in the plant operations it begins to have a much greater influence. As particle size drops, greater flocculant concentrations are required to flocculate the aggregates to an acceptable level. A decrease in particle size also generally decreases the optimum solids concentration for flocculation (that which gives the highest settling flux, i.e. solids throughput) and the underflow density that can be achieved. This places greater demands on the thickener operation.

The dry particle density also declined with increasing feed Si:Fe ratios in the residue, which is explained by the increasing silica to ferrihydrite ratio. Ferrihydrite (3.96 g cm^{-3}) is denser than silica (2.63 g cm^{-3}) due to silica being more porous and iron being a heavier element than silicon (Iler 1979; Cornell 1996).

3.3.4.2. Surface Chemistry

The surface area of the particles increased with greater initial silicate concentrations (Table 3.1). This is most likely due to silica having a higher surface area than ferrihydrite and is indicative of a surface association. If all of the silica was encapsulated in the ferrihydrite aggregate, or even structurally associated, there would be little or no effect.

In a similar manner, there was a significant change in the co-precipitate surface charge with increasing silicate in the feed, which would only occur if the surface chemistry had been altered. As referred to in chapter 2, the generally accepted isoelectric points (IEP) of silica and ferrihydrite sit on opposite sides of neutral pH; the IEP for ferrihydrite is approximately pH 8, while that for silica is taken as 2. Therefore at any pH between these values the surfaces of the two phases will be oppositely charged. This has the potential to impact greatly on the behaviour of the particles in suspension and how they interact. At reaction pH the particles repel similar particles (comprising of the same material), however, where ferrihydrite and silica coexist they will attract each other and bind favourably.

In the surface charge measurements described in chapter 2, only the steady-state samples were analysed; for the larger scale experiments, a number of different

residence times for selected systems were examined. Figure 3.4 displays the similarity in zeta potential across the majority of residence time samples for one of the co-precipitation experiments. The first residence time displays more positive values and has a greater IEP; given that silica precipitation is slower than that of the iron, it will not initially achieve the same proportion of surface coverage or constitute as much of the precipitate as it does at later residence times. Aside from the first residence time, the surface charge remained relatively constant across much of the pH range for the residence times studied.

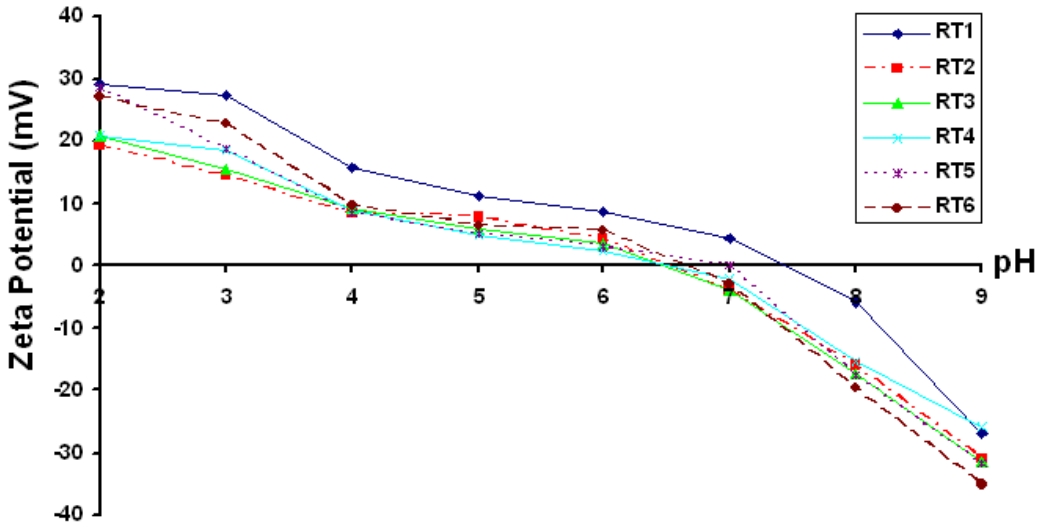

Figure 3.4: Zeta potential measurements from samples of each residence time from experiment LS-10-1.

Figure 3.5 displays a decrease in IEP as the proportion of silicate in the feed was increased. One possible consequence of having less (or no) silicic acid adsorption on the ferrihydrite surface is the opportunity for more sulfate to remain on the surface due to the lack of competition from silicic acid monomers. The greater amount of sulfate appears to decrease the IEP even further. The substantially decreased IEP observed for the sample from LS-20-2 system is of some interest, as this value was much lower than observed in any other system, even compared to those containing far greater proportions of silica in the residue (for which silica would be considered to dominate surface behaviour). This may be due to the presence of larger proportions of goethite, which generally has a lower surface area, allowing the silica to further dominate the surface behaviour. It may also be a result of the greater silica

polymerisation in the feed, providing a lack of competitive adsorption with sulfate. The combination of having greater surface coverage of ferrihydrite by sulfate and the presence of silica surfaces in the aggregate may have contributed to the shift of the IEP to a lower pH.

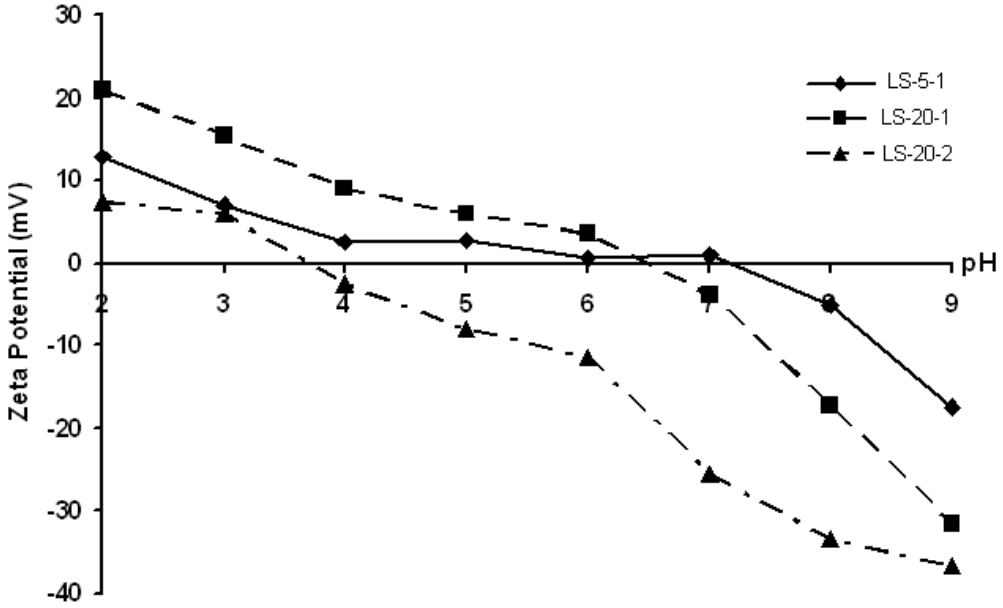

Figure 3.5: Zeta potential measurements taken from samples of LS-5-1, LS-10-1 and LS-20-2, the last of which is described in section 3.3.4.1.

The presence of sulfate has been seen to decrease the IEP of ferrihydrite to a value below those measured in nitrate and chloride media. Sulfate also appears to have the effect of minimising the magnitude of the zeta potential (figures 2.17 and 2.23). This would be expected to have a large impact on the aggregation and adsorptive properties of the residue, as at Si:Fe ratios above 0.25, the IEP would be within 1 – 2 pH units of the reaction pH. The very low surface charge at this point would favour very rapid aggregation and decrease the resistance to the adsorption of positively charged ions.

Due to the lack of precision with which silica polymerisation can be controlled in the feed before the reaction, it is difficult to discern exactly what is occurring in this process. However, there are several possible facets of the reaction to be considered. The first is the proportion of silica being removed in the reaction. The elemental

concentration data (Table 3.2) indicate that, in general, there was an increase in the proportion of the silica removed from solution as the silicate concentration in the feed increased. This is logical, as the supersaturation level in the prepared solution would be higher with a greater concentration of reagent. In addition, the saturation point would constitute a smaller percentage of the total silicate in solution, and therefore where the concentration substantially exceeds the saturation point, a greater proportion of precipitation would be required to reach equilibrium.

Table 3.2 shows that far more silica was removed ***via*** this process than would be expected from the same co-precipitation reaction in the absence of silica polymerisation in feed liquors. However, in the experiments discussed in section 3.3.1 the concentration of silicate remaining in solution after the reaction was still greater than in either the nitrate or chloride systems (tables 2.6 and 2.11). This suggests that the vast decline in IEP is not solely based on the proportion of silica in the residue compared but also the anionic media in which it is produced. Adsorbed sulfate clearly had an impact; this is evident from the similar IEP values between the small-scale nitrate and sulfate systems, despite the large difference in the Si:Fe ratio in the precipitates. The combination of the increased silica content and adsorbed sulfate has yielded the observed surface behaviour.

One aspect that has proved difficult to directly demonstrate has been whether there was a significant difference in the distribution of the silica throughout the particle aggregates. If the silica particles formed before the co-precipitation are included in the aggregates (which is almost certain), where are they located within these aggregates? Are they closer to the external surface, or are they distributed evenly throughout the entire aggregate, and how much of an influence does this play on the surface chemistry? Surface charge measurements addressing this question are presented in Figure 3.6, in which subsamples, one containing a combination of both large and small aggregates and the other only fines, were compared.

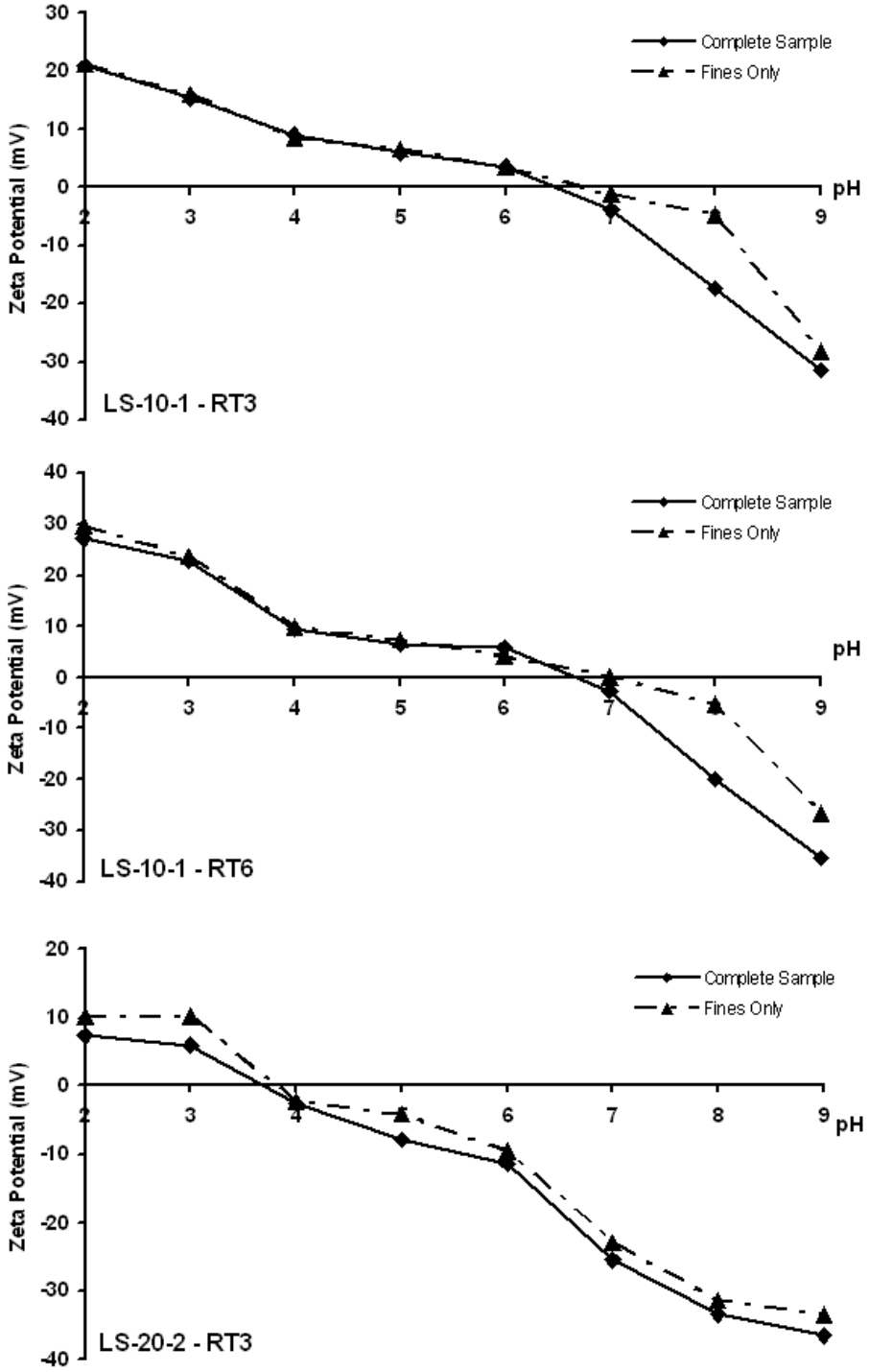

Figure 3.6: Plots from selected samples displaying the zeta potential of both complete slurry samples (all size fractions) and fines only subsamples.

For the full-scale hydrometallurgical process, members of plant staff have noted that zinc loss occurs to a more significant degree with different size fractions of the

precipitated solids. An attempt was therefore made to separate the fines fraction from selected samples prior to zeta potential measurements. This was done simplistically by measuring the sample after agitation to obtain representation of all particle sizes; after the bulk of the unflocculated suspension was allowed to settle, the supernatant was extracted and measured. In this manner, the second sample only contained particles small enough to remain suspended.

No significant difference was observed in the zeta potential behaviour of the fine and bulk particles (Figure 3.6). The finer particles may have produced a slightly less negative potential at approximately pH 8, which may suggest that adsorbed sulfate was removed more rapidly from the surface of the smaller particles. This analysis reveals that it is unlikely that zinc uptake alters between size fractions of the ferrihydrite aggregates. It is possible that different iron oxide phases are responsible for the effect observed on the plant, but the most likely cause is undissolved calcine phases. These particles are primarily in the larger size fractions of the total plant residue.

3.3.4.3. Slurry Properties

Solids concentrations in the laboratory experiments are relatively low (~ 10 g L^{-1}), such that it influences the effect of particle size on the flocculation process. While larger particles generally improve the thickening properties of the material at low solids concentration, large particles mean less particles, which leads to less collisions and poorer flocculant efficiency. A significant body of settling rate measurements was acquired from the large-scale tests, but the majority did not provide particularly useful information, and therefore are not discussed in detail. Sample slurries without flocculant addition took minutes to settle even a small distance, whereas the addition of the flocculant 800HP (1.5 mL of 0.05 % flocculant per 110 mL of sample slurry) induced settling within seconds in practically all samples. The first two residence times for each system generally displayed the poorest settling properties, which is likely due to the inconsistent conditions (e.g. pH drifting) and slower hydrolysis rate in the reactor as the reagent concentration increases from zero to steady-state. While the lower iron concentration would produce a greater proportion of more crystalline

material that should be more readily settled, the ferrihydrite residue would be produced at smaller concentrations, and this can be potentially detrimental to polymer-bridging flocculation, through the reduction in the number of bridge-forming collisions (Fawell 2009). There was also a significant proportion of fines in the suspension in such cases; no clear mud-line was observed in many of these samples, with the suspensions only becoming clear over extended settling times (i.e. more than 10 minutes).

An increase in silicon concentration in the feed appears to be linked to poorer settling properties in the absence of the flocculant, with no mud-line discernable in the LS-20-1 and LS-30-1 steady-state samples. LS-0-1, LS-5-1 and LS-10-1 all had clear mud-lines and settled at rates between 0.85 and 0.95 m h^{-1} with no evident correlation to silica content. The greater proportion of fine aggregates in the LS-20-1 and LS-30-1 are the likely cause of this effect, leaving the slurry practically opaque after the larger aggregates had settled very slowly (although the slurry clarified over time). Turbidity measurements would have been required to have any prospect of determining settling rates in these cases.

The settling rate also is affected by the fractal dimension; the less densely packed aggregates will have a lower relative density with regard to the medium and thus will be somewhat more resistant to settling. However, this would probably make a minor contribution, as aggregate size would dominate the settling rate measurement (Lamb 1994).

Rheological characterisation was undertaken on slurry samples without the addition of a flocculant. Systems LS-0-1, LS-5-1 and LS-10-1 produced negligible shear strain (<10 Pa) at the highest solids concentration achievable (506, 767 and 632 g L^{-1}, respectively). This shows very weak association between aggregates in suspension and may reflect the difficulty in concentrating the solids. There was an increase in the values measured in the latter samples (Figure 3.7). As was shown earlier (section 2.4.4) that the introduction of silica to the particles decreases the surface charge. The positive charge of the particles at the reaction pH would be reduced by the introduction of significant amounts of silica. The increase in shear stress could be partially related to the decreased repulsion due to the electrostatic interactions

between particles arising from the lower surface charge. Interestingly, there was no direct correlation between the particle size and the solids concentration that is able to be reached. This would suggest that the ability to concentrate the solids is influenced by other factors such as the morphology of the sample aggregates based on the phases present.

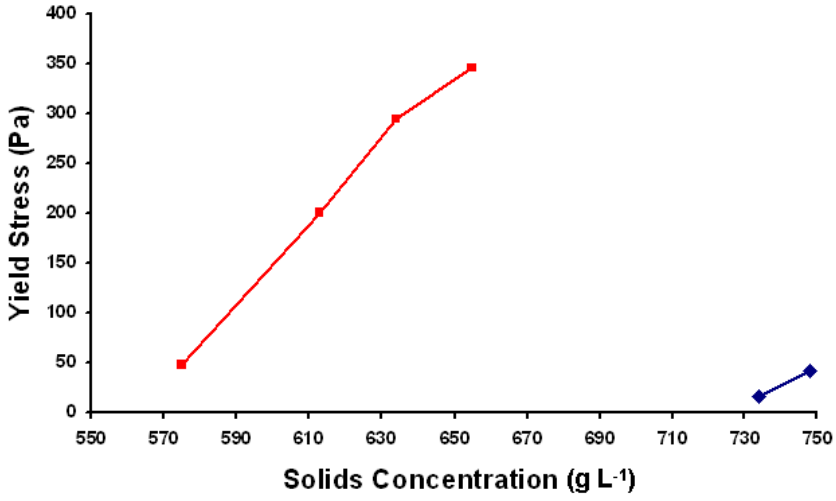

Figure 3.7: Plots of the yield stress against solids concentration, vane measurements displayed were conducted on steady-state samples of LS-20-1 (blue) and LS-30-1 (red).

3.3.5. Other Precipitation Variables

3.3.5.1. Decreased Reagent Concentration

A precipitation experiment (LS-20-2) was conducted under the same general conditions (pH, temp etc) as the earlier large-scale test LS-20-1 (see Table 3.1), except that the reagent concentrations were lowered, in order to establish whether this influences residue properties and the removal of oligomeric or colloidal silica. Section 2.8.2 highlighted the importance of the ferrihydrite surface to silica precipitation from monosilicic acid. Whether the surface is as important in aiding silica precipitation from liquor containing polymerised silica is of interest. The iron feed concentration was reduced from 5.0 to 4.0 g L^{-1}, while the silicon concentration

was reduced from 0.95 to 0.82 g L^{-1} for the LS-20-1 system. The products from this system were analysed by the same methods employed for the other large-scale samples.

Figure 3.8 displays the impact of the different reagent concentrations during the precipitation of LS-20-1 and LS-20-2 on the resultant XRD patterns. Although partially disguised by the prominent low angle reflection of goethite, a broad silica peak is observable at ~25° 2 in the LS-20-2 pattern (located between 20 and 30° 2 , beneath the intense goethite reflection). In addition, the proportion of more crystalline material has greatly increased from LS-20-1, almost to the point of rendering the ferrihydrite peaks indiscernible. This was to be expected, as the decline in hydrolysis rate caused by the lower iron concentration favours the formation of goethite (Schwertmann 2004). It is interesting to note how substantial this increase is, which leads to an explanation as to why the LS-5-1 system contained much stronger goethite reflections than the LS-0-1 sample (Figure 3.2).

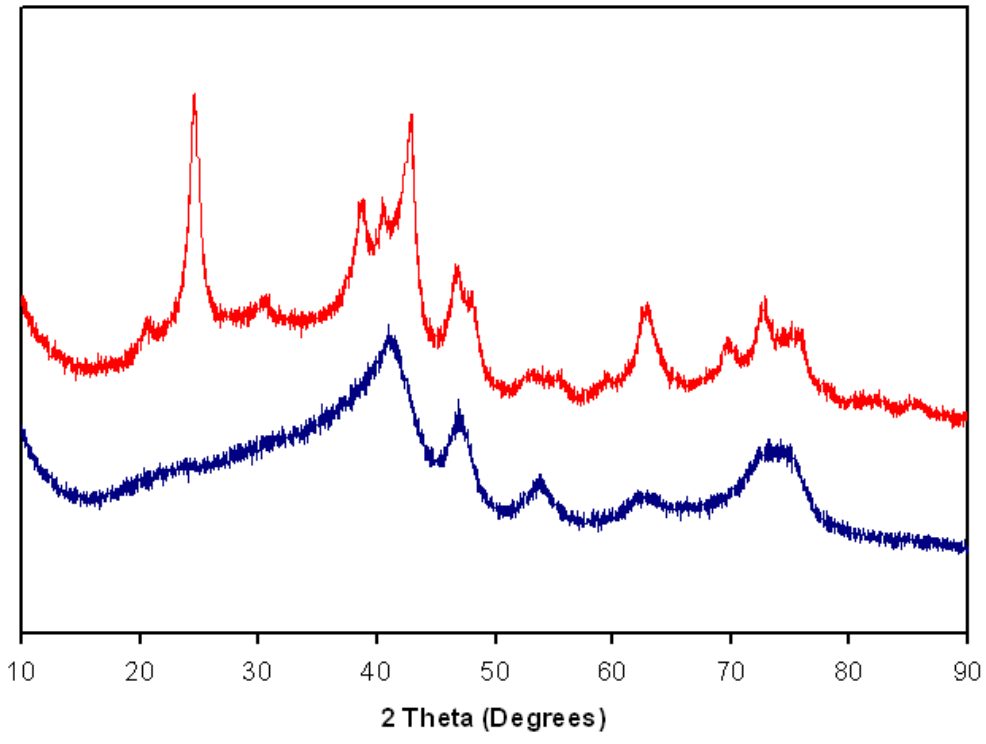

Figure 3.8: XRD traces of steady-state samples from the large-scale systems LS-20-1 (blue) and LS-20-2 (red), the latter showing the effect of reduced feed concentrations.

As noted in section 3.3.2, the ability of silica to inhibit the formation of goethite is likely to be greatly diminished in these systems as a consequence of polymerisation during the silicate feed solution preparation. By also decreasing the iron concentration, goethite formation was favoured (Schwertmann 2004), and without silica present to retard its formation, a greater proportion of goethite was produced. The LS-30-1 experiment contained the least iron, therefore if the ability of silica to inhibit the formation of more crystalline phase was completely negated by the polymerisation in the feed, the sample from that experiment would display prominent goethite reflections. However, this was not the case (Figure 3.2) as the goethite reflections are not as prominent in comparison to LS-0-1, LS-5-1 and LS-10-1. This proves that although the effect of silica was diminished, it was not completely absent.

Interestingly, the sample containing the most goethite (LS-20-2) also displayed a higher percentage of silica precipitation (Table 3.4). The result is counter-intuitive, given that LS-20-2 had lower a lower feed silicate concentration, which would result in lower supersaturation. The resulting differences in physical properties are presented in Table 3.5.

Table 3.4: Elemental concentrations of samples from the standard and reduced iron systems.

System	Fe in liquor (ppm)	% Fe precipitated	Si in liquor (ppm)	% Si precipitated
LS-20-1	11.9	99.8	261	57.6
LS-20-2	0.6	~100	131	72.9

Table 3.5: Physical properties of samples collected from the LS-20-1 and LS-20-2 systems.

Sample	Fractal Dimension	Surface Area ($m^2 g^{-1}$)	D(0.1) (m)	D(0.5) (m)	Density ($g cm^{-3}$)
LS-20-1	1.87	248.8	1.52	8.56	3.42
LS-20-2	2.18	210.2	9.71	20.73	2.78

Given that the standard samples often showed clear trends with respect to Si:Fe ratios, and exceptions were explainable, it is possible to make clear comparisons between LS-20-1 and LS-20-2. As is to be expected, the presence of a relatively large amount of goethite had a significant influence on the physical properties of the residue from LS-20-2. This reflects the larger goethite particles aggregating more tightly, with less associated water and a decreased porosity.

In the samples described in section 3.3.1, the particle size declined as the silica content was increased (Table 3.3), whereas this system contained a distribution of larger particles (Table 3.5). Goethite crystals are generally several orders of magnitude larger than ferrihydrite primary particles; the aggregation of these along with ferrihydrite will tend to form larger aggregates. The presence of silica also had less of an effect on aggregation, indicating silica oligomers/colloids are not interrupting the process to the same extent. The particle surface area results closely follow the trend observed in the other samples, showing that with similar Si:Fe ratios, the influence of silica on the surface properties remains relatively constant.

Interestingly, the dry particle density was quite low; this is not readily explained, given that this does not simply correspond to a decrease in the ferrihydrite-to-silica ratio. There was also an increase in the proportion of goethite in the sample which would generally have a greater density than ferrihydrite (Table 1.1). We were unable to ascertain the underlying cause of this effect.

Both the solids maximum concentration (reached by settling and centrifugation), and the corresponding yield stress measurements of the steady state sample of LS-20-2 produced astonishing results. While it had greater particle size measurements and a

smaller proportion of fines (less than 2.6 % below 3 m) than any of the other residues it was the most difficult to concentrate. The greatest solids concentration reached was only 291 g L^{-1} and it produced a significant yield stress (Figure 3.9 Figure 3.9).

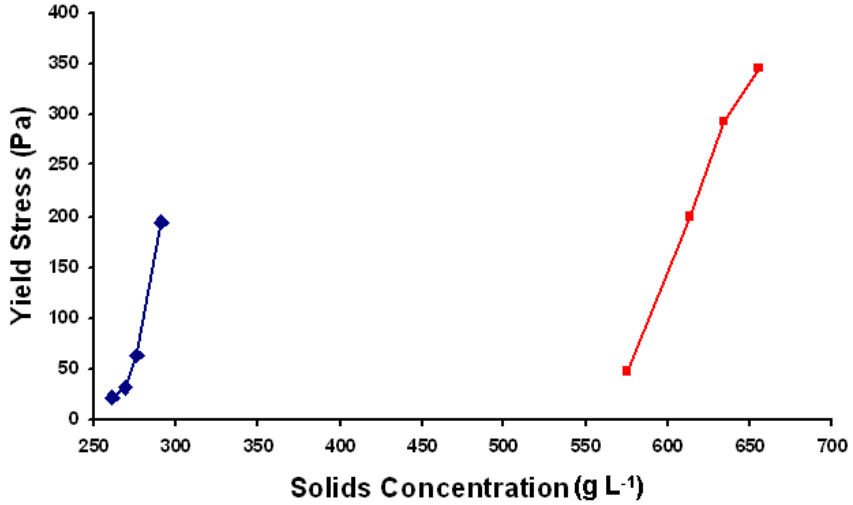

Figure 3.9: Rheology measurements displaying the difference in the solids concentration that produces significant yield stress values for steady-state samples of LS-20-2 (blue) and LS-30-1 (red).

The proportion of silica in the residue was still less than that of LS-30-1 which eliminates the Si:Fe ratio in the material as the cause of the behaviour shown in Figure 3.9. The solids concentration of the residue as it was removed from the reactor was only ~20 % lower than the other experiments which again would not account for the difficulty in concentrating the slurry. The high proportion of goethite in the residue is the only significant difference between LS-20-2 and the other experiments. Goethite has multiple morphologies (including rod-shaped particles) (shown later in Figure 4.1), all substantially different from that of ferrihydrite. The introduction of a large number of such particles in combination with the ferrihydrite aggregates is a possible explanation for the relatively high yield stress observed at relatively low solids concentrations.

3.3.5.2. Silicate Feed Preparation: Avoiding Polymerisation

An experiment was conducted under the same conditions as LS-30-1 except attempts were made to avoid or at least minimise silica polymerisation in the feed solution. This would indicate which properties polymerised silica influences, and how they differ in the presence of monomeric silica. The results would also be directly relatable to the S-30-1 experiment in the small-scale, thereby speaking to how consistent the process is when scaled-up.

Table 3.6 shows the similarities between the amounts of reagents precipitated from solution under the same conditions on the small and large scales. The agreement between the values suggest that the experiment was both a successful larger scale version of initial experiments and able to eliminate or at least minimise precipitation prior to the reaction. Also, when compared to the data given in Table 3.2, there was a marked difference in the amount of silicon remaining in solution. As seen in section 3.3.2, the induced polymerisation in the feed solution greatly increases the propensity to remove Si species ***via*** the precipitation.

Table 3.6: Elemental concentrations from samples of S-30-1 and LS-30-1.

Experiment Scale	Fe in Liquor (ppm)	% Fe Precipitated	Si in Liquor (ppm)	% Si Precipitated
S-30-1	84.5	98.1	671	32.1
LS-30-1	22.7	99.4	648	31.6

This is strong evidence that small differences involved in the scaling-up the process do not significantly affect the behaviour of the system. Some of the differences include the following; the reactor being steel as opposed to glass, the introduction of room temperature reagents at a greater rate and the large reactor containing baffles and a larger agitator to provide efficient mixing. While none of these were expected to impact heavily on the reaction, it is reassuring to provide evidence to support that assertion. The lack of an effect related to the hydrodynamics correlates well with the investigation described in section 2.8.1.

The XRD data provides further evidence of the success of the scaling-up of the reactor set-up (Figure 3.10). The LS-30-2 sample displays similar reflections to those observed in the S-30-1 product. The absence of the more crystalline material is notable which also reinforces the assertion that the goethite observed in the other large-scale sulfate systems was due to the pre-polymerisation of the silica reducing its ability to retard goethite formation.

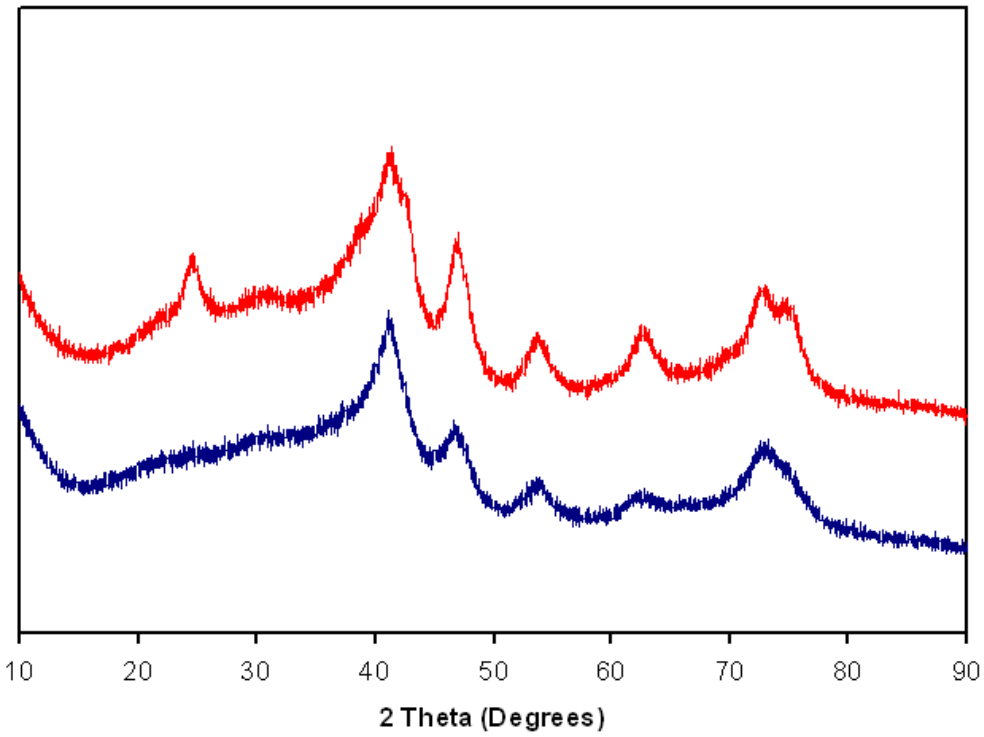

Figure 3.10: XRD patterns of steady state samples of the LS-30-1 (red) and LS-30-2 (blue), revealing a lack of more crystalline material in the latter sample.

While the difference between having monomeric vs. oligomeric species in solution may seem minor, the influence on some of the physical properties is appreciable (Table 3.7). This is most likely due to more complete surface coverage of the ferrihydrite, coupled with a much greater number of collisions occurring with the more dispersed monomers. The coverage over both particulate and aggregate surfaces would aid the stability of the clusters against solution (dissolution) and shear forces. The similarity (difference < 10%) in surface area is interesting to note, given

the large difference in the proportion of silica in the solid. This is indicative of greater surface association of the silica in the LS-30-2 sample which actually has a greater surface area.

Table 3.7: Physical properties of the LS-30-1 and LS-30-2.

System	Fractal Dimension	Surface Area ($m^2 g^{-1}$)	D (0.1) (m)	D (0.5) (m)	Density (g cm^{-3})
LS-30-1	1.45	255.3	0.90	6.74	3.05
LS-30-2	1.81	275.9	6.08	13.17	3.48

As can be seen from Table 3.7, the aggregate properties have been significantly altered by the different feed preparation. Aggregation appears to be aided where the co-precipitates form in the presence of the monomeric species. The density is higher even with the absence of more crystalline material in the product; this may be due to the lower proportion of silica in the solid. The particle size and fractal dimension values are substantially greater in the precipitate formed in the presence of the monosilicic acid. This indicates both more tightly bound aggregates and the particles being more stable against shear forces. When compared to the values of the silica-free sample (LS-0-1, Table 3.3), the introduction of polymerised silica to the precipitation is to the detriment of the physical properties in terms of solid / liquid handling. While there is a small decrease in the D (0.1), D (0.5) and fractal dimension values where monosilicic acid is present during the reaction, it is not to such a large degree as in the LS-30-1 sample and therefore would not significantly influence the separation properties.

3.4. Nitrate Systems

3.4.1. Preparation Conditions

Large-scale experiments under similar conditions to those of N-0-2 to N-30-1 were conducted, with the specifications described in Table 3.8. As in the small-scale tests, the pH in nitrate media was far more difficult to maintain, being more susceptible to drift and over-correction. It was possible that this could pose problems with the residue formation, including precipitation of more (at lower pH) or less (at higher pH) crystalline material. However, any such effects were minimised by constant monitoring during preparation.

Table 3.8: Experiments producing the samples referred to in this section, all were conducted at 85 °C and a pH_{85} of 2.65. Ideal feed concentrations are given, variation occurred due to experimental uncertainty. * LN-x-x denotes the larger scale systems (reactor volume 2.5 L) conducted in nitrate media.

System	Feed Concentrations		Si:Fe Ratio
	Iron (g L^{-1})	Silicon (g L^{-1})	
*LN-0-1	6.3	0	0
LN-5-1	6.0	0.16	0.053
LN-10-1	5.7	0.32	0.111
LN-20-1	5.0	0.63	0.25
LN-30-1	4.4	0.95	0.429

The silicate solutions were made up in batches in these experiments (as opposed to a single step preparation) in an attempt to minimise polymerisation prior to the reaction (as discussed in section 3.3.7.2). Quantities of less than 15 g of sodium metasilicate were dissolved in 500 mL of deionised water. Adjustment of pH was then conducted, followed by dilution to a volume of two litres with both iron-bearing solution and additional deionised water. The iron was also spread between these

steps in quantities of less than 150 g (although no effect would be expected from high concentrations of this species). The total feed was stirred vigorously for several minutes and (to a lesser extent) during experiments to promote homogeneity. As in section 3.3.7.2, these reactions also serve to test whether variations occur between the different scales.

3.4.2. Structural Analysis

Samples from the LN-0-1 system representing the fifth (RT5) and sixth (RT6) residence times, along with the reactor contents, were taken for XRD analysis (Figure 3.11). Collecting data from all residence times to detect structural change prior to steady-state was deemed unnecessary.

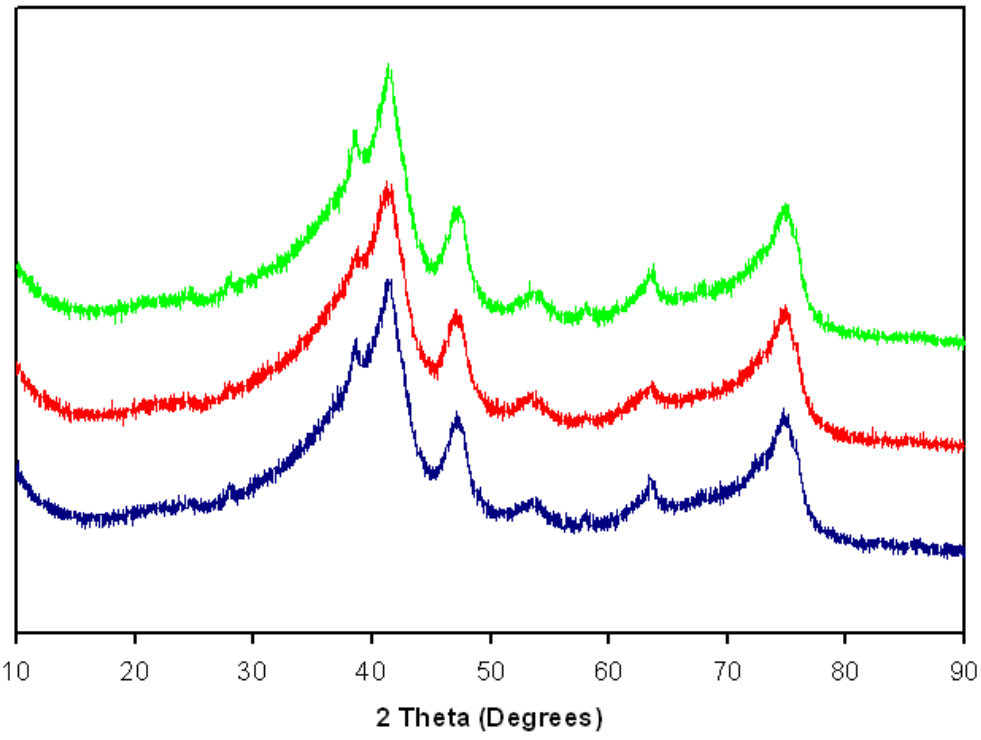

Figure 3.11: XRD patterns from samples collected during the fifth (blue) and sixth (red) residence times and reactor contents (green) of the LN-0-1 system.

In contrast to the corresponding small-scale experiments, there was almost no evidence of phases of greater crystallinity (goethite, hematite, etc.) in the steady-state (RT6) LN-0-1 sample. The shoulder at approximately 39° 2 suggests the presence of a small amount of a phase that could be goethite, hematite or a combination thereof. However, this was the only minor evidence of other phases, implying they represent a very small proportion of the sample. There also appeared to be slightly greater proportions of more crystalline material in the fifth residence time and reactor content samples. The shoulder was more prominent and there were three other very low intensity reflections that were observable above the background (two were between 20 and 30° 2 , one at approximately 58.5° 2). These demonstrated the presence of both goethite and hematite in the samples. Although there was a greater proportion of such species in these samples, they remained very minor constituents and were potentially due to fine differences in the average pH or iron concentration.

The introduction of soluble silicates removed any trace of more crystalline phases from the samples and broadening of the ferrihydrite reflections was observed (Figure 3.12). This effect was enhanced by the presence of greater quantities of silicates, as was also seen in the small-scale nitrate experiments (Figure 2.7). The increasing appearance of a broad reflection at ~25° 2 associated with amorphous silica was also observed, primarily at high initial silicate levels.

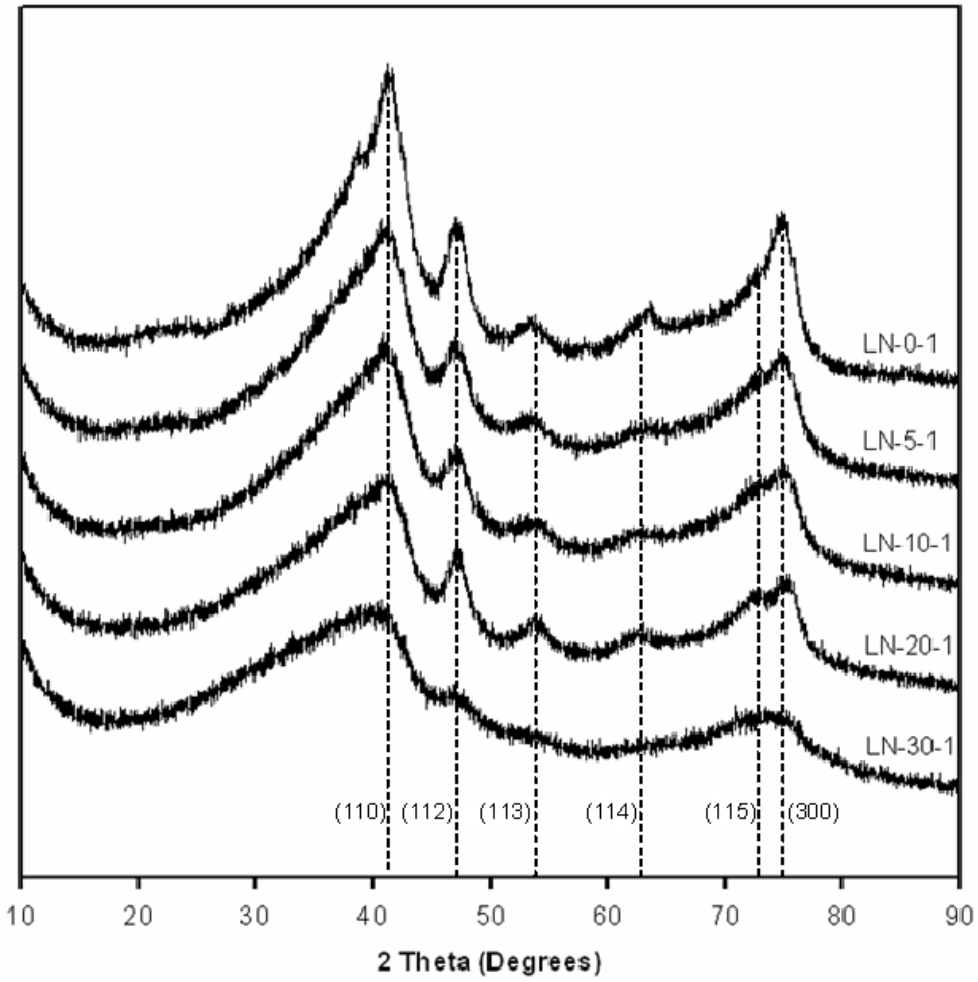

Figure 3.12: XRD patterns from the steady-state samples from each nitrate system in order of Si content from the LN-0-1 (top) to the LN-30-1 system (bottom).

The decline in crystallinity for LN-0-1 appeared to be even greater than that observed in the small-scale systems using ferric nitrate, however, this may simply be due to a slightly faster hydrolysis rate through the entire series of large-scale experiments. The small-scale silica-free precipitates displayed much greater proportions of more crystalline material than those obtained from their large-scale equivalents, indicating slightly faster hydrolysis in latter series (Figure 3.13). The lower crystallinity in the silica-containing samples from the large-scale tests may be due to a similar effect. All of the peaks had broadened significantly in LN-30-1 and the (113) and (114) peaks were practically lost to the background signal (Figure 3.14). The (115) and (300) peaks appeared as one elongated reflection and were only able to be properly resolved by peak-fitting software.

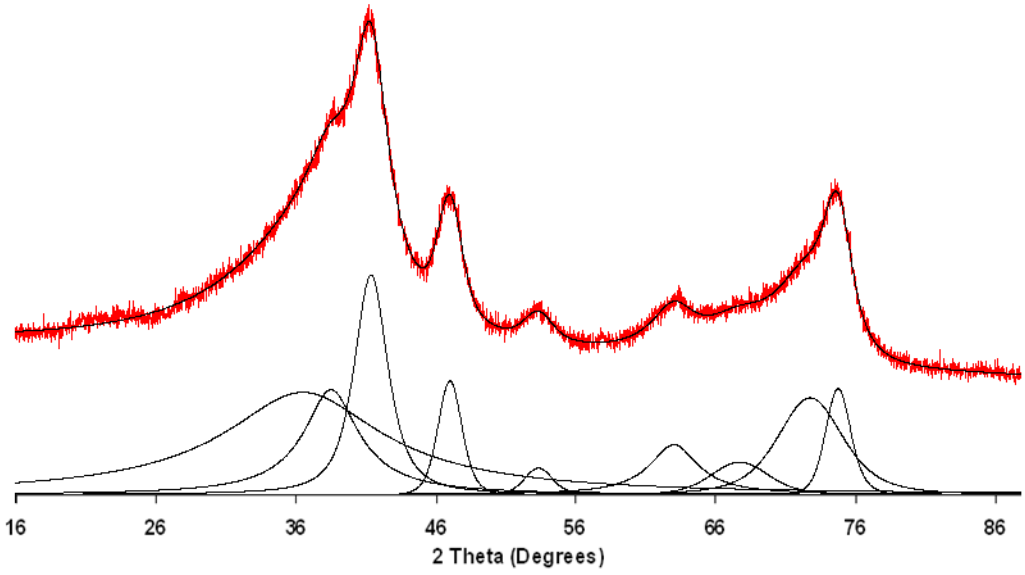

Figure 3.13: Peak fitting from xfit analysis of the XRD pattern for LN-0-1 sample.

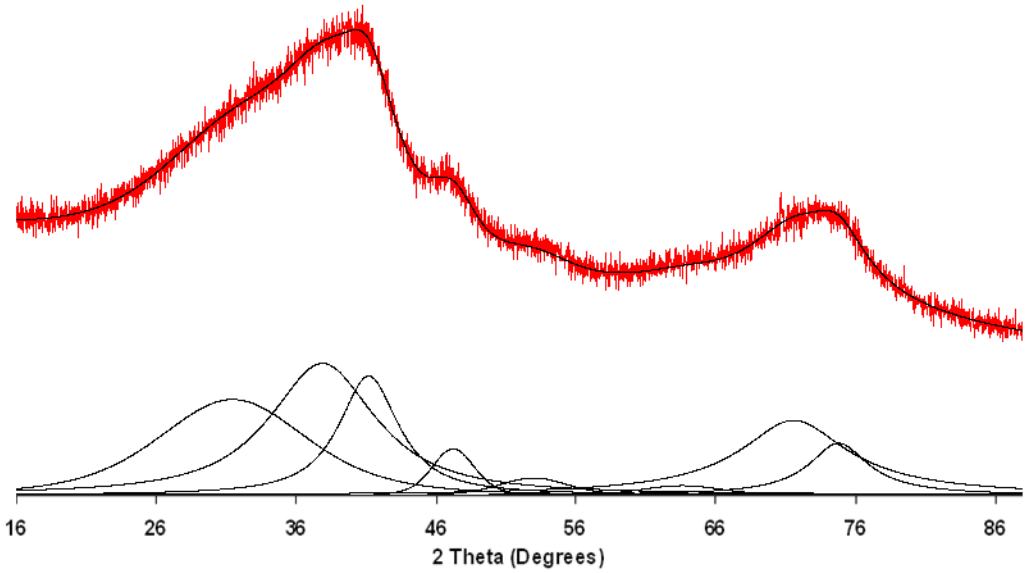

Figure 3.14: Peak fitting from xfit analysis of the XRD pattern for LN-30-1 sample.

The (113) and (114) peaks are still barely visible in the calculated peaks fitted to the LN-30-1 pattern. The errors associated with the calculations of these peaks were much greater than in those for systems with lower Si content. The broadening of other reflections was apparent from the data presented in Table 3.9. It is interesting

to note that there was only a significant increase in the FWHM values in the LN-30-1 pattern and this was supported by three of the six major peaks. The reflections from the (110), (114) and (115) planes vary sporadically and show no real trends, whereas the (112), (113) and (300) reflections remain relatively constant through the first four systems, then increase dramatically in the LN-30-1 sample. While it is obvious from Figure 3.12 that the LN-30-1 pattern displayed by far the greatest decrease in crystallinity, the other patterns did not show such a marked effect (similar to the small-scale experiments). Slight broadening of most reflections in the LN-5-1 and LN-10-1 samples can also be seen in the FWHM values presented in Table 3.9. This indicates that even at relatively low feed concentrations silica can influence ferrihydrite crystallinity.

Table 3.9: FWHM values, calculated using xfit from all peaks from the LN-0-1, LN-5-1, LN-10-1 and LN-30-1 systems.

	FWHM (° 2)					
Reflection Index	(110)	(112)	(113)	(114)	(115)	(300)
LN-0-1	2.63	1.88	2.18	3.87	5.08	1.97
LN-5-1	3.00	2.00	2.48	5.55	6.09	2.23
LN-10-1	3.22	1.99	2.70	3.58	3.40	2.95
LN-30-1	4.62	3.36	5.37	6.19	8.68	4.74

3.4.3. Elemental Composition

The concentrations of species remaining in the supernatant solutions were expected to closely correlate to those of the small-scale experiments. While the general behaviour was similar, Table 3.10 shows that there is a much greater percentage of silicon precipitated from solution in the LN-5-1 and LN-10-1 than their small-scale counterparts. This may be due to an increased efficiency of adsorption given the reactor volume and the relative position of feed and removal points.

Table 3.10: Elemental concentrations for iron and silicon in supernatant liquors of steady-state samples from each large-scale nitrate system.

System	Fe in Liquor (ppm)	% Fe Precipitated	Si in Liquor (ppm)	% Si Precipitated
LN-0-1	0.28	>99.9	-	-
LN-5-1	0.20	>99.9	9.79	94.52
LN-10-1	<0.2	100	22.9	92.68
LN-30-1	<0.2	100	80.7	91.43

The vast majority of the Si was precipitated in the nitrate experiments. As in the small-scale precipitations, a much greater percentage of silicon was present in the residue than in the corresponding sulfate experiment LS-30-2 (Table 3.6), this was the only large-scale sulfate experiment without silica polymerisation in the feed, therefore the only one with which a proper comparison can be made. This contrast represents further evidence that sulfate interrupts the silica precipitation process. As these samples were prepared with the express purpose of minimising the silicate concentration in the feed, the high proportion of silica precipitation can therefore be attributed to the influence of the ferrihydrite surface.

3.4.4. Physical Properties

Results for the large-scale nitrate series from measurements of the fractal dimension, surface area, PSD and density are given in Table 3.11. The values display several trends in properties, some of which are similar to those observed in the corresponding large-scale sulfate series of experiments, but others that are entirely the opposite.

Table 3.11: Physical data obtained from precipitates produced on the larger scale in the presence of nitrate anions.

Experiment	Fractal Dimension	Surface Area ($m^2 g^{-1}$)	D (0.1) (m)	D (0.5) (m)	Density ($g cm^{-3}$)
LN-0-1	1.55	170.9	1.12	7.44	3.16
LN-5-1	2.28	245.9	1.39	5.04	2.98
LN-10-1	1.64	277.0	1.67	12.32	3.40
LN-30-1	1.73	370.0	2.65	17.47	3.19

The surface area increased significantly with the introduction of silicate into the reaction as well as with each further increase in its concentration. Although showing the correct trend for surface area, the value obtained for LN-30-1 was far greater than was obtained for any other samples. There are two effects that are likely to combine to produce such a high surface area. Both the greater proportion of silica in the residue than others measured, and the fact that the silica is primarily surface associated would contribute to an increase the surface area.

The particle density values do not follow any observable trend, which suggests one of two possibilities. Either the densities varied with no dependence on the composition of the feed within the confines of this investigation or there were multiple effects on the density which can oppose each other.

The aggregation process was positively influenced by the co-precipitation, as is displayed by the increase in the D (0.1) and D (0.5) statistics (a reduction in fines) and the increase in the fractal dimension (especially in N-5-1). The relationship between fractal dimension and particle size appears not to correspond logically in the N-5-1 sample; while it has by far the greatest fractal dimension, it has the smallest PSD values. This may simply indicate the formation of small, very tightly packed aggregates. Interestingly, while there was a significant increase in the D (0.5) value, the increase in D (0.1) was smaller, which widens the particle size distribution. The increase in the fractal dimension and PSD indicate more tightly packed, stable aggregates.

The free settling of individual aggregates in highly diluted samples was monitored by means of the FDA (Figure 3.15). The differences between the LN-0-1 and LN-30-1 samples were marked; in general, much larger aggregates were observed in the latter, which in turn settled at a greater rate. Representative images are given in Figure 3.15. This observation further speaks to the positive influence that co-precipitated silica has on the potential solid / liquid handling of the precipitates.

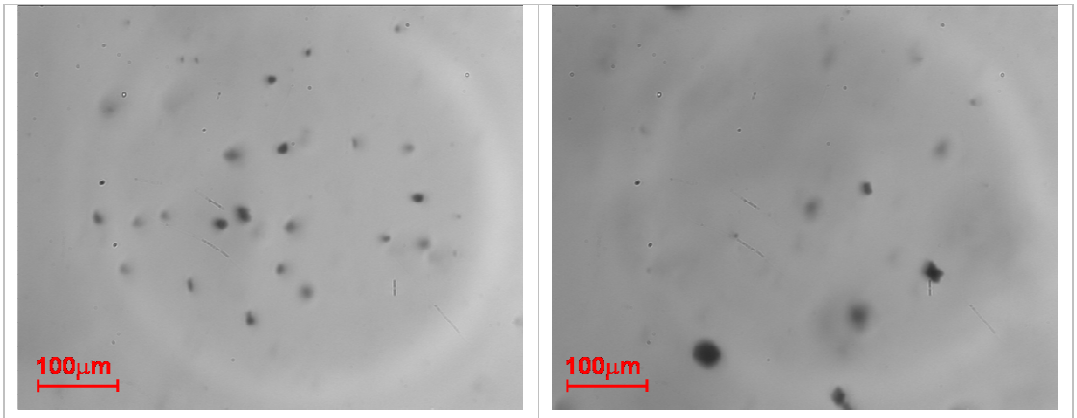

a b

Figure 3.15: Images taken from FDA sequences displaying the difference in the appearance between the smaller aggregates in LN-0-1 (a) and the larger aggregates in LN-30-1 (b).

Unfortunately, the relatively small aggregate size distribution prevents quantification of the images from these aggregated precipitates. Image analysis of the FDA video output requires a certain degree of image sharpness with regard to aggregate size and shape. Even using the camera's greatest magnification, the aggregated precipitate particles did not present the size or degree of focus required to be recognised by the software in statistically valid numbers. This is a very useful technique for a range of materials, but the equipment currently available was unable to be effectively implemented in this study.

3.5. Summary

Several important pieces of information regarding iron and silicon co-precipitation and the simulation of the Paragoethite process have been gained through the experiments described in this chapter. The first is that the continuous crystallisation process employed could be effectively scaled-up, and that all conditions remain constant. Procedures were altered to accommodate the difference in material volume and handling required.

The introduction of silicate in the feed during ferrihydrite precipitation influences several physical properties. Monosilicic acid tends to aid aggregation, producing larger, more densely aggregated particles, whereas polymerised silica interferes with the process, resulting in smaller, more open aggregate structures. The surface area is increased by the presence of surface associated silica, an effect that appears stronger where monosilicic acid is the species in solution. It is likely that polymerisation in the feed occurs in industrial process liquors, which may have a detrimental effect on the solid / liquid handling of the precipitate.

The proportion of silica precipitated during the reaction was also dependent on whether polymerisation was allowed to occur in the feed solution. In systems such as those containing sulfate that inhibit the precipitation of silica, polymerisation in the feed greatly increases the proportion of silica removed from solution. The presence of polymerised silica during iron oxide precipitation does not inhibit the formation of more crystalline phases, whereas monosilicic acid clearly does.

These outcomes indicate entirely different co-precipitate formation pathways between the two cases. While chapters 2 and 3 indicate a certain process in the formation of the co-precipitates under these conditions, more detailed evidence is required to formulate a conclusive mechanism.

4. TRANSMISSION ELECTRON MICROSCOPY AND PAIR DISTRIBUTION FUNCTION ANALYSIS

4.1. Introduction

The point of greatest interest driving this work was to determine (or at least provide supporting evidence) how silica is associated with ferrihydrite. There are many possibilities as to how silicon may appear in the residue, there may be no association at all, with the ferrihydrite and silica forming discrete particles and aggregates or particles of both species may themselves aggregate together. The likelihood is that there will be some association; the silicon may be incorporated into the ferrihydrite structure, silica may adsorb on the surface of particles, or discrete silica particles may be formed with a clear boundary between the oxide phases. It is also possible that silicate/silica will only interact with the external surfaces of already formed ferrihydrite aggregates due to the relative rates at which the processes occur. An association may be between soluble species, particles or aggregates or any combination thereof.

The methods of analysis used to this point have provided some information with regard to this question however, it is far from conclusive. While surface measurements and the slower reaction rate of silica with respect to ferrihydrite proves that some silica is present on the surface of the particles, it has not been possible to ascertain whether it is primarily surface associated or exists in large proportions within aggregates.

Detailed knowledge of the distribution of silica throughout the aggregates is highly significant as it will provide evidence as to how the co-precipitates form. The pathway to formation of the materials has been partially elucidated by the analyses discussed in chapters 2 and 3. However, these have not provided sufficient evidence to conclusively indicate a particular mechanism. The data presented in this chapter will

speak as to the validity of proposed theories of crystal structure and particle constitution. From this, the observed changes in the properties can be explained.

The aim of the TEM work described in this chapter was to obtain morphological, structural and elemental distribution information for the particles formed in the co-precipitation experiments. The morphology can be obtained using standard imaging, while the other information requires the use of high resolution TEM (HRTEM) and energy filtered TEM (EFTEM). HRTEM requires the microscope to be very accurately aligned to provide focus at the greatest possible magnification. By reaching such magnification, lattice planes are able to be resolved; these are often used to determine particle size and lattice spacings (Nesterova 2003; Liu 2006).

EFTEM uses inelastically scattered electrons and filters them based on their energy. Electrons lose energy when they interact with atoms; the amount lost is discrete and characteristic of the element (Ahn 2004). The electron energies are measured and can be observed as peaks in the electron energy loss spectrum (EELS) to determine which elements are present. An energy filter centred on these peaks will produce images based solely on interactions with the intended element(s), providing a map of where they appear within the sample. By comparing the element maps with the bright field images and images displaying sample thickness, we can determine the aggregate composition.

4.2. Experimental

For all techniques used there was no difference in sample preparation procedures. A small volume of either slurry or redispersed dried solid was obtained (where appropriate) and the liquor was removed by decantation and replaced with ethanol. This process was repeated several times to remove as much water as possible. It provides some purification, removing soluble constituents that would contaminate the sample upon drying, and ensures ease of drying given the low boiling point of ethanol. A small droplet of the solid/ethanol suspension was then placed on a 3 mm TEM grid and left to dry at room temperature. This was conducted, where possible, in a clean air-flow controlled cabinet to avoid dust contamination on the grids. Once dry, the samples were ready for analysis.

Curtin University's JEOL 2011 instrument was utilised; later work was completed with the JEOL 3000F and 2100 instruments available at the Centre for Microscopy, Characterisation and Analysis at The University of Western Australia. As discussed in section 4.1, standard TEM provides images of particles based on the transmission of electrons through the sample. The sample can not be too thick otherwise it will simply appear as a silhouette. Therefore when using particles, they must be under a few hundred nanometres in size to be suitable for imaging. As with all types of microscopy, there is also a lower size limit based on resolution. In the case of standard TEM, resolution is of the order of several nanometres (Clark 2002).

Due to the precision and scale of magnification available on the instruments, all lenses and apertures must be very accurately aligned for the desired image quality. High resolution work requires a beam tilt adjustment that is generally unnecessary for standard imaging. The electron loss energies used for the pre- and post-edge measurements on the elements to obtain the EFTEM images are given in the Table 4.1.

Table 4.1: Energy levels chosen for the EFTEM analysis of the precipitates.

Edge	Pre-edge 1	Pre-edge 2	Edge	Post-edge	Slit Width
Fe M	45	50	54	59	5
Si L	84	94	99	109	10
S	130	145	165	185	15

4.3. Microscopy

The initial tests were primarily to collect standard TEM images of product aggregates, and perform some preliminary electron diffraction, with the purpose of identifying similarities or any obvious differences to pure ferrihydrite. The co-precipitation experiments from which samples used in this analysis were obtained are given in table 4.2.

Table 4.2: Experiments producing the samples referred to in this section. Ideal feed concentrations are given, variation occurred due to experimental uncertainty.

System	Conditions					
	Feed Concentration		pH	Residence Time	Temp (°C)	Anion present
	Fe (g L^{-1})	Si (g L^{-1})				
N-0-2	6.3	0	2.65	45 min	85	NO_3^-
N-30-1	4.4	0.95	2.65	45 min	85	NO_3^-
S-30-2	4.4	0.95	2.65	45 min	85	SO_4^{2-}
S-50-1	3.2	1.6	2.65	45 min	85	SO_4^{2-}

The images displayed randomly shaped aggregates made up of sub-micron particles that appeared to be ferrihydrite (Figure 4.1). The sample also contained much larger acicular crystals (rods), which are most likely goethite. The diffraction pattern of the aggregates contained amorphous rings (indicating ferrihydrite) and the rods were far more crystalline, showing a pattern of defined points (indicating goethite).

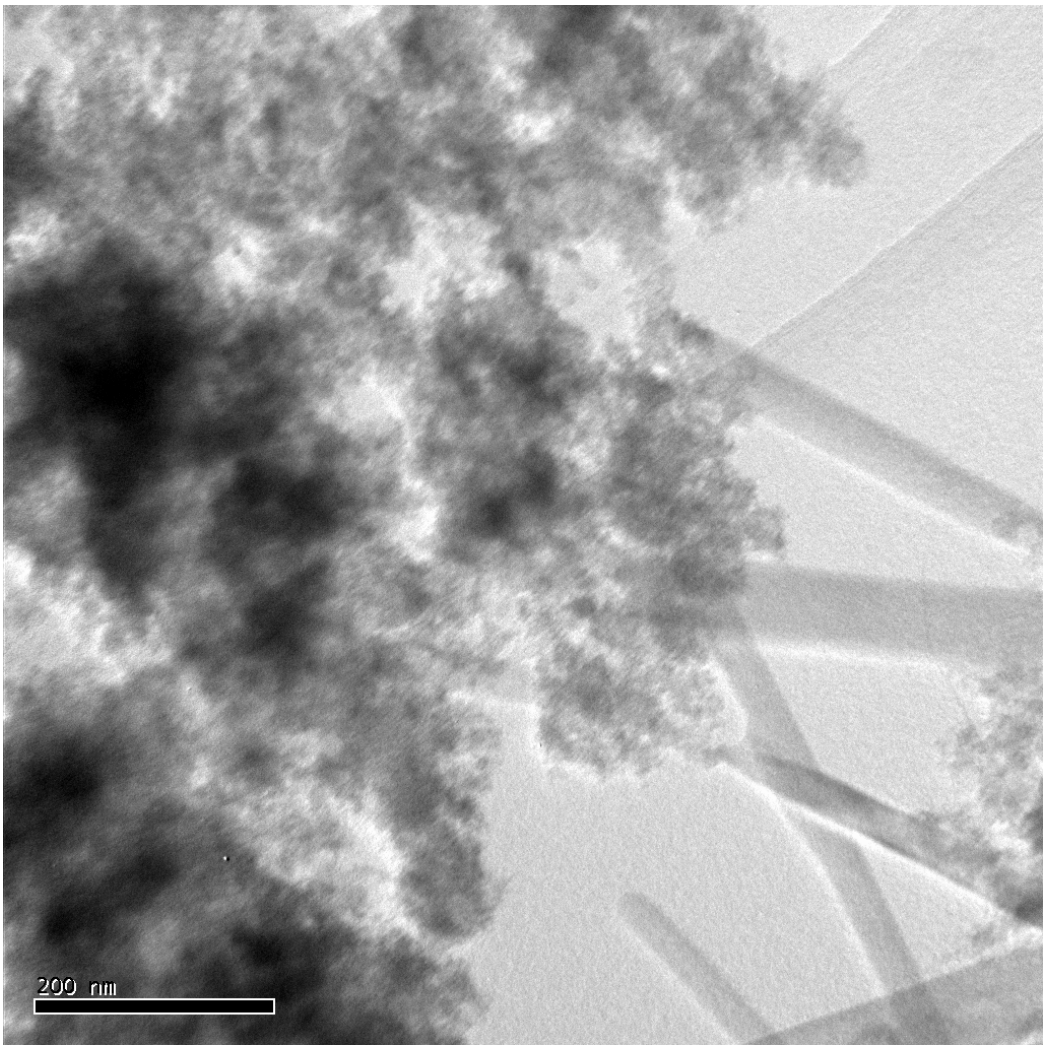

Figure 4.1: TEM image collected from a sample of N-0-2.

Further bright field imaging on silicon-containing systems (N-30-1, Figure 4.2) displayed aggregates bearing the same irregular morphology and nanoscale primary particles as the N-0-2 sample (Figure 4.1). This, coupled with strong iron, oxygen and silicon peaks in the energy dispersive spectra (EDS), was further evidence that ferrihydrite particles with associated silica appeared in the sample. Figure 4.2 shows that the primary particles are less than 10 nm in all dimensions; from general observation it was evident aggregates range in size from under 100 nm to larger than the instrument is capable of processing in a single image. Silica formation had not created a visible effect on the sample, so other forms of analysis are necessary. The

only notable difference is the absence of the acicular particles, consistent with the absence of peaks from more crystalline phases in the XRD pattern (Figure 2.5).

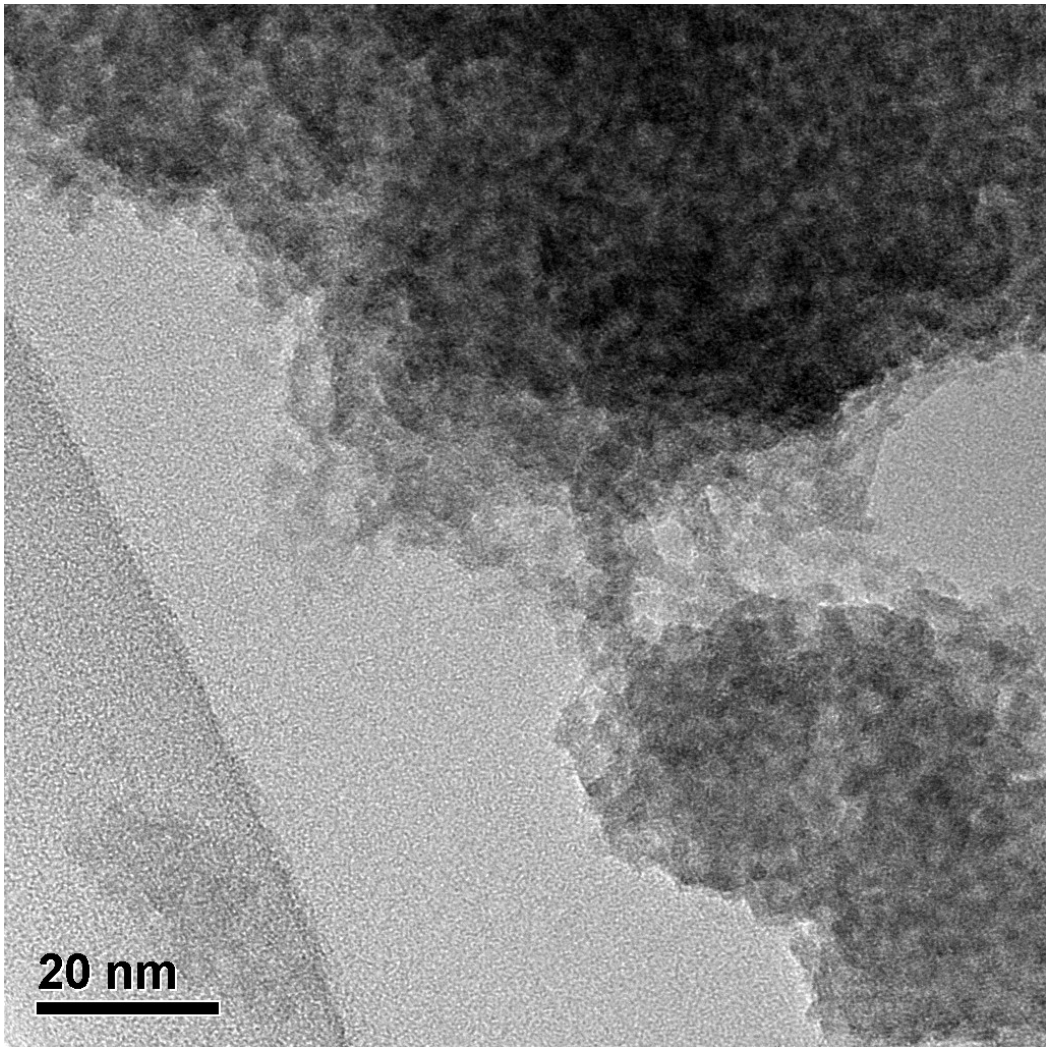

Figure 4.2: Higher magnification TEM image collected from a steady state sample of N-30-1.

Samples produced in sulfate media were analysed by TEM for comparison. The apparent presence of schwertmannite observed in XRD patterns in samples prepared in the presence of sulfate required confirmation. As mentioned in chapter one, schwertmannite aggregates form as roughly spherical cores with fine needles radiating outward in all directions. This differs from ferrihydrite, which is generally devoid of such sharp features. The XRD patterns suggest a combination of ferrihydrite and

schwertmannite; the possible absence of individual schwertmannite aggregates was a potential complication for more advanced analysis.

Figures 4.3 shows aggregates obtained from S-30-2 samples with morphology resembling standard ferrihydrite, as well as aggregates with distinct sharp features. No characteristic schwertmannite aggregates were found in S-30-2 samples, although there were several large masses that appear to have roughly similar features to schwertmannite aggregates. Unfortunately these aggregates are too large to be effectively imaged ***via*** TEM, as they can not be captured in their entirety. However, the effect is visible through the images of sample sections of these particles. The best example of the presence of material resembling schwertmannite is figure 4.3 (f), which shows an image of one aggregate containing a dense core and radiating needles as part of a larger aggregate.

In general, pure schwertmannite is produced at lower hydrolysis rates (lower pH and supersaturation) and over shorter reaction times than used in these experiments, which can form a significant proportion of single schwertmannite aggregates (Claassen 2007). Hockridge et al. (Hockridge 2009) showed that schwertmannite is produced within the first hour and transformation to goethite is seen within the first 2 hours. They also concluded that it is actually a ferrihydrite aggregate with goethite nanocrystals forming the radiating needles.

Experiments in this investigation involve much greater hydrolysis rates (a consequence of higher iron concentrations and pH) as well as the opportunity for increased reaction times if the species remains in the reactor for more than a single residence time. The effect of these conditions is to favour ferrihydrite formation, creating the mixture of phases observed in these samples. The presence of ferrihydrite, schwertmannite and surface associated silica could be the driving force behind the aggregation of schwertmannite hedgehog particles. The presence of a large amount of silica could induce the further aggregation of the schwertmannite aggregates by creating a surface more favourable to aggregation. However, it could simply be due to the greater amount of particles in suspension in these experiments. Having greater hydrolysis rates will increase the number of nucleation events; this in

turn will produce more particles which will experience a greater number of collisions. By virtue of this, there is a greater likelihood of agglomeration.

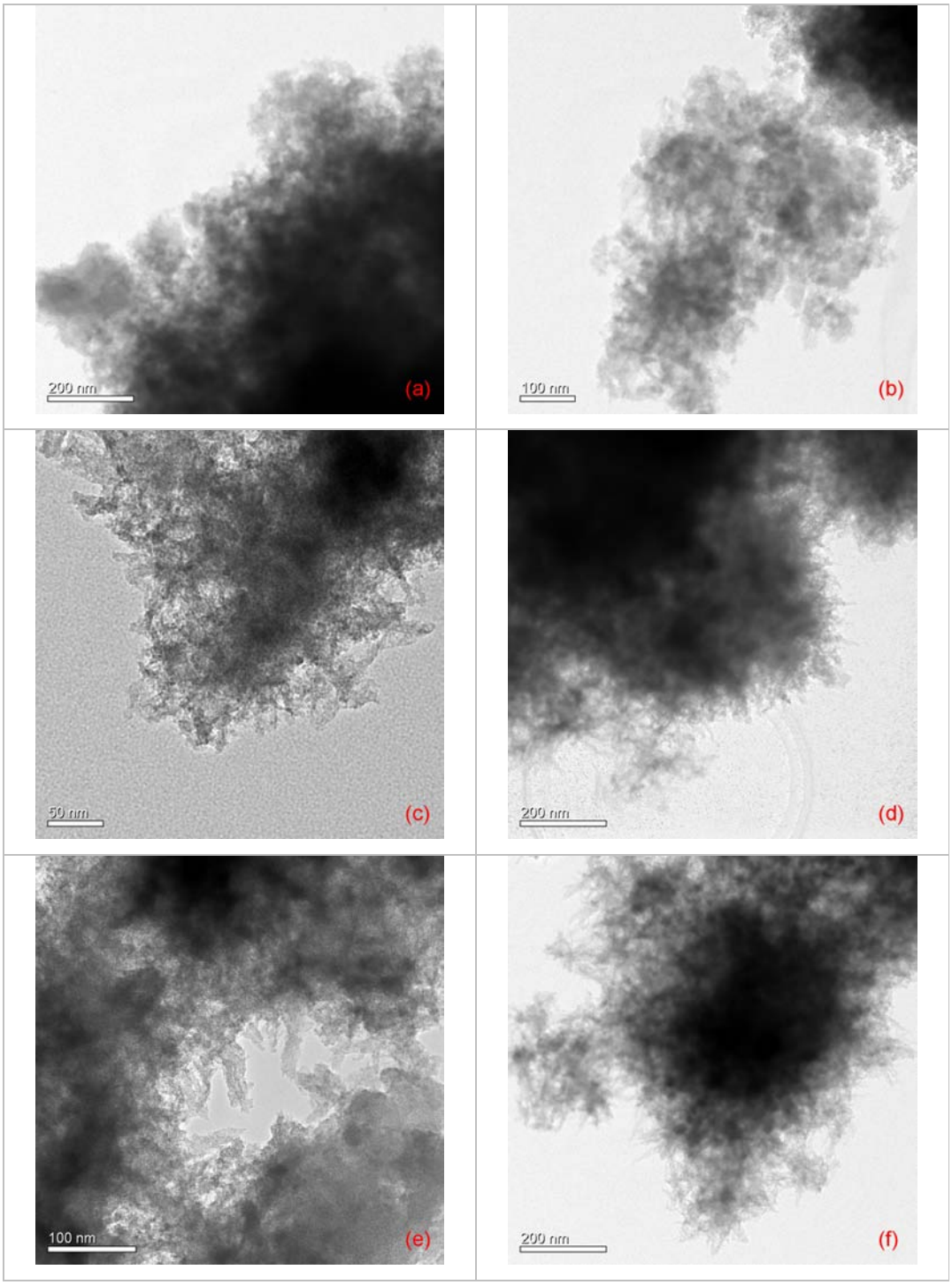

Figure 4.3: Images of aggregates from S-30-2 which is a duplicate of S-30-1.

4.3.1. Phase Identification

HRTEM was employed in an attempt to obtain evidence of the difference between the pure ferrihydrite and the silica containing precipitates. As mentioned above, at high enough magnification (assuming it is within the capabilities of the instrument) the atomic planes of crystalline samples can be resolved. The purpose of this analysis was to attempt to observe the how silicon/silica was associated with the ferrihydrite in the samples. This may appear as defects in the lattice plains where silicon had been introduced into the crystal structure. However, more likely would be regions of crystallinity relating to ferrihydrite primary particles and regions of amorphous, material, being silica. While ferrihydrite is often referred to as amorphous this is misleading. Each individual particle is crystalline but structural strain, a high surface to volume ratio and very small scattering domains give fairly amorphous responses to bulk techniques.

HRTEM images were obtained from the N-0-2 sample, all showing the discrete particles of the order of approximately 4 nm by contrasting the directions in which lattice planes appear (Figure 4.4). These images were obtained to measure the mean primary particle size or measure lattice spacings. However, it was not possible to obtain equivalent images under the same microscope alignment and conditions with the silica-containing sample N-30-1 (Figure 4.5). This may suggest that an amorphous ferrihydrite / silica phase had been formed. However, the difference in these particles was not likely to be due to the presence of a completely different material, as the XRD patterns showed that ferrihydrite was still the predominant phase. A more likely explanation is that a surface layer of silica was obscuring the coherently scattered electrons from the ferrihydrite.

Repeated efforts to optimise the microscope alignment failed to provide resolution of atomic information. It would appear that the silica layer covering both sides of the aggregate interfered with any structural information from the crystalline particles. There was no solution to this problem - a significant amount of silica was required for it to be visible, while at the same time the higher the silica content, the less the information that could be extracted. A different approach was therefore required.

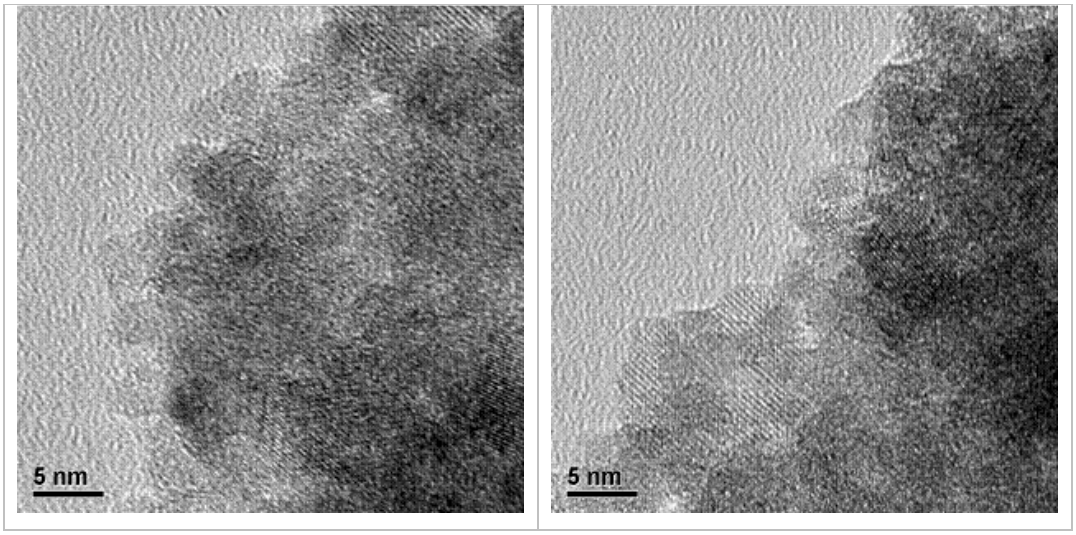

Figure 4.4: High resolution TEM images of N-0-2.

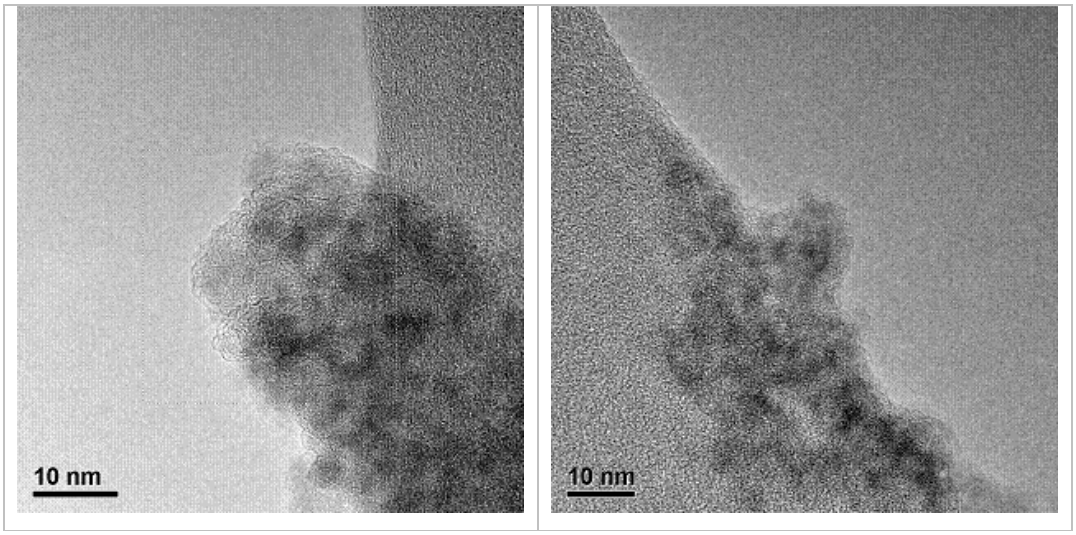

Figure 4.5: Images taken from particles produced in N-30-1.

4.3.2. Elemental Distribution

4.3.2.1. Stationary Measurements

EFTEM was conducted on selected samples with a view to obtaining maps of elements throughout aggregates. Images of the dispersion of elements throughout

aggregates should provide information on how the aggregates are formed with relation to each species, such as elucidating which point in the reaction the ferrihydrite / silica association occurs. The EELS spectra were taken and positions selected for the energies at which to analyse the relative intensities of electrons for iron, silicon and sulphur. Thickness maps, elemental maps and unfiltered images were obtained for each aggregate and position.

While a bright field TEM image appears darker in thicker areas (since fewer electrons will pass through) the thickness map from EFTEM contains little or no surface detail and is brightest (most intense) in the thickest regions of the aggregate. The elemental maps operate in a similar manner, displaying the brightest signal in regions containing the greatest amount of that element. This can be due to the thickness of the sample (as thicker areas contain more material and therefore often more of the selected element) or it can be due to discrete pockets of high concentration of the element.

The images displayed in Figures 4.6 and 4.7 provided a visual representation from which a mechanism of how the co-precipitate particles were formed could be proposed. The iron maps (Figure 4.6c and Figure 4.7c) tended to closely mimic the thickness maps throughout the aggregates, suggesting that the bulk of the material consisted of the iron containing phase. In contrast, the silicon map seemed to display a more surface oriented dispersion. The thicker regions of the aggregates didn’t produce significantly greater intensities on the silicon map, consistent with there being little or no additional silicon in thick areas. There was also a region of greater intensity around the edges of aggregates, which may indicate a greater depth of silica around the edge. This is consistent with surface related silica as the edges of aggregates would have had vertical layers of silica. The silicon maps of all the aggregates analysed show undulations related to surface association, demonstrating common and therefore representative behaviour.

A clear example of this behaviour is shown by the bright region on the left of the thickness map in Figure 4.7b. This also appears as a bright region in the iron map but there is no corresponding spike in intensity in the silicon map, providing further evidence that the bulk of the silica forms a coating on the outside of the ferrihydrite aggregates as opposed to being simultaneously precipitated with ferrihydrite; the

silica precipitation process is both slower and reliant on a suitable surface. It appears that there is a small proportion of silicon throughout the aggregates but the majority of the silicon is surface-related. There are limitations to the resolution of this technique, which makes it impossible to conclude whether silica is on the surface of primary particles or only on entire aggregates. It is also beyond the scope of this technique to determine whether silicon has been incorporated into the ferrihydrite structure.

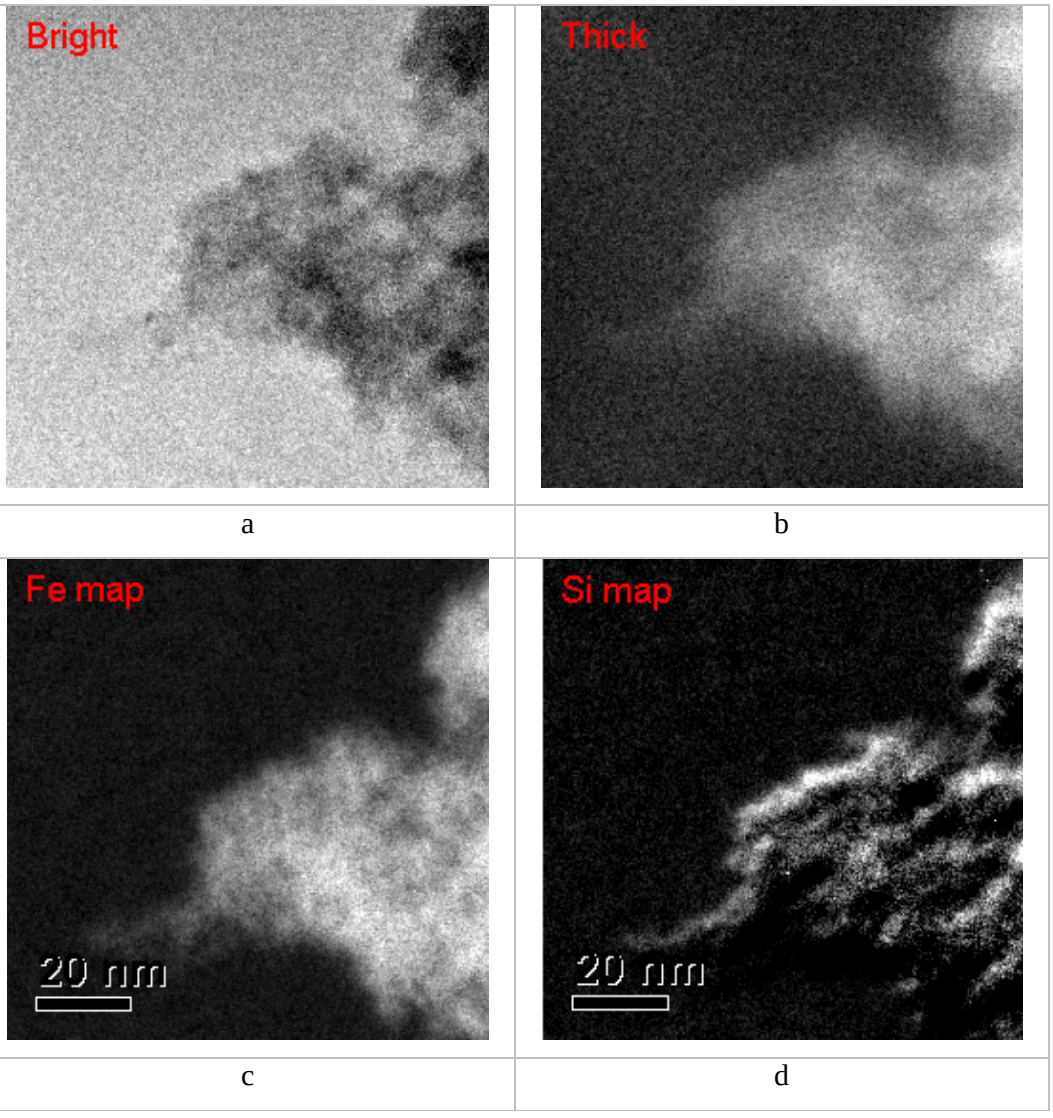

Figure 4.6: EFTEM image series taken of the edge of a particle from N-30-1, where (a) is the bright field image (b) is the thickness map, (c) is the iron map and (d) is the silicon map.

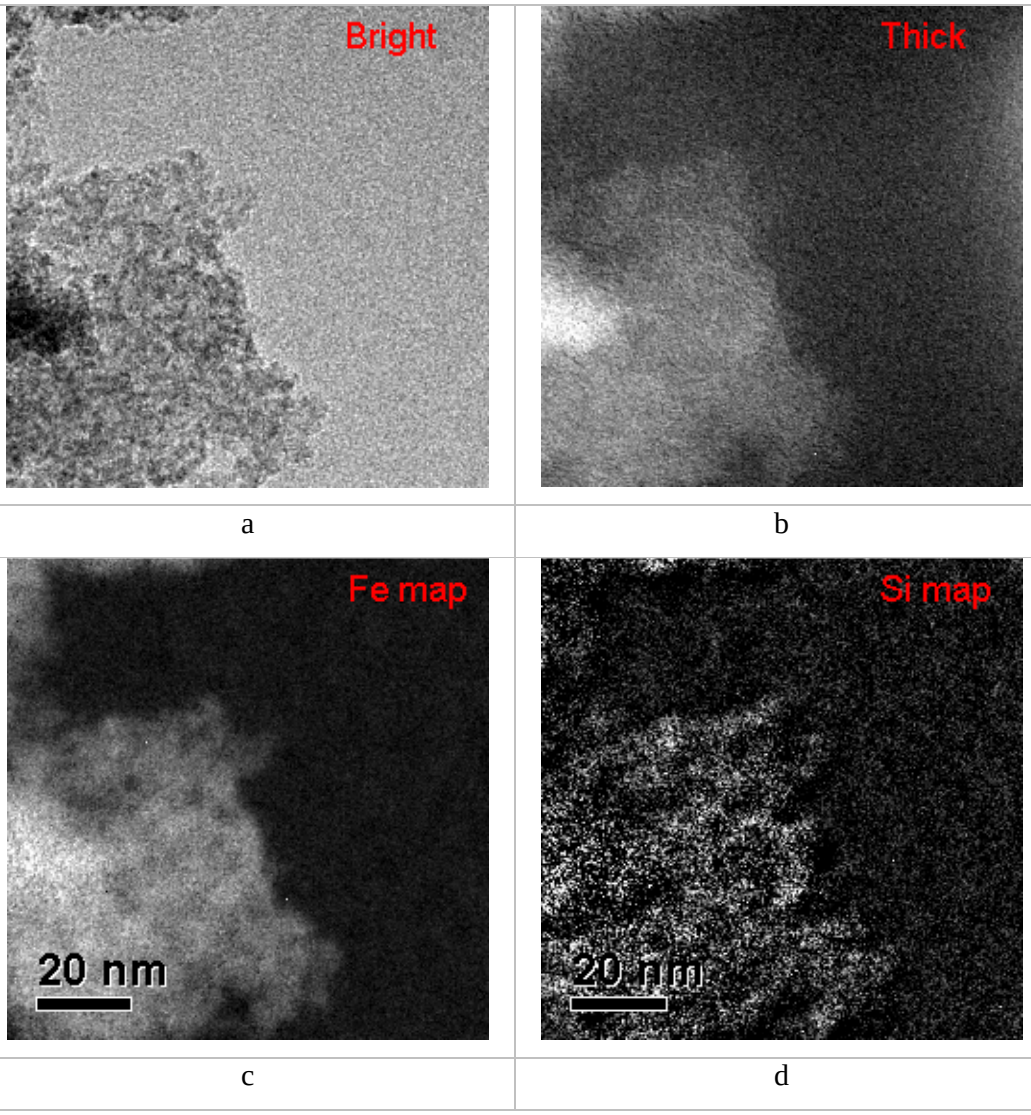

Figure 4.7: EFTEM image series taken of the edge of a different particle from N-30-1, where (a) is the bright field image (b) is the thickness map, (c) is the iron map and (d) is the silicon map.

For a complete analysis of the co-precipitates and to provide supporting evidence of the surface association of silica, it was necessary to examine the sulfate systems. This also provided the opportunity to investigate the distribution of elements throughout both the standard ferrihydrite aggregates and the schwertmannite-like fine needles within the samples. The silicon levels in the samples produced in sulfate media are much lower than those produced in nitrate, which complicates acquisition of the silicon map. Where an element is present in low proportions, the signal intensity of the related electrons is low, therefore a greater acquisition time is required. This introduces problems, one of which is greater sample drift. While it is very difficult to

keep the sample perfectly stationary, very small amounts of drift are generally insignificant under normal circumstances. However, larger acquisition times allow more drift to occur and affect the image obtained. Attempts to amplify the signal intensity can also decrease the contrast obtained and features can be lost.

The element maps show similarities between samples produced in nitrate and sulfate media with regard to the physical distribution of iron and silicon (Figure 4.8 and Figure 4.9, both produced in sulfate media). The iron map displays ferrihydrite forming the bulk of the aggregate peaking in intensity in the thickest regions of the aggregates, while the silicon map shows surface feature association and limited response to thickness. Figure 4.8 displays images of the needles described above that are indicative of schwertmannite. In the unfiltered image (Figure 4.8(a)), the individual particles can be observed, which correspond to the goethite particles proposed by Hockridge et al. (Hockridge 2009).

The sulphur map also presented in Figure 4.9e exhibits how sulfate is present throughout the aggregate. The distribution appears to have some relation to thickness as well as surface features. This would suggest a combination of surface coverage of constant concentration and significant dispersal through the aggregate bulk. It is possible that a strong surface association is the driving force behind the formation of the hedgehog morphology in the crystallisation of schwertmannite (Hockridge 2009). The distribution of sulfate observed here may indicate an association with both ferrihydrite and silica.

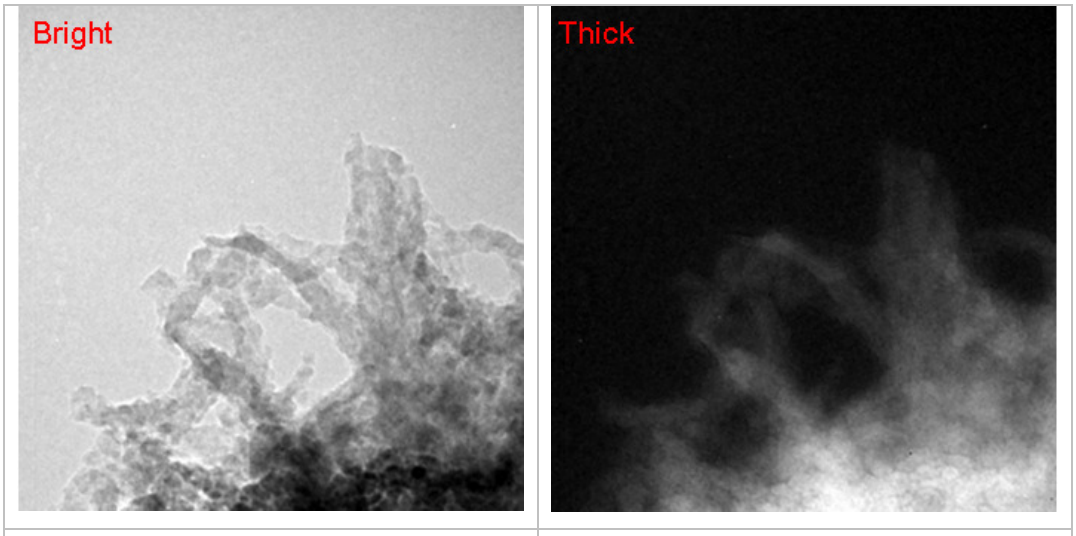

Figure 4.8: EFTEM image series obtained from S-50-1, where a) is the bright field image b) is the thickness map, c) is the iron map and d) is the silicon map.

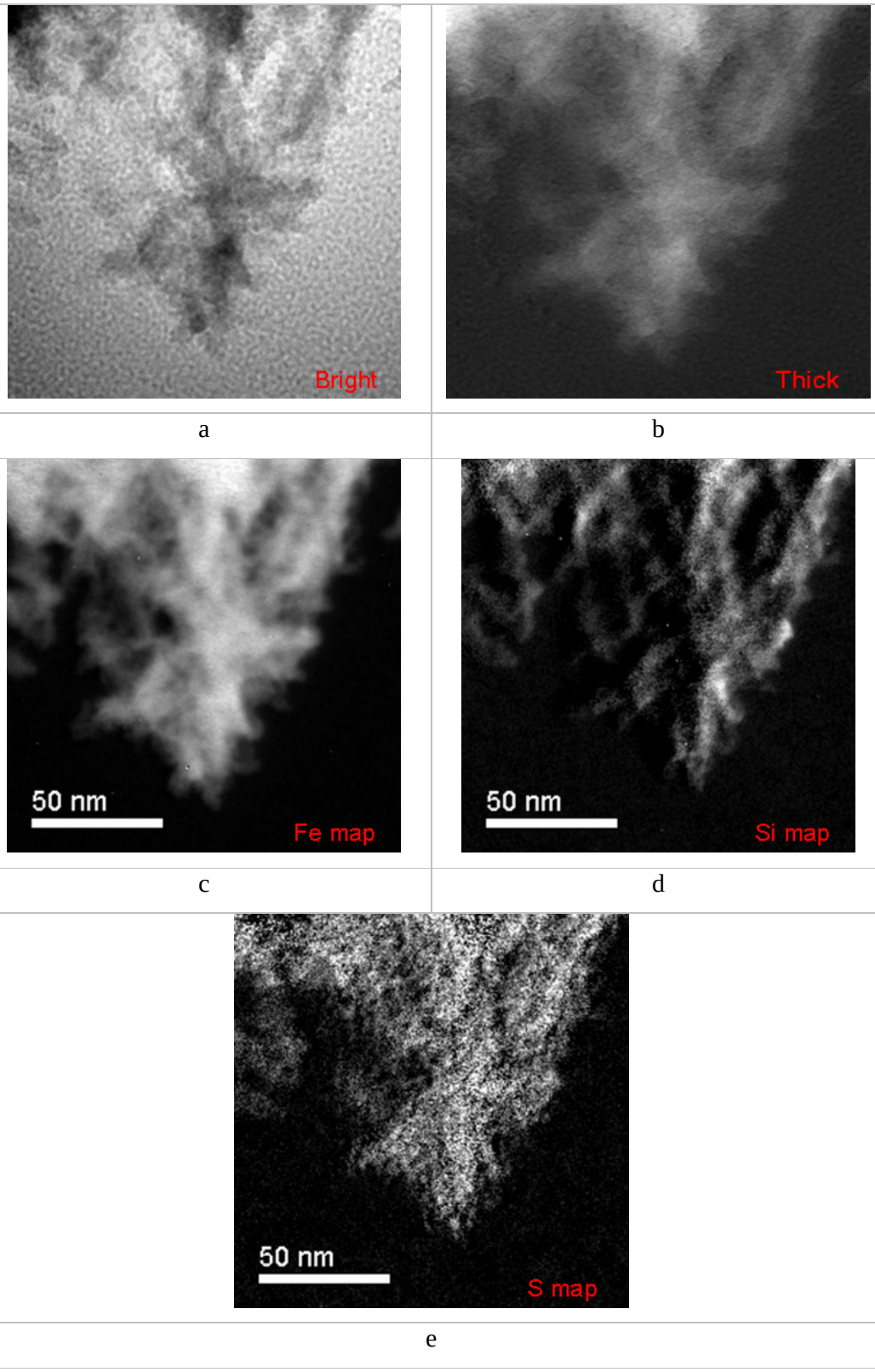

Figure 4.9: EFTEM image series obtained from S-30-2, where a) is the unfiltered image b) is the thickness map, c) is the iron map, d) is the silicon map and e) is the sulfur map.

4.3.2.2. Sample Rotation

Tomography involves imaging or data collection in segments, which is generally reconstructed to provide a three-dimensional representation of the object in question. Electron tomography is the collection of images while the sample is rotated through a series of angles, and this technique was conducted on N-30-1. These measurements were carried out on a Jeol 2100 microscope, as the capabilities for angular rotation do not exist on the other available instruments. A specific sample holder was also required to allow the sample to be manipulated in such a way. The microscope was aligned in a similar manner as for HRTEM to provide the best resolution and focus and preparations were conducted for EFTEM. The sample was rotated away from the normal in one direction and set to the angular range required. The data acquisition was automated; the microscope rotated the sample by one degree and then takes the designated images (Boudier 2005; Xu 2008; Alloyeau 2009; Ke 2010; Okuda 2010).

Collecting a series of maps from different angles was expected to provide further information with respect to how silica was dispersed throughout the particles. This procedure raised several complications in relation to image collection. The microscope must be extremely accurately aligned to allow the sample to rotate without moving laterally or vertically while maintaining focus. Acquiring an EFTEM image series also takes a significant amount of time, which can introduce difficulties with sample drift and degradation. Obviously conducting these measurements for up to 80 times on a single sample magnifies these problems. The time taken is also an issue with regard to the use of the instrument. The process requires hours for completion, meaning that only a single attempt can be made per microscope session.

The above problems were evident during the first attempt at acquiring a series of images at different angles, which was unsuccessful due to the selected aggregate moving out of focus early in the series. The second series provided images that remained in focus over a 50 degree angular range. The sample is shown at either end of this angular range in Figure 4.10 and Figure 4.11 and similarities of the elemental distribution can be seen. Like previous samples, the bulk of the aggregate appeared to

be primarily ferrihydrite, as the iron maps correlate well with the aggregate thickness. There is a distinct intense layer on the edge of the aggregate in the silicon maps taken at both angles, which is further evidence of surface-associated silica, and also suggests that the silica coating the surface of the aggregate was dispersed over the entire aggregate.

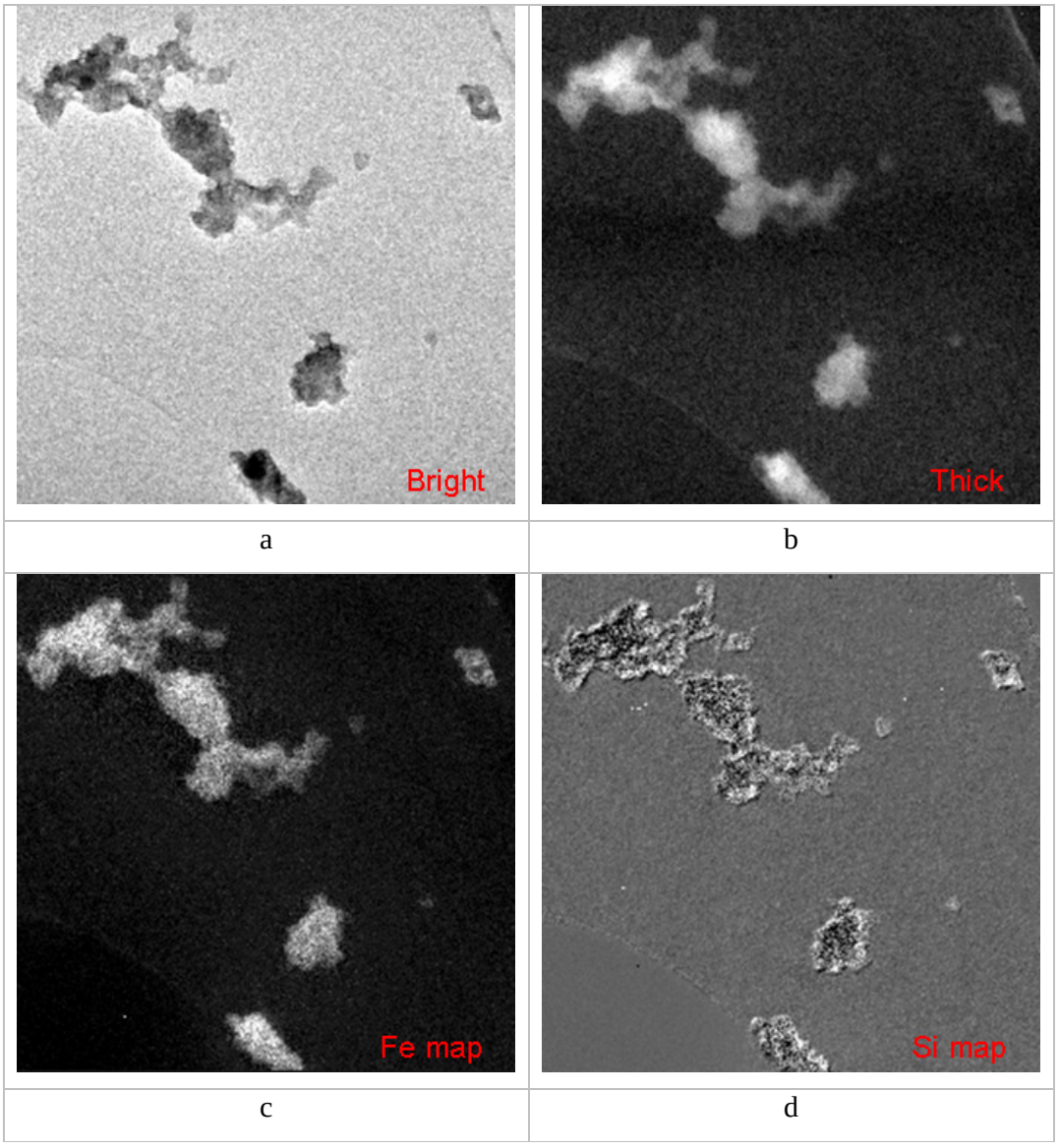

Figure 4.10: EFTEM image series taken of a particle from N-30-1 at -10 degrees tilt, where (a) is the bright field image (b) is the thickness map, (c) is the iron map and (d) is the silicon map.

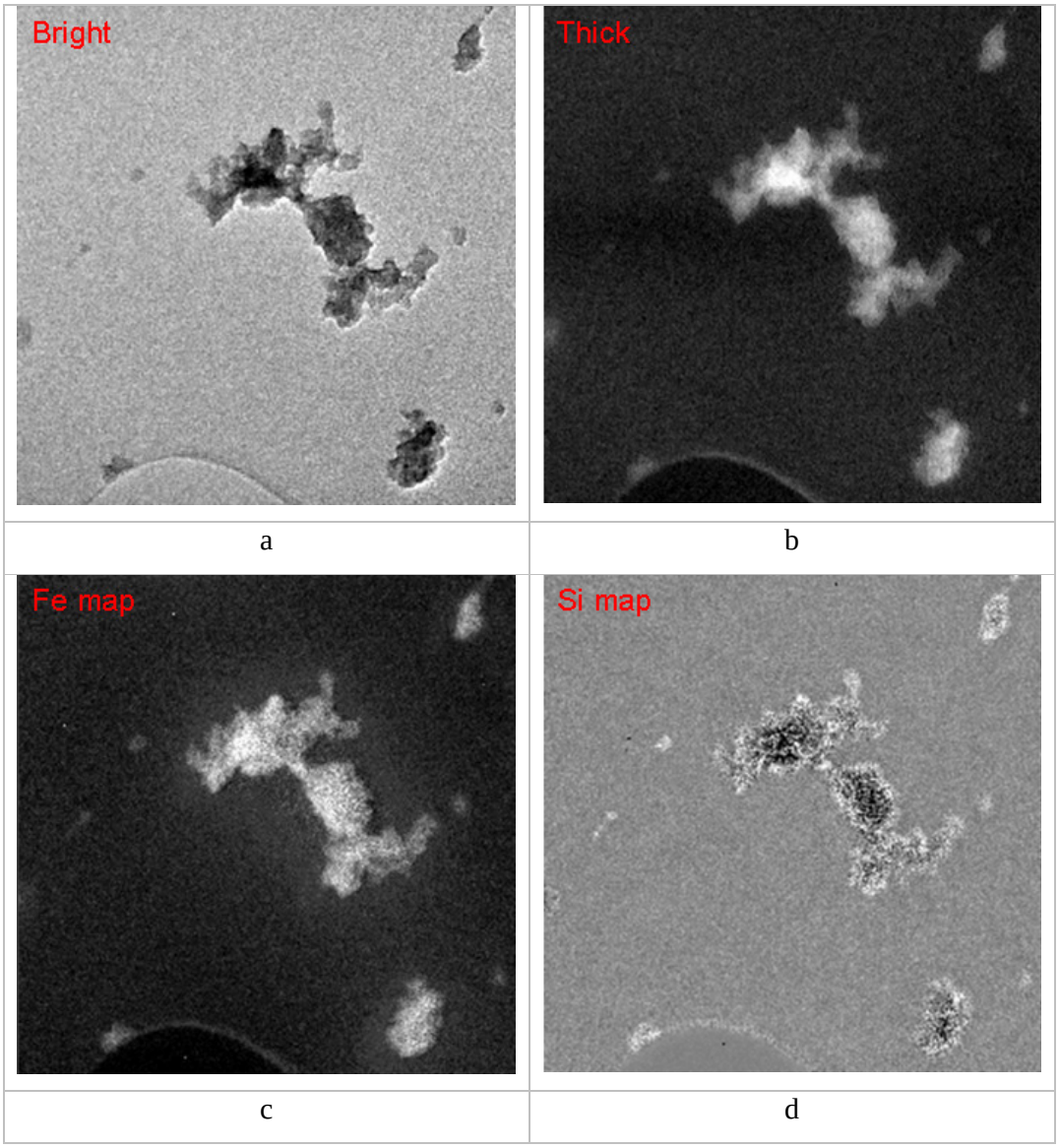

Figure 4.11: EFTEM image series taken of a particle from N-30-1 at +40 degrees tilt, where (a) is the bright field image (b) is the thickness map, (c) is the iron map and (d) is the silicon map.

The above observation is highly significant, as it provides a three-dimensional examination of the co-precipitate. While previously it had been assumed that the surface layer would be present around the surface of the particle, there was no definitive evidence. The indications displayed in these images would also suggest that most of the silicon signal observed in the bulk of the sample is also from the surface layer. It would appear that there was very little of the silica within the aggregate itself.

The fact that there were multiple particles in view (two throughout the entire series) in this series adds to the significance of the results. The behaviour displaying the bright surface layer is seen in all of the particles in view. This suggests that the data obtained can be likely to be representative of the general aggregate composition throughout the precipitate mass.

While the aggregate had drifted during the process of the measurement, this did not affect the analysis significantly across the 50 degrees shown. If overlays of the maps were required, this may create a problem with correctly aligning features. The silicon map lost focus beyond -10 degrees tilt, which may have been caused by the drift, or by a change in height due to the rotation. Considerable degradation of the sample had also occurred, due to prolonged exposure to the beam. However, given that there was little resulting change in the morphology, the elemental distribution of iron and silicon throughout the aggregate should have remained constant.

All of the data collected has indicated that silica generally forms on the surface of aggregates. The data presented suggests that it is unlikely that large amounts of silica are present on the primary particles within the aggregates. However, it can be concluded that, if silica is associated within the aggregates, it would be a relatively small fraction of the total silica, as the majority of the silicon signal is associated with the aggregate surface. These techniques are also unable to determine whether the ferrihydrite has been altered due to the inclusion of silicon in the structure. PDF analysis will be required for this determination.

4.4. Pair Distribution Function Analysis

4.4.1. Introduction

Laboratory-based X-ray sources used for energy emission, while extremely useful, do not necessarily have the beam intensity required for some analyses. Synchrotron X-ray installations provide the beam intensity and experimental apparatus to conduct experiments and analyses that would otherwise be impossible on most laboratory instruments.

Pair distribution function (PDF) analysis was considered highly desirable for this study, as it can provide detailed information regarding the structure of materials. X-ray scattering data is obtained from passing a high energy beam through the sample, the scattered photons are collected by a circular detector stationed on the opposite side of the sample. A calibration material is measured to obtain values for certain required variables, such as the sample-to-detector distance. The data obtained from the sample measurement is then averaged and integrated to form a one-dimensional plot of intensity against scattering angle.

A background subtraction is conducted to remove scattering from other media that the beam traverses such, as containers (e.g. capillaries) and liquids (e.g. samples dispersed in solution). Other corrections for a significant number of factors related to the instrument, beam type and energy, sample and sample container shape are required to remove interference from the data (Chupas 2003). Knowledge of the contributions is required to extract the structure function S(Q) (Q is a three-dimensional point in reciprocal space). A Fourier transform is applied to the structure function to convert the intensities into values relative to real space distances. Any errors in the corrections applied to the data throughout the analysis will result in faults in the PDF produced.

The PDF describes the probability of finding a pair of atoms at a given distance (Qui 2004). The data is a representation of the distances between neighbouring atoms

which can be related to not only a crystal structure but also bonding environment. The scattering data (in this case X-rays) is compiled and manipulated by software to convert the raw data to the intended 2D representations. These can be modelled to derive the structure of the sample or compared to others to visualise structural similarities or differences.

Experiments conducted by Michel et al. (Michel 2007) demonstrated that the difference between 2- and 6-line ferrihydrite is the size of the primary particles. They found that both systems displayed similar PDF traces to the point at which the 2-line signal was attenuated due to the restriction of smaller scattering domains (attenuation in this context refers to the decline in signal strength; complete attenuation would see the signal lost to background). This occurs because there is no coherent structure beyond a certain distance and is generally seen in nano-sized materials at the particle boundaries. The 2-line trace showed no significant signal above 20 Å, which is approximately the mean primary particle size. For a sample of intermediate crystallinity lying between (2- and 6-line ferrihydrite) and for pure 6-line ferrihydrite, the signal continued to approximately 30 and 60 Å, respectively, corresponding to their measured mean particle sizes.

Experiments involved in this investigation are based on this theory and are directed at determining whether silicon is included in the ferrihydrite structure and if the effect of silica on the crystallinity is through a restriction of the primary particle size. Such information is of great importance, as no other technique has been able to provide compelling evidence as to whether co-precipitation produces a ferrihydrite structure containing silicon. This knowledge, coupled with the possible alteration of particle size by silica, will provide insight as to how the precipitates are formed. These are key requirements to conclusively determine the path that the reaction follows.

4.4.2. Experimental

A pure silica sample (Si-045, Table 4.3) was prepared by a method modified from Cooper's (Cooper 1998) preparation of zinc orthosilicate. An acid solution containing 15.5 mL of 98% sulphuric acid and 314.5 mL milliQ® water was prepared and heated

to 95 °C. To this a solution of 10.61 g of sodium metasilicate dissolved in 70 mL of milliQ® water was added. The mixture was thoroughly agitated and left to react at 95 °C for 5 days. The suspension was allowed to cool followed by several days of dialysis against milliQ® water. The resulting gel was filtered, washed twice with milliQ® water and oven-dried at 60 °C for 5 days; it was then crushed using a mortar and pestle to create a coarse powder. This sample was used for comparison of the PDF response of pure silica with that of the co-precipitated material.

The PDF measurements require large beam intensities and a wide span detector to get high resolution and Q-range, which is the maximum interatomic distance that is measured. In many investigations the data at low distances is most important, as it describes the local bonding environment; however, the data at higher distances is required for comparison of longer range order. The measurements were conducted at the Advanced Photon Source (APS) at Argonne National Laboratory in Chicago, Illinois. The 11-ID-B beamline was utilised; it was the instrument with which Michel et al. conducted their PDF analysis of ferrihydrite, proving it could provide the conditions and range for this purpose(Michel 2007). It is also one of the few beamlines that have the desired energy range and can accommodate the necessary detector to extend data to a high Q-range, (a requirement for these experiments).

X-ray scattering data was obtained by passing a high energy X-ray beam (11-ID-B beamline) through the sample with an MAR345 image plate detector on the other side capturing scattered photons up to wide angles. The detector collects radial intensities in two dimensions arranged across a circular surface, of which small portion is obscured by the beam stop.

Only small volumes of powder were needed in such experiments, and therefore subsamples were taken from those used for XRD analysis. Two types of sample holder were used - the first were 1 mm kapton capillaries and the second were flat, thin metal rings. One side of the ring was lined with kapton and the sample placed in the hole in the centre, the other side was then covered with kapton creating a thin flat sample of powder with kapton on either side. This removes any interference from possible changes in sample depth that might be present using the cylindrical

capillaries. Two beam energies (60 and 90 keV) were used, as each provides different advantages. The wavelength for each was accurately given and recorded as 0.2128 and 0.13072 nm, respectively. The experiments from which samples were taken for this analysis are described in table 4.3.

The modelling was done using two programs. The first is fit2D (Hammersley 1996), which produces a chi plot which is then used in the second program (PDFgetX2, (Qui 2004)), which is used to extract a PDF plot. The raw data is fed into fit2D, which allows multiple measurements to be averaged and plots the 2D intensities. Using a CeO_2 standard, the sample-to-detector distance is calculated, and masking the influence of the beam stop, the pattern is integrated to produce the 1D chi plot. This data is then introduced into PDFgetX2. Information such as sample composition, radiation parameters, scattering type, corrections, etc. is required to provide the most accurate PDF.

4.4.3. Discussion

Fifteen samples were supplied for analysis; N-0-2, N-30-1, N-10-1, S-0-1, S-10-1, S-30-1, N-2Line, (Si-045), S-0-10Z, S-10-10Z, and S-30-10Z. The general purpose was to compare the PDF plots from the ferrihydrite produced in the absence of silica, pure silica and physical mixtures of the two with co-precipitate samples. The physical mixtures were produced by adding silica powder to the N-0-2 and S-0-1 samples in proportions calculated to simulate those in the co-precipitates. The proportion of ferrihydrite and silica in the N-30-1, N-10-1, S-10-1 and S-30-1 samples were roughly calculated based on the feed and supernatant element concentrations.

Co-precipitate samples showing the same PDF pattern as a mixture of the silica-free samples and pure silica would suggest that silicon has not been included in the ferrihydrite structure. Also a great enough decline in the particle size corresponding to attenuation in the PDF occurring at a shorter distance would indicate that silica restricts ferrihydrite particle growth. This would both add further credibility to the findings of Michel et al. (Michel 2007) and demonstrate that the silica is limiting particle growth, thereby decreasing the apparent crystallinity. The zinc-containing

systems were introduced to observe whether the zinc would significantly influence the structure.

Table 4.3: Experiments producing the samples referred to in this section. Ideal feed concentrations are given, variation occurred due to experimental uncertainty.

System	Conditions					
	Feed Concentration		pH	Residence Time	Temp (°C)	Anion present
	Fe ($g\ L^{-1}$)	Si ($g\ L^{-1}$)				
N-0-2	6.3	0	2.65	45 min	85	NO_3^-
N-30-1	4.4	0.95	2.65	45 min	85	NO_3^-
N-10-1	5.7	0.32	2.65	45 min	85	NO_3^-
S-0-1	6.3	0	2.65	45 min	85	SO_4^{2-}
S-10-1	5.7	0.32	2.65	45 min	85	SO_4^{2-}
S-30-1	4.4	0.95	2.65	45 min	85	SO_4^{2-}
S-30-A	4.4	0.95	2.65	45 min	85	NO_3^-
S-50-1	3.2	1.6	2.65	45 min	85	NO_3^-
N-50-1	3.2	1.6	2.65	45 min	85	NO_3^-
LN-30-1	6.3	0	2.65	45 min	85	NO_3^-
N-2Line	12.9	0	5.25	45 min	85	NO_3^-
Si-045	Pure silica sample, see section 4.2 for preparation.					
Physical Mixture	This sample is a 1:1 mixture of Si-045 (pure silica) and N-2Line (pure 2-line ferrihydrite).					
S-0-10Z*	6.3	0	2.65	45 min	85	SO_4^{2-}
S-10-10Z*	5.7	0.32	2.65	45 min	85	SO_4^{2-}
S-30-10Z*	4.4	0.95	2.65	45 min	85	SO_4^{2-}

*Samples produced in the presence of 10 $g\ L^{-1}$ soluble Zn.

A problem was encountered with N-0-2 and S-0-1; although they were devoid of any silica, they were not pure ferrihydrite. The small amounts of goethite and hematite contained in the samples influenced the PDF response, especially at higher R values. This makes direct comparison between the silica-free and silica-containing samples difficult. Despite this, several tentative conclusions were able to be made.

Another problem became apparent with the samples produced in sulfate media. The presence of schwertmannite in the samples alters the structure and thus would likely modify the PDF response. It was impossible to determine the proportion of schwertmannite in the samples and it remains unknown whether silica affects that value. Therefore it is likely that there would be differences in the PDFs of the S-0-1, S-10-1 and S-30-1 that are not attributable to the ferrihydrite / silica association.

PDFs of N-0-2 and S-0-1 were overlaid for comparison (Figure 4.12). This highlights the problems with comparisons between samples produced in the two different media. Due to the presence of schwertmannite, goethite and hematite in the samples, the patterns are only similar to approximately 7 Å, beyond which the correlation deteriorates. It is suggested that the greatest contribution to this difference is schwertmannite as, of the undesired phases (given pure ferrihydrite was the aim), it is likely present in the largest proportion.

Plotting the responses from samples N-0-2, N-10-1 and N-30-1 together shows the similarities between the peak positions in each of the traces (Figure 4.13). The majority of the peak positions are identical and the intensities decrease with increasing silica content. There is a small contribution from silica in the samples, indicated by the arrows in Figure 4.14, which highlights R values up to 10 Å. This refers to the effect of the presence of silica in the samples causing differences in the pattern between the silica-free and silica-containing samples. This is a relatively minor influence resulting from the fact that silica constitutes less than 30% (by moles) of the sample produced even at the greatest Si concentration. Figure 4.15, focussing on the region between 30 and 40 Å, shows the differences between the samples due to the presence of more crystalline phases. Again these highlighted peaks do not occur often in the pattern, allowing a comparison to be made.

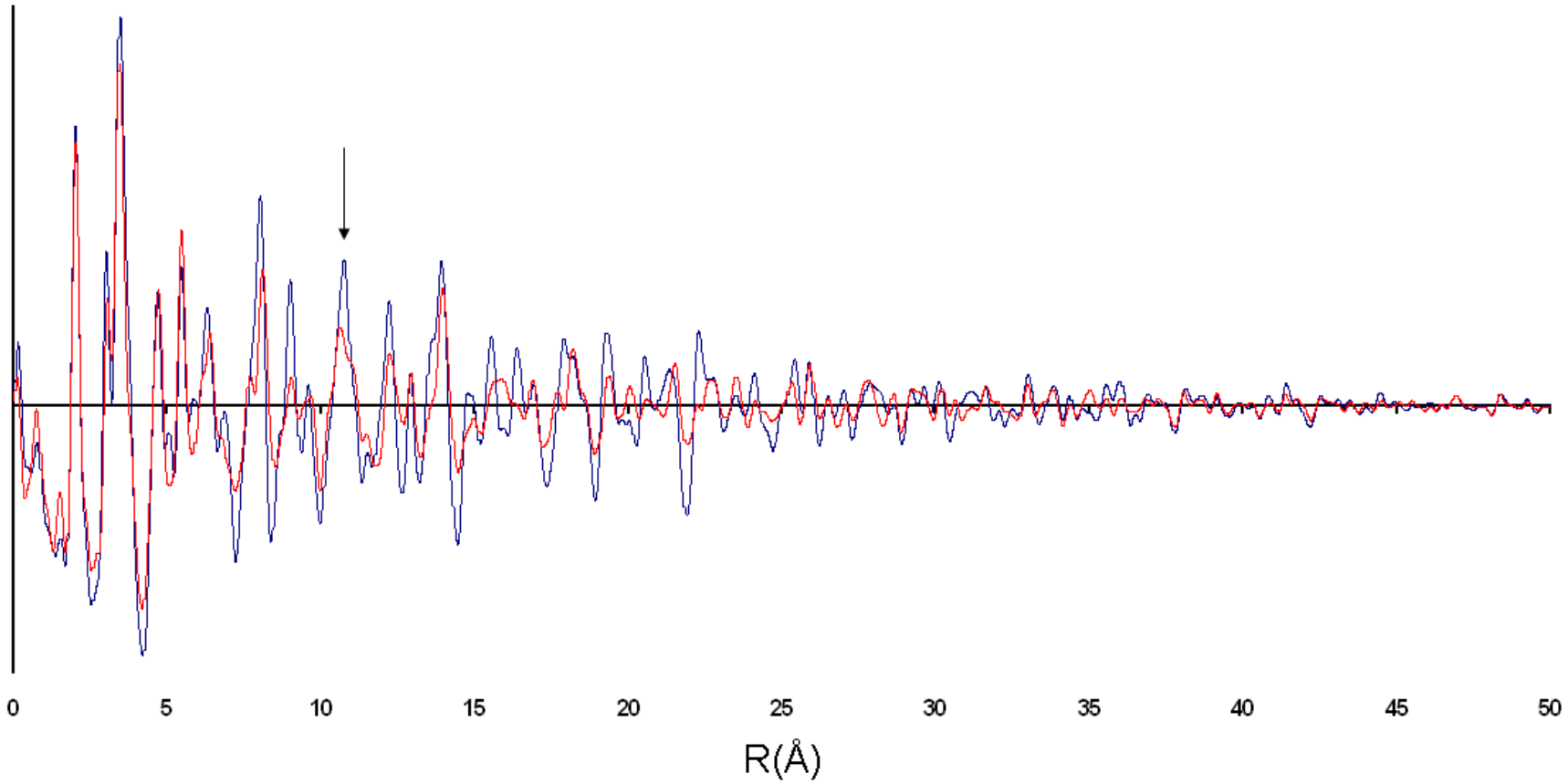

Figure 4.12: PDF plots obtained from N-0-2 (blue) and S-0-1 (red), the difference in the peak positions can be seen beyond the point indicated by the arrow.

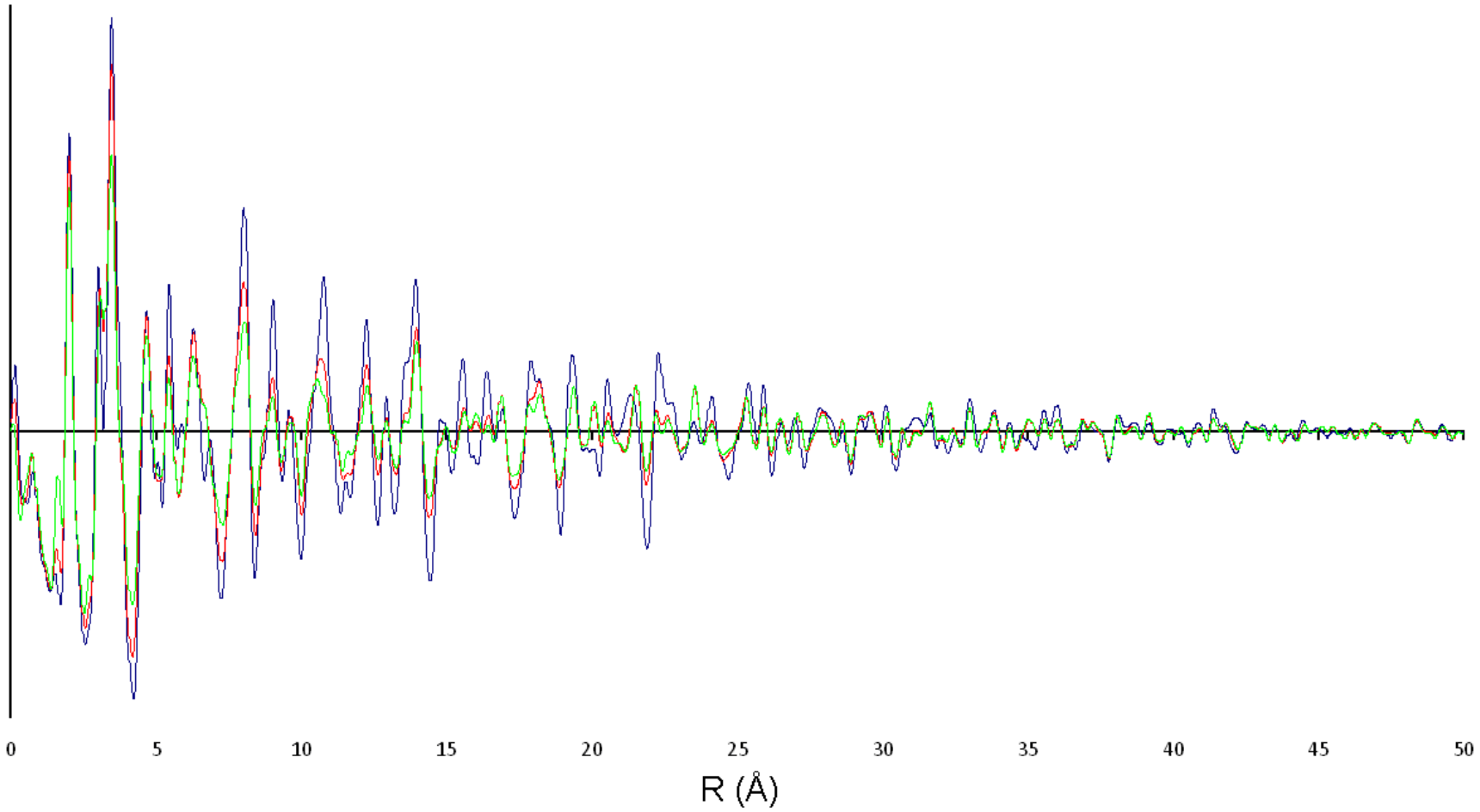

Figure 4.13: PDF plots obtained from N-0-2 (blue), N-10-1 (red) and N-30-1 (green).

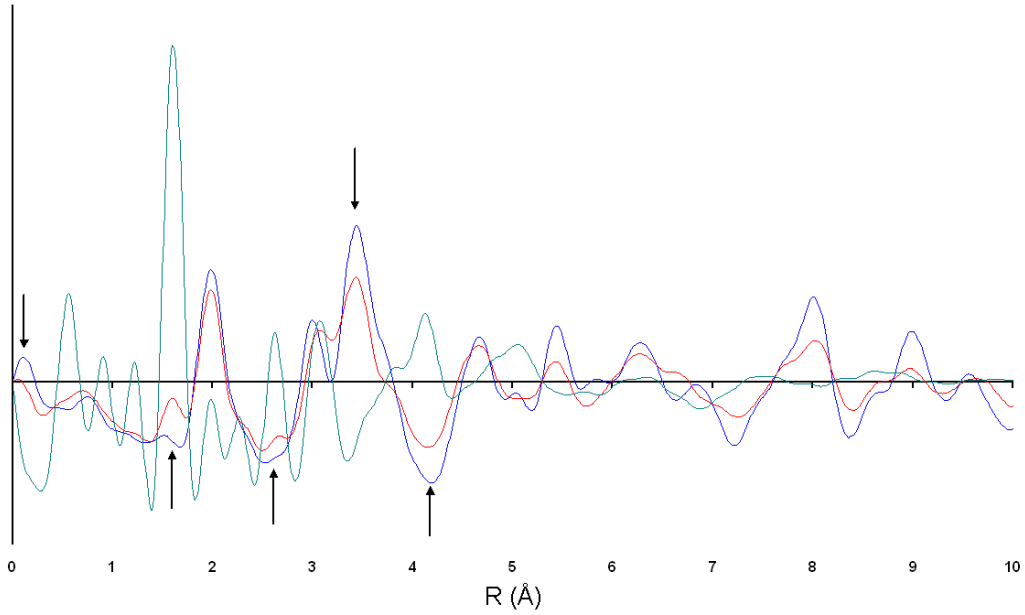

Figure 4.14: PDF plots of N-0-2 (blue), N-30-1 (red) and Si-045 (teal). The arrows indicate areas in which the plots differ due to the influence of the silica signal.

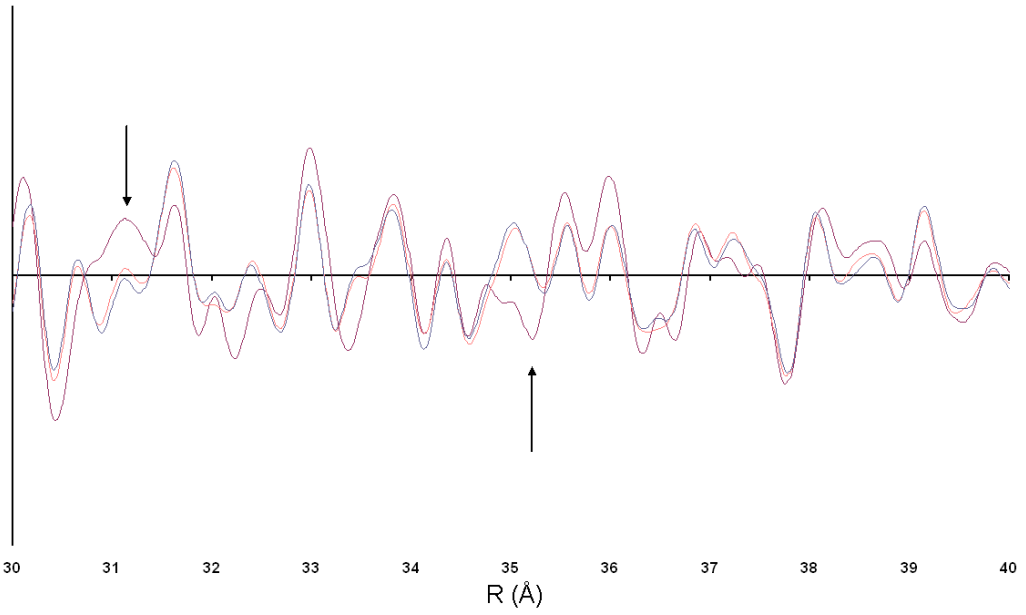

Figure 4.15: PDF plots obtained from N-0-2 (blue), N-30-1 (red) and N-10-1 (green). The arrows indicate the areas where the plots differ due to the presence of more crystalline material.

Aside from the contributions of silica and more crystalline iron oxide phases, there are very few structural differences between the samples. The decrease in intensity seen in most of the features is due to dilution of the sample (less ferrihydrite per mass of sample) and possibly from slight attenuation that can be attributed to minor changes in particle size. If any difference in the average primary particle size exists between the samples, it is not able to be determined ***via*** this method. It is our belief that this is because there is not a great enough change to be observed in the Q range examined.

Figure 4.16 illustrates the effect of having a lower proportion of ferrihydrite in the sample (the dilution effect mentioned above) on the peak intensities. These samples are the physical mixtures prepared by adding S-0-1 and Si-045 in the ratios of 9:1 and 7:3. The only difference between them is the proportion of each material; they are structurally identical. Beyond 10 Å, the contribution by the silica phase can be discounted due to the expected loss of signal from this point (as seen in Figure 4.14 for Si-045) but there is a general decrease in the intensity of the peaks. This is due to the lower proportion of ferrihydrite in the 7:3 sample providing less scattered X-rays.

The samples produced in sulfate media show the similar trends with respect to the presence of silica, except to a smaller degree at low r, and a higher degree at greater distances (Figure 4.17). This is displayed by the high degree of similarity in the peaks up to 7-8 Å, but the PDFs of the silica-containing samples differ from the pattern of the silica-free sample significantly beyond this point. The decreased amount of silica precipitated from these systems is the reason behind a weaker effect on the response from the atomic arrangement in the first 10 to 15 Å. This is a result of the samples not having been diluted as much with respect to ferrihydrite and having a smaller contribution from silica to the signal. The drop-off in the signal of the co-precipitates relative to S-0-1 suggests a smaller primary particle size. Since there was very little decrease in the apparent crystallinity observed in the XRD patterns of these systems (Figure 2.8), it would suggest that the six characteristic ferrihydrite XRD peaks are still observable in a range of particle sizes as low as 4 nm. It is also possible that the continued signal beyond this point in S-0-1 is due to the presence of goethite and that there is no difference in the particle size between this sample and the co-precipitates.

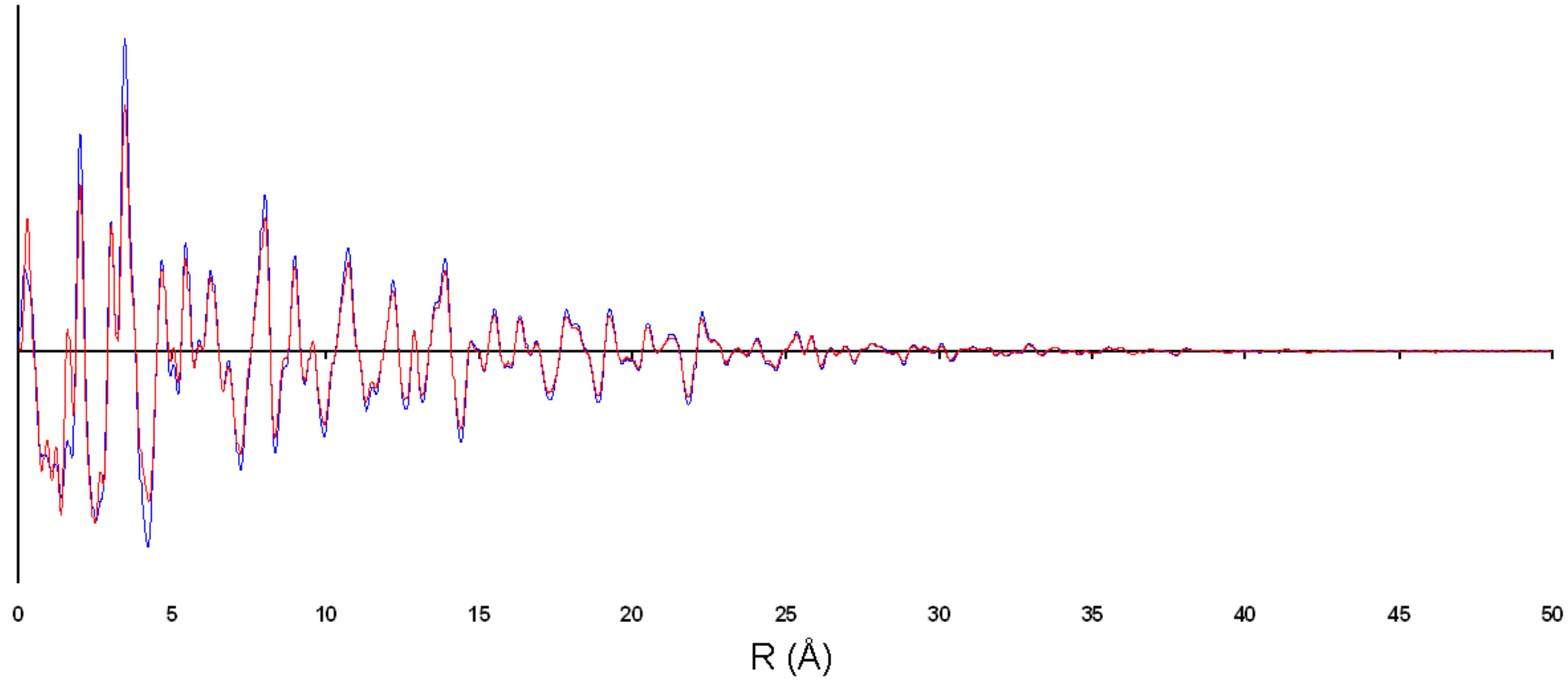

Figure 4.16: PDF plots collected from the physical mixtures of N-0-1 and Si-045 at proportions of 9:1 (blue) and 7:3 (red).

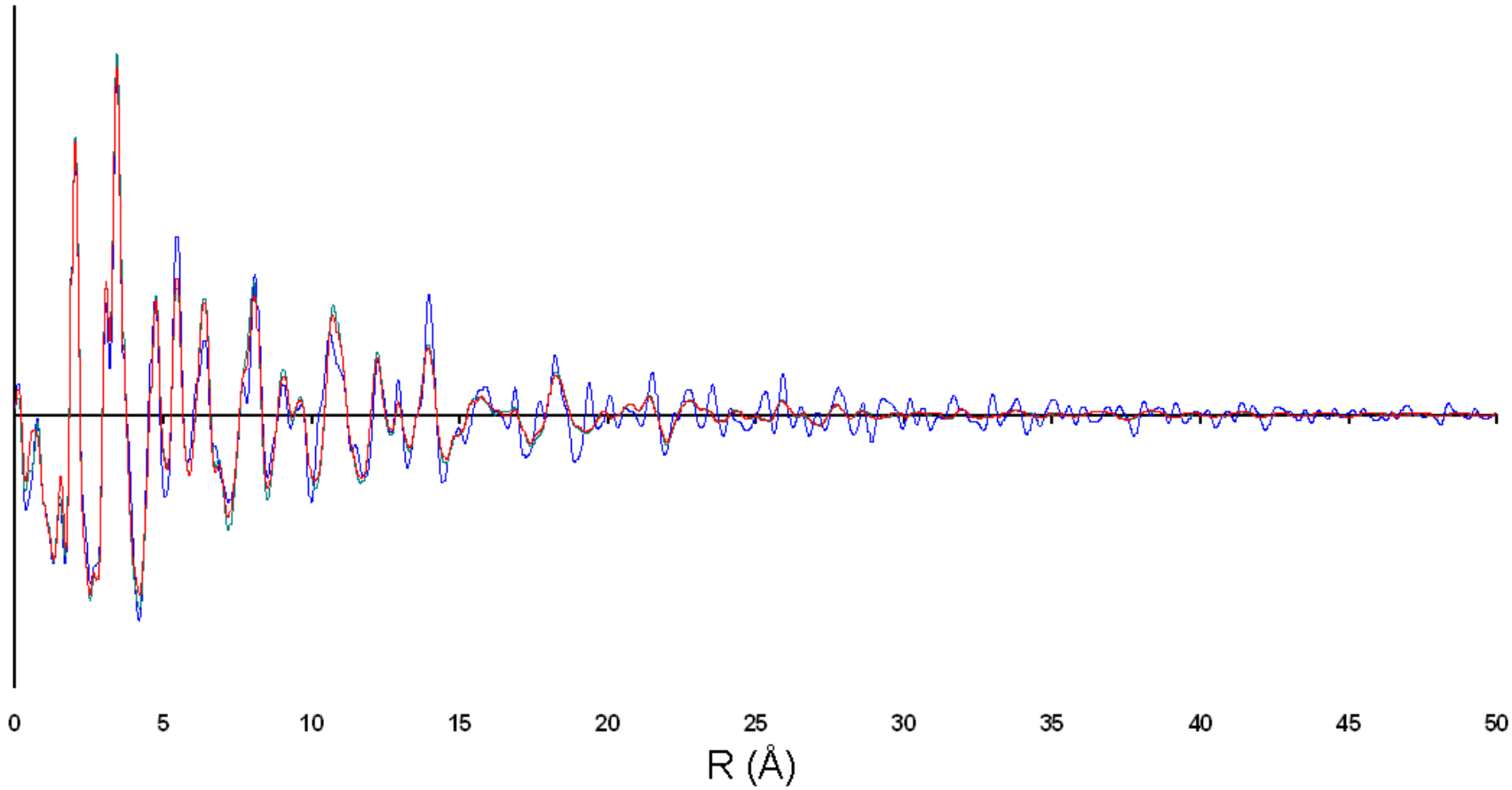

Figure 4.17: PDF plots obtained from S-0-1 (blue), S-10-1 (red) and S-30-1 (teal).

Comparison of the XRD pattern of N-50-1 in Figure 2.20 and that of pure silica and 2-line ferrihydrite in Figure 4.18 revealed that N-50-1 resembled 2-line ferrihydrite and contained the characteristic broad peak of amorphous silica. This should allow a direct comparison to be made between the PDF plots of N-2Line and Si-045 and the pure 6-line product to be made.

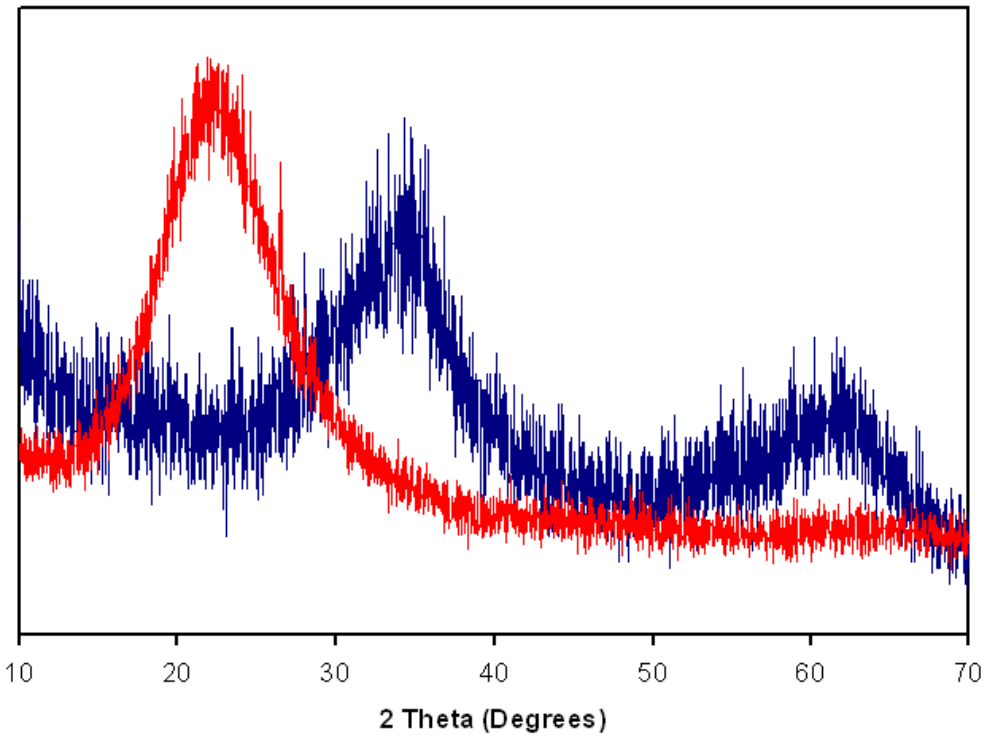

Figure 4.18: XRD traces of Si-045 (red) and N-2Line (blue). These patterns were obtained very quickly to demonstrate that the correct materials (2-line ferrihydrite and amorphous silica) had been produced.

Figure 4.19 contains PDF plots displaying the similarity between the physical mixture of silica and 2-line ferrihydrite and the sample N-50-1. The PDF responses were not expected to be identical, given that there is no chemical association between the two phases in the mixed sample. The co-precipitation of the species will most likely form the Fe – O – Si bonds referred to in previous chapters. Such bonds would be absent in the mixed sample and should thus ensure a certain amount of difference in the pairing in regions of the PDF.

In general, the traces display great similarity and the signals deteriorate at a similar distance. This attenuation would suggest a similar coherent scattering domain related to the primary particle size of the ferrihydrite phase. It can be seen in the trace of a sample of pure silica that the signal attenuates at approximately 11 Å, therefore it would not contribute to the signal reaching as far as 20 Å (2 nm, Figure 4.19). Using the same rationale as Michel et al. (Michel 2007), the attenuation of the signal occurring somewhere between 15 and 20 Å (1.5 and 2 nm) suggests an average primary particle size of approximately 2 nm, which correlates well with literature values (Cornell 1996; Janney 2000). This observation agrees with the assertion that the crystallinity of ferrihydrite is related to the particle size.

The similarity in peak position and attenuation point is strong evidence that the systems are somewhat alike in crystal structure. While there are some variations in peak positions below 1 Å these are most likely due to the existence of siloxane bridges joining the regions of silica and ferrihydrite as mentioned above. Beyond that, although there are differences in intensity, the peaks show a high degree of similarity with respect to R. This would suggest that it is unlikely that there is any silicon included in the ferrihydrite structure.

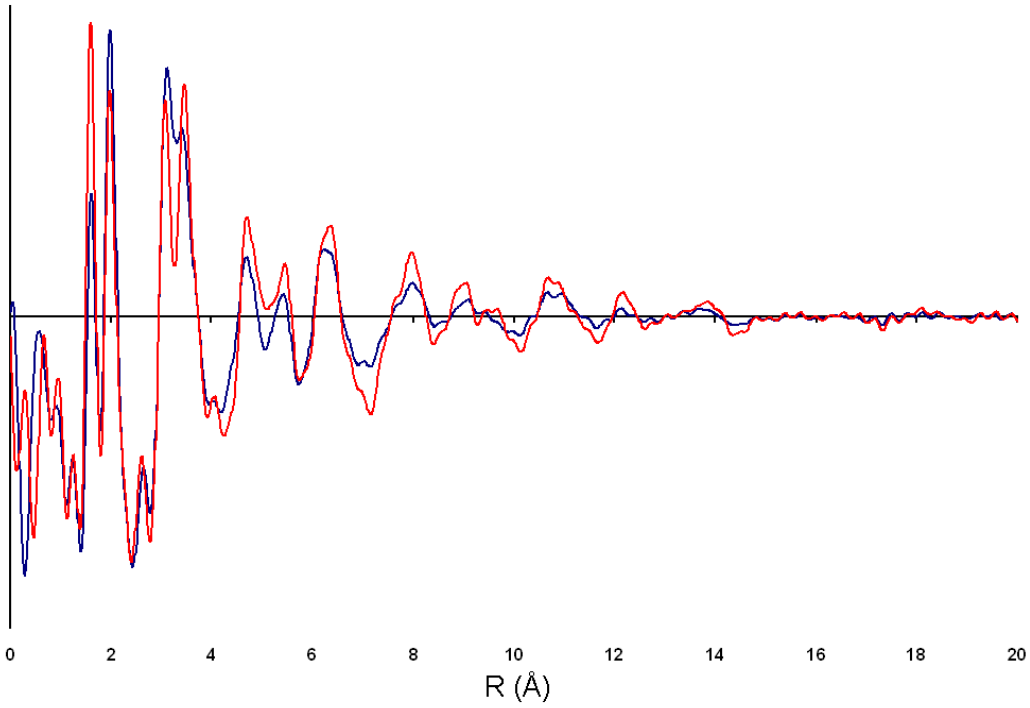

Figure 4.19: PDF plots obtained from N-50-1 (blue) and the mixture sample (red).

From comparison of the traces for a high-silica co-precipitate (N-50-1) and silica-free sample (LN-0-1) shown in Figure 4.20, it can be seen that in the first 15 to 20 Å before the N-50-1 signal is lost, the peak positions correspond well with LN-0-1. As with the different peak positions between N-50-1 and the mixture, the different peaks in this figure are evident at low R. This is due to the presence of silica in the N-50-1 sample. The silica signal is quite strong at low R values and the sample will contain Fe – O – Si bonds that are absent in LN-0-1.

The work by Michel et al. (Michel 2007) shows that 2 and 6 nm particles produce traces that are fairly similar in both peak position and intensity over the first 10 Å, which is not the case for the data presented here. The intensity of N-50-1 is always significantly lower and drops off very rapidly with respect to the LN-0-1 data. This is due to the high proportion of silica in the sample (one effect of which is seen in Figure 4.16). The presence of a large amount of silica also dilutes the powder with respect to ferrihydrite decreasing the amount of scattering from the iron oxide phase.

The feature of greatest significance with respect to Figure 4.20 is the large difference between the attenuation of the signal in the two PDF plots. This raises the proposition that the decrease in the apparent crystallinity of the co-precipitates is in fact related to a decline in particle size of the ferrihydrite phase. This is demonstrated clearly in these samples due to the high degree of change in both crystallinity and particle size. In combination with the correlation of the peaks between these samples it would suggest that the ferrihydrite crystal structure has not been altered, simply restricted in this case. This is evidence to the fact that the presence of silica in the precipitation process restricts the particle size of the ferrihydrite. It also adds further evidence to the argument of Michel et al. that the difference between 2-line and 6-line ferrihydrite is the size of the coherent scattering domain.

The signal from the LN-0-1 sample attenuates somewhere between 40 and 45 Å (4 and 4.5 nm), suggesting an average primary particle size between 4 and 5 nm. This is interesting, as this signal actually attenuates before those from the N-30-1 sample which contains a significant percentage (~28 %) of silica. However, this can be explained by the fact that the N-30-1 sample was prepared under conditions that would favour the production of a moderate proportion of more crystalline material if it weren't for the presence of silica. While this was not the intention, it is proven by the XRD trace of N-0-2 (Figure 2.7). This suggests that a slightly slower hydrolysis rate was occurring than would be required to produce pure ferrihydrite. Such a reaction would result in the precipitation of both goethite and hematite species along with a ferrihydrite phase with the greatest possible crystallinity and primary particle size. Although a decrease in crystallinity is observed between N-0-2 and N-30-1, due to the presence of silica, N-30-1 still contains the six characteristic ferrihydrite peaks. This means that the particle size is large enough to contain this degree of order.

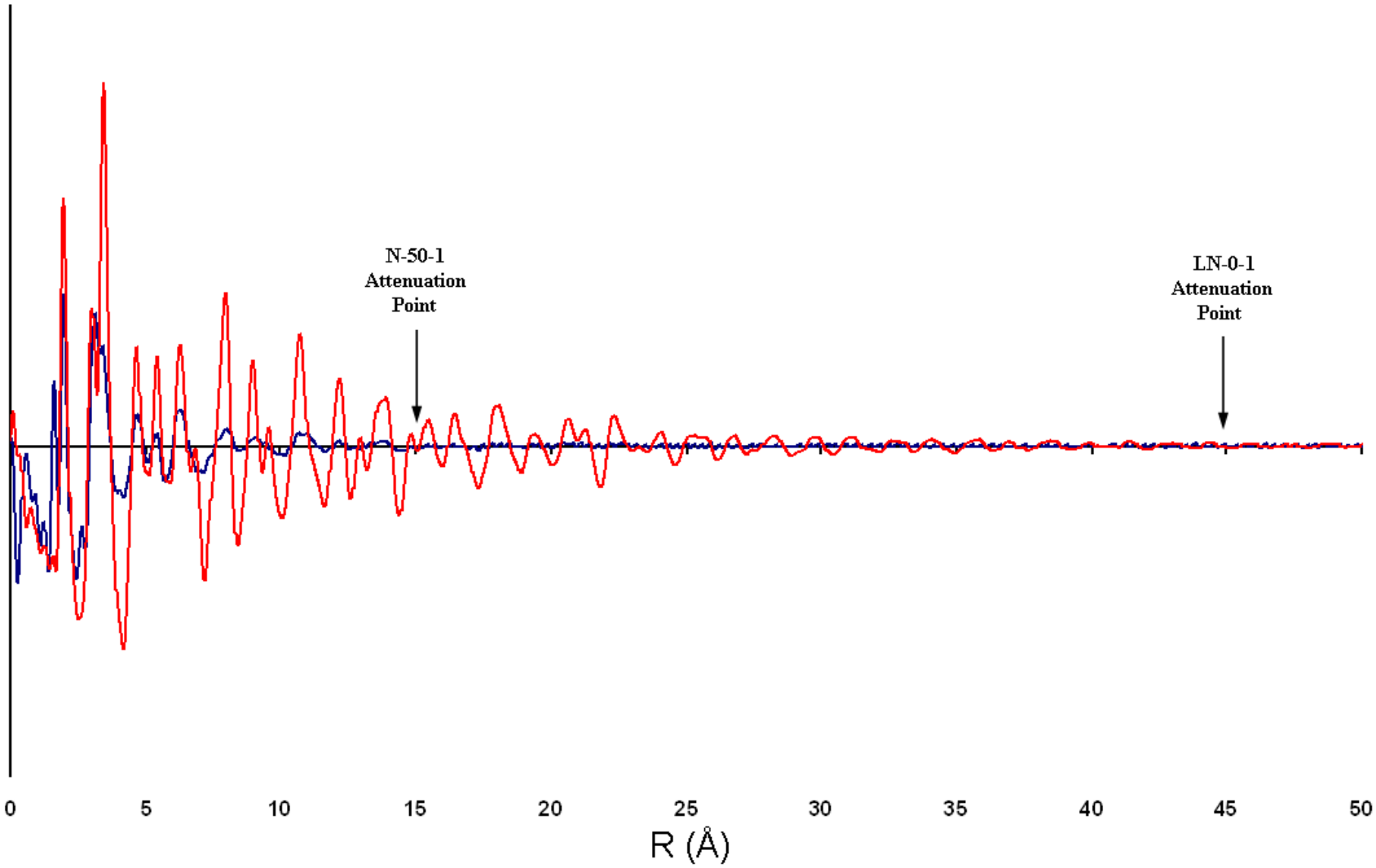

Figure 4.20: PDF plots from N-50-1 (blue) and LN-0-1 (red).

Conversely, while the LN-0-1 sample did not contain any Si during precipitation, it was formed at a fast enough hydrolysis rate as to almost eliminate the formation of more crystalline phases. This increased hydrolysis rate would give rise to the smaller particle size observed. In addition, the fifth characteristic peak, generally appearing as a shoulder at 72° 2 , is not visible from the XRD pattern (Figure 3.12). Its presence is detected by modelling the asymmetry of the peak at 75 degrees, but is less prominent than in pure 6-line ferrihydrite. This could be due to a decrease in at least one dimension of the primary particles. However, it can be seen from examining Figure 3.12 and Figure 4.20 that signal attenuation at approximately 4 nm does not necessarily coincide with an obvious decrease in crystallinity. Michel et al. showed that their sample containing 3 nm ferrihydrite particles, which produced a signal that attenuated at approximately 3 nm, still displayed all six characteristic X-ray diffraction peaks, although broader than the sample of 6 nm particles.

Supplementary plots are provided in Figure 6.6 and Figure 6.7 in the appendix. Figure 6.6 displays the comparison of the PDF plots of N-30-1 and a mixture of N-0-2 and Si-045 in which it can be seen that the co-precipitate signal attenuates slightly earlier than the mixed sample. This provides complimentary evidence reinforcing the assertion that co-precipitated silica restricts the primary particle size. Figure 6.7 contains the PDF plots of S-10-1 and S-10-10Z which indicate that zinc is not structurally incorporated into ferrihydrite when it is present during precipitation.

4.5. Summary

The data presented in this chapter provides information regarding the distribution of elements throughout the precipitates, the structural similarities and differences between systems and the co-precipitation process itself. There is enough evidence to conclude that samples produced in the presence of sulfate contain schwertmannite. HRTEM has shown, that within the scope of this investigation, high resolution imaging of samples containing large proportions of silica is unable to provide lattice information.

The elements in the co-precipitates were not all uniformly distributed throughout the aggregates. It was revealed that iron is distributed evenly across the bulk of the aggregate in high concentrations, while silicon tends to be dispersed around the aggregate surface. This agrees with the proposition that monosilicic acid adsorbs on the particulate surface provided upon precipitation of the ferrihydrite. This has been shown to cover the entire particle surface where the initial silicic acid concentration is sufficient. Sulfur is present on the surface, but displays enough correlation with the thickness to suggest it is also distributed throughout the aggregates. It would appear that sulfate anions are present on the surface of individual particles as well as the aggregate as a whole.

The pair distribution function results presented display the different responses of atomic arrangement within the materials. From the data collected, it appears that there is no incorporation of silicon into the ferrihydrite structure. Corresponding peak positions speak to the structural similarity of the pure ferrihydrite samples and co-precipitates. This is in agreement with the XRD and line profile analysis (chapter 2) results that did not show evidence of structural changes. The difference between the samples produced in nitrate and sulfate media also correlates with XRD and TEM results.

These experiments have provided information with regard to the behaviour of the constituents in the co-precipitation reactions. A great decline in particle size was observed in a sample that had shown the greatest decrease in crystallinity due to the

presence of Si during precipitation. The sample produced in the N-50-1 reaction was similar in both crystallinity and particle size to a physical mixture of 2-Line ferrihydrite and silica powders. However, the samples were not identical due to the presence of the Fe – O – Si bonding arrangement produced by the association of the two species.

5. CONCLUSION

This project was aimed at gaining a better understanding of the co-precipitation of ferrihydrite and silica, particularly the effect of silica on ferrihydrite crystallinity, primary particle size and aggregate structure. Establishing the implications of the presence of substantial silicate concentrations in process liquors on the Paragoethite process (specifically operations at Nyrstar Hobart) was also a priority.

The experimental crystallisation process employed in this study is continuous, in that reagents are constantly fed into the reactor and product slurry is removed. This approach was favoured, as the chemical system being analysed occurs both industrially and naturally as a continuous process. While batch experiments give some insight into the reaction of focus, the reagent concentration is not maintained over time and therefore multiple reactions can occur due to altering saturation levels.

Structural analyses, including XRD and PDF studies, were conducted on a raft of samples to determine how the iron and silicon were associated and what impact that had on the ferrihydrite structure and particle size. Measurements of aggregate properties such as fractal dimension and shear yield stress, gave insights into how the association of silica influences ferrihydrite aggregation.

The multiple facets of the co-precipitation process were analysed in an effort to understand the formation pathway and associated properties of the materials produced. While primarily fundamental information was gained during this study, it allowed some possible industrial implications of the co-precipitation to be determined. Understanding of the process has also provided possible measures that may be employed to both utilise the positive and minimise the negative aspects of the co-precipitates.

5.1. Influence of Silicates on Crystal Structure

5.1.1. Monomeric Silica

The XRD patterns presented in chapters two and three display a decrease in ferrihydrite crystallinity due to the presence of soluble silicates that had been well catalogued in the known literature. It has also been shown that elevating the silicate concentration increases the effect. However, little information had been previously offered as to why this occurs. Line profile analysis detailed in chapter two provides evidence that silicon is not incorporated into the ferrihydrite structure, a conclusion reinforced by the PDF analysis described in chapter four. As a consequence, such incorporation can now be ruled out as a potential cause of the alteration in crystallinity.

While some literature states that the difference between ferrihydrite samples of varying crystallinity is based on different crystal structures, there is certainly not a consensus. If structural differences were to be invoked then how would the presence of silicates alter the structure of the iron oxide phase? It has already been shown that the silicon is not incorporated into the ferrihydrite structure, therefore the silicon species would have to either increase the iron hydrolysis rate or somehow increase the tendency to form one structure over the other.

Similarities in the PDF results for ferrihydrite samples of varying crystallinity obtained by Michel et al. (Michel 2007) produced further evidence that no structural difference exists. The observed decline in the crystallinity correlated in general terms with decreases in the primary particle size, which represents a more likely cause. The PDF measurements described in this thesis also support this theory, showing a distinct difference in the size of the coherent scattering domains between samples of 6- and 2-line ferrihydrite. This would suggest that silicate retards the crystal growth of the primary particles. The PDF plots also display the fact that, other than the presence of silica (Si – O – Si bonding) and Si – O – Fe surface bonds in the co-

precipitates, the bonding environment remains the same; that is, silicate molecules are being adsorbed on the ferrihydrite primary particles.

It has previously been proposed that during both adsorption of silica on ferrihydrite and the co-precipitation of the species that Si – O – Fe bonding is the first association formed with silicate molecules. Where significant silicate concentrations remain, silica polymerisation then occurs across the surface of ferrihydrite particles once ferrihydrite surface binding sites are occupied (Doelsch 2001). It has been shown here that silicon is not structurally incorporated; along with significant changes in surface charge, surface area and a dependence of the amount of silica precipitated on the available ferrihydrite, this is indicative of surface adsorption during the co-precipitation process. This determination stands to reason, as adsorption is a faster process than silica polymerisation (Iler 1979).

Chapter two describes the ability of co-precipitated silica to retard the transformation of ferrihydrite into more crystalline phases, such as hematite. This phenomenon has again been well documented, but it has been shown here that this is due to surface binding of silica that inhibits the formation of hematite and goethite in precipitation experiments. The lack of such phases in all experiments containing predominantly soluble silicate in the feed (monosilicic acid as opposed to silica oligomers or particles) indicates that ferrihydrite-silica association is the cause.

The ability of silica to stabilise ferrihydrite against transformation in solution would also suggest a strong surface association. The predominant mechanism of ferrihydrite transformation in solution is via a dissolution / reprecipitation process, in which low molecular weight iron species are cleaved from the ferrihydrite surface, providing growth units for goethite (Cornell 1996). Stabilisation of ferrihydrite against dissolution by surface associated silica would impede such a process. Other proposed mechanisms of transformation involve reordering of the crystal structures of primary particles in ferrihydrite aggregates to eventually form a single crystal containing consistent long-range order. However, these mechanisms would also be inhibited by the presence of silicate molecules adsorbed on the surface of ferrihydrite primary particles.

The ability of silica to stabilise ferrihydrite against transformation is also shown to a lesser extent by the hedge-hog shaped schwertmannite particles obtained from sulfate experiments in chapter four. In the absence of silicate, the characteristic needles are relatively long and well formed, whereas when silicate is present the needles are shorter and less well defined. As it is proposed that the needles are comprised of goethite nanocrystals; it is likely that silicic acid adsorption and polymerisation is inhibiting the formation of these nanocrystals or aggregation to some degree.

Thus evidence has been obtained supporting the premise that the silicate species adsorbs on ferrihydrite primary particles once they have formed, retarding their further growth and inhibiting transformation into more crystalline material.

5.1.2. Polymerised Silica

Where polymerisation was induced in the feed solution, prior to co-precipitation, the silica level did not influence the ferrihydrite crystallinity or the presence of more crystalline phases (chapter three). Such observations can be explained by the inability of the silica oligomers or small particles to cover a significant number of the ferrihydrite surface sites. The remaining silicic acid in solution is not at a great enough concentration to bind to all sites across the ferrihydrite, allowing dissolution and therefore transformation to occur. As a consequence, the aggregates would likely be a mixture of silica and ferrihydrite particles, possibly with ferrihydrite forming on the surface of silica particles.

The plant conditions during hydrometallurgical zinc processing are conducive to silica polymerisation in the process liquors themselves, with low pH, extremely high ionic strength, and extended tank residence times. The results obtained here would then indicate that this is the reason that multiple iron oxide phases, including more crystalline material such as goethite, are observed in the residue, regardless of the silica concentration. It has also provided the basis for a proposed formation process in systems containing polymerised silica (Figure 5.1).

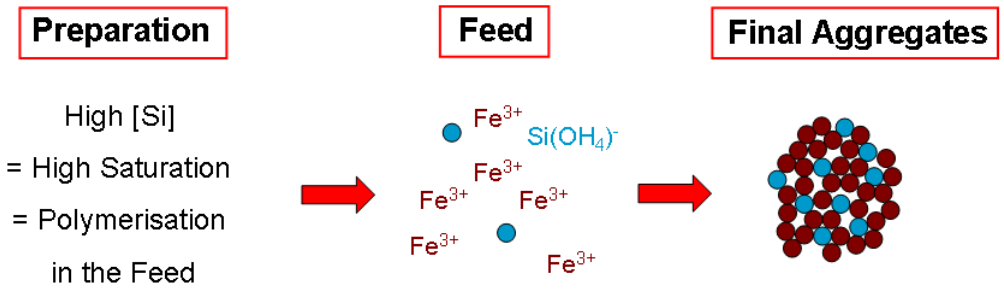

Figure 5.1: Diagram depicting a simplified process through which the co-precipitate forms where silica polymerisation has occurred in the feed solution.

The data presented in chapter three displays the implications of silica polymerisation in the feed solution. There is a much greater proportion of silica removed under these conditions and ferrihydrite is allowed to transform to more crystalline material. The separation properties are detrimentally influenced, the PSD falls along with the fractal dimension suggesting weaker, more open aggregates. There are also indications that the yield stress becomes a factor at lower solids concentrations.

5.2. Aggregate Composition

The assertion made by Hockridge et al. (Hockridge 2009) that schwertmannite is in fact a combination of ferrihydrite and goethite nanocrystals suggests that there is no sulfate inclusion in the structure, or at least not to a large enough extent to explain a large uptake of sulfate from solution. This would therefore suggest that the sulfate is surface adsorbed, which was confirmed in this study using EFTEM (chapter four).

This investigation has shown that the proportion of silica precipitated during co-precipitation is dependent on the ferrihydrite surface; the lower the available surface binding sites, the lower the silica precipitation. The inhibition of silica precipitation observed in sulfate media would thus indicate that sulfate is competitively adsorbed on the ferrihydrite surface. High ferrihydrite surface coverage by sulfate interrupts the adsorption of silicate units, which are then unable to polymerise as effectively across the ferrihydrite particle.

The EFTEM data has shown that in these co-precipitates the silica is predominantly associated with the aggregate surface. It would appear that the ferrihydrite particles initially form, with a small amount of silicate molecules then adsorbed, halting growth, but the rapid aggregation of these particles proceeds and further adsorption and silica polymerisation occurs on the surface of the aggregates (Figure 5.2). As the processes of ferrihydrite particle nucleation, silicate molecule adsorption and particle aggregation are all much faster reactions than silica polymerisation, it is logical that they should proceed in such a manner.

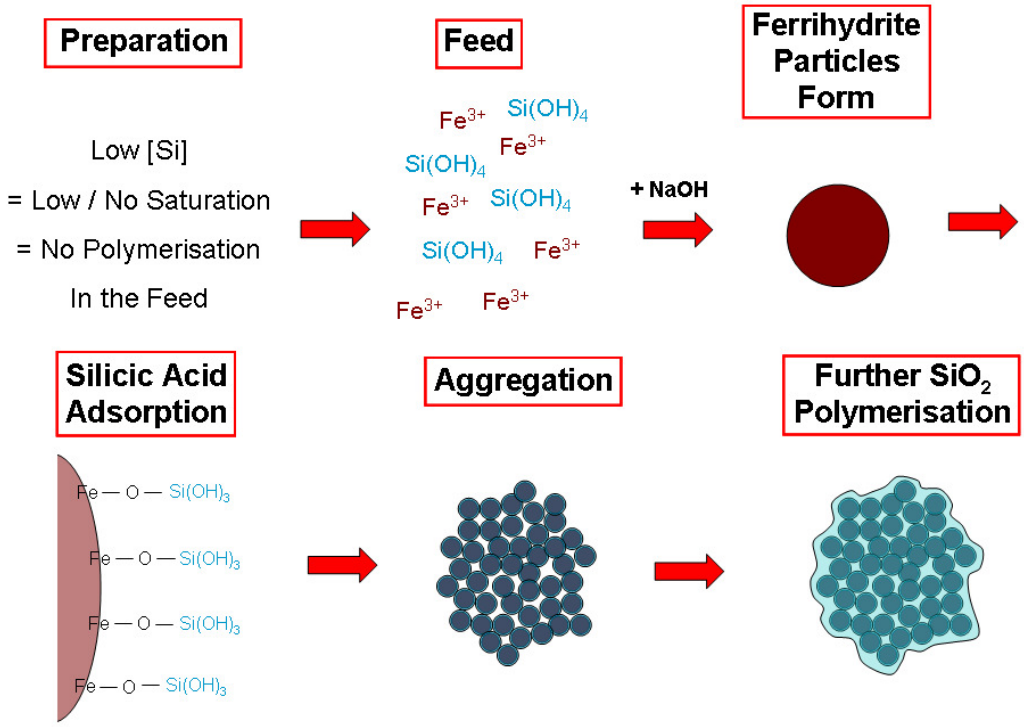

Figure 5.2: Diagram depicting a simplified process through which the co-precipitate forms from a solution containing monomeric silica (silicic acid).

5.3. Co-precipitate Characteristics

5.3.1. Surface Properties

Some key properties of these co-precipitate materials lie in their surface chemistry. This study has shown that the introduction of silicon to any of the systems producing ferrihydrite increases the surface area, which in turn increases the ability to adsorb soluble species from solution. Furthermore, the IEP is shifted to a lower pH by the inclusion of silica in aggregates. These results are further evidence supporting the formation process described in Figure 5.2, as only small amounts of Si are needed to significantly influence the surface properties of the aggregates. The decrease in IEP increases the affinity for adsorption of positively charged species and decreases the adsorption of anions.

This investigation has also shown that the adsorption of other anionic species have some influence on the surface charge. An example is the presence of sulfate, which contributes to a decrease in IEP due to its negative charge and strong binding to the ferrihydrite surface. This provides fundamental knowledge as a basis for work in the areas of synthesised adsorbents and soil science in which similar materials maintain the levels of ions in natural systems.

Specifically, in terms of the Paragoethite process, surface charge should not significantly impact upon the adsorption of anionic impurities. The reason for this is that much higher Si:Fe levels than exist in plant solutions would be required to decrease the IEP to the reaction pH. While in cases such as the removal of cationic impurities (e.g. lead) a decreased IEP would be constructive, it would also increase the affinity for the adsorption of zinc. This may have an impact on plant operations, as zinc is lost in the thickener, in which a slight increase in pH is observed. If the increase in pH is responsible, a lower iso-electric point would exacerbate the problem.

5.3.2. Aggregation Properties

One of the biggest concerns for the Paragoethite process is solid/liquid handling. Currently, the residue can be difficult to separate from liquors, as it often has poor settling properties and high water content. Fractal dimension values reported in this thesis have shown some interesting features. Where monosilicic acid alone was present in the feed, in nitrate and chloride media, there were small variations in the fractal dimension. An initial decrease was observed at low silicate levels (Si:Fe = 1:19) and slightly higher values than in the silica-free samples were obtained at higher ratios. A different trend was observed in the large-scale sulfate systems, with the high silica-content experiment, in which no polymerisation occurred before the reaction had a much lower fractal dimension than the silica-free sample.

The samples obtained from experiments in which polymerisation was induced prior to the precipitation showed a decreasing trend in fractal dimension with increasing silica content. A lower fractal dimension is indicative of poorly bound, open aggregates, which would tend to display poorer settling behaviour and contain large amounts of associated water. Such a trend may be due to the introduction of silica particles impeding the ferrihydrite aggregate formation and structure. However, in combining this with the value obtained from the LS-30-2 sample, it may suggest that the interaction between silicic acid or silica and the surface-adsorbed sulfate detrimentally affects aggregate formation.

Rheology measurements have brought two effects to light. The first is that an increase in the silica content in sulfate systems increases the associated shear stress of the settled residue at a fixed solids concentration. The other concerns the significant difficulty in increasing the solids concentration in preparation for rheology in some samples. Problems associated with these effects may have implications for the removal of solids from the Paragoethite slurry. Yield stress will probably not be a factor of concern in the process until thickening as the solids concentration will be relatively low. However, beyond this point it will impede handling and filtration, as will the associated difficulty in increasing solids concentration.

5.4. Summary

The mechanism of ferrihydrite / silica co-precipitation and aggregation described in Figure 5.2 was one of the major fundamental outcomes of this study. The understanding of the process by which the co-precipitates are formed allows predictions of reactions and precipitate behaviour to be made based on the conditions of a particular system and potentially the manipulation of operating conditions for a desired application. Associated properties such as surface chemistry and those related to aggregation can also be explained and even controlled to some degree. While of direct relevance to zinc hydrometallurgy and the Paragoethite process, conclusions of this study will aid research in fields such as the removal of iron and silicon from aqueous systems, soil science and water treatment.

Evidence has been provided towards a previous point of contention with regard to ferrihydrite and composites. The results obtained align with those of Michel et al. suggesting that there is no structural difference between 2-line and 6-line ferrihydrite, and that the observed change in crystallinity is dependent on the size of the coherent scattering domain (primary particle size). In addition, the propensity of the simultaneous polymerisation of silica to decrease ferrihydrite crystallinity is based on retarding particle growth.

While it is difficult to definitively determine whether silica will have significant impact on the Paragoethite, process suggestions as to possible impacts can be made. As mentioned earlier in this chapter, the plant conditions are likely to induce silica polymerisation in liquors prior to the PG precipitation step. The combination of the high levels of sulfate and silicate polymerisation will influence many facets of the process. Critically, the length of time that the silica spends in solution and the residue spends in slurry will maximise the amount of both iron and silica removed from solution, counteracting the interference of the sulfate.

While the surface charge shifts toward negative values, it is unlikely to alter the adsorption of the trace impurities but, may increase the amount of zinc adsorbed by the precipitate. The greatest effect would be observed from the slight increase in pH

and decrease in temperature in the thickener creating conditions that would be close to the IEP of the material.

Ideally, to remove such issues the reaction would be conducted in the presence of nitrate as opposed to sulfate, which is obviously unrealistic. Therefore, to minimise the effect of the polymerised silica, inducing maximum polymerisation and coagulation of silica particles and subsequent removal prior to liquor introduction to the precipitation vessel would solve several problems. However, this may also prove unrealistic in terms of capital and any processes would have to have minimal collateral impact on the liquor. Silica removed may also contain large levels of adsorbed zinc, then requiring recovery.

In terms of realistic possibilities, maintaining the reaction conditions to be as constant as possible will form a product that is most conducive to separation. There are competing considerations with regard to silica polymerisation in feed solutions. Where polymerisation occurs the silica precipitation is maximised, but there are associated declines in the fractal dimension and PSD, which result in poor settling and filtration properties. Conversely, the presence of monomeric silica during co-precipitation produces aggregates that will settle and filter more favourably, but reduces the proportion of silica precipitated. As seen in data obtained from samples produced in LS-20-1, it is possible to reach a compromise between high silica precipitation and less impact on aggregate properties. LS-20-1 samples did not contain more crystalline iron oxide phases, displayed a higher fractal dimension than any other system containing polymerised silica, and did not reach a significant yield stress until a solids concentration of 734 g L^{-1}, which are all positive outcomes. However, in steady-state samples from LS-20-1 the polymerisation of the silica occurred to a slightly lesser degree (57 % as opposed to >60 %) than that of LS-10-1 and LS-30-1, and there was no improvement to particle size. Therefore a control of the degree of silica polymerisation in feed liquors by varying the time spent in solution or silicate concentration may provide a suitable compromise of effects on co-precipitation.

REFERENCES

Adachi, Y., Kobayashi, M., Ooi, S. (1998). "Applicability of fractals to the analysis of the projection of small aggregates." Journal of Colloid and Interface Science **208**: 353-355.

Ahn, P., Ahn, C. C. (2004). Transmission electron energy loss spectrometry in materials science and the EELS atlas. Weinheim, Germany, John Wiley and Sons.

Alexander, G. B., Heston, W. M., Iler, R. K. (1953). "The solubility of amorphous silica in water." **58**: 453-455.

Allen, L. H., Matijevic, E. (1970). "Stability of colloidal silica III. Effect of hydrolyzable cations." Journal of Colloid and Interface Science **35**(1): 66-76.

Alloyeau, D., Ricolleau, C., Oikawa, T., Langlois, C., Le Bouar, Y., Loiseau, A. (2009). "Comparing electron tomography and HRTEM slicing methods as tools to measure the thickness of nanoparticles." Ultramicroscopy **109**: 788-796.

Amal, R., Raper, J. A., Waite, T. D. (1990). "Fractal structure of hematite aggregates." Journal of Colloid and Interface Science **140**(1): 158-168.

Anderson, P. R., Benjamin, M. M. (1985). "Effects of silicon on the crystallisation and adsorption properties of ferric oxides." Environmental Science and Technology **19**(11): 1048-1053.

Armstrong, R. D., Bell, M. F. (1976). "The effect of silicate ion addition on the dissolution of zinc in alkaline solution." Electrochimica Acta **21**(2): 155-156.

Arregui, V., Gordon, A. R., Steintveit, G. (1979). "Jarosite process - past, present and future." Journal of Metals **31**(12): 22.

Bagnall, C. M., Howarth, L. G., James, P. F. (1990). "Modelling of aggregation kinetic of colloidal silica particles." Journal of Non-Crystalline Solids **121**(1): 56-60.

Balas, F., Rodriguez-Delgado, M., Otero-Arean, C., Conde, F., Matesanz, E., Esquivias, L., Ramirez-Castellanos, J., Gonzalez-Calbet, J., Vallet-Regi, M. (2007). "Structural characterisation of nanosized silica spheres." Solid State Sciences **9**: 351-356.

Berthoud, A. (1912). "Theorie de la formation des faces d'un crystal." Journal de Chimie Physique et de Physico-Chimie Biologique **10**: 624.

Bigham, J. M., Carlson, L., Murad, E. (1994). "Schwertmannite, a new iron oxyhydroxy-sulphate from Pyhasalmi, Finland, and other localities." Mineralogical Magazine **58**(4): 641-648.

Blesa, M. A., Matijevich, E. (1989). "Phase transformation of iron oxides, oxyhydroxides, and hydrous oxides in aqueous media." Advances in Colloid and Interface Science **29**: 173-221.

Bodas, M. G. (1996). "Hydrometallurgical treatment of zinc silicate ore from Thailand." Hydrometallurgy **40**(1-2): 37-49.

Bogush, G. H., Zukoski, C. F. (1991). "Uniform silica particle precipitation: An aggregate growth model " Journal of Colloid and Interface Science **142**(1): 19-34.

Boudier, T., Lechaire, J. P., Frebourg, G., Messoudi, C., Mory, C., Colliex, C., Gaill, F., Marco, S. (2005). "A public software for energy filtered transmission electron tomography (EFTET-J): Application to the study of granular inclusionsin bacteria from Riftia pachyptila." Journal of Structural Biology **151**: 151-159.

Bouguerra, W., Ben Sik Ali, M., Hamrouni, B., Dhahbi, M. (2007). "Equilibrium and kinetic studies of adsorption of silica on to activated alumina." Desalination **206**: 141-146.

Brady, G. W., Kurkjian, C. R., Lyden, E. F. X., Robin, M. B., Saltman, P., Spiro, T., Terzis, A. (1968). "The structure of an iron core analog of ferritin." Biochemistry **7**: 2185-2192.

Buckley, H. E. (1952). Crystal Growth. London, Chapman and Hall.

Buekers, J., Amery, F., Maes, A., Smolders, E. (2008). "Long-term reactions of Ni, Zn and Cd with iron oxyhydroxides depend on crystallinity and structure and on metal concentrations." European Journal of Soil Science **59**: 706-715.

Campbell, A. S., Schwertmann, U., Stanjek, H., Friedl, J., Kyek, A., Campbell, P.A. (2002). "Si incorporation into hematite by heating Si-ferrihydrite." Langmuir **18**: 7804-7809.

Cannas, C., Musinu, A., Navarra, G., Piccaluga, G. (2004). "Structural investigation of Fe2O3-SiO2 nanocomposites through radial distribution functions analysis." Physical Chemistry Chemical Physics **6**(13): 3530-3534.

Carlson, L., Schwertmann, U. (1981). "Natural ferrihydrites in surface deposits from Finland and their association with silica." Geochimica et Cosmochimica Acta **45**: 421-429.

Carlson, L., Schwertmann, U. (1987). "Iron and manganese oxides in finnish ground water treatment plants." Water Research **25**(2): 165-170.

Chang, S. M., Lee, M., Kim, W. S. (2005). "Preparation of large mondispersed spherical silica particles using seed particle growth." Journal of Colloid and Interface Science **286**: 536-542.

Chatellier, X., West, M. M., Rose, J., Fortin, D., Leppard, G. G., Ferris, F. G. (2004). "Characterisation of iron oxides formed by oxidation ferrous ions in the presence of

various bacterial species and inorganic ligands." Geomicrobiology Journal **21**: 99 - 112.

Cheary, R. W., Coelho, A. A. (1996). Programs XFIT and FOURIYA, deposited in CCP14 powder diffraction library. Engineering and Physical Sciences Research Council, Daresbury Laboratory, Warrington, England.

Chen, C.-T. A., Marshall, W. L. (1982). "Amorphous silica solubilities IV. Behaviour in pure water and aqueous sodium chloride, sodium sulfate, magnesium chloride, magnesium sulfate solutions up to 350^{o}C." Geochimica et Cosmochimica Acta **46**: 279-287.

Cheng, J., Ni, X., Zheng, H., Li, B., Zhang, X., Zhang, D. (2006). "Preparation of Fe (core)/ SiO2 (shell) composite particles with improved oxidation-resistance." Materials Research Bulletin **41**: 1424-1429.

Chukin, G. D., Malevich, V. I. (1977). "Infrared spectra of silica." Journal of Applied Spectroscopy **26**(2): 223-229.

Chupas, P. J., Qui, X., Hanson, J. C., Lee, P. L., Grey, C. P., Billinge, S. J. L. (2003). "Rapid-aquisition pair distribution function (RA-PDF) analysis." Journal of Applied Crystallography **36**: 1342-1347.

Claassen, J. O., Meyer, E. H. O., Rennie, J., Sadenburgh, R. F. (2002). "Iron precipitation from zinc rich solutions: defining the Zincor Process." Hydrometallurgy **67**(1-3): 87-108.

Claassen, J. O., Sandenbergh, R. F. (2007). "Influence of mixing on the quality of iron precipitates in zinc-rich solutions." Hydrometallurgy **87**: 112-123.

Claassen, J. O., Sandenbergh, R. F. (2007). "Influence of temperature and pH on the quality of metastable iron phases produced in zinc-rich solutions." Hydrometallurgy **86**: 178-190.

Clark, A., Eberhardt, C. (2002). Microscopy techniques for materials science. Boca Raton, CRC Press/Worldwide Publications.

Combes, J. M., Manceau, A., Calas, G., Bottero, J. Y. (1989). "Formation of ferric oxides from aqueous solutions: A polyhedral approach by X-ray adsorption spectroscopy: I. Hydrolysis and formation of ferric gels." Geochimica et Cosmochimica Acta **53**: 583-594.

Cooper, R. M. G. (1998). Silica precipitation from electrolytic zinc solutions. Applied Chemistry. Perth, Western Australia, Curtin University of Technology.

Cornell, R. M., Schwertmann, U. (1996). The Iron Oxides: Structure, Properties, Reactions, Occurrence and Uses. Weinheim, VCH.

Davis, C. C., Chen, H-W., Edwards, M. (2002). "Modelling silica sorption to iron hydoxide." Environmental Science and Technology **36**: 582-587.

Davis, J. A., Leckie, J. O. (1978). "Surface ionisation and complexation at the oxide/water interface: II. Surface properties of amorphous iron oxyhydroxide and adsorption of metal ions." Journal of Colloid and Interface Science **67**(1): 90-107.

Dietzel, M. (2000). "Dissolution of silicates and the stability of polysilicic acid." Geochimica et Cosmochimica Acta **64**(19): 3275-3281.

Doelsch, E., Rose, J., Masion, A., Bottero, J. Y., Nahon, D., Bertsch, P. M. (2000). "Speciation and crystal chemistry of iron(III) chloride hydrolysed in the presence of SiO4 ligands .1. An Fe K-edge EXAFS study." Langmuir **16**: 4726-4731.

Doelsch, E., Stone, W. E. E., Petit, S., Masion, A., Rose, J., Bottero, J. Y., Nahon, D. (2001). "Speciation and crystal chemistry of iron(III) chloride hydrolysed in the presence of SiO4 ligands .2. Characterisation of Fe-Si aggregates by FTIR and 29Si Solid State NMR." Langmuir **17**: 1399-1405.

Drits, V. A., Sakharov, B. A., Salyn, A. L., Manceau, A. (1993). "Structural model for ferrihydrite." Clay Minerals **28**: 185-207.

Dutrizac, J. E. (1987). An overview of iron precipitation in hydrometallurgy. International Symposium of Crystallisation and Precipitation, Saskatoon, Saskatchewan, Canada, Pergamon Press.

Dyer, J. A., Trivedi, P., Scrivner, N.C., Sparks, D.L. (2004). "Surface complexation modelling of zinc sorption onto ferrihydrite." Journal of Colloid and Interface Science **270**: 56-65.

Edwards, G. R., Evans, L. F. (1962). "Effective surface charge on ice nucleation by AgI." Transactions of the Faraday Society **58**(1649).

Eggleton, R. A., Fitzpatrick, R. W. (1988). "New data and a revised structural model for ferrihydrite." Clays and Clay Minerals **36**(2): 111-124.

El-Ammouri, E. G., Distin, P. A., Lempka, B. M.-A., Hagens, R. G. (1997). Method for the removal of metals from solution by means of activated silica. U. S. Patents. Canada, McGill University.

Farrow, J. B., Swift, J. D. (1991). Improving thickener technology. 5th AusIMM Conference on Extractive Metallurgy. Perth, AusIMM**:** 227-232.

Fawell, P. D., Owen, A. T., Grabsch, A. F., Benn, F. A., Labbett, D. M., Swift, J. D. (2009). Factors affecting flocculation within gravity thickeners. Water in Mining, Perth, Western Australia, The Australian Institute of Mining and Metallurgy.

Flynn Jr., C. M. (1984). "Hydrolysis of inorganic iron(III) salts." Chemical Reviews **84**: 31-41.

Franks, G. V., Zhou, Y., Yan, Y-d., Jameson, G. J., Biggs, S. (2004). "Effect of aggregate size on sediment rheological properties." Physical Chemistry Chemical Physics **6**: 4490-4498.

Gallup, D. L. (1997). Inhibition of silicate scale formation. U. S. Patents. United States, Union Oil Company of California**:** 242.

Gibbs, J. W. (1928). Collected Works. London, Longmans Green.

Glasauer, S., Friedl, J., Schwertmann, U. (1999). "Properties of goethites prepared under acidic and basic conditions in the presence of silicate." Journal of Colloid and Interface Science **216**: 106-115.

Glasauer, S. M., Hug, P., Weidler, P. G., Gehring, A. U. (2000). "Inhibition of sintering by Si during the conversion of Si-rich ferrihydrite to hematite." Clays and Clay Minerals **48**(1): 51-56.

Gun'ko, V. M., Mironyuk, I. F., Voronin, E. F., Turov, V. V., Pakhlov, E. M., Goncharuk, E. V., Nychiporuk, Y. M., Vlasova, N. N., Gorbik, P. P., Mishchuk, O. A., Chuiko, A. A., Kulik, T. V., Palyanytsya, B. B., Pakhovchishin, S. V., Skubiszewska-Zieba, J., Janusz, W., Turov, A. V., Leboda, R. (2005). "Morphology and surface properties of fumed silica." Journal of Colloid and Interface Science **289**: 427-445.

Hammersley, A. P., Svensson, S. O., Hanfland, M., Fitch, A. N., Hausermann, D. (1996). "Two-dimensional detector software: From real dectector to idealised image or two-theta scan." High Pressure Research **14**: 235-248.

Han, Y.-S., Jeong, G-Y., Lee, S-Y., Kim, H-K. (2007). "Hematite template route to hollow-type silica spheres." Journal of Solid State Chemistry **180**: 2978-2985.

Hanna, R. (1965). "Infrared absorption spectrum of silicon dioxide." Journal of The American Ceramic Society **48**(11): 595-599.

Herbillon, A. J., Tran Vinh An, J. (1969). "Heterogeneity in silica-iron mixed hydroxides." Journal of Soil Science **20**(2): 223-235.

Hernandez, A. V., Torchynska, T. V., Vazquez, A. L. Q., Matsumoto, Y., Khomenkova, L., Shcherbina, L. (2007). "Emission and structure investigations of Si non-crystals imbedded in amorphous silicon." Journal of Physics: Conference Series **61**: 1231-1235.

Hiemstra, T., Van Riemsdijk, W. H. (2009). "A surface structural model for ferrihydrite I: Sites related to primary charge, molar mass, and mass density." Geochimica et Cosmochimica Acta **73**: 4423-4436.

Hildebrand, J. H., Scott, R. L. (1950). Solubility of non-electrolytes. New York, Reinhold.

Hingston, F. J., Raupach, M. (1967). "The reaction between monosilicic acid and aluminium hydroxide I. The kinetics of adsorption of silicic acid by aluminium hydroxide." Australian Journal of Soil Research **5**: 295-309.

Hlavay, J., Jonas, K., Elek, S., Inczedy, J. (1977). "Characterisation of the particle size and crystallinity of certain minerals by infrared spectrophotometry and other instrumental methods - I. Investigations on clay minerals." Clays and Clay Minerals **25**: 451-456.

Hockridge, J., Jones, F., Loan, M., Richmond, W. R. (2009). "An electron microscopy study of the crystal growth of schwertmannite needles through the oriented aggregation of goethite nanocrystals." Journal of Crystal Growth **311**: 3876-3882.

Hong, R. Y., Fu, H. P., Di, G. Q., Zheng, Y., Wei, D. G. (2007). "Facile route to gamma-Fe2O3/SiO2 nanocomposite used as a precursor of magnetic fluid." Materials Chemistry and Physics.

Icopini, G. A., Brantley, S. L., Heaney, P. J. (2005). "Kinetics of silica oligomerisation and nanocolloid formation as a function of pH and ionic strength at 25^{o}C." Geochimica et Cosmochimica Acta **69**(2): 293-303.

Iler, R. K. (1979). The Chemistry of Silica: Solubility, Polymerisation, Colloid and Surface Properties, and Biochemistry. New York, John Wiley & Sons.

Jambor, J. L., Dutrizac, J. E. (1998). "Occurrence and constitution of natural and synthetic ferrihydrite, a widespread oxyhydroxide." Chemical Reviews **98**(7): 2549-2585.

James, R. O., Healy, T. W. (1972). "Adsorption of hydrolyzable metal ions at the oxide-water interface. II. Charge reversal of SiO2 and TiO2 colloids by adsorbed Co(II), La(III), and Th(IV) as model systems." Journal of Colloid and Interface Science **40**(1): 53-64.

Janney , D. E., Cornell, R. M., Buseck, P. R. (2000). "Structure of synthetic 2-line ferrihydrite by electron nanodiffraction." American Mineralogist **85**: 1180-1187.

Janney , D. E., Cornell, R. M., Buseck, P. R. (2000). "Transmission electron microscopy of synthetic 2- and 6-line ferrihydrite." Clays and Clay Minerals **48**(1): 111-119.

Janney , D. E., Cornell, R. M., Buseck, P. R. (2001). "Structure of synthetic 6-line ferrihydrite by electron nanodiffraction." American Mineralogist **86**: 327-385.

Jansen, E., Kyek, A., Schafer, W., Schwertmann, U. (2002). "The structure of six-line ferrihydrite." Applied Physics A. Materials Science and Processing **74s**: s1004-s1006.

Janusz, W., Patkowski, J., Chibowski, S. (2003). "Competetive adsorption of Ca^{2+} and Zn(II) ions at monodispersed SiO_2/electrolyte solution interface." Journal of Colloid and Interface Science **266**: 259-268.

Jarvis, P., Parsons, S. A., Henderson, R., Nixson, N., Jefferson, B. (2008). "The practical application of fractal dimensionin water treatment practice - the impact of polymer dosing." Seperation Science and Technology **43**: 1785-1797.

Jones, A. M., Collins, R. M., Rose, J., Waite, T. D. (2009). "The effect of silica and natural organic matter on the Fe(II)-catalysed transformation and reactivity of Fe(II) minerals." Geochimica et Cosmochimica Acta **73**: 4409-4422.

Jullien, R., Botet, R. (1987). Aggregation and fractal aggregates. Singapore, World Scientific Publishing.

Kauffman, K., Hazel, F. (1975). "Infrared and Mossbauer spectroscopy, electron microscopy and chemical reactivity of ferric chloride hydrolysis products." Journal of Inorganic and Nuclear Chemistry **37**: 1139-1148.

Ke, X., Bals, S., Cott, D., Hantschel, T., Bender, H., Van Tendeloo, G. (2010). "Three-dimensional analysis of carbon nanotubenetworks in interconnects by electron tomography without missing artifacts." Microscopy and Microanalysis **16**: 210-217.

Kershaw, M. G. (1995). "Modernisation of the leaching circuit at pasminco metals - EZ." Hydrometallurgy **39**(1-3): 129-145.

Khare, V., Mullet, M., Hanna, K., Blumers, M.,Abdelmoula, M., Klingelhofer, G., Ruby, C. (2008). "Comparative studies of ferric green rust and ferrihydrite coated sand: Roles of synthesis routes." Solid State Sciences **10**: 1342-1351.

Kim, S. S., Kim, H. S., Kim, S. G., Kim, W. S. (2004). "Effect of electrolyte additives on sol-precipitated nano silica particles." Ceramics International **30**: 171-175.

Kinniburgh, D. G., Syers, J. K., Jackson, M. L. (1975). "Specific adsorption of trace amounts of calcium and strontium by hydrous oxides of iron and aluminium." Soil Science Society of America Journal **39**(3): 464-470.

Kinrade, S. D., Pole, D. L. (1992). "Effect of alkali-metal cations on the chemistry of aqueous silicate solutions." Inorganic Chemistry **31**(22): 4558-4563.

Kodaira, K., Ito, S., Matsushita, T. (1975). "Hydrothermal growth of willemite single crystals in acidic solutions." Journal of Crystal Growth **29**: 123-124.

Kosmulski, M. (2002). "The pH-dependent surface charging and the points of zero charge." Journal of Colloid and Interface Science **253**: 77-87.

Kosmulski, M. (2003). "A literature review of the differences between the reported isoelectric points and their discussion." Colloids and Surfaces A: Physiochemical and Engineering Aspects **222**: 113-118.

Kozawa, A. (1961). "Ion-exchange adsorption of zinc and copper ions on silica." Journal of Inorganic and Nuclear Chemistry **21**: 315-324.

Krauskopf, K. B. (1956). "Dissolution and precipitation of silica at low temperatures." Geochimica et Cosmochimica Acta **10**: 1-26.

Lamb, H. (1994). Hydrodynamics 6th Edition, Cambridge University Press.

Lewin, S. (1960). The solubility product principle. London, Pitman.

Lewis, D. G., Cardile, C. M. (1989). "Hydrolysis of Fe^{III} solution to hydrous iron oxides." Australian Journal of Soil Research **27**(1): 103-115.

Liu, G., Debnath, S., Paul, K. W., Han, W., Hausner, D. B., Hosein, H. A., Michel, F. M., Parise, J. B., Sparks, D. L., Strongin, D. R. (2006). "Characterisation and surface reactivity of ferrihydrite nanoparticles assembled in ferritin." Langmuir **22**(22): 9313-9321.

Loan, M. (2004). The paragoethite process: Fundamentals of ferrihydrite, schwertmannite and goethite precipitation. Applied Chemistry. Perth, Western Australia, Curtin University of Technology.

Loan, M., Crowley, J. M., Hart, R., Parkinson, G. M. (2004). "Evidence on the structure of synthetic schwertmannite." American Mineralogist **89**: 1735-1742.

Loan, M., Newman, O. M. G., Cooper, R. M. G., Farrow, J. B., Parkinson, G. M. (2006). "Defining the paragoethite process for iron removal in zinc hydrometallurgy." Hydrometallurgy **81**(2): 104-129.

Loan, M., Newman, O. M. G., Farrow, J. B., Parkinson, G. M. (2006). "Continuous reactive crystallisation of nanoscale six-line ferrihydrite." Crystal Growth and Design **6**(1): 79-86.

Loan, M., Parkinson, G. M., Richmond, W. R. (2005). "The effect of zinc sulfide on the phase transformations of ferrihydrite." American Mineralogist **90**: 258-261.

Loan, M., Richmond, W. R., Parkinson, G. M. (2005). "On the crystal growth of nanoscale schwertmannite." Journal of Crystal Growth **275**: e1875-e1881.

Loan, M., St. Pierre, T. G., Parkinson, G. M., Newman, O. M. G., Farrow, J. B. (2002). "Identifying nanoscale ferrihydrite in hydrometallurgical residues." Fine Particle Characterisation **54**(12): 40-43.

Luxton, T. P., Eick, M. J., Rimstidt, D. J. (2008). "The role of silicate in the adsorption/desorption of arsenite on goethite." Chemical Geology **252**: 125-135.

Manceau, A. (2009). "Evaluation of the structural model for ferrihydrite derived from real-space modelling of high-energy X-ray diffraction data." Clay Minerals **44**: 19-34.

Manceau, A., Combes, J. M., Calas, G (1990). "New data and a revised structural model for ferrihyrite: Comment." Clays and Clay Minerals **38**(3): 331-334.

Manceau, A., Marcus, M. A., Tamura, N., Proux, O., Geoffroy, N., Lanson, M. (2004). "Natural speciation of Zn at the micrometer scale in a clayey soil using X-ray flourescence, adsorption and diffraction." Geochimica et Cosmochimica Acta **68**(11): 2467-2483.

Marshall, W. L. (1980). "Amorphous silica solubilities I. Behaviour in aqueous sodium nitrate solutions: 25-350^{o}C, 1-6molal." Geochimica et Cosmochimica Acta **44**: 907-913.

Marshall, W. L., Chen, C-T. A. (1982). "Amorphous silica solubilities VI. postulated sulfate silicic acid solution complex." Geochimica et Cosmochimica Acta **46**: 367-370.

Marshall, W. L., Warakomski, J. M. (1980). "Amorphous silica solubilities II. Affect of salt solutions at 25^{o}C." Geochimica et Cosmochimica Acta **44**: 915-924.

Martin, S., Zhu, C., Rule, J., Nuhfer, N. T., Ford, R., Hedges, S., Soong, Y. (2005). "A high-resolution TEM-AEM, pH titration, and modelling study of Zn^{2+} coprecipitation with ferrihydrite." Geochimica et Cosmochimica Acta **69**(6): 1543-1553.

Martinez, C. E., McBride, M. B. (1998). "Solubility of Cd^{2+}, Cu^{2+}, Pb^{2+} and Zn^{2+} in aged coprecipitates with amorphous iron hydroxides." Environmental Science and Technology **32**(6): 743-748.

Masion, A., Doelsch, E., Rose, J., Moustier, S., Bottero, J. Y., Bertsch, P. M. (2001). "Speciation and crystal chemistry of iron(III) chloride hydrolysed in the presence of SiO4 ligands. 3. Semilocal scale structure of the aggregates." Langmuir **17**: 4753-4757.

Mason, B. J. (1957). The physics of clouds. Oxford, Clarendon.

Matjie, R. H., Engelbrecht, R. (2007). "Selective removal of dissolved silicon and aluminium ions from gas liquor by hydrometallurgical methods." Hydrometallurgy **85**: 172-182.

Mayer, T. D., Jarrell, W. M. (1996). "Formation and stability of iron(II) oxidation products under natural concentrations of dissolved silica." Water Research **30**(5): 1208-1214.

Mazzetti, L., Thistlethwaite, P. J. (2002). "Raman spectra and thermal transformations of ferrihydrite and schwertmannite." Journal of Raman Spectroscopy **33**: 104-111.

Meakin, P. (1988). "Fractal Aggregates." Advances in Colloid and Interface Science **28**: 249-331.

Michel, F. M. (2007). "The structure of ferrihydrite, a nanocrystalline material." Science **316**: 1726.

Michel, F. M., Ehm, L., Liu, G., Han, W. Q., Antao, S. M., Chupas, P. J., Lee, P. L., Knorr, K., Eulert, H., Kim, J., Grey, C. P., Celestian, A. J., Gillow, J., Schoonen, M. A. A., Strongin, D. R., Parise, J. B. (2007). "Similarities in 2- and 6-line ferrihydrite based on pair distribution function analysis of x-ray total scattering." Chemistry of Materials **19**(6): 1489-1496.

Miers, H. A. (1927). "The growth of crystals from supersaturated liquids." Journal of the Institute of Metals **37**: 331.

Mirnezami, M., Restrspo, L., Finch, J. A. (2003). "Aggregation of sphalerite: role of zinc ions." Journal of Colloid and Interface Science **259**: 36-42.

Miyazake, A., Yokoyama, T. (1999). "Effects of anions on local structure of Al and Si in aluminosilicates." Journal of Colloid and Interface Science **214**: 395-399.

Morioka, T., Kimura, K., Tsuda, N., Kaito, C., Saito, Y., Koike, C. (1998). "Study of the structure of silica film by infrared spectroscopyand electron diffraction analysis." Monthly Notices of the Royal Astronomical Society **299**: 78-82.

Mullin, J. W. (1972). Crystallisation. Oxford, U.K., Butterworth-Heinemann.

Mullin, J. W. (1993). Crystallization. Oxford, U.K., Butterworth-Heinemann.

Mustafa, S., Dilara, B., Nargis, K., Naeem, A., Shahida, P. (2002). "Surface properties of the mixed oxides of iron and silica." Colloids and Surfaces A: Physiochemical and Engineering Aspects **205**: 273-282.

Namasivayam, C., Prathap, K. (2007). "Adsorptive removal of silica onto 'waste' Fe(III)/Cr(III) hydroxide: Kinetics and isotherms." Colloids and Surfaces A: Physiochemical and Engineering Aspects **295**: 55-60.

Natesaiyer, K. C., Hover, K. C. (1992). "Chemical reagents for reducing the solubility of silica in 1N sodium hydroxide." Cement and Concrete Research **22**: 653-662.

Nesterova, M., Moreau, J., Banfield, J. F. (2003). "Model biomimetic studies of templated growth and assembly of nanocrystalline FeOOH." Geochimica et Cosmochimica Acta **67**(6): 1177-1187.

Noyes, A. A., Whitney, W. R. (1897). "Rate of solution of solid substances in their own solution." Journal of the American Chemical Society **19**: 930.

Ocana, M., Andres-Verges, M., Pozas, R., Serna, C. J. (2006). "Spherical iron-silica nanocomposites from core-shell particles." Journal of Colloid and Interface Science **294**: 355-361.

Ochs, H., Bublak, D., Wild, U., Muhler, M., Kolbesen, B. O. (1998). "Depth distribution of zinc adsrobed on silicon surfaces out of aqueous alkaline solutions." Applied Surface Science **133**: 73-83.

Okada, K., Otsuka, N. (1986). "Characterisation of the spinel phase from SiO_2-Al_2O_3 xerogels and the formation process of mullite." Journal of The American Ceramic Society **69**(9): 652-656.

Okuda, M., Takeguchi, M., O Ruairc, O., Tagaya, M., Zhu, Y., Hashimoto, A., Hanagata, N., Schmitt, W., Ikoma, T. (2010). "Structural analysis of hydroxyapatite coating on magnatite nanoparticlesusing energy filtered imaging and electron tomography." Journal of Electron Microscopy **59**(2): 173-179.

Pankhurst, Q. A., Pollard, R. J. (1992). "Structural and magnetic properties of ferrihydrite." Clays and Clay Minerals **40**(3): 268-272.

Parks, G. A. (1967). Equilibrium concepts in natural water systems. Advances in Chemistry. Stanford, American Chemical Society. **67:** 121-160.

Pauling, L. (1929). "The principles determining the structure of complex ionic crystals." Journal of the American Chemical Society **51**(4): 1010-1026.

Phan, T. N. T., Louvard, N., Bachiri, S.-A., Persello, J., Foissy, A. (2004). "Adsorption of zinc on colloidal silica, triple layer modellisation and aggregation data." Colloids and Surfaces **244**: 131-140.

Pokrovski, G. S., Schott, J., Farges, F., Hazemann, J-L. (2003). "Iron (III)-silica interactions in aqueous solution: insights from X-ray adsorption fine structure spectroscopy." Geochimica et Cosmochimica Acta **67**(19): 3559-3573.

Porcu, M., Orru, R., Cao, G. (2004). "On the use of industrial scraps for the treatment of zinc hydrometallurgical wastes by self-propagating reactions." Chemical Engineering Journal **99**(3): 247-256.

Prado, A. G. S., Miranda, B. S., Zara, L. F. (2005). "Adsorption and thermochemical data of divalent cations onto silica gel surface modified with humic acid at solid/liquid interface." Journal of Hazardous Materials **B120**: 243-247.

Predoi, D., Crisan, O., Jitianu, A., Valsangiacom, M. C., Raileanu, M., Crisan, M., Zaharescu, M. (2007). "Iron oxide in a silica matrix prepared by the sol-gel method." Thin Solid Films **515**: 6319-6323.

Queneua, P. B., Berthold, C. E. (1985). Silica in hydrometallurgy: An overview. Impurity Control and Disposal. Vancouver, Canada, CIM Metallurgical Society.

Qui, X., Billinge, S. J. L. (2004). PDFGetX2 Manual, Department of Physics and Astronomy, Michigan State University, Michigan, U.S.A.

Qui, X., Thompson, J. W., Billinge, S. J. L. (2004). PDFGetX2: A GUI driven program to obtain the pair distribution data from X-ray powder diffraction data.

Rancourt, D. G., Meunier, J.-F. (2008). "Constraints on structural models of ferrihydrite as a nanocrystalline material." American Mineralogist **93**: 1412-1417.

Rashchi, F., Xu, Z., Finch, J. A. (1998). "Adsorption of silica in Pb- and Ca-SO_4-CO_3 systems." Colloids and Surfaces **132**: 159-171.

Reardon, E. J. (1979). "Complexing of silica by iron(III) in natural waters." Chemical Geology **25**: 339-345.

Richmond, W., Loan, M., Morton, J., Parkinson, G. M. (2004). "Arsenic removal from aqueous solution via ferrihydrite crystallisation control." Environmental Science and Technology **38**(12): 2368-2372.

Richmond, W. R., Loan, M., Newman, O. M. G., Parkinson, G. M. (2005). "Zinc sulfide as a solid phase additive for improving the processing characteristics of ferrihydrite residues." Hydrometallurgy **78**(1-2): 172-179.

Rimstidt, J. D., Barnes, H. L. (1980). "The kinetics of silica-water reactions." Geochimica et Cosmochimica Acta **44**: 1683-1699.

Rivera-Rubero, S., Baldelli, S. (2004). "Influence of water on the surface of hydrophilic and hydrophobic room-temperature ionic liquids." Journal of the American Chemical Society **126**(38): 11788-11789.

Roberts, D. R., Ford, R. G., Sparks, D. L. (2003). "Kinetics and mechanisms of Zn complexationon metal oxides using EXAFS spectroscopy." Journal of Colloid and Interface Science **263**: 364-376.

Rose, J., Manceau, A., Masion, A., Bottero, J.-Y. (1997). "Structure and mechanisms of formation of FeOOH(NO_3) oligomers in the early stages of hydrolysis." Langmuir **13**: 3240-3246.

Sartoratto, P. P. C., Caiado, K. L., Pedroza, R. C., da Silva, S. W., Morais, P. C. (2007). "The thermal stability of maghemite-silica nanocompsites: An investigation using X-ray diffraction and Raman spectroscopy." Journal of Alloys and Compounds **434-435**: 650-654.

Schaer, E., Ravetti, R., Plasari, E. (2001). "Study of silica particle aggregation in a batch agitated vessel." Chemical Engineering and Processing **40**(3): 277-293.

Schlomach, J., Kind, M. (2004). "Investigation on the semi-batch precipitation of silica." Journal of Colloid and Interface Science **277**: 316-326.

Schwartz, C. H., Ulery, A. L., Gschwend, P. M. (1997). "An AEM-TEM study of nanometer-scale mineral associations in an aquifer sand: Implications for colloid mobilization." Geochimica et Cosmochimica Acta **61**(4): 707-718.

Schwertmann, U. (1982). "The point of zero charge of natural and synthetic ferrihydrites and its relation to adsorbed silicate." Clay Minerals **17**: 471-476.

Schwertmann, U., Cornell, R. M. (2000). Iron Oxides in the Laboratory: Preparation and Characterisation. Weinheim, Wiley-VCH.

Schwertmann, U., Friedl, J., Kyek, A. (2004). "Formation and properties of a continuous crystallinity series of synthetic ferrihydrites (2- to 6-line) and their relation to FeOOH forms." Clays and Clay Minerals **52**(2): 221-226.

Schwertmann, U., Friedl, J., Pfab, G. (1996). "A new iron(III) oxyhydroxynitrate." Journal of Solid State Chemistry **126**(2): 336.

Schwertmann, U., Friedl, J., Stanjek, H. (1999). "From Fe(III) ions to ferrihydrite and then to hematite." Journal of Colloid and Interface Science **209**: 215-223.

Schwertmann, U., Wagner, F., Knicker, H. (2005). "Ferrihydrite-humic associations: Magnetic hyperfine interactions." Soil Science Society of America Journal **69**(4): 1009-1015.

Scott, J. P., Fawell, P. D., Ralph, D. E., Farrow, J. B. (1996). "The shear degradation of high-molecular-weight flocculant solutions." Journal of Applied Polymer Science **62**: 2097-2106.

Seehra, M. S., Roy, P., Raman, A., Manivannan, A. (2004). "Structural investigations of synthetic ferrihydrite nanoparticles doped with silica." Solid State Communications **130**: 597-601.

Selomulya, C., Amal, R., Bushell, G., Waite, T. D. (2001). "Evidence of shear rate dependenceon restructuring and breakup of latex aggregates." Journal of Colloid and Interface Science **236**: 67-77.

Sheikholeslami, R., Bright, J. (2002). "Silica and metals removal by pretreatment to prevent fouling of reverse osmosis membranes." Desalination **143**: 255-267.

Sjoberg, S. (1996). "Silica in aqueous environments." Journal of Non-Crystalline Solids **196**: 51-57.

Smith, S. D., Edwards, M. (2005). "The influence of silica and calcium on arsenate sorption to oxide surfaces." Journal of Water Supply: Research and Technology: 201-211.

Soderberg, O., Ge, Y., Haimi, E., Heczko, O., Oja, M., Laine, J., Suhonen, T., Aaltonen, A., Kalliokari, K., Borak, B., Jasiorski, M., Baszczuk, A., Maruszewski, K., Hannula, S-P. (2007). "Morphology of ferromagnetic sol-gel submicron silica powders doped with iron and nickel particles." Materials Letters **61**: 3171-3173.

Sperlich, A., Werner, A., Genz, A., Amy, G., Worch, E., Jekel, M. (2005). "Breakthrough behaviour of granular ferric hydroxide (GFH) fixed-bed adsorption filters: modelling and experimental approach." Water Research **39**: 1190-1198.

Sugimoto, T., Sakata, K., Muramatsu, A. (1993). "Formation mechanism of monodisperse pseudocubic alpha-Fe_2O_3 particles from condensed ferric hydroxide gel." Journal of Colloid and Interface Science **159**: 372-382.

Swedlund, P. J., Webster, J. G. (2001). "Cu and Zn ternary surface complex formation with SO_4 on ferrihydrite and schwertmannite." Applied Geochemistry **16**: 503-511.

Swedlund, P. J., Webster, J. G., Miskelly, G. M. (2003). "The effect of SO_4 on the ferrihydrite adsorption of Co, Pb, and Cd: Ternary complexes and site heterogeneity." Applied Geochemistry **18**: 1671-1689.

Swedlund, P. J., Webster, J.G. (1999). "Adsorption and polymerisation of silicic acid on ferrihydrite, and its affect on arsenic adsorption." Water Research **33**(16): 3413-3422.

Takemori, M. (1993). "Hydrometallurgical methods for extraction and purification of silica." Minerals Engineering **6**(3): 279-290.

Tewari, P. H., McLean, A. W. (1972). "Tempreature dependence of point of zero charge of alumina and magnetite." Journal of Colloid and Interface Science **40**(2): 267-272.

Thordarson, H., Tomasson, T. H. (1989). "Brine clarification at Svartsengi, Iceland: effect of pH and temperature on the precipitation of silica and its properties." Geothermics **18**(1): 287-294.

Tongpool, R., Jindasuwan, S. (2004). "Sol-gel synthesis and characterisation of iron oxide-silica nanocomposites." Surface and Interface Analysis **36**: 1130-1132.

Towe, K. M., Bradley, W. F. (1967). "Mineralogical constitution of colloidal "hydrous ferric oxides"." Journal of Colloid and Interface Science **24**: 384-392.

Trivedi, P., Axe, L. (2001). "Ni and Zn sorption to amorphous versus crystalline iron oxides: macroscopic studies." Journal of Colloid and Interface Science **244**: 221-229.

Trivedi, P., Dyer, J. A., Sparks, D. L., Pandya, K. (2004). "Mechanistic and thermodynamic interpretations of zinc sorption onto ferrihydrite." Journal of Colloid and Interface Science **270**: 77-85.

Turnbull, D. (1950). "Kinetics of heterogeneous nucleation." Journal of Chemical Physics **18**: 198.

Turnbull, D., Vonnegut, B. "Nucleation Catalysts." 1292.

Unob, F., Wongsiri, B., Phaeon, N., Puanngam, M., Shiowatana, J. (2007). "Reuse of waste silica as adsorbent for metal removal by iron oxide modification." Journal of Hazardous Materials **142**: 455-162.

Valdeavella, C. V., Perkyns, J. S., Pettitt, B. M. (1994). "Investigations into the common ion effect." Journal of Chemical Physics **101**(6): 5093-5109.

Vempati, R. K., Loeppert, R. H., Cocke, D. L. (1990). "Mineralogy and reactivity of amorphous si-ferrihydrites." Solid State ionics **38**: 53-61.

Vogel, A. A. (1996). Vogel's qualitative inorganic analysis. New York, Longman.

Vogelsberger, W., Lobbus, M., Sonnefeld, J., Seidel, A. (1999). "The influence of ionic strength on the dissolution process of silica." Colloids and Surfaces **159**: 311-319.

Voight, W. (1912). Sitzungsber. Bayerische Akademie der Wissenschaften **42**: 603.

Volmer, M. (1939). Kinetik der Phasenbildung. Dresden and Leipzig, Steinkopff.

Walton, A. G. (1967). Chemical Anlysis: The formation and properties of precipitation. New York, U.S.A., Interscience Publishers.

Wang, S., Cao, H., Gu, F., Li, C., Huang, G. (2007). "Synthesis and magnetic properties of iron/silica core/shell nanostructures." Journal of Alloys and Compounds.

Waychunas, G. A., Fuller, C. C., Davis, J. A. (2002). "Surface complexation and precipitate geometry for aqueous Zn(II) sorption onto ferrihydrite: I. X-ray absorption extended fine structure spectroscopy analysis." Geochimica et Cosmochimica Acta **66**(7): 1119-1137.

Waychunas, G. A., Fuller, C. C., Davis, J. A., Rehr, J. J. (2003). "Surface complexation and precipitate geometry for aqueous Zn(II) sorption on ferrihydrite: II. XANES analysis and simulation." Geochimica et Cosmochimica Acta **67**(5): 1031-1043.

Wells, A. F. (1946). "Crystal growth " Annual Reproduction of the Chemical Society **43**: 62.

Williams, R. A., Kelsall, G. H. (1988). "An investigation of the surface properties of atomised FexSi powders." Journal of Colloid and Interface Science **132**(1): 210-219.

Xu, G., Zhang, J., Song, G. (2003). "Effect of complexation on the zeta potential of silica powder." Powder Technology **134**: 218-222.

Xu, J., Thompson, S., O'Keefe, E., Perry, C.C. (2004). "Iron oxide-silica nanocomposites via sol-gel processing." Materials Letters **58**: 1696-1700.

Xu, X., Saghi, Z., Yang, G., Gay, R., Mobus, G. (2008). "Electron tomography of CeO_2 nanostructures." Journal of Physics: Conference Series **126**: 012016.

Xu, Y., Axe, L. (2005). "Synthesis and characterisation of iron oxide-coated silica and its effect on metal adsorption." Journal of Colloid and Interface Science **282**: 11-19.

Xue, J., Huang, P. M. (1995). "Zinc adsorption-desorptionon on short-range ordered iron oxides influenced by citric acid during its formation." Geoderma **64**: 343-356.

Zeng, H., Fisher, B., Giammar, D. E. (2008). "Individual and competitive adsorption of arsenate and phosphate to a high-surface-area iron oxide-based sorbent." Environmental Science and Technology **42**: 147-152.

Zeng, L. (2003). "A method for preparing silica-containing iron(III) oxide adsorbents for arsenic removal." Water Research **37**: 4351-4358.

Zhang, J., Buffle, J. (1996). "Multi-method determination of the fractal dimension of hematite aggregates." Colloids and Surfaces A: Physiochemical and Engineering Aspects **107**: 175-187.

Zhou, Y., Franks, G. V. (2006). "Flocculation mechanism induced by cationic polymers investigated by light scattering." Langmuir **22**: 6775-6786.

Zimmerman, H. K. (1952). "The experimental determination of solubilities." Chemical Reviews **51**: 25.

6. APPENDIX

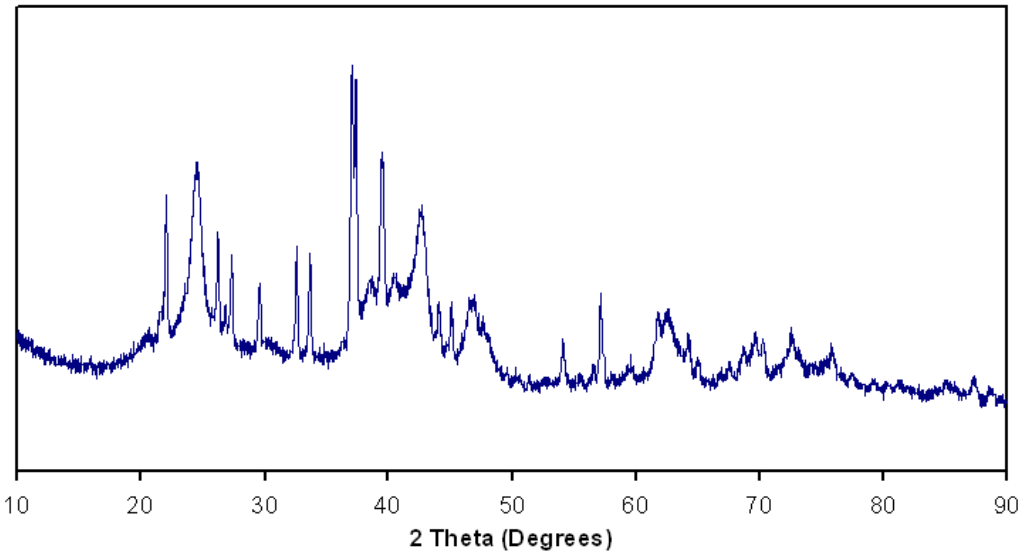

Figure 6.1: X-ray diffraction pattern obtained from the steady-state sample of the first experiment doped with excess sulfate. Many sharp peaks appeared corresponding to the presence of a substantial amount of re-precipitated sodium sulfate.

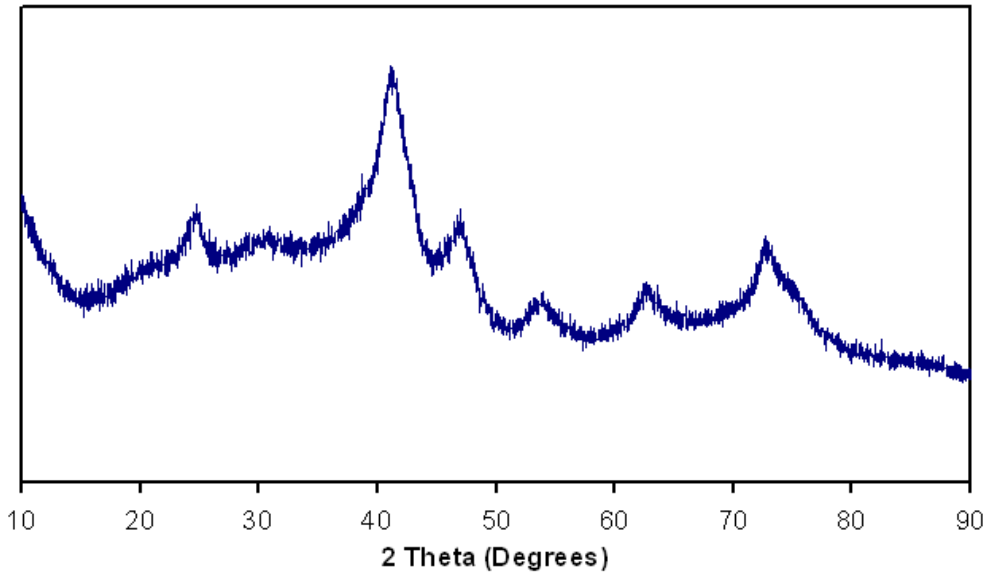

Figure 6.2: X-ray diffraction pattern obtained from the steady-state sample of LD071 (successful sulfate doping experiment). The peak at approximately 25 ° suggests the presence of goethite where none was observed in the steady-state continuous sample.

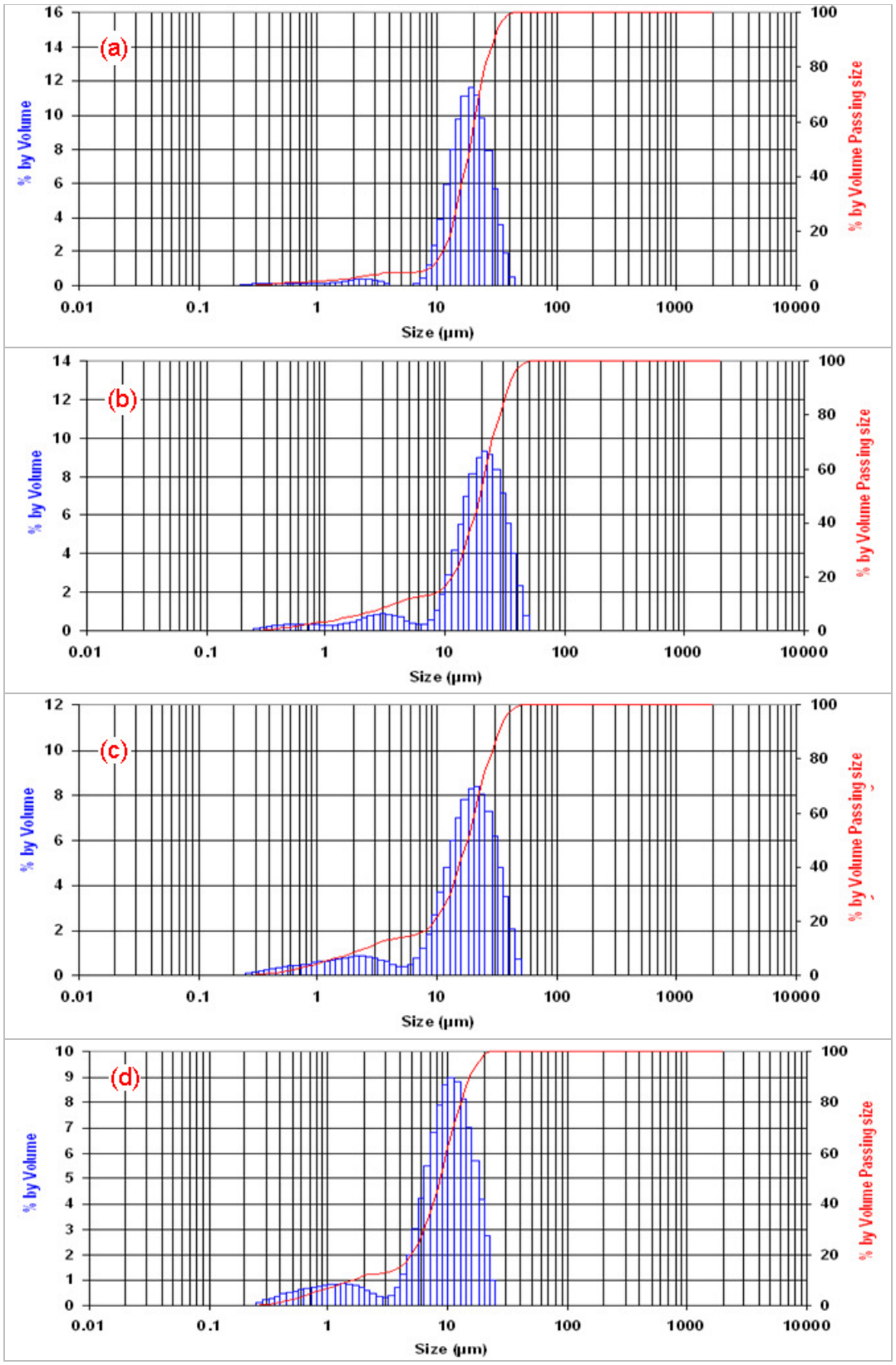
(a)
% by Volume
% by Volume Passing size
Size (µm)
0.01
0.1
1
10
100
1000
10000
(b)
% by Volume
% by Volume Passing size
Size (µm)
(c)
% by Volume
% by Volume Passing size
Size (µm)
(d)
% by Volume
% by Volume Passing size
Size (µm)

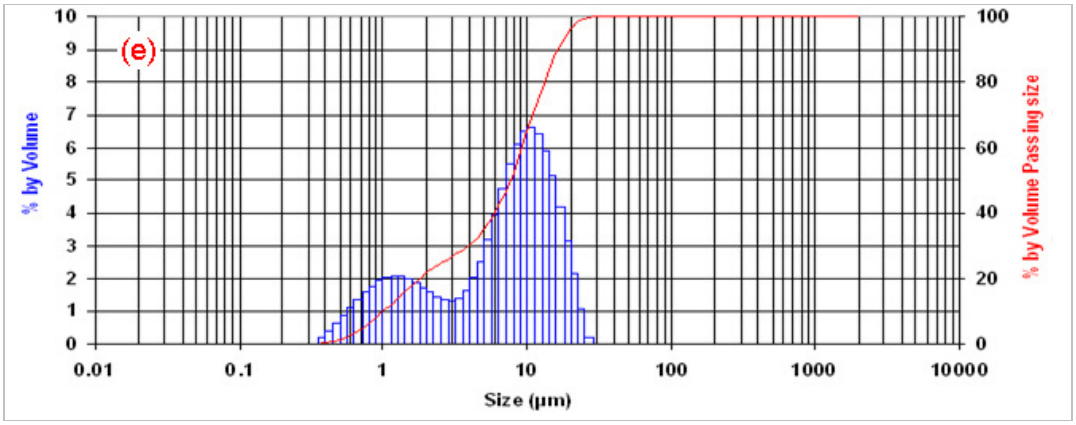

Figure 6.3: Particle size distribution data from (a) LS-0-1, (b) LS-5-1, (c) LS-10-1, (d) LS-20-1 and (e) LS-30-1. There is a significant increase in the proportion of aggregates falling below 3 m in size based as the Si:Fe ratio increases.

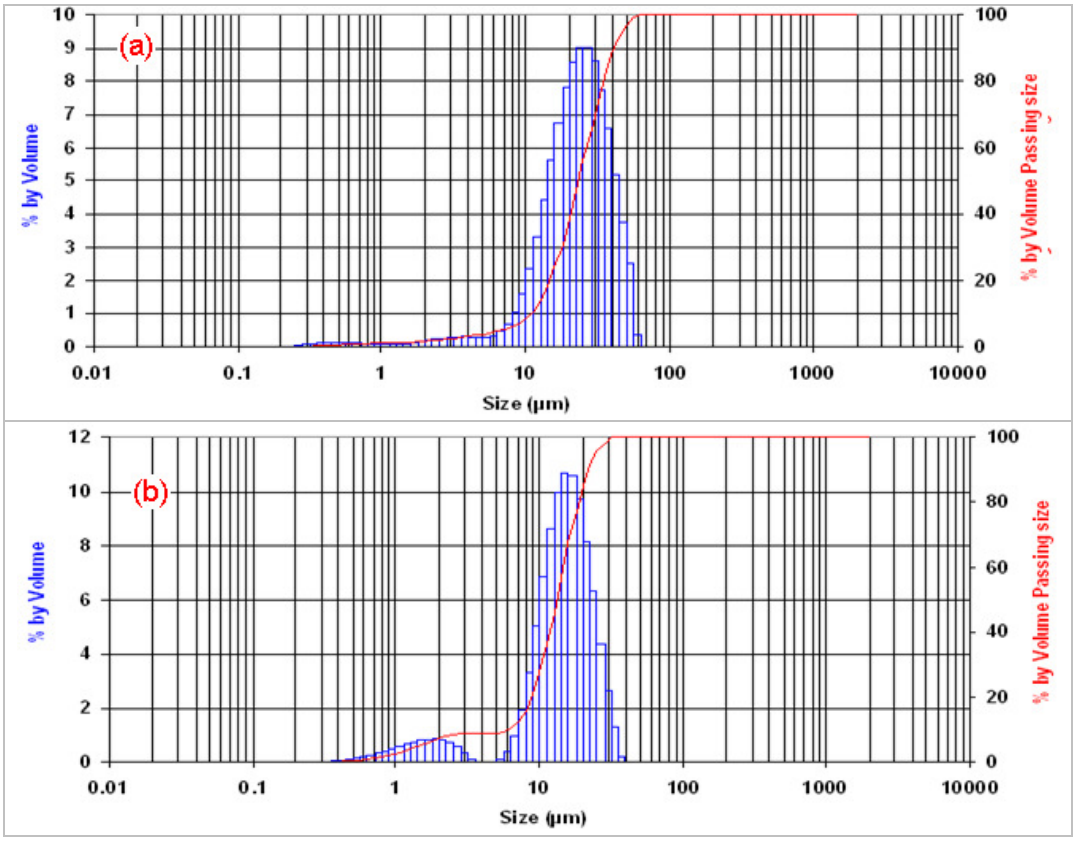

Figure 6.4: Particle size distribution data from (a) LS-20-2, (b) LS-30-2. These samples have comparatively less fines (below 3 m) than the experiments using the same Si:Fe ratios in Figure 6.3. This is due to a slower hydrolysis rate in LS-20-2 and the monomeric state of the silicate in LS-30-2.

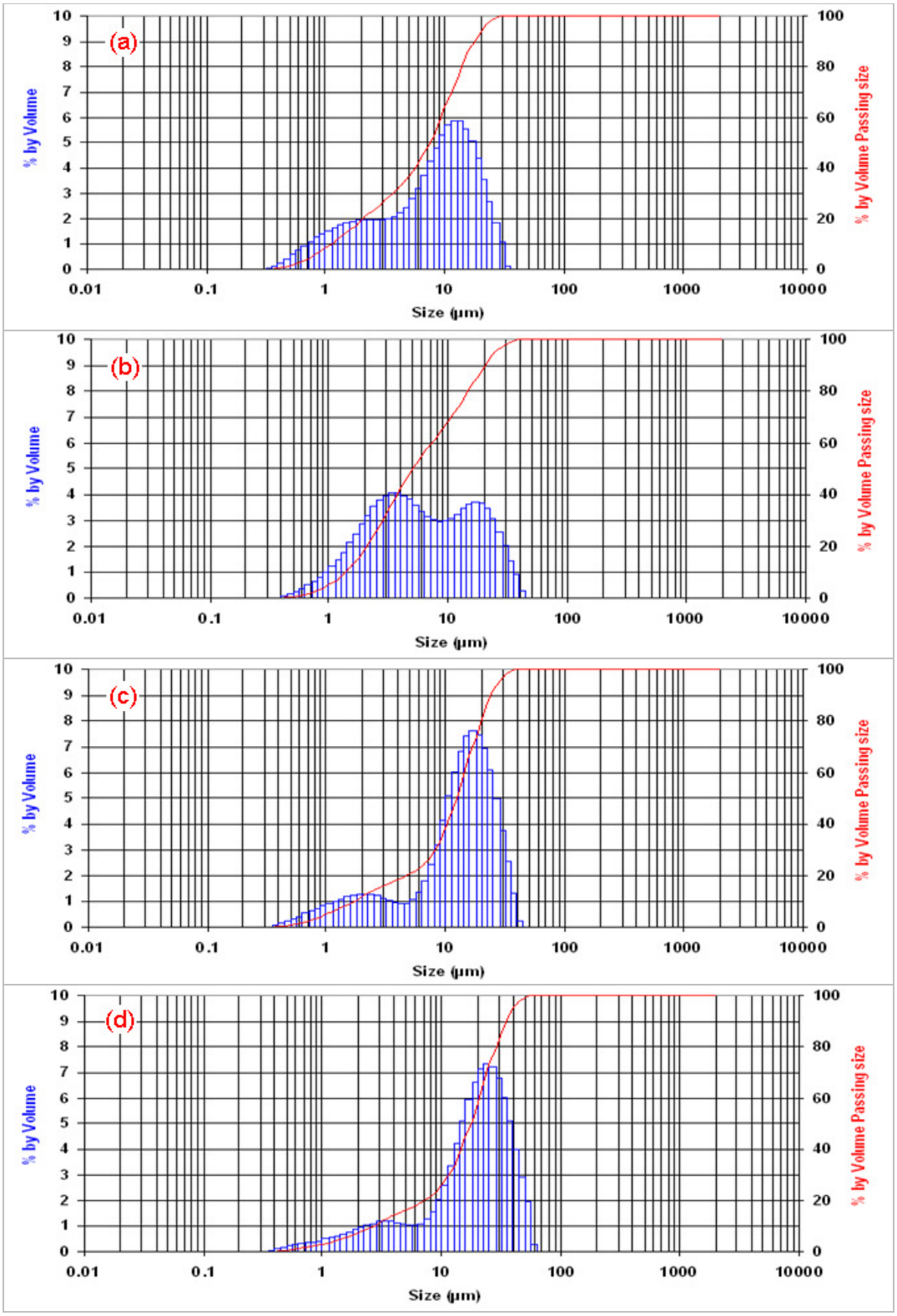

Figure 6.5: Particle size distribution data from (a) LN-0-1, (b) LN-5-1, (c) LN-10-1 and (d) LN-30-1. Above the initial introduction of silicate to the feed (LN-5-1) increase in Si:Fe ratio decreases the amount of fines and increases the average aggregate size.

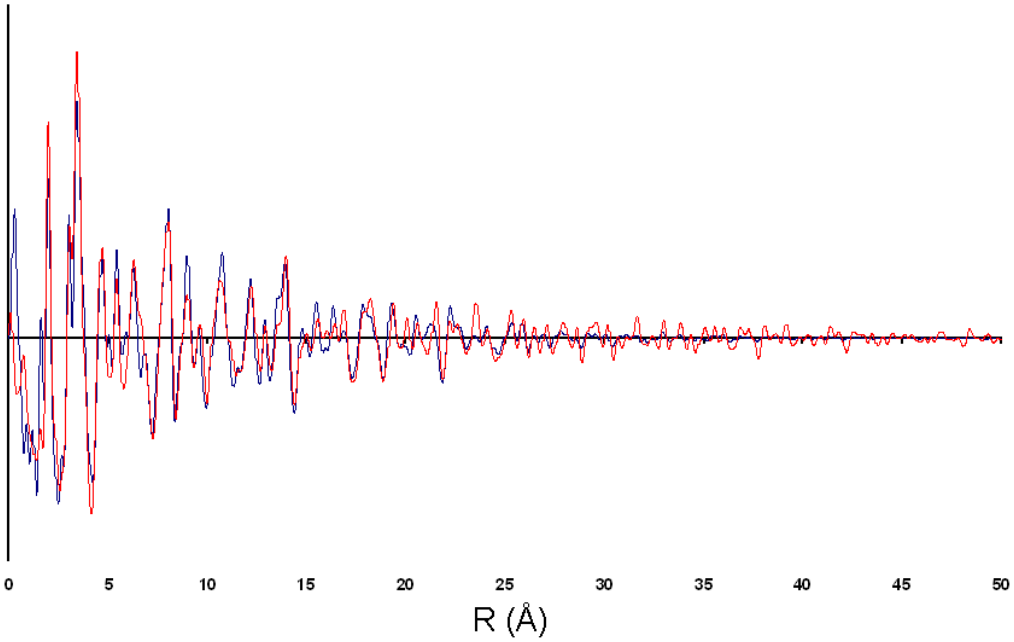

Figure 6.6: Pair distribution functions obtained from samples of N-30-1 (red) and a physical mixture of N-0-2 and pure silica (Si-045) (blue). Structural information is able to be obtained at greater R values for the mixture compared with the co-precipitate is further evidence of the decline in ferrihydrite particle size caused by the association with silica during formation.

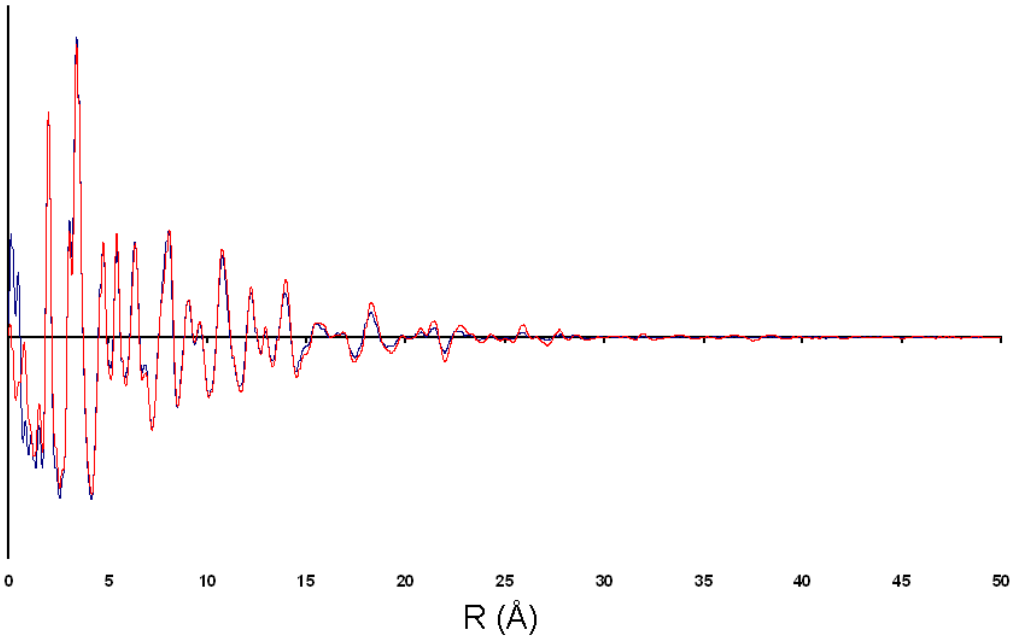

Figure 6.7: Pair distribution function obtained from samples of S-10-1 (red) and S-10-10Z (blue). The similarity between the two plots suggests that zinc has little or no impact on the ferrihydrite structure.